

EFFECT OF ELECTRON BEAM IRRADIATION ON ORGANIC FILMS AND DEVICES

By

Nishant Chaudhary

(PHYS01201304011)

Bhabha Atomic Research Centre, Mumbai

*A thesis submitted to the
Board of Studies in Physical Sciences
in partial fulfillment of requirements
for the Degree of*

DOCTOR OF PHILOSOPHY

of

HOMI BHABHA NATIONAL INSTITUTE

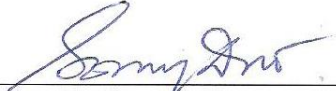
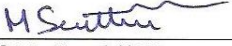


December, 2017

Homi Bhabha National Institute

Recommendations of the Viva Voce Committee

As members of the Viva Voce Committee, we certify that we have read the dissertation prepared by **Nishant Chaudhary** entitled “**Effect of electron beam irradiation on organic films and devices**” and recommend that it may be accepted as fulfilling the thesis requirement for the award of Degree of Doctor of Philosophy.

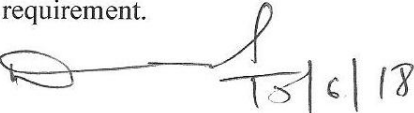
Chairperson:	 Prof. Anita V. Topakar	15/6/2018 Date:
Guide/Convener:	 Prof. D. K. Aswal	15/6/18 Date:
Examiner:	 Dr. Soumya Dutta	15/06/2018 Date:
Member 1:	 Prof. Archana Sharma	15-6-18 Date:
Member 2:	 Prof M. Senthil Kumar	15/06/18 Date:
Member 3:-	 Dr. Ajay Singh	15-6-18 Date:
Technology Adviser:	Sh. S. Acharya 	Date: 15/06/2018

Final approval and acceptance of this thesis is contingent upon the candidate's submission of the final copies of the thesis to HBNI.

I hereby certify that I have read this thesis prepared under my direction and recommend that it may be accepted as fulfilling the thesis requirement.

Date: 15-06-2018

Place: MUMBAI


15/6/18

(Prof. D. K. Aswal)

(Guide)

STATEMENT BY AUTHOR

This dissertation has been submitted in partial fulfillment of requirements for an advanced degree at Homi Bhabha National Institute (HBNI) and is deposited in the Library to be made available to borrowers under rules of the HBNI.

Brief quotations from this dissertation are allowable without special permission, provided that accurate acknowledgement of source is made. Requests for permission for extended quotation from or reproduction of this manuscript in whole or in part may be granted by the Competent Authority of HBNI when in his or her judgment the proposed use of the material is in the interests of scholarship. In all other instances, however, permission must be obtained from the author.

Nishant Chaudhary
Nishant Chaudhary

DECLARATION

I, hereby declare that the investigation presented in the thesis has been carried out by me. The work is original and has not been submitted earlier as a whole or in part for a degree / diploma at this or any other Institution / University.

Nishant Chaudhary
Nishant Chaudhary

List of Publications arising from the thesis

Journals

1. “Electron beam induced modifications in electrical properties of Poly(3,4-ethylenedioxythiophene):poly(styrenesulfonate) films” Nishant Chaudhary, M. Bharati, A. Singh, D. K. Aswal, S. P. Koiry, A. K. Debnath, S. Acharya, *Vacuum* **2018**, *152*, 243 - 247.
2. “Electron beam modified zinc phthalocyanine thin films for radiation dosimeter application”, Nishant Chaudhary, Ajay Singh, D. K. Aswal, A. K. Debnath, S. Samanta, S. P. Koiry, S. Sharma, K. Shah, S. Acharya, K. P. Muthe, S. C. Gadkari, *Synthetic Metals* **2017**, *231*, 143-152.
3. “Electron beam induced modifications in flexible biaxially oriented polyethylene terephthalate sheets: improved mechanical and electrical properties”, Nishant Chaudhary, S. P. Koiry, Ajay Singh, A. R. Tillu, P. Jha, S. Samanta, D. K. Aswal, R. K. Mondal, S. Acharya, K. C. Mittal, *Materials Chemistry & Physics* **2017**, *189*, 237-244.
4. “Electron beam modified organic materials and their applications”, Nishant Chaudhary, Ajay Singh, A. K. Debnath, S. Acharya, D. K. Aswal, *Solid State Phenomena* **2015**, *239*, 72-97.
5. “Electron beam induced modifications of polyaniline silver nano-composite films: electrical conductivity and H₂S gas sensing studies”, Nishant Chaudhary, Ajay Singh, D. K. Aswal, P. Jha, S. Samanta, A. K. Chauhan, A. K. Debnath, S. Acharya, K. Shah, K. P. Muthe, S. C. Gadkari, *Radiation Physics & Chemistry* **2017** (under review) Ref: RPC_2017_532.

Conferences

1. “Electron beam induced amendment in electrical conductivity of PEDOT:PSS films”, Nishant Chaudhary, Meetu Bharti, Ajay Singh, D. K. Aswal, S. Samanta, A. K. Debnath, S. Acharya, *International Conference on Thin Films (ICTF) 2017*, CSIR-NPL, New Delhi.
2. “High energy electron beam radiation effect on electrical conductivity of zinc phthalocyanine thin film”, Nishant Chaudhary, Ajay Singh, A. K. Debnath, D. K. Aswal, A. R. Tillu, R. Prasad, S. Acharya, *Symposium on Condensed Matter Physics under Extreme Conditions (CoMPEC) 2016*, BARC, Mumbai.
3. “Investigation of high energy electron beam effect on BOPET”, Nishant Chaudhary, Shankar P. Koiry, P. Jha, D. K. Aswal, S. Acharya, K. C. Mittal, *Organic Devices: The Future Ahead (ODeFA) 2014*, BARC, Mumbai.

Nishant Chaudhary

*To my maa – babuji & wife Minakshi, their
faith in me has
brought me up to this stage of life*

ACKNOWLEDGEMENTS

Words cannot express my deep sense of gratitude towards my guide Prof. D. K. Aswal and technology advisor Shri S. Acharya for their invaluable guidance, consistent encouragement and active support during this thesis work.

I am equally grateful to Dr. Ajay Singh for his tireless cooperation, encouragement, fruitful discussions and invaluable patience in every stages of the present study.

I would like to express my gratitude to my former division head Dr. K. C. Mittal and present head Shri R. K. Rajawat for permitting me to pursue the research work and providing all the administrative supports. I am also thankful to Dr. (Smt.) Archana Sharma and Smt. K. P. Dixit for their moral supports and encouragements.

I would like to give my special thanks to Dr. A. K. Debnath, Dr. A. K. Chauhan, Shri R. Prasad, Dr. S. Samanta, Dr. (Smt.) Vibha Saxena, Dr. S. P. Koiry, Dr. P. Jha, Dr. Ashwani Kumar and Dr. K. Shah for providing the necessary facilities and assistance to carry out the experimental works. I am grateful to Miss Meetu Bharati for her cooperations not only during experiments but also during correction and finalization of the thesis.

I owe my deepest gratitude to my colleagues Shri Mukesh Kumar, Shri A. R. Tillu, Shri R. B. Chavan, Shri H. Sarukte, Shri S. P. Dwangan and Smt. S. S. Gaikward for their co-operations to complete the irradiation experiments at EBC Kharghar, BARC.

My heartiest thanks are due to my sisters Mrs. Anju and Mrs. Aradhana & brother in laws Mr. S. Jha and Mr. M. Thakur for their constant emotional support during these years.

Last, but not least, I express my hearty thanks to my friends K. K. Singh, Ram Niranjan, H. K. Patni, Smt. Sherya and others for sharing interest in my Ph.D.

December, 2017

(Nishant Chaudhary)

CONTENTS

	Page No.
SYNOPSIS	xiii
List of Figures	xix
List of Tables	xxvi
Chapter 1 Introduction	1
1.1 An overview of organic devices	3
1.2 Introduction to radiation and its sources	5
1.3 Classification of organic materials	7
1.3.1 Insulators	8
1.3.2 Organic semiconductors	9
1.3.2.1 Molecular semiconductors	10
1.3.2.2 Conducting polymers	17
1.4 Charge transport in organic semiconductors	20
1.4.1 Films- electrode interface-controlled charge transport	23
1.4.2 Bulk limited charge transport	23
1.4.2.1 Ohmic conduction	23
1.4.2.2 Space charge limited conduction	24
1.4.3 Hopping conduction	26
1.5 Basic processes of interaction of radiation with organic materials	28
1.5.1 Physical phase	29
1.5.2 Physico-chemical phase	29
1.5.3 Chemical phase	30
1.6 Modifications of organic materials through radiation	30
1.6.1 Crosslinking	31

1.6.2	Scissioning	33
1.6.3	Crosslinking versus main-chain scission	33
1.6.4	Curing	34
1.6.5	Grafting	35
1.6.6	Unsaturation	36
1.6.7	Gas evolution	36
1.7	Applications of electron beam modified organic materials	37
1.8	Basic characteristics of chemiresistive gas sensors	39
1.8.1	Gas sensing mechanism in metal phthalocyanines	40
1.8.2	Gas sensing mechanism in conducting polymers	41
1.9	Literature review on irradiation induced benefits in organic materials	42
1.10	Outline of the thesis	44
Chapter 2	Experimental techniques	49
2.1	Introduction	50
2.2	Methods of thin film depositions	50
2.2.1	Thermal vapour deposition	50
2.2.2	Film growth by photo-polymerization	52
2.2.3	Film growth by drop cast method	54
2.3	Electron beam irradiation of synthesized samples	55
2.3.1	10 MeV RF Linac	56
2.3.2	1-3 MeV DC accelerator	57
2.3.3	Dosimetry characterization of accelerators	59
2.4	Characterization techniques	61
2.4.1	X-ray photoelectron spectroscopy (XPS)	61
2.4.2	Fourier transform infrared spectroscopy (FTIR)	63

2.4.3	UV-Visible spectroscopy (UV-Vis)	65
2.4.4	Photoluminescence spectroscopy (PL)	67
2.4.5	X-ray diffraction (XRD)	69
2.4.6	Atomic force microscopy (AFM)	71
2.4.7	Scanning electron microscopy (SEM)	73
2.4.8	Contact angle measurement	76
2.4.9	Mechanical characterizations	77
2.4.10	Crosslinking analysis	78
2.4.10.1	Sol-Gel test	79
2.4.10.2	Solubility test	81
2.5	Electrical characterizations	81
2.5.1	Electrical conductivity measurement	82
2.5.2	Chemiresistive gas sensing measurement	83
Chapter 3	Electron beam induced modifications of biaxially oriented polyethyleneterephthalate sheets	85
3.1	Introduction	87
3.2	Sample preparation & electron beam irradiation	89
3.3	Mechanical characterizations	89
3.4	Electrical characterizations	91
3.5	Structural characterizations	92
3.5.1	FTIR spectroscopy	92
3.5.2	XRD	93
3.6	Surface characterizations	94
3.6.1	XPS	94
3.6.2	Contact angle measurements	97

3.7	Sol-gel test for crosslinking analysis	98
3.8	Plausible mechanism for modification of BOPET by EB irradiation	100
3.9	Conclusions	101
Chapter 4	Electron beam induced modifications in zinc phthalocyanine films	103
4.1	Introduction	105
4.2	Deposition of flexible ZnPc films and thickness optimization	107
4.3	Electron beam irradiation of ZnPc films	110
4.4	Surface characterizations using XPS	110
4.5	Structural and morphological characterizations	114
4.5.1	UV-Visible spectroscopy	114
4.5.2	X-ray diffraction	116
4.5.3	Atomic force microscopy	117
4.6	Electrical characterizations	118
4.7	Chemiresistive gas sensing	120
4.8	Charge transport and gas sensing behavior	122
4.9	Plausible mechanism for electron beam induced change in gas sensing behavior	125
4.10	Conclusions	128
Chapter 5	Modifications in conducting polymer films through electron beam	130
5.1	Introduction	132
5.2	Photopolymerization of PANI-Ag nanocomposite films	134
5.2.1	Modifications of BOPET substrate using APTMS	134
5.2.2	Preparation of PANI-Ag nanocomposite films on APTMS modified BOPET	137
5.3	Preparation of PEDOT:PSS flexible polymer films	139

5.4	Electron beam irradiation of conducting polymer films	140
5.5	Surface and morphological characterizations of PANI-Ag nanocomposite films	140
5.5.1	Scanning electron microscopy	140
5.5.2	X-ray photoelectron spectroscopy	141
5.6	Structural characterization of PANI-Ag nanocomposite films	143
5.6.1	Fourier transform infrared spectroscopy	143
5.6.2	Photoluminescence spectroscopy	145
5.6.3	UV-Visible spectroscopy	147
5.7	Crosslinking characterizations	148
5.8	Electrical characterization and charge transport analysis	150
5.9	Chemiresistive gas sensing	153
5.10	Characterizations of PEDOT:PSS films	155
5.10.1	XPS	155
5.10.2	Contact angle measurement	157
5.10.3	Solubility test	158
5.10.4	Electrical conductivity	160
5.11	Conclusions	162
Chapter 6	Summary	165
	References	171

SYNOPSIS

During past two decade the basic research based on the organic thin films of small molecules (e.g. metal phthalocyanines, pentacene, etc.) as well as conducting polymers (polypyrrole, polyaniline, poly(3-hexylthiophene), etc.) is primarily driven by their potential applications in flexible, low cost and light-weight electronic devices. These applications include flexible / bendable displays for electronic paper and flexible computers, human-machine interfaces, electronic artificial skin, gas sensors, radiation dosimeters, field effect transistors, solar cells, photo detectors, radio frequency identification (RFID) tags, etc. Along with potential application, organic electronic devices are currently being investigated for their electro-mechanical stability and long term stable operation under ambient conditions. However, the studies pertaining to the effect of high radiation environment on organic electronic devices is not well understood. On the other hand radiation often employed to modify the physico-chemical properties of materials to cater different societal and research applications. In order to create significant changes in the physico-chemical properties of organic materials, the energy of the incident radiation should be higher than their ionization potential (typically 10 – 15 eV). There are various sources of such high energy radiation such as gamma rays, electron beam etc. The electron beam that can be generated by electron-beam accelerators have more public acceptability and outweighs than conventional gamma ray sources as i) the throughput for electron accelerators is around 10^3 - 10^7 Gy/h, which is constant with time; whereas for gamma ray throughput is lower by three orders in magnitude and it also decreases with time as activity is a function of time, (ii) The penetration depth of 10 MeV electron-beam is ~ 35 mm (for a material of unit density), whereas the same for gamma ray source (Co-60) is around 330 mm and hence the electron beam is suitable for the treatment of moderately thick materials like organic thin films, polymer sheets etc, (iii) Electron-beam is produced using accelerators that are fully controlled systems, oppositely

gamma rays are obtained from radioactive source which is not controllable. Therefore the motivation of current research work is to understand the effect of electron beam irradiation induced modification in electrical and mechanical characteristics of three important organic films, which are insulating (bi-axially oriented polyethyleneterephthalate), semiconducting (zinc phthalocyanine) and conducting (doped polyaniline) in nature with emphasis to utilize modified films for device application as gas sensors and radiation dosimeters.

Based on the results obtained the content of the thesis is organized with following six chapters:

Chapter1: Introduction

This chapter confers a detailed review of literature about the interaction of electron-beam with organic materials (eg. polymers, organic solvents, organic acids, organic semiconductors etc) to modify their physico-chemical properties and their applications in variety of societal benefits. The energetic electrons create free radicals in organic materials, which in turn, lead to modification through various mechanisms such as cross-linking, scissioning, curing and grafting. It also emphasizes on the tremendous applications of electron-beam modified organic materials in society, such as, bio-medical, textiles, environment protection, electronics, radiation dosimetry etc.

Chapter2: Experimental techniques

The chapter deals with the different experimental techniques and instrumentations used in the present thesis work. The principle of electron beam accelerator and their dosimetry characterizations are explained. All irradiation experiments were carried out at linear accelerator (Energy 10 MeV) available at Electron Beam Centre Kharghar. Along with details of accelerator the protocol for irradiation experiments is discussed in this chapter. The details of the physical vapor deposition (PVD) system used for the deposition of the zinc phthalocyanine (ZnPc) thin film and photo polymerization technique used for polyaniline

silver (PANI-Ag) nanocomposite thin films growth, have been illustrated. Brief descriptions of various characterization techniques including x-ray photoelectron spectroscopy (XPS), fourier transformation infrared spectroscopy (FTIR), UV-visible spectroscopy (UV-vis), photoluminescence spectroscopy (PL), scanning electron microscopy (SEM), atomic force microscopy (AFM), x-ray diffraction (XRD) etc have been presented. The details of electrical measurements of organic thin films using two probe method and gas sensing have been discussed. The quantification of crosslinking or scissioning of polymers through sol-gel analysis and solubility tests are also elaborated along with the mechanical characterization techniques of organic polymers.

Chapter3: Electron beam induced modifications of biaxially oriented polyethylene terephthalate films

The present chapter describes the effect of electron beam induced modifications in organic insulator namely biaxially oriented polyethylene terephthalate (BOPET). The irradiation was done with 10 MeV electron beam in dose range 2-32 kGy. The sol-gel analysis, FTIR, XPS, characterizations of the irradiated BOPET sheets suggest partial cross-linking of PET chains through diethylene glycol (DEG) formation. The mechanical properties of BOPET, such as, tensile strength, Young's modulus and electrical resistivity enhances with increasing dose and saturate for doses > 10 kGy. The improved mechanical properties and enhanced electrical resistivity of electron beam modified BOPET sheets may have additional advantages in applications, such as, packaging materials for food, medical product sterilization and electronic industries.

Chapter4: Electron beam induced modifications in zinc phthalocyanine film

This chapter is focused upon electron beam modified organic semiconducting film ZnPc. It deals with electron beam irradiation effect on electrical and gas sensing properties of 20 nm ZnPc thin film prepared on flexible BOPET substrate. The irradiation of ZnPc films

were carried out using a 10 MeV electron beam under different radiation dose levels from 1 kGy to 30 kGy. The pristine and irradiated films were characterized by using XPS, AFM, UV-Vis and XRD. The films exhibit linear enhancement of electrical conductance due to increasing content of adsorbed oxygen up to dose 18 kGy. Beyond 18 kGy the sample exhibits saturation in the content of adsorbed oxygen as well as in electrical conductance. The pristine ZnPc films exhibits excellent chemi-resistive response towards H₂S gas in 1-20 ppm range at room temperature. The response of the irradiated films decreases monotonically with increasing electron beam dose due to the strong binding of oxygen at the Zn sites. A plausible mechanism of electron beam induced modification of ZnPc films and its implication on charge transport as well as chemi-resistive gas sensing behavior are discussed. This work highlight the utilization of ZnPc thin films as potential radiation dosimeter based upon linear rise in electrical conductance as well as lowering of H₂S response, for fixed concentration, with electron beam dose. In addition the enhancement of electrical conductivity of ZnPc as result of electron beam treatment concludes that these films can be operated at lower voltage after irradiation, compared to pristine film, to get sufficient current for different applications (e.g. gas sensor, organic field effect transistor etc.) with the advantage of power-saving.

Chapter5: Modifications in conducting polymer films through electron beam

In this chapter the electron beam induced modifications in organic conducting film polyaniline-silver (PANI-Ag) nanocomposite has been elaborated. The PANI-Ag films were grown on (3-aminopropyl)trimethoxysilane (APTMS), which acts like a coupling agent to improve adhesion, treated BOPET substrate by in-situ photo polymerization and post deposition doped with HCl to convert in emeraldine salt. The modification in electrical conductivity and gas sensing characteristic after irradiation with 10 MeV electron beam, at different doses up to 100 kGy, have been discussed. After electron beam exposure the electrical conductivity of the PANI-Ag films was initially found to be enhanced by two

orders of magnitude up to 30 kGy of dose and later it falls with increasing dose. As compared to pristine film, electron beam modified PANI-Ag films exhibit higher sensitivity towards ppm level of H₂S gas. The rigorous characterization of the films suggests that enhanced conductivity up to 30 kGy of electron beam dose is due to scissioning as well as additional doping of chlorine in PANI chain as result of electron beam irradiation. At higher dose cross-linking of polymer chains dominates and results in lowering of electrical conductivity. The results of different characterizations including FTIR, UV-Vis, XPS, SEM, solubility test and PL spectroscopy have been explained with proper analysis.

The chapter also includes the effect of high radiation on the electrical properties of conducting polymer film composite poly(3,4-ethylenedioxythiophene):poly(styrenesulphonate) i. e. PEDOT:PSS. Thin films of PEDOT:PSS were deposited on flexible polyimide (Kapton) sheets and irradiated up to 75 kGy dose with 1 MeV electron beam. The conductivity of as deposited polymer film was ~ 3.2 S/cm which consistently falls to ~ 0.76 S/cm after getting 75 kGy. The detailed characterization results and analysis, using XPS, contact angle measurement and crosslinking analysis, have been presented.

Chapter6: Summary

This chapter encapsulates the summary of the important outcomes obtained during the thesis work. Briefly these important results will be summarized as follows:

- (i) Irradiation of BOPET films by electron beam, in dose range 2-32 kGy, leads to the formation of diethylene glycol that cross-link's the PET chains, resulting in improved mechanical properties and enhanced electrical resistivity.
- (ii) Electron beam exposure of ZnPc films to different doses leads to a linear enhancement in the electrical conductance and concomitant lowering of chemi-resistive response for H₂S with dose, suggesting their possible application as radiation dosimeter. In addition

the enhancement in electrical conductivity reckons that it can be operated at lower voltage after irradiation for different applications (e.g. gas sensor, organic field effect transistor etc.) with the benefit of power-saving.

(iii) The electron beam irradiation of PANI-Ag nanocomposite films resulted in tailoring of electrical conductivity and H₂S sensitivity due to enhanced doping, scissioning and cross-linking of PANI chains.

(iv) The electron beam irradiation causes crosslinking in PEDOT polymer chain and dissociation of PSS ultimately leads to fall in electrical conductivity of PEDOT:PSS. The observed systematic dependence of electrical conductivity on the electron beam dose may expect to use PEDOT:PSS films for radiation dosimeter applications. Also the study suggest the importance of electron beam as an alternative of tedious chemical crosslinking approaches used for PEDOT:PSS films.

In addition the chapter deals with the realistic and societal potential applications of the results obtained during this work. It also narrates the future scope of the work.

List of Figures

Figure No.	Figure caption	Page No.
1.1	Molecular structures of polymeric insulators: BOPET, linear polyimide, aromatic heterocyclic polyimide	9
1.2:	Structures of molecular semiconductors: pentacene, CoPc (Cobalt phthalocyanine), CuPcTs (Copper phthalocyanine tetrasulfonate) and DIP (Diindeno(1,2,3,-cd,10,20,30-lm)perylene)	11
1.3	Schematics representation of π -orbitals in benzene (C_6H_6) molecule responsible for its semiconducting properties	12
1.4	Schematic view of the splitting of the energy levels due to the interactions in the π -orbitals of a molecule leads to the formation of HOMO and LUMO energy bands	12
1.5	Molecular structure of metal phthalocyanines	14
1.6	Schematics of crystalline (a) α -ZnPc, (b) β -ZnPc	16
1.7	Molecular structures of conducting polymers: PA (Polyacetylene), PPV (Poly(phenyl vinylene)), PPy (Polypyrrole), PANi (Polyaniline), PEDOT (Poly(ethylenedioxythiophene)), PTh (Polythiophene) and PSS (Poly(styrenesulphonate))	17
1.8	Oxidation states of polyaniline	20
1.9	Acid doping of emeraldine base polyaniline to emeraldine salt polyaniline	20
1.10	(a) Schematic of energy diagram of a typical metal and organic semiconductor with separation, (b) Schematic of energy level alignment at metal/organic semiconductor interface with interface dipole	21
1.11	Schematic of hopping transport in the organic semiconductor	27
1.12	Temporal phases for interaction of organic molecule with electron beam	28

1.13	Schematic representation of interaction of radiation with organic materials	31
1.14	Permanent main chain scission in polymer contains side branches in monomeric unit	33
1.15	Schematic of electron beam induced radiation curing	34
1.16	Schematic of electron beam induced radiation grafting	35
1.17	Basic requirement and performance parameters of chemiresistive gas sensors	40
1.18	Chemisorption model of ZnPc interaction with oxygen and coordinating analytes A	41
1.19	Motivation for the research	45
2.1	(a) Schematic of thermal evaporation method for thin film deposition (b) Actual photograph of physical vapor deposition system used for thin film deposition	51
2.2	Schematic for recovering pure aniline monomers by vacuum distillation method	53
2.3	10 MeV RF electron LINAC at EBC, BARC facility at Kharghar Navi Mumbai (a) schematic representation, (b) its photograph	57
2.4	1-3 MeV Dynamitron at EBC, BARC facility at Kharghar, Navi Mumbai (a) schematic representation, (b) its photograph	58
2.5	Photograph of spectrophotometer and radiochromic film dosimeters	60
2.6	Calibration curve for dosimeter films that are used for the dose measurements in accelerators	60
2.7	Dose profile over 1 m scan length in dynamic mode at different speeds for (a) 10 MeV RF accelerator, (b) 1 MeV DC accelerator	61
2.8	Schematic of XPS set up in which x-ray produced by electron	

	bombardment on Mg anode	62
2.9	Ray diagram of recording FTIR spectra	64
2.10	Ray diagram of recording FTIR spectra in ATR mode	65
2.11	Electronic energy levels and possible electronic transitions of σ , π and n electrons	66
2.12	Block diagram of a typical double beam single monochromator UV spectrometer	67
2.13	Energy diagram showing the photoluminescence	68
2.14	Schematic representation of photoluminescence set up	69
2.15	Schematic diagram of powder x-ray diffractometer	69
2.16	Schematic showing (a) interaction of the AFM tip with the sample surface, (b) variation in force with the separation between AFM tip and the sample surface	71
2.17	(a) Photograph showing Dimension Icon AFM system, (b) block diagram of AFM	72
2.18	Typical sketch of scanning electron microscope	74
2.19	Schematic showing Tear drop model of electron interaction with sample and the depth/volume from which the different signals originates	75
2.20	Schematic representation of contact angle measurement by water droplet method	77
2.21	Schematic diagram of the mechanical property measurement setup	78
2.22	Schematic of Soxhlet-Extract setup	79
2.23	Schematic of two probe method for conductivity (I - V) measurements	83
2.24	Schematic representation of gas sensing measurement setup	83
3.1	Variation in mechanical properties of BOPET with dose (a) tensile	

strength, (b) elongation at break	90
3.2 Variation in Young's modulus of BOPET with respect to dose	90
3.3 (a) Current-voltage characteristics of pristine and irradiated BOPET sheets	
(b) variations of sheet resistance with dose	92
3.4 FTIR results for BOPET irradiated with different doses	93
3.5 XRD data recorded for the pristine and irradiated BOPET samples	94
3.6 Survey XPS result for pristine and irradiated (16 kGy) BOPET sheets	95
3.7 Convolutd XPS result for pristine and irradiated (16 kGy) BOPET sheets	
(a) C1s spectra, (b) O1s spectra	96
3.8 Static contact angle variations with electron beam dose for BOPET sheets	97
3.9 (a) Gel fraction of irradiated BOPET under different electron beam doses	
(b) Charlesby-Pinner plot for electron beam irradiated BOPET samples	99
3.10 Schematic revealing the mechanism of the formation of DEG in BOPET polymer chains as a result of electron beam irradiation	100
4.1 (a) Schematic configuration of chemiresistive sensor, (b) its equivalent circuit	106
4.2 Current -voltage plots of ZnPc films during first and subsequent scans for thickness (a) 10 nm, (b) 20 nm and (c) 50 nm; (d) <i>I-V</i> plot for ZnPc films of different thicknesses under stable condition	108
4.3 XPS survey spectrum of 20 nm ZnPc film grown on BOPET substrate	110
4.4 High resolution XPS spectra for pristine and irradiated ZnPc films (a) C1s, (b) N1s, (c) Zn2p, (d) O1s	111
4.5 (a) Atomic ratios (O/Zn) with respect to dose, (b) variation in area ratio C1s peak at 288.2 eV to total C1s peak with dose, (c) FWHM of Zn 2p _{3/2} peak changes with dose	113

4.6	(a) UV-Visible spectra for pristine and EB irradiated ZnPc films	
	(b) variations of intensity ratio of Q band peaks at 688 to at 632 with dose	115
4.7	X-ray diffraction pattern for the pristine and EB irradiated ZnPc films	117
4.8	AFM images (size: 5 μ m x 5 μ m) of the pristine and irradiated ZnPc films	118
4.9	(a) Current-voltage characteristics of ZnPc films at room temperature	
	(b) electrical conductance variation with EB dose for ZnPc film	119
4.10	(a) Alteration in electrical resistance of the pristine ZnPc thin film on exposure to reducing gas H ₂ S and oxidizing gas NO ₂ , (b) Selectivity histogram at 5 ppm of each gas of ZnPc thin film based chemiresistive gas sensor	120
4.11	Response curves of ZnPc films, for different concentration of H ₂ S irradiated with dose (a) pristine, (b) 11 kGy and (c) 18 kGy; (d) repeatability of the response curve at 5 ppm H ₂ S for pristine ZnPc films	122
4.12	Response of pristine and EB irradiated ZnPc films towards H ₂ S gas sensing	124
4.13	Variation in response of ZnPc films as function of irradiation dose for fixed concentration of H ₂ S gas (a) 2 ppm, (b) 5 ppm	124
4.14	(a) Response time, (b) recovery time for pristine and EB irradiated ZnPc films for different concentrations of H ₂ S gas	125
4.15	Gas analytes dipole interacting with image charges at metal-semiconductor interface and with the charge at grain boundary of p-type organic semiconductor	126
4.16	Schematic diagram showing the detection of H ₂ S gas by ZnPc thin film	127
4.17	Slope of response versus dose as function of H ₂ S concentration	128
5.1	Representative schemes for surface modification of BOPET substrate with APTMS	135
5.2	XPS survey spectra of BOPET and APTMS treated BOPET substrate	136

5.3	XPS convoluted spectra of (a) Si2p, (b) N1s for APTMS treated BOPET	136
5.4	Mechanism of photo-polymerization of PANI in presence of AgNO ₃	138
5.5	Representative scheme for growth of PANI-Ag nanocomposite films on APTMS modified BOPET substrate	138
5.6	Structure of PEDOT:PSS composite film	139
5.7	FE-SEM images of pristine and EB irradiated PANI-Ag films	140
5.8	XPS survey scan of pristine PANI-Ag films	141
5.9	Convoluted XPS for (a) N1s, (b) Cl2p of PANI-Ag films pre and post EB irradiation	142
5.10	FTIR spectra of (a) APTMS treated BOPET substrate and pristine as well as EB irradiated PANI-Ag films, (b) characteristic conductive band showing shift from 1264 cm ⁻¹ to 1250 cm ⁻¹ after irradiation up to 30 kGy	144
5.11	Photoluminescence spectra of pristine and EB irradiated PANI-Ag films	146
5.12	UV-Visible spectra of pristine and EB irradiated PANI-Ag films	148
5.13	Actual photographs of PANI-Ag film on APTMS treated BOPET after solubility test: (a) pristine, (b) 10 kGy, (c) 30 kGy, (d) 50 kGy, (e) 75 kGy, (f) 100 kGy	149
5.14	Change in solubility of PANI-Ag film in DMSO with electron beam dose as compared to pristine film	150
5.15	(a) <i>I-V</i> characteristics of pristine and EB irradiated PANI-Ag film (b) electrical conductivity as function of dose	151
5.16	(a) Response curve of pristine and irradiated with 75 kGy EB dose PANI-Ag film at various H ₂ S concentration, (b) response of pristine and irradiated PANI-Ag film towards various H ₂ S concentrations	154
5.17	XPS survey spectra of pristine PEDOT:PSS films	156

5.18	Convolutd XPS for S2p of PEDOT:PSS films pre and post EB irradiation	157
5.19	Static contact angle variations with electron beam dose for PEDOT:PSS films	158
5.20	Actual photographs of PEDOT:PSS film grown on Kapton after solubility test using DMSO as solvent: (a) pristine, (b) 20 kGy, (c) 30 kGy, (d) 50 kGy, (e) 75 kGy	159
5.21	Relative change in solubility of PEDOT:PSS film in DMSO with electron beam dose as compared to pristine	160
5.22	(a) <i>I-V</i> plot of pristine and EB treated PEDOT:PSS films, (b) electrical conductivity of PEDOT:PSS films as function of dose	161
5.23	Electrical conductivity and H ₂ S response of flexible PANI-Ag films as function of EB dose	163
6.1	Schematic summarizing the outcomes of the present research work	169

List of Tables

Table No.	Table caption	Page No.
3.1	Chemical composition of the pristine and irradiated BOPET surface determined from the analysis of XPS data	96
5.1	N ⁺ /N ratio of pristine and electron beam irradiated PANI-Ag film based up on XPS	143
5.2	FTIR band intensity ratio of pristine and EB irradiated PANI-Ag films	145
5.3	Area ratio of sulphonate group (S2p) of PSS and thiophene group (S2p) of PEDOT in pristine and EB irradiated PEDOT:PSS film samples	157

CHAPTER-1

INTRODUCTION

In this chapter we begin by providing a brief overview about radiation and sources of electron beam. The interaction of electron beam with organic materials, such as insulating polymers, molecular semiconductors and conducting polymers, is known to modify their physico-chemical properties and in many cases such modified materials are being used for various societal applications including bio-medical, textile, environment protection, electronics, radiation dosimetry and sensors. The energetic electrons on interaction with organic materials create free radicals that lead to modifications in material through various mechanisms such as, cross-linking, scissioning, curing and grafting. These mechanisms will be discussed in this chapter in details for organic polymers and molecular semiconductors. One of the major device applications of organic material namely conducting polymer and molecular semiconductor is as chemiresistive gas sensor which is presented in this chapter. The electrical conduction and chemiresistive gas sensing mechanisms of organic molecular semiconductor and conducting polymer have been discussed along with the detailed charge transport mechanisms in these materials. The state-of-art activity in the present domain has also been discussed based upon detailed literature survey. The chapter is concluded by bringing out the major objective of the thesis work and the outcomes along with the structure of the thesis.

1.1 An overview of organic devices

During the past few decades, organic materials owing to their interesting electrical and optical properties have attracted a strong focus by many research groups world-wide. Their low cost, flexibility along with amenability towards doping has made them most suitable candidates for futuristic smart electronic devices [1 – 4]. Moreover, organic molecules are potential candidates for extending the present scaling limits of the existing silicon-based microelectronics to nanoscale [5 – 7]. Typical advantages that can be realized by using organic molecules in case of the nanoscale devices are: (i) small sizes (typically 0.5 to 2.5 nm); (ii) easy tuning of electronic properties through modification in the chemical structure of the molecule; and (iii) possibility of forming self-assembled monolayer on various substrates (e.g. thiols on Au, silanes on Si). In recent years, various nanoelectronics molecular devices, such as, rectifiers, memory-chips, resonant tunnel diodes and transistors have been established with two-dimensional ordered molecular monolayers and multilayers [8 - 14]. Similarly, thin and thick films of various organic semiconductors are being investigated for their applicability in new electronics applications such as flexible and low-cost large-area electronics which is difficult to be accomplished through inorganic semiconductors as well as for having better understanding of the physics behind the charge transport. Due to many developments in this field, the researchers have become capable to manage the material properties at the molecular scale [15]. Moreover, many efforts are being made in the industrial development of the organic electronic devices. Many applications of organic semiconductors have been demonstrated and some of them have already created their place commercially. These include: mobile phones display based on organic field effect transistor (OFET) by Philips and Polymer Vision, automobile stereo display from Pioneer, organic light emitting devices (OLEDs) from Philips and full color displays in Kodak digital cameras. On the development of organic electronics, Forrest has commented: “*If the field*

continues to progress at its current rapid pace, electronics based on organic thin-films materials will soon become a mainstay of our technological existence” [16]. However, despite of these developments, organic devices have limitations in terms of their low charge carrier mobility ($0.001 - 10 \text{ V.s/cm}^2$), which is several orders of magnitude lower than that in traditional inorganic semiconductors (e.g. Silicon 1400 V.s/cm^2) [17, 18]. In order to improve the performance of organic devices, the mobility needs to be increased significantly.

For the past two-decades, the basic research has been focused mainly on the organic films of small molecules (such as metal phthalocyanines, pentacene, etc.) along with many conducting polymers like polypyrrole, polyaniline, poly(3-hexylthiophene) etc. Use of such organic films can be extended to many areas like flexible / bendable displays for electronic paper and flexible computers, human-machine interfaces, electronic artificial skin, gas sensors, radiation dosimeters, field effect transistors, solar cells, photo detectors and radio frequency identification (RFID) tags [19 - 22]. Along with these potential applications, organic electronic devices are also currently being investigated for their electro-mechanical and long-term stability under ambient conditions. In many applications, it is expected that the electronic devices should remain stable under high radiation environment. However, the effect of high radiation environment on organic electronic devices is still not well-understood. On the other hand, radiations are often employed for modification of the physico-chemical properties of the materials to cater different societal and research applications [23 - 25]. In order to create significant changes in the physico-chemical properties of organic materials, the energy of the incident radiation should be higher than their ionization potential (typically $10 - 15 \text{ eV}$) [26]. There are various sources of such high energy radiations such as gamma rays, electron beam etc. However, the electron beam that is generated by the accelerators has more public acceptability and outweighs conventional gamma ray sources. Therefore, the present thesis has been focused to investigate the electron beam irradiation

induced modifications of electrical and mechanical parameters for all the three important categories of organic films; materials selected for these three categories are: bi-axially oriented polyethyleneterephthalate (insulating); zinc phthalocyanine(semi-conducting); doped polyaniline and doped poly (3,4-ethylenedioxythiophene) (conducting). Such electron-beam modified films have also been investigated for their suitability in device applications as gas sensors and radiation dosimeters.

1.2 Introduction to radiation and its sources

High energy radiations are used for bringing out the desired modifications in the physico-chemical properties of the organic materials depending upon their use in various societal applications. These high energy beams can be obtained from various radiation sources that can be broadly classified into three types:

- (i) Positively charged particles, e.g. proton beam, alpha particles and heavy ions
- (ii) Neutral particles, e.g. gamma rays, x-rays and neutrons
- (iii) Negatively charged particles, e.g. electron beam and beta particles.

Among these, positively charged particles and neutrons are not suitable for the modification of materials properties because of their very small penetration depth in the bulk of materials and possibility of induced radioactivity that depends upon atomic number of the interacting nuclei. However, heavy ion irradiation does find highly specialized applications like ion implantation in semiconductors in electronic industry. On the other hand, gamma and electron-beam (limited up to 10 MeV) pose relatively less risk of induced radioactivity and therefore they often commercially employed for radiation processing of materials [27]. The electron-beam irradiation has more public acceptability and it outweighs over gamma ray irradiation due to the following reasons:

- (i) The throughput for electron-beam is around $10^3 - 10^7$ Gy/h which remains constant as a function of time; whereas for gamma irradiation throughput is lower by three orders in

magnitude (i.e. $1 - 10^4$ Gy/h) and it also decrease with time as activity decays with time.

- (ii) The irradiation thickness is typically 35 mm (for unit density material of unit density) in case of 10 MeV electron-beam, whereas the same for gamma source (Co-60) is around 330 mm and hence the electron beam is very much suitable for the treatment of moderately thick materials like polymer films, pipes, insulated wires, liquids, etc [28]. However, the modification in case of thick materials is achieved by irradiating samples with electron beam from both sides.
- (iii) Electron-beam is produced from the accelerators that are fully controlled systems and therefore electron beam irradiation is a well controlled process. On the other hand, gamma rays are obtained from radioactive source, which demands special requirements for their storage transportation and disposal.

When energetic electrons are impinged onto organic materials, their energy is absorbed by the materials and active species (such as radicals) are created, which in turn, initiate various chemical reactions. The amount of radiation energy absorbed per unit mass is known as radiation dose (D) and is measured in joules per kg and its unit is gray (Gy). The quantification of induced chemical changes is referred to as “G values”, known as radiation chemical yield. G value is expressed in terms of the number of molecular events arising per 100 eV of absorbed energy in the medium. D and G are related: $D \text{ (kGy)} = 9.65 \times 10^6 / (G \times \text{mol. wt.})$. Typical G-values for many reactions are in the range of 0.1-10. The relation between D and G clearly explains that higher the molecular weight of compound lower is the amount of dose required for irradiation. This is the reason why most of the industrial applications of electron beam are focused to organic materials which have higher molecular weights in comparison to inorganic compounds [29].

Electron beams that are used for radiation processing have energy ranging from 0.3 – 10 MeV. Electrons having energy less than 0.3 MeV cannot penetrate materials up to noticeable depth and hence are not suitable for industrial applications. The machine which is used to generate energetic electron beam is known as electron accelerator. It consists of two main components: electron-gun and electron accelerating system (under electric field). Electron gun consists of metallic filament (cathode), which on heating to high temperatures (approx. up to 1600°C) ejects electrons from the surface via thermionic emission. These electrons are accelerated under an electric field, which is either generated by producing a potential difference across an insulating column (called direct acceleration method) or by producing relatively smaller electric field repeatedly to get acceleration in bunches (called induction acceleration method). Accelerated electrons then enter into the air from high vacuum field through a thin metallic (usually made of titanium) foil window to be used for irradiation applications. The main accelerator parameters of interest are the electron beam energy, which decides the thickness of the product that can be uniformly irradiated, and the beam current which decides the dose rate. Electron accelerators based on their energy range are classified into following three broad categories: (i) low energy electron accelerators (up to 0.75 MeV); (ii) medium energy electron accelerators (0.75 – 5 MeV); and (iii) high energy electron accelerators (5 – 10 MeV). Brief descriptions of the accelerators, used in present studies, have been given in chapter 2.

1.3 Classification of organic materials

Organic materials can be classified in many ways depending upon their characteristics and various applications. In view of device applications the electrical properties of organic materials are extremely important and thus they can be broadly classified into two categories: insulator and semiconductors. The organic semiconductors are further categorized into two groups as molecular semiconductors and conducting polymers.

1.3.1 Insulators

The organic insulators are basically organic polymers having electrical conductivities of the order less than 10^{-10} S.cm⁻¹. These are being utilized for development of portable, flexible and foldable electronics [30]. The important applications of organic polymer materials include production of insulation panel for electronic appliances as well as substrate for fabrication of flexible devices. Organic insulators can also provide a clean and smooth surface for efficient device operation and besides they being inexpensive serve as potential materials for commercial use. Chemical structure some common organic insulators are shown in Fig. 1.1. Biaxially oriented polyethylene terephthalate (BOPET) and poly(imide) (also called Kapton) are widely used because these are normally inert to the solvent that are used for dissolving polymers. In addition, their thermal properties are suitable for fabricating polymer electronic devices. BOPET is a flexible insulating polymer of great interest due to its application as packaging material for food and medical commodities as well as a substrate for flexible electronic devices. These wide applications of BOPET have become possible due to its physical, electrical and mechanical properties. It is manufactured from molten PET by biaxially orienting it through the process called drawing and then subsequently allowing it to heat-set under tension at the temperature greater than 200°C [31]. The heat setting step prevents the sheet from shrinking back to its original un-stretched shape and locks it in the molecular orientation in sheet plane. The molecular orientation induces the formation of many crystalline nuclei or regions.

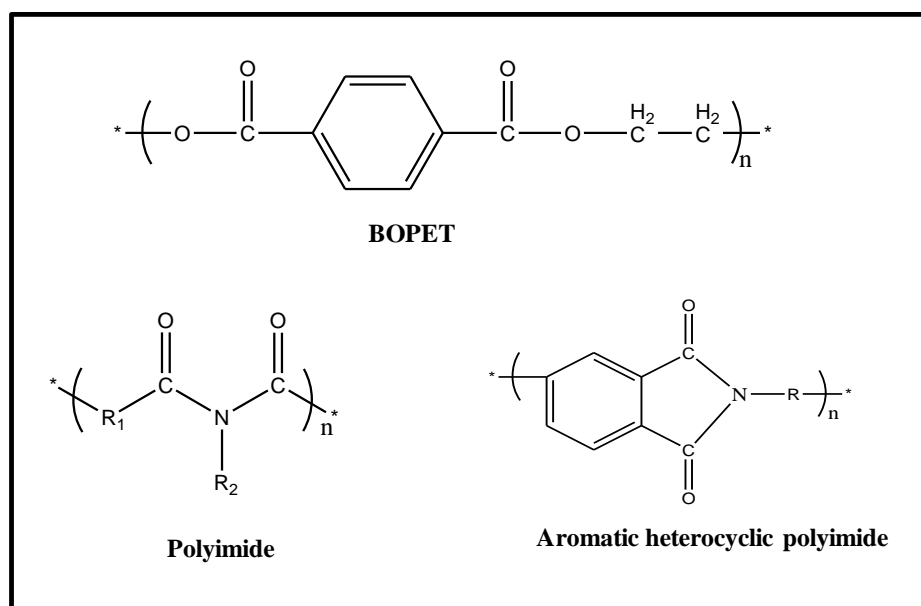


Figure 1.1: Molecular structures of polymeric insulators: biaxially oriented polyethylene terephthalate (BOPET), linear polyimide, aromatic heterocyclic polyimide.

In case of the organic insulating polymers, the hopping of charge carriers from one chain to another chain is responsible for electrical conduction (discussed later in the chapter). Due to irradiation effect, phenomenon called crosslinking is observed in these organic insulators. This crosslinking of polymers causes swelling in molecule and ultimately increases the distance between two chains. As a result, the inter chain hopping of charge carriers is reduced and hence, the insulating properties of organic polymers are improved. Chapter 3 describes in detail about the mechanism behind improvement of insulating properties of organic insulators.

1.3.2 Organic semiconductors

Organic semiconductors can be classified into two major categories: (i) molecular semiconductors having single molecules (polycyclic aromatic compounds, such as, pentacene, rubrene, phthalocyanines etc) and oligomers (short chain comprising few monomers) and (ii) conjugated polymers or conducting polymers: which consist of many monomers bonded together in a long chain such as poly(3-alkylthiophene), poly(p-phenylene

vinylene), polyfluorene etc. The molecular semiconductors have a well defined structure and weight whereas conjugated polymers consist of variable repetition unit and thus, they can have a different molecular mass. However, π -conjugation i.e. the arrangement of carbon atoms in a series of alternating single and double bonds is the common characteristic of both the classes. Also, polymers form disordered phases whereas small molecules show ordered and crystalline structures frequently. These materials exhibit a strong anisotropy in their optical and transport properties perpendicular and parallel to the molecular plane. Molecular semiconductors, in general, have high vapour pressures and are poorly soluble in different solvents. Therefore, the films of molecular semiconductors are usually deposited from the gas phase by sublimation or evaporation techniques. On the other hand, conducting polymers being solution processable can be easily deposited in form of films using cost effective techniques such as spin-coating, photo-polymerization or screen-printing. However, the major advantage of molecular films in comparison to the polymer films is that they can be grown with very high purity and crystalline order both of which are the two major requirements for obtaining high charge carrier mobility.

1.3.2.1 Molecular semiconductors

Some of the typical molecular semiconductors are shown in Fig. 1.2. Semiconducting properties in organic materials is feasible because carbon atoms have the ability to form sp^2 hybridization in which sp^2 orbitals are formed within a plane and the p_z orbitals exist in the perpendicular plane [32]. Basically, in sp^2 hybridization, $2s$ orbital get mixed with only two (out of the three) available $2p$ orbitals. It means that three hybrid sp^2 orbitals are formed leaving the p_z orbital unaltered. For organic molecules, σ bond is formed between two carbon atoms by axial overlapping of the two sp^2 hybrid orbitals. It creates a large energy difference between occupied bonding orbitals and unoccupied anti-bonding orbitals that leads to the insulating properties in the organic molecules. However, the mutual overlapping between the

remaining non-hybridized p_z orbitals of adjacent carbon atoms cause formation of π bonds perpendicular to the plane of sigma bonds. The electrons of overlapping p_z orbitals form a delocalized electronic orbital over the whole conjugation length. These π electrons are delocalized over the whole molecule and are more loosely bound compared to the σ electrons. Therefore, these delocalized electrons become responsible for semiconducting properties of molecular semiconductors. The π -orbitals which are responsible of semiconducting property in case of benzene (C_6H_6) molecule are illustrated in Fig. 1.3.

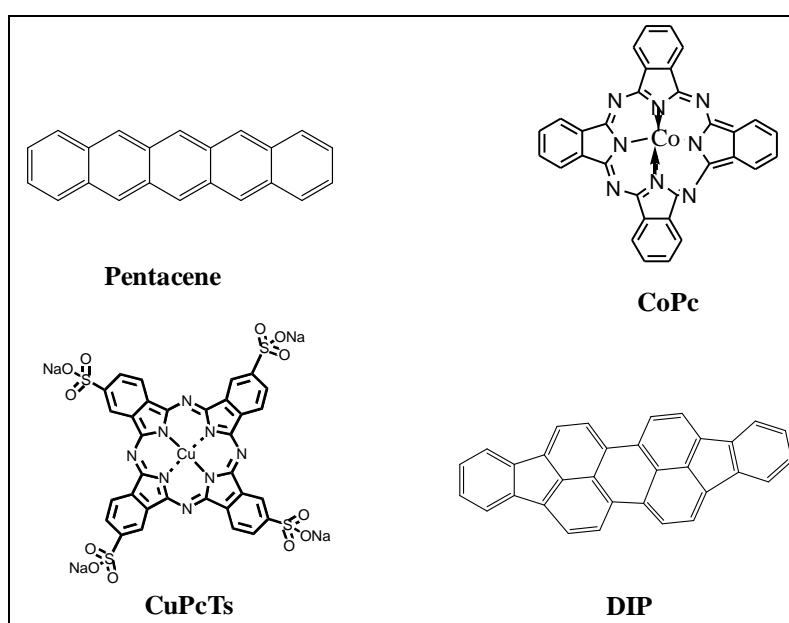


Figure 1.2: Structures of molecular semiconductors: pentacene, CoPc (Cobalt phthalocyanine), CuPcTs (Copper phthalocyanine tetrasulfonate) and DIP (Diindeno(1,2,3,-cd,10,20,30-lm)perylene).

These π molecular orbitals split into a bonding (π) and anti-bonding (π^*) molecular orbitals as shown in Fig. 1.4 (according to Pauli's exclusion principle) due to the interaction among π electrons. The two electrons occupy the highest occupied molecular orbital (HOMO) while the other which remains empty is called lowest unoccupied molecular orbital (LUMO). The extended chain of overlapped p orbitals along with the delocalization of

electrons over the whole molecule results in the further splitting of HOMO and LUMO to cause formation of band (Fig. 1.4).

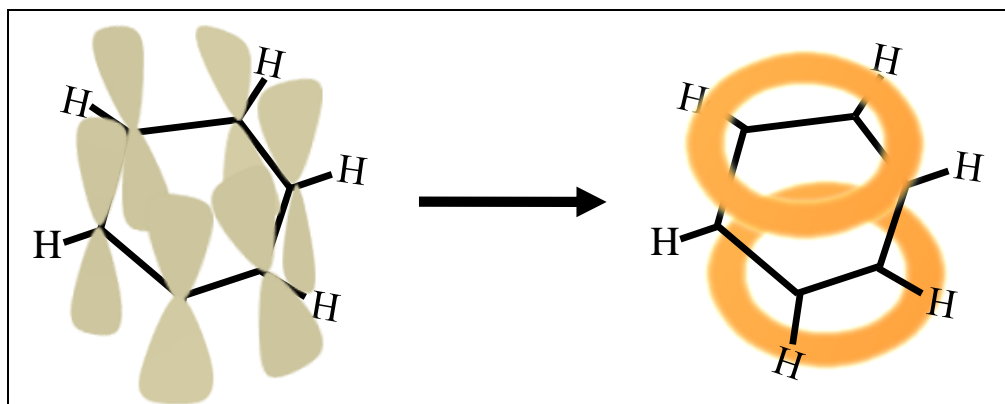


Figure 1.3: Schematic representation of π -orbitals in benzene (C_6H_6) molecule, responsible for its semiconducting property. In case of the solids, the overlap between π -orbitals of adjacent molecules will allow the charge transport.

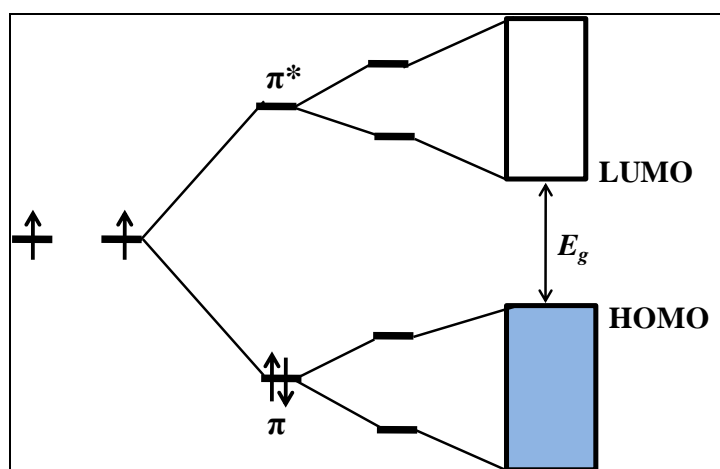


Figure 1.4: Schematic view of the splitting of the energy levels due to the interactions in the π -orbitals of a molecule which results in the formation of HOMO and LUMO energy bands. Molecular interactions in the solid give rise to further splitting of the molecular orbitals.

The HOMO and LUMO for organic semiconductors are analogous to the valence and conduction bands of the conventional inorganic semiconductor. Optical and thermal excitation can promote an electron to an unoccupied level and so the energy band gap for

organic semiconductor corresponds to the gap between HOMO and LUMO of the molecule. The HOMO-LUMO separation in these conjugated molecules depends strongly on the overlapping of neighbouring p orbitals, which in turn related to the planarity of the molecule and side groups. The HOMO-LUMO energy gap is relatively small (~ 1 to 3 eV) and the molecules can be doped to assume n - or p -type character. In this way, the π -conjugated molecules can act as the semiconducting channels in organic molecular devices. However, the band formation is not sufficient for organic molecular material to behave as a semiconductor. There must be a transfer of charge carriers between molecules. This is achieved due to the overlap of the π -orbitals from one molecule to those of its adjacent molecule. Therefore, a close packing of molecule and a crystalline structure free of defects is essential to maximize the π -orbital overlap that improves the conduction properties of the material.

(A) **Metal phthalocyanines:** Among various molecular semiconductors, both the metal and metal free phthalocyanines have been extensively studied because their chemical properties can be easily tuned through variation of the metal centre as well as functionalization of the macrocycle. Moreover, they have not shown any noticeable degradation up to several hundred degrees centigrade of temperatures in air as well as in vacuum. They posse intense colour and are highly economical also in comparison to other materials in this category. The word 'Phthalocyanine' has been derived from the Greek term 'naphtha' (rock oil) and 'cyanine' (dark blue). The first phthalocyanine was produced accidentally in 1907 by Braun and Tcherniac as a minor product in the synthesis of o-cyanobenzamide from phthalamide and acetic anhydride [33]. C. E. Dent *et al* had reported the structure of the planar phthalocyanine molecule for the first time [34]. Phthalocyanines are an intensely blue-green colored macrocyclic compound and traditionally have been used as dyes or pigments. Phthalocyanines form coordination complexes with most of the elements

in the periodic table (especially first row of transition metals) and exhibit semiconducting properties. Therefore, they are currently being explored for their possible applications in the organic electronics. Majority of the research has been focused on the mononuclear phthalocyanines i.e. molecule containing only one metal atom.

Phthalocyanines, both metal and metal free form, are a class of coordination complexes which is composed of a di-anionic macrocyclic ring with a metal centre (MPc) or two central protons (H_2Pc , also called metal free phthalocyanine). Metal phthalocyanines (MPcs) have a general formula $C_{32}H_{16}N_8M$ (M stands for corresponding metals like Co, Cu, Zn etc.) whereas metal-free phthalocyanine (H_2Pc) is represented as $C_{32}H_{18}N_8$. It is chemically designated as 5, 10, 15, 20 tetraazatetrabenzporphyrin or tetrabenzporphyrazin [35]. The structure of MPc molecule is a planar one which consists of four isoindole molecules linked together at the corners of the pyrrole ring by four nitrogen atoms as shown in Fig. 1.5.

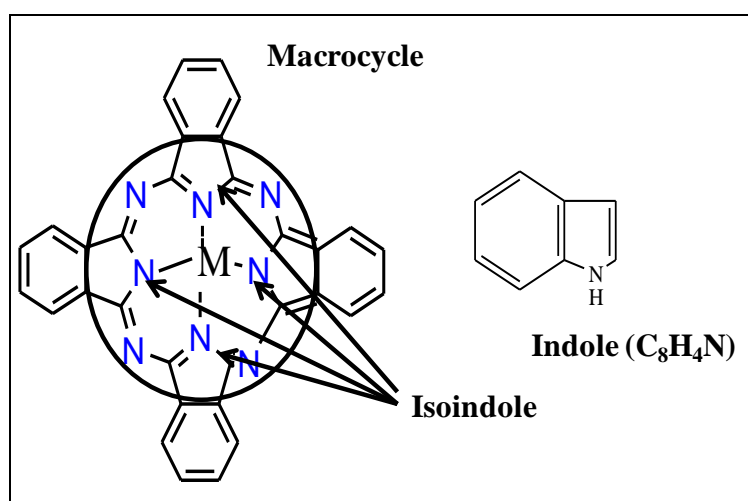


Figure 1.5: Molecular structure of metal phthalocyanines.

In the simple metal phthalocyanines, such as $ZnPc$, the two central nitrogen atoms are coordinately bonded with metal atom (Zn). MPc offer some interesting properties, including:

- (i) Pc's are easily sublimed and can be crystallized with very high purity (10^{14} - 10^{15} traps cm^{-3}) that is rare/ exceptional in organic chemistry.
- (ii) Pc's show an exceptional thermal and chemical stability. MPcs do not show any noticeable degradation up to temperature 400 - 500°C in air whereas in vacuum most of them do not decompose below 900°C. Moreover, they remain unaffected by strong acids or bases [35, 36].
- (iii) Pc's are highly conjugated molecule and contains 18 π electrons in the macrocyclic ring which results in very intense absorption band in visible range (400-700 nm).
- (iv) Pcs are very versatile systems as there are possibilities of tuning their electronic properties (more than one thousand types of Pcs can be synthesized) by manipulating with different side groups and central metal atoms. The replacement of central metal atom and side group, though, modifies their electronic properties but keep their molecular structure unchanged in most of the cases. For example, CuPc is a *p*-type molecular semiconductor but the replacement of sixteen hydrogen atoms by fluorine makes the molecule (F_{16}CuPc) *n*-type semiconductor. In fact, F_{16}CuPc is one of the most stable *n*-type organic semiconductor known at present and it has been used to fabricate the first *n*-channel organic transistor [37] and also in complementary logic circuits [38, 39].

The above important characteristics of metal phthalocyanines have made them a hot topic of research for applications as various organic devices such as solar cells, gas sensors, organic light emitting diodes (OLEDs) and organic field effect transistors (OFETs) [40 - 43]. Phthalocyanines appear in various crystalline forms due to different growth techniques and/or conditions; this is called polymorphism which is purely a consequence of different packing in the unit cells. The most common polymorphs of phthalocyanines are α and β phases as shown in Fig. 1.6. These two phases differ in the tilt angle of the molecular stack from the b-axis,

which is 26.11° for α -phase and 44.81° for β -phase [44 - 46]. Both the phases crystallize in monoclinic structure. The α -form is obtained in thin films when the substrate temperature is maintained below a phase transition temperature during growth [47]. As shown in Fig.1.6, α and β phases are formed by quasi-orthorhombic and monoclinic unit cells respectively [44]. Besides α and β phases, γ , δ , and χ phases have also been observed on rare occasions [45].

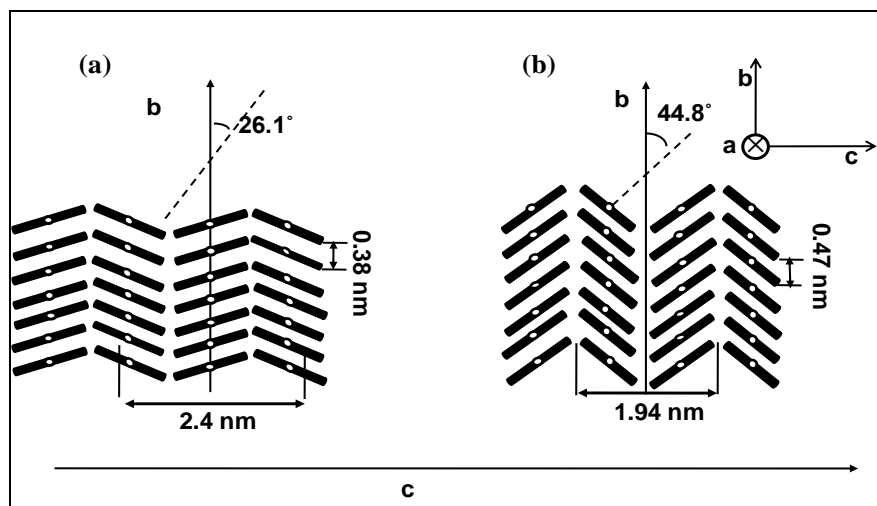


Figure 1.6: Schematics of crystalline (a) α -ZnPc, (b) β -ZnPc.

It has been observed that MPCs are highly electrically insulating in dark or high vacuum environment but majority of MPCs exhibit *p-type* semiconducting characteristics. On exposure to air, improvement in their electrical conductivity is observed [48]. The air induced conductivity in phthalocyanine films has been attributed to different mechanisms. Since in planar MPCs due to strong π - π interactions the molecules are arranged in a compact fashion and therefore, there occurs very less probability to be affected by air. As a result, O_2 gets absorbed only at air/MPC interface and at the grain boundaries.

The formation of charge transfer complexes by coordination of O_2 with MPC metal centres at the air/MPC interface causes formation of MPC^+ and O_2^- charged species and injection of holes as charge carriers into the bulk solid.



The presence of superoxide species has been observed in several electron paramagnetic resonance (EPR) studies [49]. The crystal structure of MPcs generally remain unaffected on exposure to air, therefore, it can be concluded that the reaction occurs through adsorption of O_2 on the surface of the molecule.

1.3.2.2 Conducting polymers

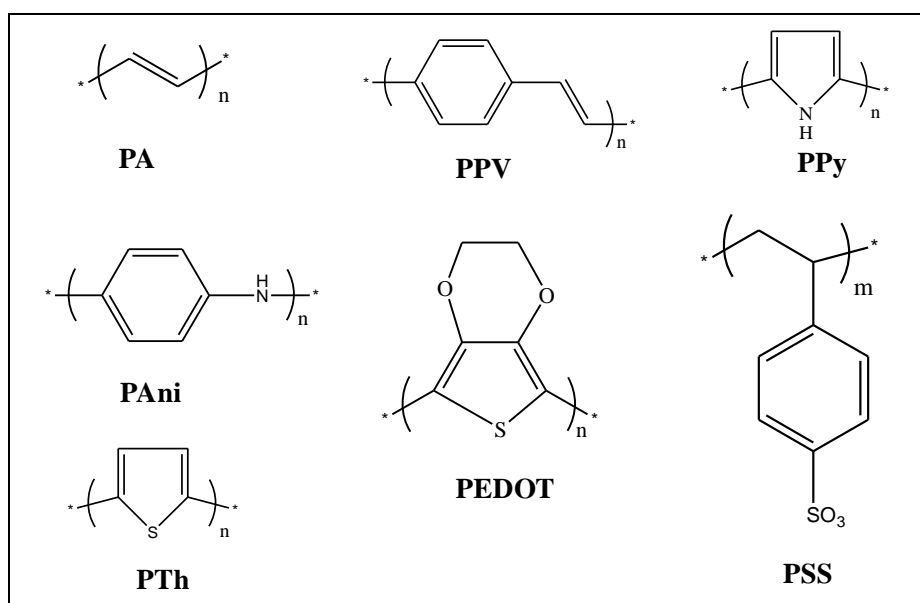


Figure 1.7: Molecular structures of conducting polymers: PA (Polyacetylene), PPV (Poly(phenyl vinylene)), PPy (Polypyrrole), PAni (Polyaniline), PEDOT (Poly(ethylenedioxythiophene)), PTh (Polythiophene) and PSS (Poly(styrenesulphonate)).

Conducting polymers are basically conjugated and these are characterized by repeated units in which atomic valence is not fulfilled by covalent bonds. The remaining valence electrons of adjacent carbon atoms overlap and form double bonds which give rise to π -bonds. These π -electrons are delocalized over large segments of the polymer chain and therefore, are responsible for the electronic properties of the conjugated polymers. Normally polymers consists of around $10^4 - 10^6$ monomers linked together to form a macromolecular

chain while the conjugated polymers include straight chain units. Chemical structures of some commonly known conducting polymers are shown in Fig. 1.7.

However, the bond conjugation alone is not enough to achieve the desired conductivity in the conducting polymers. In order to achieve high conductivity, doping must be done and this can be achieved by redox (or in some case non-redox like in polyaniline) and protonation reactions. However, when an electron is added to or withdrawn from a conducting polymer, a chain deformation takes place around the charge which cost the elastic energy and puts the charge in lower electronic state. The competition between elastic energy and electronic energy determines the size of the lattice deformation and it can be long enough as order of 20 polymer units. The localized charged particle along with the chain deformation is known as polaron. The hopping of polaron governs the charge transport in conducting polymers. Sometimes the charge transport is described by bipolarons which are similar to polarons but having double charge. In bipolaron there are two charges which are bonded together by the same chain deformations.

The variety of conducting polymers can be formed through the addition of heteroatoms (i.e. atoms other than carbon and hydrogen) and side chains. The π -bonding scheme of the conjugated polymers decreases the gap between HOMO and LUMO states. The band gap of the conducting polymers lies in the same range as that of inorganic semiconductors i.e. 1.5 to 3 eV [50].

Various methods that are used for thin film deposition of conducting polymers include Langmuir-Blodgett (LB) technique, electrochemical deposition, spin coating, dip coating and drop casting. In LB technique, thin films can be synthesized with very regular multilayers with a well defined molecular orientation. In electrochemical deposition, a conducting substrate (like indium tin oxide, ITO, or highly doped Si) is required and the film thickness is controlled by the flow of charge through the electrochemical cell during film growth. In spin

coating process, the conducting solution is spread on a rotating substrate and after evaporation of solvent, thin film is formed. Here, thickness can be controlled by controlling the viscosity of solution and rotating rate of substrate. In dip coating, the substrate is dipped into a chemical solution to polymerize through UV or thermal energy. The part of polymer thus gets deposited onto its surface and dipping time controls the film thickness. In drop casting, a polymer solution is drop casted on a substrate and dried, therefore, the films obtained in this case are usually not uniform.

(A) Polyaniline: Among various conducting polymers, polyaniline (PANI) has attracted much attention due to ease of synthesis, tuneable electrical conductivity, biocompatibility and excellent stability under environmental conditions [51, 52]. In addition, it has unique acid base chemistry that is elaborated ahead in details. In a conducting polymer like PANI, the doping can take place without changing in oxidation level of the polymer. PANI is referred as a class of polymers which has the generalized composition with different oxidation states as given in Fig. 1.8. The different oxidation states of the PANI referred as per value of 'y' which can vary from 0 to 1. It can exist in several oxidation states varying from $y = 0$ (completely oxidized pernigraniline base state) to $y = 1$ (completely reduced leucoemeraldine base state). The 'half' oxidized emeraldine base state of polyaniline i.e. ($y = 0.5$) is semiconductor and have alternate sequence of two benzenoid units and one quinoid unit. The emeraldine base of polyaniline can be non-redox doped with acid to yield the conductive emeraldine salt state of polyaniline as shown in Fig. 1.9.

The non-redox doping process differs from redox doping process that it does not involve the addition or removal of electrons from the polymer backbone [53]. The same type of non-redox doping takes place as result of electron beam irradiation.

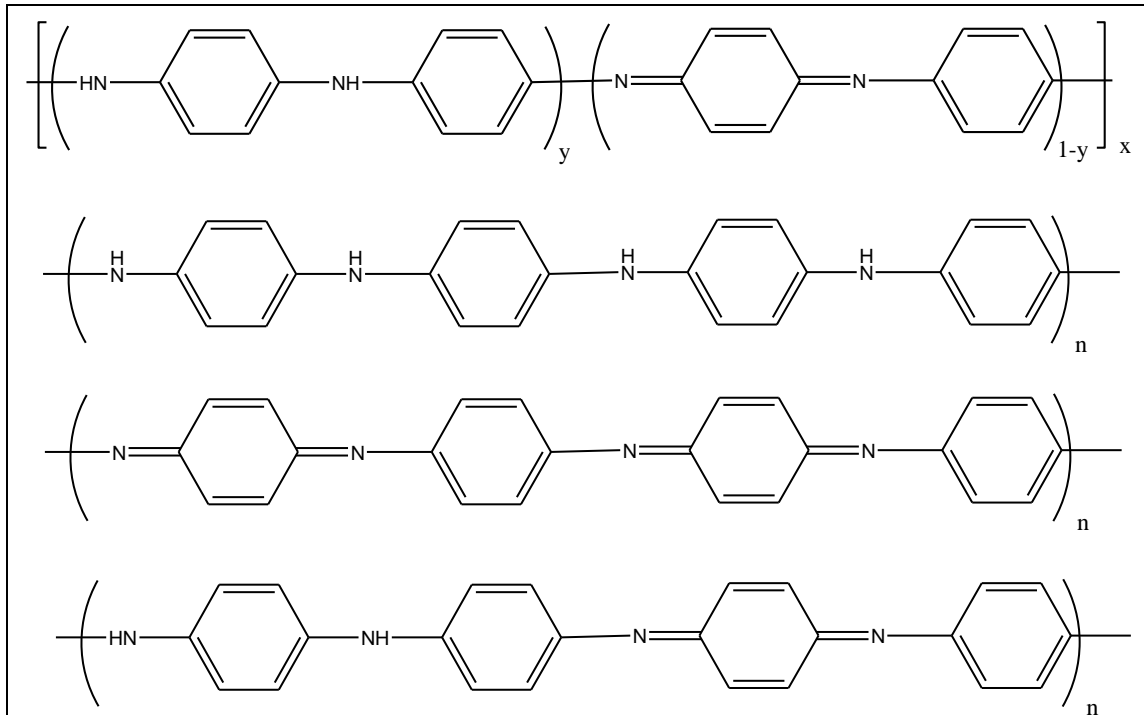


Figure 1.8: Oxidation states of polyaniline.

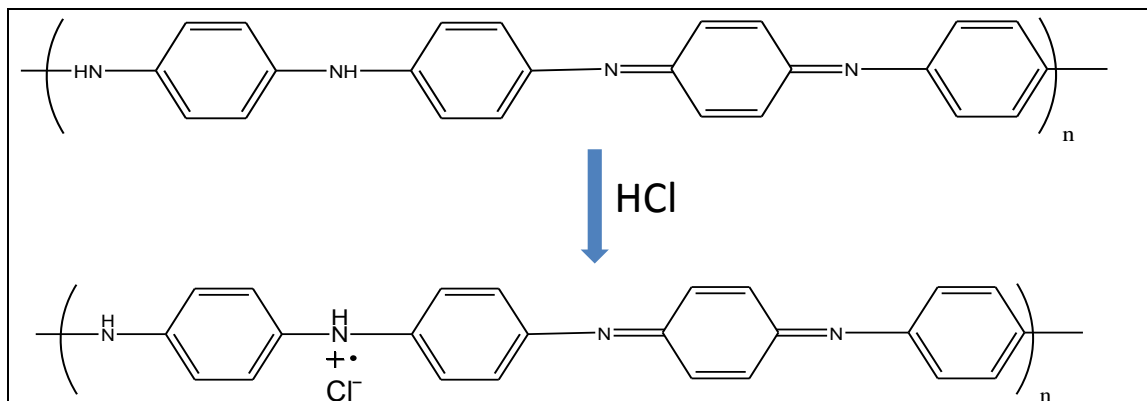


Figure 1.9: Acid doping of emeraldine base polyaniline to emeraldine salt polyaniline.

1.4 Charge transport in organic semiconductors

The mechanism of charge transport in organic materials (semiconductors or insulator) is governed by two processes:

- (i) injection of charge carrier from electrode to organic semiconductor and
- (ii) transportation of charge carriers in the bulk.

The relative position of Fermi level of both the electrode metal & organic material governs the potential barrier at their interface. The typical energy band diagram of metal and organic material, when they are separated, has been given in Fig. 1.10a. The electrode Fermi level (E_F); the semiconductor HOMO (i.e. hole transport level) and LUMO (i.e. electron transport levels); and the vacuum level (E_{vac}) of each material are the critical energy levels. The energy difference between vacuum level and Fermi level for the metal is called work function of the electrode (ϕ_m) and the same between vacuum level and HOMO or LUMO are respectively defined as ionization energy (IE) or electron affinity (EA), respectively, of the semiconductor.

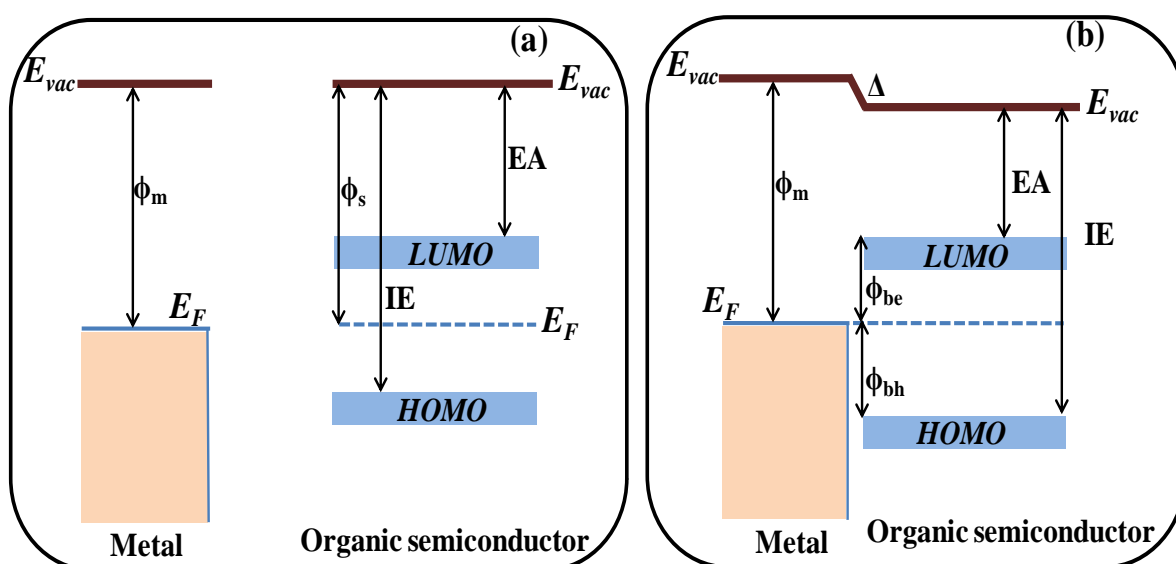


Figure 1.10: (a) Schematic of energy diagram of a typical metal and organic semiconductor with separation, (b) Schematic of energy level alignment at metal/organic semiconductor interface with interface dipole.

When a metal and a semiconductor (organic) are brought together to form an interface, a dipole barrier (Δ) appears because of interface gap states (shown in Fig. 1.10b). There are reasons for creation of gap states like chemical and induced density interface states (IDIS). Chemical reason indicates the formation of chemical bonds or defects between metal

and the semiconductor [54, 55]. The induced density of interface states (IDIS) are generated due to overlap between continuum of metal surface and the semiconductor state which induces a density of states in the gap of semiconductor [56, 57]. As a result, there exists an injection barrier for electron (ϕ_{bn}) and holes (ϕ_{bh}) are generated and thus standard metal semiconductor interface treatment leads to the following equation for the electron injection barrier [58].

$$\phi_{bn} = \phi_m - EA - \Delta \quad (1.2)$$

$$\phi_{bh} = IE - \phi_m + \Delta \quad (1.3)$$

For non-interactive metal-semiconductor interfaces the density of interface states are negligible i.e. $\Delta \approx 0$ and thus the electron and hole barriers are given by $\phi_{bn} = \phi_m - EA$ and $\phi_{bh} = IE - \phi_m$. These types of contacts are known as neutral contacts. However, whether the charge conduction process will be dominated by the electrode or bulk, depends on the value of ϕ_{bn} (or ϕ_{bh}) for electron (or hole) injection and the relative Fermi level positions of metal and semiconductor. Normally an ohmic contact is considered if the metal work function (ϕ_m) is less than the semiconductor work function (ϕ_s) for n-type and vice versa for p-type semiconductor. On the other hand, a Schottky barrier appears when metal work function (ϕ_m) is greater than semiconductor work function (ϕ_s) for n-type semiconductor. In this case the barrier height is given by the value of ϕ_{bn} for electrons. Similar reasoning is also applicable to p-type semiconductors. However, an ohmic contact between metal and semiconductor may be established if ϕ_{bn} or ϕ_{bh} is in the order of few kT. For example, in case of metal phthalocyanine semiconductors usually electrodes were made using Au material due to the fact that Au has a work function of 5.1 eV while phthalocyanine has work function of ~ 4.8 eV. A typical interface of Au and MPc has ϕ_{bh} of 0.3 eV, at room temperature, hence contacts at Au/MPc interface are ohmic in nature.

1.4.1 Films- electrode interface-controlled charge transport

The electrodes in semiconductor is controlled by the electrodes (or charge injection) if the contacts between metal electrodes and organic semiconductors are Schottky in nature. The injection mechanisms that may occur at the metal/semiconductor interfaces depend upon the applied electric bias, temperature and active layer thickness. If the barrier is too thick to allow tunneling of charge carriers from one electrode to other, the current flowing through the semiconductor is limited mainly by the rate at which electrons are thermally excited over the interfacial potential barrier into the semiconductor transport level. In this case current is given by the Richardson thermionic emission [59].

$$J = \frac{4\pi me k^2 T^2}{h^3} \exp\left(-\frac{\phi}{kT}\right) \equiv AT^2 \exp\left(-\frac{\phi}{kT}\right) \quad (1.4)$$

Where A is the Richardson constant ($1.2 \times 10^6 \text{ Am}^{-2}\text{K}^{-2}$) and ϕ is potential barrier independent of applied voltage. But in practice ϕ changes with applied field as the image forces originate due to the polarization of electrode surface by the ejected electrons. Thus current does not saturate, but rather becomes a function of applied field. The current density with modified barrier height is given by Richardson-Schottky equation [60]

$$J = AT^2 \exp\left(-\frac{\phi_0}{kT}\right) \exp\left(\frac{\beta_s F^{1/2}}{kT}\right) \quad (1.5)$$

1.4.2 Bulk limited charge transport

The charge transport is governed by the bulk of the semiconductor if the ohmic type metal/organic interface is present. Various charge transport mechanisms can operate in the films depending on the bias, temperature and nature of the traps. These mechanisms are explained in the following sections.

1.4.2.1 Ohmic conduction

Ohmic conduction takes place if the injected charge carriers are very less as compared to the thermally generated carriers. Since in low bias region, the injected charge carriers are

negligible and therefore charge carriers will drift from one electrode to the other due to the applied electric field. Under such conditions, the current density, which is linearly proportional to the applied bias, is given by Eq. 1.6.

$$J = n_0 e \mu V/L \quad (1.6)$$

Where n_0 is the free charge carrier density and μ is the mobility of charge carrier.

1.4.2.2 Space charge limited conduction (SCLC)

In the higher bias region, the free charge carriers, that are injected from electrode, exceed than the number of thermally generated carriers. These injected carriers start piling up in the vicinity of injecting electrode leading to create a space charge which influence the conduction processes in the semiconductor. In space charge limited condition (SCLC), the J - V characteristics depend on the applied bias, temperature as well as the nature and density of traps in the semiconductor. Now SCLC has been briefed in two cases: (i) trap free organic semiconductors and (ii) semiconductors with traps.

(A) Charge transport in trap-free organic semiconductor: The perfect intrinsic semiconductor is considered free of traps and has small density of thermally generated free charge carriers (n_0). The J can be written as

$$J = \rho v \quad (1.7)$$

Where ρ is the average charge density and v is the average drift velocity. A semiconductor can hold total charge per unit area, at a particular voltage, depending upon its capacitance ($C = \epsilon/L$; L is the cathode-anode spacing and ϵ is the permittivity of the medium).

The total charge per unit area, Q at a particular voltage V , is given by equation 1.8.

$$Q = \rho L = CV \approx \epsilon V/L \quad (1.8)$$

Assuming that the charges are injected from the ohmic contacts i.e. current is not injection limited and combining Eq. 1.7 and 1.8 resulted as

$$J \approx \epsilon v V / L^2 \quad (1.9)$$

When strength of field is low, the average drift velocity is proportional to the average applied field (E) and given by

$$v = \mu E \approx \mu V / L$$

where μ is the free electron drift velocity. Substituting for v into Eq. 1.9 gives

$$J \approx \epsilon \mu V^2 / L^3 \quad (1.10)$$

The more rigorous result can be derived by solving current equation and Poisson equation that leads to

$$J \approx \frac{9\epsilon \mu V^2}{8L^3} \quad (1.11)$$

It is known as Mott- Gurney law describing current-voltage relation in a trap free insulator. In this mathematical expression, current density varies with square of voltage and by knowing the value of permittivity, mobility can be evaluated from slope of J - V^2 plot. But in case that density of thermal free carriers (n_0) cannot be neglected in the semiconductor and hence this expression is not valid. In such cases, Ohm's law is valid at low voltages and with the increase in voltage the density of injected carrier (n_i) increases and finally, at a particular voltage, becomes comparable to thermal free carriers (n_0). Thus, the crossover from Ohm's law (Eq. 1.6) to trap-free square law (Eq. 1.11) is observed. The crossover voltage can be derived as:

$$V_X = \frac{9en_0L^2}{8\epsilon}$$

At this particular voltage, the transit time of electron and dielectric relaxation time are equal. If the voltage is further raised then the transit time for electron becomes too short for their charge to be relaxed by the thermally generated carriers. Thus, the injected electrons dominate the thermally generated electrons and SCLC condition is satisfied.

(B) Charge transport in organic semiconductors having traps: In the practical samples, the local states are always present in the form of traps which reduce the current at lower injection level by capturing and immobilizing most of the injected charge carrier. On the other hand, the trapped electrons do contribute to the $Q=CV$ relation and the Eq. 1.8 in this case becomes

$$Q = (\rho + \rho_t)L = CV \simeq \varepsilon V/L \quad (1.12)$$

Where, ρ_c is the average trapped charge density. The space charge limited J - V relation can be derived, as trap free case, subjected to the relationship of ρ and ρ_c . The relationship can be derived if the free and trapped carriers are in quasi-thermal equilibrium. The free to total carrier density ratio (Θ) can be defined as

$$\Theta = \frac{n}{n+n_t} = \frac{\rho}{\rho+\rho_t} \quad (1.13)$$

Combining Eq. 1.12 and Eq.1.13 results in

$$Q = (\rho + \rho_t)L = \rho L/\Theta \simeq \varepsilon V/L \quad (1.14)$$

Substituting ρ , Eq. 1.7 becomes

$$J \simeq \Theta \varepsilon \mu \frac{V^2}{L^3} \quad (1.15)$$

For the trap-free case, the correct analytically derived result has the numerical factor 9/8. It is evident from the Eq. 1.15 that SCL J - V characteristics should not be necessarily proportional to the square of the voltage but also depends on the voltage dependent Θ . In other word the shape of the SCL current-voltage characteristic depends on the position of the quasi-Fermi level (voltage dependent) with respect to energies of the distribution of traps.

1.4.3 Hopping conduction

In inorganic semiconductors, the charge conduction is realized through free wave-like propagation of charge carriers in well-known conduction or valance bands and those energy bands extend continuously in the bulk. This is possible because the atoms are strongly

bonded together by covalent bond with well long range ordered configurations. Oppositely in case of molecular semiconductors, the constituting molecules are bond together with weak vander Waals force and so the convention of band formation is not very true. In these materials, band widths are typically smaller than kT and charges are intrinsically localized due to the weak wave function overlap between two adjacent molecules [61, 62]. Thus, the facile propagation of charge carriers in analogy to inorganic semiconductors no longer remains valid and therefore, the charge conduction mechanism in organic semiconductors cannot be same as that observed in crystalline inorganic semiconductors. Basically, it is a rate-limiting process where in each step charge carriers need to overcome an activated energy barrier and the mobility is given by Arrhenius relation

$$\mu \propto \exp(-\Delta E/kT) \tag{1.16}$$

where ΔE is the activation energy.

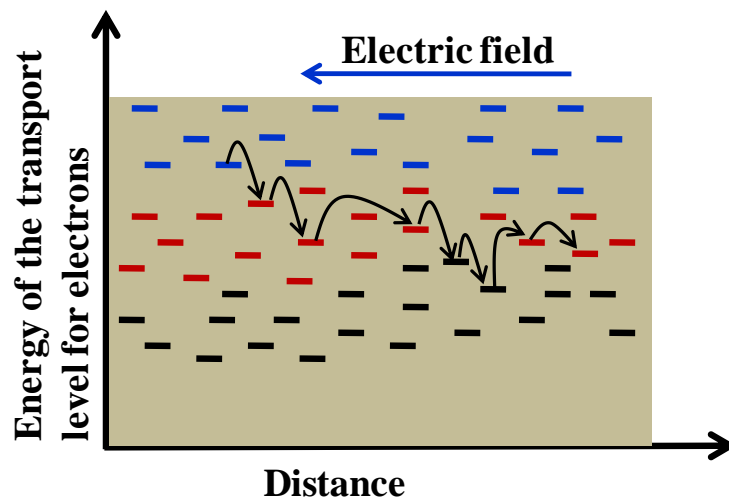


Figure 1.11: Schematic of hopping transport in the organic semiconductor.

The schematic representation of charge hopping transport in the organic semiconductor is shown in Fig. 1.11. It implies that as a result of applied electric field, the charge carrier will hop from one localized state to another localized state. It is a thermally activated process and a dominant transport mechanism in organic semiconductors. Thus, the mobility or the conductivity of (disordered) molecular semiconductor increases exponentially

with temperature, contrasting the inorganic semiconductor. The hopping process involves thermionic emission (called phonon-assisted hopping) or direct tunneling of carriers between localized states. Phonon assisted hopping occurs if the carriers that are trapped in localized states, absorb a phonon and classically jump to the next localized state. But the tunnelling can only take place between two localized states if the electronic wave functions of the two localized states effectively overlap.

1.5 Basic processes of interaction of radiation with organic materials

When energetic electron-beam is impinged on the organic materials, the energy of electron beam gets dissipated in the material, which causes occurrence of various processes. The temporal processes of electron beam interaction with organic molecules can be divided in three phases as shown in Fig. 1.12 on time scale [63].

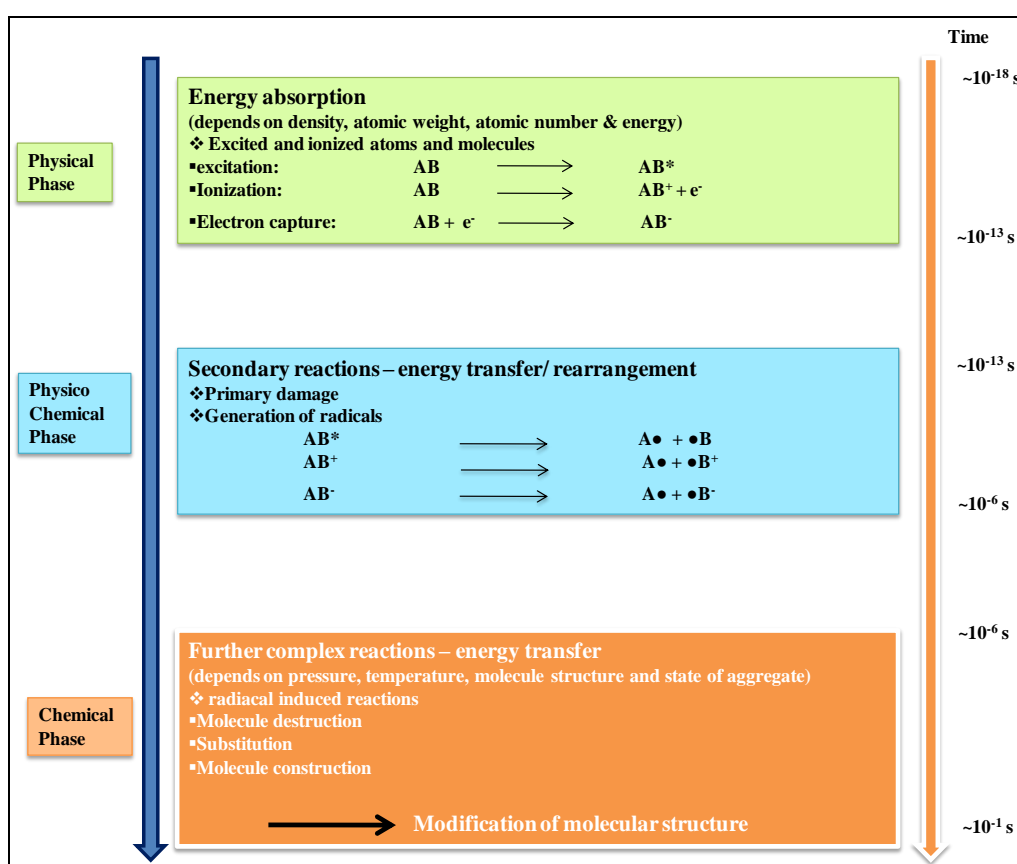


Figure 1.12: Temporal phases for interaction of organic molecule with electron beam.

1.5.1 Physical phase

This is the initial phenomena of interaction of e-beam with organic materials, known as physical phase, and concludes in less than 10^{-13} s after electron beam is exposed. The electric charge that appears in a material which is subjected to electron beam is observable. This is the result of the extraction of electrons from the irradiated molecules due to transfer of sufficient amount of energy by e-beam and positive ions are created. The binding energy of the most labile electrons is called ionization potential which exists in the range of 10–15 eV for polymers and organic molecules. It is also known as the threshold energy for ionization. Since electron-beam generated by accelerators carries high energy, ionization has very high probability. Also it follows that only a fraction of the deposited energy is used in ionization while the remainder causes electronic excitation. Thus, the processes that take place in this phase are collectively called ionization and excitation and can be represented as:

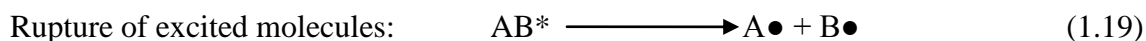


The symbol $\xrightarrow{\sim}$ used to designate radiation induced phenomena, AB an organic molecule, AB^+ a positive ion, e^- an electron, AB^* excited molecules.

1.5.2 Physico-chemical phase

The formation of free radicals in the materials is second stage of basic processes called physico-chemical phase and normally this is finished in 10^{-13} s to 1 μs after trigger of the electron beam radiation. The electrons extracted from the irradiated molecules are subjected to the strong electric field of positive charges (ions) formed. Therefore, charge recombination is a frequent event, both at the time of irradiation and after the end of irradiation, as an after-effect. In this process the ionization potential (10–15 eV) is recovered and this generates highly excited molecules, carrying an amount of energy much larger than

any bond strength. In organic molecules, the molecular bond strength is in the 3-4 eV range. As a result, there is very high probability that such excited molecules will break down into free radicals. Ions also get fragmented into free radicals. In solid polymers, ions and free radicals may remain trapped for a significant amount of time.



where AB^* denotes excited molecules, $A\bullet$ and $B\bullet$ both stands for uncharged fragments (free radicals).

These active species (ions and free radicals) are responsible for the changes observed in organic molecules subjected to electron beam irradiation. In polymers, some transformations are explained as of ions; however, most reactions can be accounted for by conventional free-radical processes.

1.5.3 Chemical phase

The final stage of interaction of e-beam with material is termed as chemical phase in which chemical reactions take place due to the active species generated in the earlier phases. The completion of chemical phase occurs in 1 μ s to 0.1 s after irradiation. This phase results in modification of molecular structure and generates the organic materials having enhanced or degraded characteristics.

1.6 Modifications of organic materials through radiation

Chain reactions are crucial chemical reactions in modification of organic materials as they offer the prospect of relatively large yield of product for a small investment in radiation energy. Accelerated electrons have sufficient energy to break the chemical bonds in organic materials including polymers. The most common result of the cleavage of chemical bonds is the formation of free radicals (and/or ions also). Electron-beam applications take advantage of the many processes that arise from the formation of these radicals because high dose rates

do not allow transient recombination. These radicals as intermediate products initiate chain reactions which result in crosslinking (polymerisation), scissioning, curing and grafting. The chain reaction mechanism confirms that it takes place in four steps: initiation, propagation, termination and chain transfer. In addition the free radicals are also responsible for other reactions including unsaturation, gas evolution, and oxidation [29]. The scheme of interactions of electron beam radiation with organic material is represented in Fig. 1.13. The crosslinking, scissioning, curing and grafting occur in case of polymeric materials whereas mechanism like unsaturation, gas evolution etc are predominantly take place in case of molecular semiconductors.

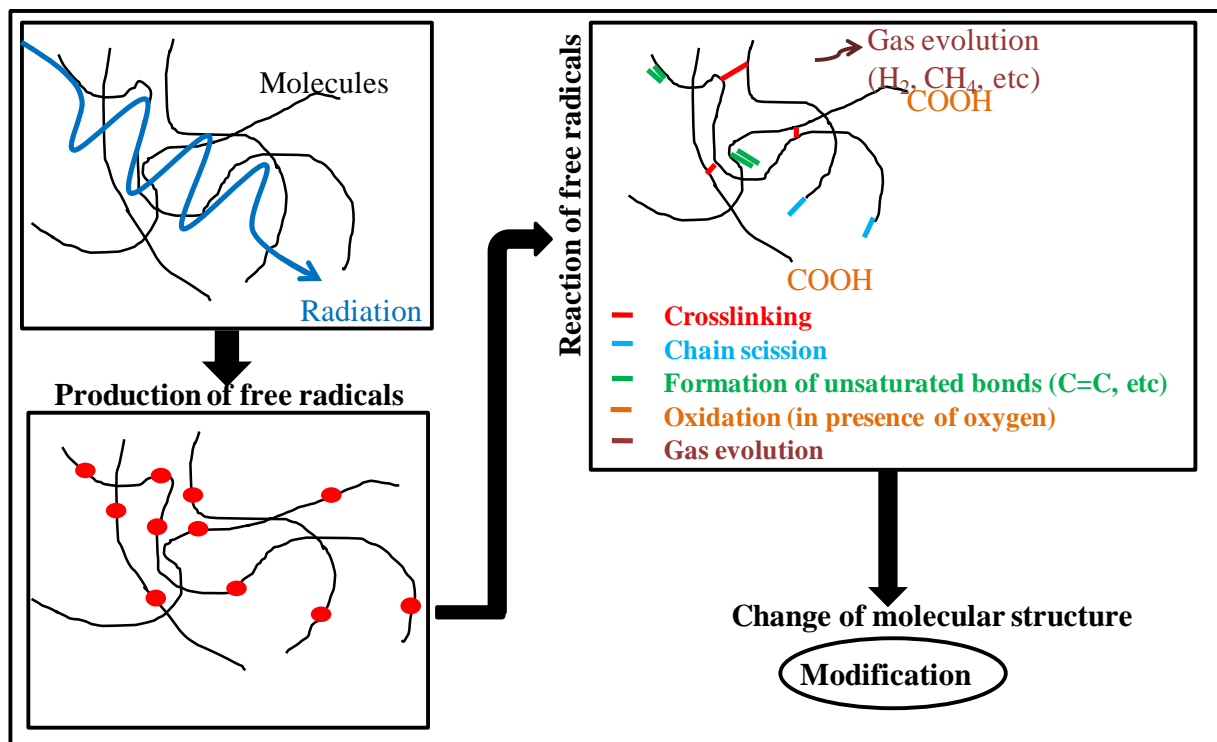
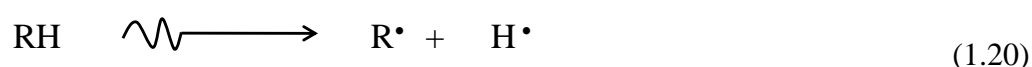


Figure1.13: Schematic representation of interaction of radiation with organic materials.

1.6.1 Crosslinking

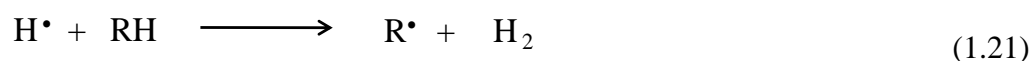
Crosslinking is basically creation of three dimensional network of high molecular weight by covalent linkage among comparatively lower molecular weight polymer chains. The active sites may be free radical centres (atoms with an unpaired electron) or positive ions

(cations, with an electron pair deficiency on a carbon atom) or negative ions (anions, with a nonbonding electron pair on carbon atom). Depending on the intermediates involved, crosslinking is described as radical crosslinking, anionic crosslinking or cationic crosslinking. However, the mechanism is common as chain reaction in any intermediate active species. From several studies it was concluded that, in most cases, radiation-initiated crosslinking or polymerizations follow normal free-radical kinetics. The free radicals that are generated during irradiation readily react with most of the monomers resulting in their polymerization. Radiation initiated polymerisation is temperature independent, hence the process can be carried out at room temperatures with significant rates. Crosslinking is the process which follows reactions in which carbon hydrogen bond is broken by radiation and two polymeric radicals R^\bullet arise. These radicals combine to form an intermolecular bond or cross-link as reaction from (1.20) to (1.22).



where RH is hydrogen containing polymer, R^\bullet a polymer radical and H^\bullet a hydrogen atom.

This step is followed by hydrogen atom abstraction:



The comparison of reactions (1.20) and (1.21) with (1.22) resulted that the formation of one cross-link corresponds to the evolution of one hydrogen molecule. The yield of cross-linking is enhanced in the presence of polyunsaturated compounds, such as polyfunctional vinyl monomers.

1.6.2 Scissioning

Chain scissioning or degradation causes the reduction in the average size (i.e. molecular weight) of the macromolecules present. It is different from the process of depolymerisation in which complete or partial reversion of the polymer to the original monomer takes place because radiation induced degradation normally produces no monomers (or little bit). Main-chain scission involves the break of a chemical bond of the polymeric backbone chain. In linear (unbranched) polymers, the resulting two polymeric radicals are trapped in close vicinity and readily recombine to restore the original structure. However, if the polymer contains side branches (methyl groups) in its monomeric unit, particularly if two branches are attached to the same carbon atom, the two polymeric radicals interact with transfer of a hydrogen atom and formation of a double bond dominated results in scissioning which becomes permanent as illustrated in Fig. 1.14 [26].

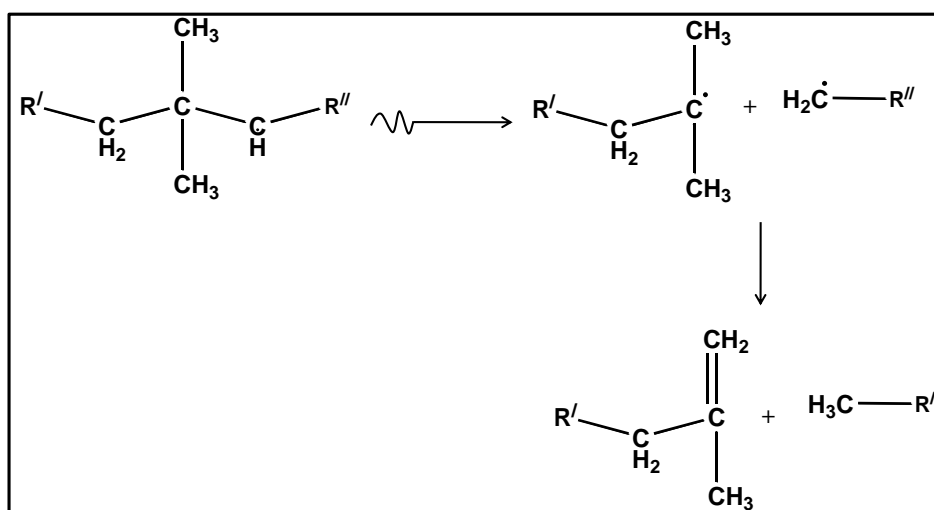


Figure 1.14: Permanent main chain scission in polymers that contain side branches in monomeric unit.

1.6.3 Crosslinking versus main-chain scission

Crosslinking is the most important consequence of polymer irradiation because it can result in improvement of the mechanical, thermal and electrical properties as well as the

chemical, environmental and radiation stabilities of preformed parts and bulk materials. Both polymer crosslinking and degradation by chain scission occur during treatment, but one or the other of these effects may be predominant depending on the material properties, state and chemical structure [64]. Materials with G(S)/G(X) ratio (Here G(S) and G(X) respectively defines the radiation chemical yield of scissioning and cross-linking) below 1.0 are favoured for crosslinking applications. For instance, polyethylene has an attractive ratio because its G(S) values are about half of its G(X) values. Natural rubber also has a very favourable ratio because of its very low G(S) value. Usually G(S) would increase more than G(X) with increasing dose. So, it is possible that upon reaching a certain dose level, crosslinking dominated polymers, e.g. polyethylene or natural rubber latex, will change to be degradation dominated polymers or vice versa. G(X) and G(S) are also dependent on irradiation conditions, such as temperature and atmosphere.

1.6.4 Curing

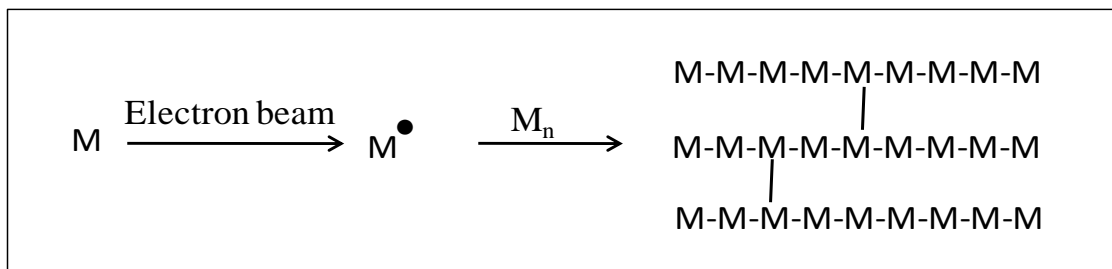


Figure 1.15: Schematic of electron beam induced radiation curing.

Radiation curing is said to occur when a specifically formulated reactive liquid is converted into the solid on a surface through irradiation. This is simply a combination of polymerization and crosslinking of monomers and oligomers by radiation. Major advantages of radiation curing include reduction or elimination of volatile organic compounds (VOCs) and it is a faster process than chemical curing. Electron-beam is the most suitable for radiation curing processes. The schematic of radiation curing is shown in Fig. 1.15. For

curing, the most suitable electron accelerators are those operating in the range of 0.3–0.8 MeV. The penetration of the electron beam has to be high enough to cure the deposited layer lying in depth. In majority of the cases, radiation curing is a free-radical process and it may get affected by the environmental oxygen. Since oxygen has a prominent inhibiting effect, it is desirable to carry out the irradiation process in a chemically inert atmosphere.

1.6.5 Grafting

Graft copolymerization involves two consecutive (or simultaneous) processes in which active sites formed on or near the surface of an existing polymer by irradiation, followed by polymerization of monomer on these sites (Fig. 1.16). Graft copolymerization is normally accompanied by some homo polymerization of the monomer. The important quantity is degree of grafting and it is expressed as the percentage increase in mass of the polymer upon grafting. Graft copolymers can be considered as polymeric alloys. The binding of two polymers by covalent bonds gives rise to an unlimited range of new materials which has created interest in graft copolymers. Electron beam (or radiation) induced grafting can proceed by radical, ionic and mixed radical – ionic mechanisms in a manner similar to block polymerization.

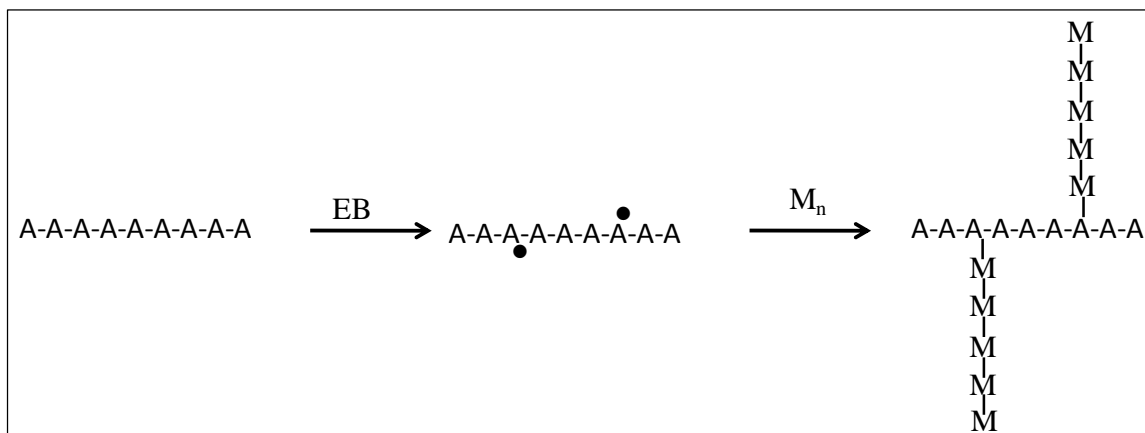


Figure 1.16: Schematic of electron beam induced radiation grafting.

1.6.6 Unsaturation

As is indicated above, double bonds are formed in the interaction of branched free radicals. Moreover, if we compare the radiation chemical yields in polyethylene for hydrogen evolution and for cross-linking (1.21) and (1.22) respectively, it appears that cross-linking only accounts for one-half of the hydrogen produced. In addition, hydrogen is generated in the formation of intra-chain double bonds as:



Double bonds arise with much higher yields in chlorinated polymers, such as polyvinylchloride (PVC), where HCl is formed by a chain process. It may cause severe corrosion on metal parts located in the vicinity of irradiated PVC.

1.6.7 Gas evolution

Gases are generated during all irradiation process of polymers, as in any organic molecule hydrogen can account for a substantial fraction of the gas. The hydrogen formation results from a two-step process. First a carbon-hydrogen bond is broken by radiation followed by hydrogen atom in accordance with reactions (1.20) and (1.21). Also, hydrogen formation would lead to unsaturation reaction shown in (1.23). Carbon monoxide and carbon dioxide arise among the gases that are evolved from polyacrylates and polymethacrylates. Acidic gases such as HCl and HF are generated from halogenated polymers. However, in vitreous or partially crystalline polymers, the gases that are generated by irradiation remain trapped and result in potential cracks or even rupture due to the rise of strains in the irradiated specimen. In this case, a post-irradiation heat treatment also leads to the diffusion of the gases and releases the strain. The released gas causes extra doping in case of organic semiconductors and conducting polymers and hence, results in enhancement in electrical conductivity.

1.7 Applications of electron beam modified organic materials

The electron beam modified organic materials (especially polymers) can be employed in various industrial sectors including biomedical, textile, waste water treatment, electrical, membrane, coatings, rubber goods, tires and wheels, foam, footwear, printing rolls, aerospace and pharmaceutical industries. Electron-beam induced radiation cross linking and curing have been recognized as techniques which result in products with improved properties. Requirement of sterilized plastic medical supplies insists the utilization of electron beam as radiation source for the same application. Medical supplies are irradiated in finished form in air tight bags just prior to shipment. For bio-medical applications, hydrogel are in the forefront because of their bio-compatibility. The hydrogels are polymeric materials having capability to swell in water, i.e. they do not dissolve in water in spite of retaining a momentous fraction of water within themselves [65]. This property originates because of cross linking of polymer, which leads to an increase in the average molecular mass and intrinsic viscosity. Electron beam initiated scissioning in polymer chains favours molecular weight control. Also, some graft copolymers can also be prepared commercially with radiation initiation.

Some organic molecules (or material in large) possess a standard response to radiation and therefore they can be used as radiation detector or dosimeter. Polystyrene calorimeters are widely used as primary dosimeter as it evaluates dose from basic physical quantities. Its response is independent of meteorological parameters and used for calibration of standard dosimeters. Organic crystals as alanine pellet used to measure absorbed dose in material irradiated with electron or photon. The radiation induced free radicals generated from amino acid alanine is responsible for the change in magnetic property and the change which is related to the incident radiation intensity is quantified by electron paramagnetic resonance (EPR) spectroscopy. The dosimeter is in the form of alanine pellets prepared by using α –

alanine, (CH₃-CH(NH₂)-COOH). The suitable radiation energy for good response is ranging from 0.1 MeV to 28 MeV. Since the measurement of the concentration of free radicals by EPR spectroscopy is non-destructive and can be read out repeatedly and hence it can be used for archival (standard reference) purposes. It is useful as transfer dosimetry as well as for calibration of routine dosimeters. Radiochromic film contains a special dye that degrades upon exposure to radiation and causes fading of the film. B3 (GEX make) is a radiochromic film cast from polyvinyl butyral (PVB) resin mixed with the radiochromic dye. The irradiation events activate the dye centres which in turn cause the film to undergo a predictable colour change from clear to deepening shades of pink magenta (which is read at 554 nm wavelength). The radio chemical yield of the dye results in a colour change that is easily related to absorbed dose and it is independent of the dose rate. The cellulose triacetate (CTA) dosimeter is also based up on radiation induced modifications in optical absorption properties of organic molecules near ultra-violet region (read at 280 nm). The dosimeter, in this case, is a film containing cellulose triacetate and plasticizer. These two types of film dosimeters are frequently used as routine dosimeters in electron-beam irradiation facilities because most of the dose requirements lie within their range. Moreover, they map dose both on the surface and within the bulk of materials because they can be used at material-material interface and material-air interface. Ethanol chlorobenzene solution has found good success as reference dosimeter in high dose applications [66].

Chain scission reduces the molecular weight of the macromolecules of a polymer and it has commercial application especially in the field of the retrieval of polymer wastes. This includes electron-beam irradiation of polyisobutylene (butyl rubber), polytetrafluoroethylene (teflon) and cellulose. For instance, electron beam exposure of butyl rubber, under high doses, converts wastes of this polymer into valuable lubricating oils. Teflon is a polymer which remains unaffected by chemical treatments or fire treatments especially under natural

conditions. The wastes of this polymer used to accumulate in teflon production plants [23]. When such a teflon waste is exposed to the electron doses of 100–200 kGy, it degrades into the low-molecular-weight polymer which finds application in sprays or in aqueous suspensions used for coating on various metals for improvement of sliding properties.

1.8 Basic characteristics of chemiresistive gas sensors

The electron beam irradiation effect on the organic molecules and polymers can easily result in tailoring of their physical and chemical properties. The electrical conductivity of the organic materials such as conducting polymer or molecular semiconductor can be easily modified through doping and the doping levels can be easily modified due to interaction with many gases, therefore these organic materials are used as chemiresistive gas sensors. The electrical resistance of a chemiresistive gas sensor changes significantly when it gets exposed to the molecule of analyzing gas. But the increase or decrease in resistance depends upon the nature of the active layer material (p-type or n-type) as well as the kind of analyzing gas (oxidising or reducing). For example, a p-type semiconductor will exhibit the rise in resistance on exposing it to the reducing gases (such as H₂S, NH₃ etc.) while the resistance will reduce if the gas is oxidising (such as NO₂, Cl₂ etc). The response curve of a chemiresistive gas sensor is defined by the following parameters (also shown in Fig. 1.17) [67].

- (i) Sensitivity: It is also called response and defined in percentage. It is the ratio of resistance in air to that gas and mathematically represented by using the relation:

$$\text{Response(\%)} = \frac{|R_g - R_a|}{R_a} \times 100 \quad (1.24)$$

where R_g and R_a stand for the resistance values of the sensor films in test gas and fresh air respectively.

- (ii) Response time: It is the time interval in which sensor resistance attains a 90% of final saturation value after exposing the full-scale concentration of the gas.
- (iii) Recovery time: It is time interval in which sensor resistance reduces to 10% of the saturation value attained for full scale gas concentration after exposing to clean air. For a good sensor the response and recovery time both should be small so that sensor can be used over and over again.
- (iv) Selectivity: It gives the idea that whether the sensor is selective to a particular gas.
- (v) Repeatability: The sensor should give same response for a fixed concentration of particular gas repeatedly. In addition, it should not degrade on continuous operations for long durations.

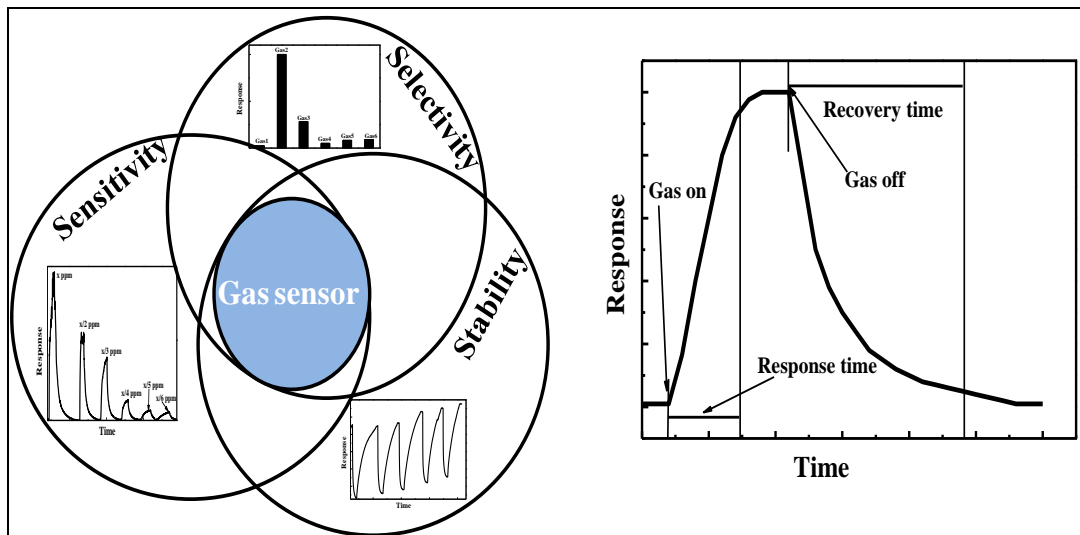


Figure 1.17: Basic requirement and performance parameters of chemiresistive gas sensors.

1.8.1 Gas sensing mechanism in metal phthalocyanines

The electrical charge carriers are introduced by oxygen doping in MPCs and as a surface dopant, oxygen occupies only a fraction of the binding sites on the MPC films. Hence the interaction with analyte vapours in air could result in two different mechanisms of analyte binding as shown in Fig. 1.18 [48]. It has been assumed that the analytes could bind to open

surface metal coordination sites or could compete with oxygen for occupied metal surface sites. There is additional possibility of weak binding (physisorption) to the organic region of the MPc molecule for non-coordinating analytes that may be governed by weak hydrophobic and possibly charge transfer interactions.

When MPc films are exposed to reducing gases, eg H_2S , the charge transfer complexes are formed and electrons are injected causing trapping of charge carriers or lowering in hole concentration which ultimately leads to reduction in current value [68]. The interaction of phthalocyanines with oxidizing gases, such as NO_x , has opposite effect.

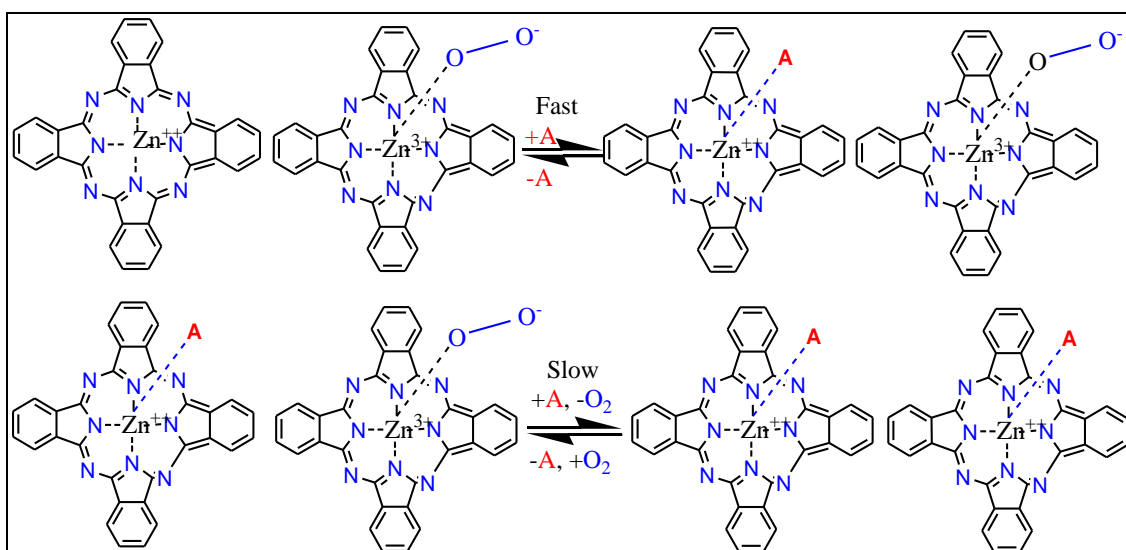


Figure 1.18: Chemisorption model of ZnPc interaction with oxygen and coordinating analytes A.

1.8.2 Gas sensing mechanism in conducting polymers

The mechanism of interaction of the analyte with the conducting polymer (CP) can be explained with following considerations.

(A) **Sensors based on change in doping levels:** The physical properties of conducting polymers highly depends upon their doping levels and the conducting polymers can be doped / dedoped (called primary doping) by using redox reaction or acid base reactions. These reactions lead to transfer of electrons from / to the analyte and can be

achieved chemically or electrochemically. Thus the doping levels of conducting polymers can be easily changed through chemical reactions with many analytes at room temperature which offers a simple technique to detect the analyte.

(B) Sensors based on weak interactions: It has been widely observed that the CPs used as sensor based on Lewis acids and bases detection and the interaction of CPs with neutral molecules such as alcohols or other volatile organic compounds (VOCs) like benzene, toluene etc is not significant [69]. In addition to redox reactions, a partial charge transfer between the analyte and conducting polymer may result in formation of charge transfer complex which leads to change in electrical and optical signal [70]. Also, the charge transfer depends upon the electro-negativity of the analyte and the work function of the conducting polymer [71]. The dipole-dipole interaction or hydrogen bonding may occur between analyte and the nitrogen atoms.

1.9 Literature review on irradiation induced benefits in organic materials

In literature, interesting studies, related to the irradiation effect on the organic molecules and polymers with different types of radiation sources including electron beam, heavy ion beam, gamma rays and UV-rays, have been presented. Organic molecules can easily decompose or polymerize by high energy radiations and it can produce doping effects into the host materials [72]. It has been explained nicely by Yoo *et al*, that electron beam irradiation causes the up shift in LUMO level and down shift in HOMO level of [6, 6]-phenyl-C61-butyric acid methyl ester (PCBM) molecules [73]. The variation in band structure is attributed to the modification in molecular structure of PCBM, as result of e-beam irradiation, which can be tuned with dose. Thus, e-beam irradiation technique can be utilized as a strategy to control the electronic band structures of the organic semiconductors for tailoring their performance. Recently the electron beam effect on organic semiconductor rubrene has been investigated by Kim *et al* and it was found that n-doping occurred along

with change in molecular conjugation system of the crystalline film [74]. This n-doping diminished the charge carrier injection from electrode to HOMO level of rubrene as the HOMO-LUMO energy gap was increased. Also the diversified conjugation systems of irradiated rubrene molecule and the additional traps created, due to e-beam, discourage the intermolecular charge transportation. These ultimately results in lowering down of mobility up to 50% in case of 10 kGy as compared to un-irradiated samples. The electron beam induced tuning of semiconducting properties can be utilized to modify the performance of rubrene based thin film transistors (TFTs) and also to enable its use as highly sensitive radiation dosimeters. Electron beam irradiation has also been used to fabricate patterned rubrene TFT with very good charge mobility $\sim 1.3 \text{ cm}^2\text{V}^{-1}\text{s}^{-1}$ and on/off ratios higher than 10^8 [75]. In present case, the dielectric layer of polystyrene has been modified with electron beam, resulting in crystallization of rubrene. Electrical conductivity modification of copper phthalocyanine (CuPc) thin film with γ -rays, in low dose ranging up to 50 Gy, has been studied by Raval *et al.* The application of CuPc thin film as radiation dosimeter has been demonstrated based up on resistivity and OFET characteristic of the film [76]. In CuPc film p-doping occurred because of chemical transformation in the material when exposed to the radiation, resulted in conductivity increase. Similar observations have been reported in semiconducting oligomer-pentacene thin film, as its resistance falls linearly from 2 G Ω to 0.5 G Ω as γ -rays dose varies from 0 to 100 Gy [77]. This has occurred due to enhanced p-type doping along with formation of energy states in between HOMO and Fermi energy levels which resulted in facile hopping of charge carriers in the organic semiconductors.

The crosslink density and electrical conductivity of polymer-based Bakelite material, used as resistive plate chambers (RPC) detector, have been modified with 8 MeV electron beam and it improves the performance of these RPC detectors [78]. The conductivity enhances from $1.23 \times 10^{-8} \text{ S/m}$ to $50.3 \times 10^{-8} \text{ S/m}$ after delivering 40 kGy e-beam dose and

with further increase of dose it falls to 1.08×10^{-8} S/m in case of 100 kGy. The chain scissioning occurred as dominant phenomena in lower dose regime (up to 40 kGy) followed by crosslinking due to radical reactions in higher dose regime (beyond 40 kGy). The modification in electrical properties and other characteristics of polymers largely depends upon its type and source of radiation as well as dose. Raghu *et al* reported a comparative study on irradiation effect of electron beam and gamma rays on polymer electrolyte film made of polyethylene oxide [79]. The AC conductivity of the polymer electrolyte film has been enhanced, as result of 150 kGy dose, from 8.626×10^{-4} S/m to 1.749×10^{-2} S/m. It is because modification in chemical structure in the form of crosslinking and crystallinity. A large number of dipoles arise in the polymer matrix due to irradiation and it leads to faster ionic transportation through the crosslinked polymer matrix. At the same time the frequency exponent falls to 0.108, in case of 150 kGy irradiated sample, from 0.177 for pristine sample. It indicates that ac conduction mechanism follows the barrier hopping model of charge transport in this polymer film. In addition, it has also concluded that electron beam is more effective tool as compared to gamma irradiation.

1.10 Outline of the thesis

As discussed in previous sections, the organic material based devices are keys for futuristic technologies owing to their low cost, flexibility, chemical & environmental stability and capability to blend with textiles. Moreover, they have found applications in food wraps, radio frequency identification (RFID) tags etc. So far, very little work has been reported to understand the effect of high energy and high intensity electron-beam induced modifications in organic materials and devices. Therefore, the motivation behind current research work is to understand the effect of high energy & high intensity electron-beam induced modifications in organic materials. The thesis has been directed towards investigating the effect of irradiation on electrical and mechanical characteristics of three important types of organic films

(conducting, semiconducting and insulating also elaborated in Fig. 1.19). Feasibility of such radiation modified organic films for device applications such as gas sensors or dosimeters have also been investigated.

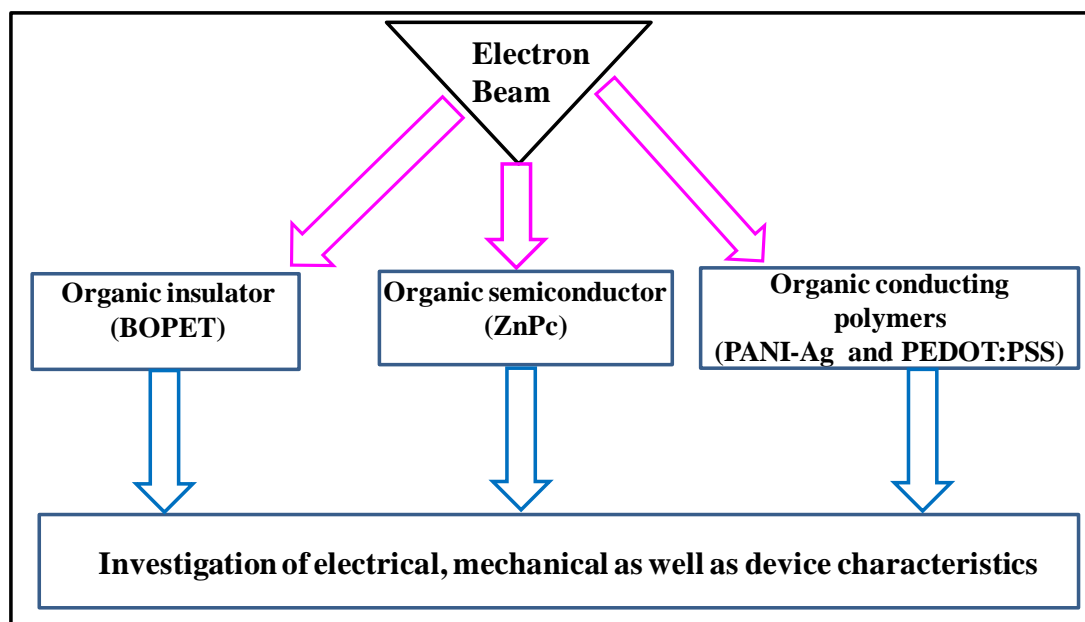


Figure 1.19: Motivation for the research.

The major objectives of this thesis are:

- (i) To understand the different types of interaction processes of electron-beam with the organic materials and find the applications of tailored organic materials in different aspects of life.
- (ii) To study electron-beam induced changes in mechanical as well as electrical properties of flexible organic insulator, bi-axially oriented polyethyleneterephthalate (BOPET). It is generally used as substrate / support for organic devices as well as packaging material for food and medical commodities. Therefore, sustainability of BOPET with high radiation dose has to be investigated to make its use as a packaging material for food and medical products.
- (iii) Investigation on the electrical conductivity modification of organic semiconducting film ZnPc through high energy electron beam and its feasibility to use as radiation

dosimeter. In addition, the variation in gas sensing characteristic of ZnPc as result of electron beam irradiation has also to be examined.

(iv) Analysis on high energy high intensity electron beam stimulated amendment on electrical conductivity and H₂S gas sensing of organic conducting polymer film (PANI-Ag nanocomposite). Also the tailoring in electrical conductivity of commercial organic conducting polymer PEDOT:PSS films, as result of electron beam, has to be probed.

The various experimental techniques used, results, observations and their discussions are organized in the thesis with following chapters.

Chapter2 deals with various experimental techniques used in the thesis work including deposition techniques, electron beam irradiation, mechanical testing techniques, structural and spectroscopic characterization techniques etc. It also describes the experimental methods which have been employed for charge transport and gas sensing studies as well as polymeric characterization.

Chapter3 describes the effect of electron beam on mechanical and electrical properties of organic insulator BOPET in the dose range of 2 - 32 kGy with 10 MeV electron beam. The crosslinking dominance leads to improved mechanical properties (Tensile strength, Young's Modulus etc) and enhanced electrical resistivity of BOPET sheets and such modified properties can have use in many applications such as packaging materials for food, medical product sterilization and electronic industries.

Chapter4 illustrates the electron beam induced modifications in electrical and gas sensing properties of zinc phthalocyanine (ZnPc) thin film (organic semiconductor) prepared on flexible BOPET substrate. The irradiation of ZnPc films were carried out using a 10 MeV electron beam under different radiation dose levels from 1 kGy to 30 kGy. The films exhibit linear enhancement of electrical conductance up to 18 kGy due to increasing content of

adsorbed oxygen and beyond that dose they exhibit saturation. ZnPc films shows excellent response for ppm level of H₂S gas among other gases at room temperature and it decreases monotonically with increasing electron beam dose due to the strong binding of oxygen at the Zn sites. A plausible mechanism of electron-beam induced modification of ZnPc films has also been proposed. Charge transport as well as chemi-resistive gas sensing behavior in such modified ZnPc films along with their use as potential radiation dosimeter has also been presented.

Chapter5 elaborates the electron beam induced amendment on conductivity of organic conducting film polyaniline silver (PANI-Ag) which was synthesized on (3-aminopropyl)trimethoxysilane (APTMS) treated BOPET substrate by in-situ photo polymerization and post deposition doped with HCl. The studies have been done up to dose range of 100 kGy with 10 MeV electron beam and the electrical conductivity of the PANI-Ag films was initially found to be enhanced by two orders of magnitude up to 30 kGy of dose but after that it falls with the increasing dose. The rigorous characterizations of the films suggest that enhanced conductivity up to 30 kGy is due to scissioning as well as additional doping of chlorine in PANI chain as result of electron beam irradiation but at higher dose cross-linking of polymer chains dominates causing the lowering of electrical conductivity. The higher sensitivity of PANI-Ag film towards ppm level of H₂S gas as result of electron beam irradiation has also been explained. Electron beam induced changes in conductivity of commercial conducting polymer PEDOT:PSS film have also been discussed. The conductivity of as deposited polymer film was ~ 3.2 S/cm which consistently falls to ~ 0.76 S/cm after getting 75 kGy with 1 MeV electron beam. Detailed characterizations of the samples suggest that the lowering of electrical conductivity in irradiated sample is attributed to the crosslinking of PEDOT chains and dissociation of PSS.

Chapter6 summarizes the main results that are obtained during the course of research work and the future possibilities that can be realized for device applications through irradiation by electron-beam.

EXPERIMENTAL TECHNIQUES

2.1 Introduction

In this chapter we discuss different techniques utilized to prepare, irradiate and characterize the different organic films. Organic films are prepared using physical vapour deposition and photo polymerization as well as by drop cast method. These films were irradiated with high energy electron beam using accelerators followed by characterization done through many techniques including x-ray photoelectron spectroscopy (XPS), fourier transformation infrared spectroscopy (FTIR), UV-Vis spectroscopy (UV-Vis), x-ray diffraction (XRD), atomic force microscopy (AFM), scanning electron microscopy (SEM), photoluminescence spectroscopy (PL), static contact angle measurements, sol gel analysis etc. The details of the mechanical and electrical characterizations of the films have also been presented.

2.2 Methods of thin film deposition

The details of processes that were used for thin film deposition/growth such as using physical vapor deposition, photo-polymerization and drop casting have been elaborated in this section.

2.2.1 Thermal vapor deposition

Thin film deposition through thermal evaporation is very simple and conventional technique, also called vapor deposition (PVD) method. The schematic of thermal evaporation technique for thin film deposition is shown in Fig. 2.1a along with actual photograph of the system (Fig. 2.1b). We have used a thermal evaporation system from M/s Hind High Vacuum model 12A4T for depositing zinc phthalocyanine (ZnPc) thin films and gold for making contacts. The ZnPc films have been prepared on BOPET substrate by using the process described as follow.

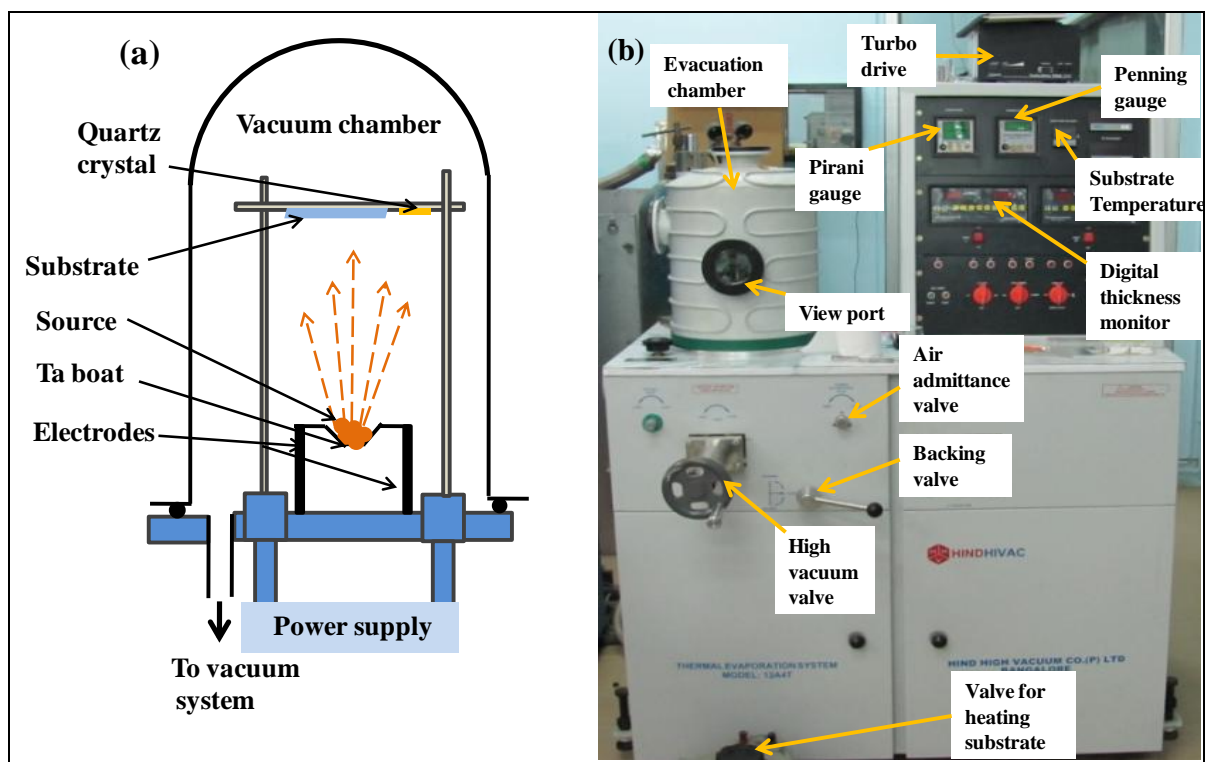


Figure 2.1: (a) Schematic of thermal evaporation method for thin film deposition, (b) actual photograph of physical vapor deposition system used for thin film deposition.

(A) **Substrate preparation:** To prepare the flexible film we have used biaxially oriented polyethylene terephthalate (BOPET) sheets as substrate which was procured from M/s Dupont, having thickness $\sim 100 \mu\text{m}$, and used as received after cleaning. The cleanliness of substrate is very crucial for film's growth as well as for the uniformity and purity of the films. Therefore, the substrates require thorough cleaning before proceeding to next steps. BOPET sheets were cut in desired size and cleaned in ultrasonic bath using methanol as solvents for 10 minutes. The other solvents like trichloroethylene, acetone etc should be avoided because they may roughen the BOPET surface. After ultrasonic cleaning the substrate was removed from solvent and thoroughly dried under the jet flow of dry high purity argon gas.

(B) **Induction of source-substrate into PVD system and deposition:** Now the pre-cleaned substrates were loaded with help of holder in chamber along with source (for

which ZnPc powder was used as procured) kept in tantalum boat. The distance between source and the substrate was about 12 cm. The base pressure of the chamber during the deposition was $\sim 2 \times 10^{-6}$ mbar and it was achieved in two stages. First low pressure $\sim 5 \times 10^{-2}$ mbar (rough vacuum) was achieved with direct driven rotary vacuum pump, model ED-15. After that a turbo molecular pump (M/s LEYBOARD, model TURBOVAC361) was connected to the chamber which was continuously backed up by the rotary pump and the desired base vacuum was realized. The system is comprised with Pirani gauge (for measuring rough pressure up to 1×10^{-3} mbar) and Penning gauge (for measuring high vacuum in the chamber ranging 1×10^{-3} to 1×10^{-7} mbar). High electrical current was passed through the tantalum boat to evaporate the material at a controlled rate which is measured with a Quartz crystal based thickness monitor. The deposition rate was controlled $\sim 1 \text{ \AA/s}$ and as a result, the thickness of ~ 20 nm was achieved for ZnPc films. The film preparation was concluded by keeping the substrate at room temperature (during deposition) followed by in-situ vacuum annealing at 100°C for 15 minutes. For electrical and gas sensing measurements, a few pairs of gold electrodes (thickness ~ 50 nm) of size $3 \text{ mm} \times 3 \text{ mm}$ having separation of $\sim 12 \text{ }\mu\text{m}$, were thermally evaporated on the ZnPc thin film using a metal mask.

2.2.2 Film growth by photo polymerization

In this process, organic films are grown by making the monomers to polymerize under UV photons using some photo-initiators as catalysts and allowing the polymerized material to in-situ deposit on the specific substrates. The process of photo-polymerization for deposition of polyaniline films is described as follow.

(A) Purification of aniline monomers: Aniline (procured from Sigma-Aldrich, purity 98 %) was refrigerated in the dark prior to synthesis. Before using, it was passed through the basic alumina powder (MERCK, size $\sim 63 \text{ }\mu\text{m}$) filled column to remove the impurities. The pure aniline monomers were recovered through distillation method

schematically shown in Fig. 2.2. The recovered aniline monomers were refrigerated to properly in dark to avoid any moisture contamination.

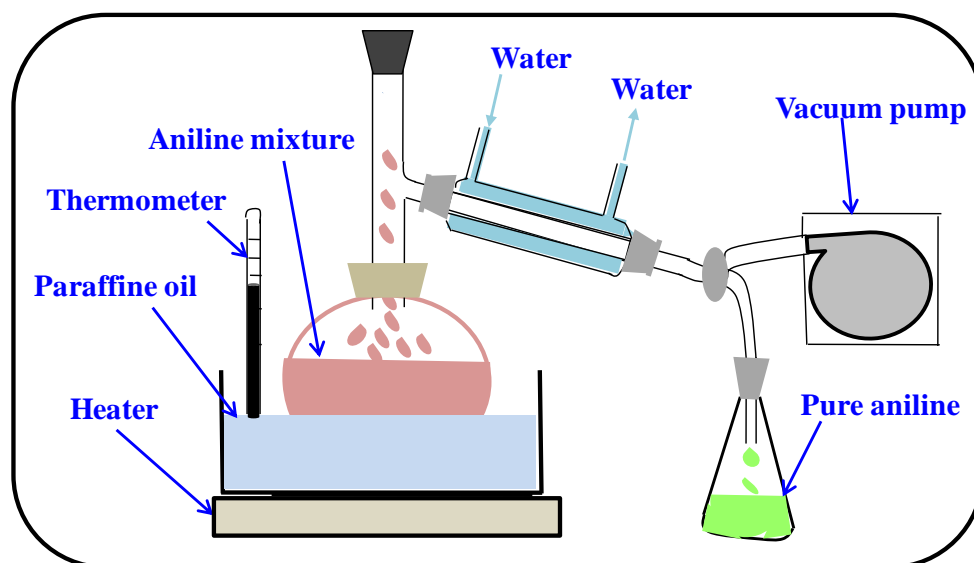


Figure 2.2: Schematic for recovering pure aniline monomers by vacuum distillation method.

(B) Surface modification of BOPET substrate by grafting of APTMS: The surface modification of BOPET sheets were carried out by the APTMS i.e. (3-aminopropyl)trimethoxysilane layer. The organic solvents of analytical grade were used for solution preparation and deionized (DI) water was used for washing. BOPET sheets of thickness $\sim 100 \mu\text{m}$ (procured from DuPont) were cut into size of $30 \text{ mm} \times 20 \text{ mm}$ using steel scissor for the experiments. BOPET substrates were ultrasonically washed with chloroform, and ethanol for 20 min and after that dried for 4 hrs. at 60°C in an oven.

To graft APTMS on BOPET, first the surface of BOPET was hydroxylated by dipping it in the potassium hydroxide (KOH) containing dimethyl sulphoxide (DMSO) solution (160 mg of KOH dissolved in 30 ml of DMSO) with 5 ml DI water. The sheets were left to react with KOH for 30 min., then thoroughly washed in DI water and dried through nitrogen purging. The hydroxylated sheets were then dipped in an APTMS solution containing $112 \mu\text{l}$ APTMS in 25 ml ethanol with 1 ml acetic acid and left to react for 72 hrs. After this the

substrates were thoroughly cleaned using ethanol and dried for 1 hr. at 60°C in an oven. Thus, we prepared APTMS modified BOPET substrate which can provide enhanced adhesion as well as directional growth to the polyaniline films on the substrate.

(C) Preparation of PANI-Ag nanocomposite films on APTMS modified BOPET: Silver nitrate (procured from Sigma-Aldrich, purity ~ 99.9%) was of analytical grade and used as received. The photo-polymerization of aniline on APTMS modified BOPET sheets was done in an air tight glass bottle containing fixed amount of distilled aniline 0.913 ml along with 2M HNO₃ in 10 ml of DI water. HNO₃ is added to aniline 10 min. prior to the photo-polymerization for the protonation of monomer. After protonation of aniline, 3.4 g (2 M) AgNO₃ is added and finally after a uniform mixing, the solution which was obtained after the uniform mixing of both these solutions was placed under a UV lamp (Spectrolinker, XL-1500UV cross linker) for 6 hrs. The UV light has wavelength ~ 365 nm, intensity ~5 mW/cm² and UV source to sample distance was ~13 cm. After UV exposure the samples were thoroughly cleaned with deionized water and ethanol to remove the unreacted monomer species. This washing treatment might have caused partially de-doping of the PANI-Ag films and therefore, the films were subsequently exposed to the HCl vapors for about 3 min. Finally, the samples were dried for 1hr. at 60°C in an oven.

2.2.3 Film growth by drop cast method

Drop-casting is a very simple technique through which polymers that can be dissolved in a solvent are dropped on a substrate. However, films deposited by this method are non-uniform in thickness. We have use this method to deposit thin films of conducting polymer Poly(3,4-ethylenedioxythiophene):poly(styrenesulphonate) (i.e. PEDOT:PSS) which is already available commercially in solution form. PEDOT:PSS solution was procured from M/s Ossila (make-M122 PH1000) and it was subjected to ultrasonication before deposition. For substrates, polyimide sheets (procured from M/s Dupont) were cut into proper size and

cleaned with Helmanex II soap solution and de-ionized (DI) water. Ultrasonic cleaning was also done using chloroform and methanol. After the cleaning of substrates, they were pasted on glass slides to provide flat surface for uniform deposition and PEDOT:PSS solution was drop casted on them. The films were dried in air and annealed at 160°C for 45 min.

2.3 Electron beam irradiation of synthesized samples

Electron-beams generated by electron accelerators having high energy from 0.3 MeV to 10 MeV have been used to irradiate the samples. Electrons having energy less than 0.3 MeV do not penetrate in the material thoroughly, hence, are not suitable for irradiation and processing. On the other hand, the electron-beam having energy greater than 10 MeV will potentially generate neutron activations. Electron accelerators constitutes of two components. One is electron gun (source) and second is electric field for acceleration. Electron gun has cathode which is raised up to sufficiently high temperature (approx. up to 1600°C) to eject electrons from the surface by thermionic emission. Electric field can be produced in different manners, either by producing potential difference across an insulating column (called direct acceleration method) or by producing relatively smaller electric field repeatedly to get acceleration in bunches (called induction acceleration method). Accelerated electrons pass, into the air from high vacuum field, through a thin titanium-foil window for irradiation applications. The path of electron from the point of generation to exit window is maintained under the vacuum of $\sim 1 \times 10^{-6}$ mbar. Thus, the titanium exit window through which the electrons enter in air (to be bombarded on the products/samples) acts as a boundary for vacuum and air. The accelerator parameters of significance are the electron beam energy (which decides the thickness of the product that can be uniformly irradiated) and beam current on which dose rate depends. Electron acceleration can be done through following two ways: (i) direct acceleration method and (ii) induction acceleration method. We have used two types of accelerators for the present irradiation experiments.

2.3.1 10 MeV RF Linac

In this machine 10 MeV electron beam is generated through the oscillating electric fields, established in an electromagnetic cavity structure (called LINAC), which is driven at resonance by a suitable microwave (or RF) power source. The microwave is powered, by a source such as klystron or magnetron, to the LINAC which consists of a series of coupled cavities. The microwave source is operated in pulsed mode, with high voltage pulses provided by a modulator - pulse transformer combination and it supplies output pulses (micro pulses) of certain duration at the modulator repetition frequency. Application of a micro pulses to the LINAC produces a stream of electron pulses (macro pulses) at the frequency of microwave radiation. LINACs are of two types: travelling wave LINAC and standing wave LINAC. In travelling wave electric field travels from one end of accelerator to other, while in later case there is no energy flow along the system and electrons are accelerated as they pass through the pattern of oscillating local electric fields. High energy accelerators come under this category are used for medical product sterilization, radiation treatment of food commodities, cross linking of polymers and enhancement of characteristic of semiconducting diodes & chips. A 10 MeV RF electron LINAC based upon standing wave principle is indigenously developed by Bhabha Atomic Research Centre (BARC) facility at Electron Beam Centre (EBC), Kharghar, Navi Mumbai, India [29]. The schematic of 10 MeV RF Linac is shown in Fig. 2.3.

In this accelerator the resonating frequency is 2856 MHz and it has 10 μ s pulse duration. The Linac generates 100 mA pulsed beam current with pulse repetition frequency of 300 Hz and beam scanning is done over a 1 meter long exit window with scan frequency of 1 Hz, so that desired uniformity of radiation dose can be realized. The accelerated electron beam comes out in air, for product irradiation, through the exit window. This exit window is made of 50 micron thick titanium so that it doesn't attenuate beam significantly and thus it

acts as boundary between air and high vacuum. To avoid any significant temperature changes or thermal damages to the samples, they are kept on a conveyor located just below the exit window (at around 45 cm) and the conveyor has the ability of to and fro motion with sufficient time gaps. The speed of conveyor is fixed as 1 m/min and number of passes is set accordingly to ensure delivery of the requisite dose.

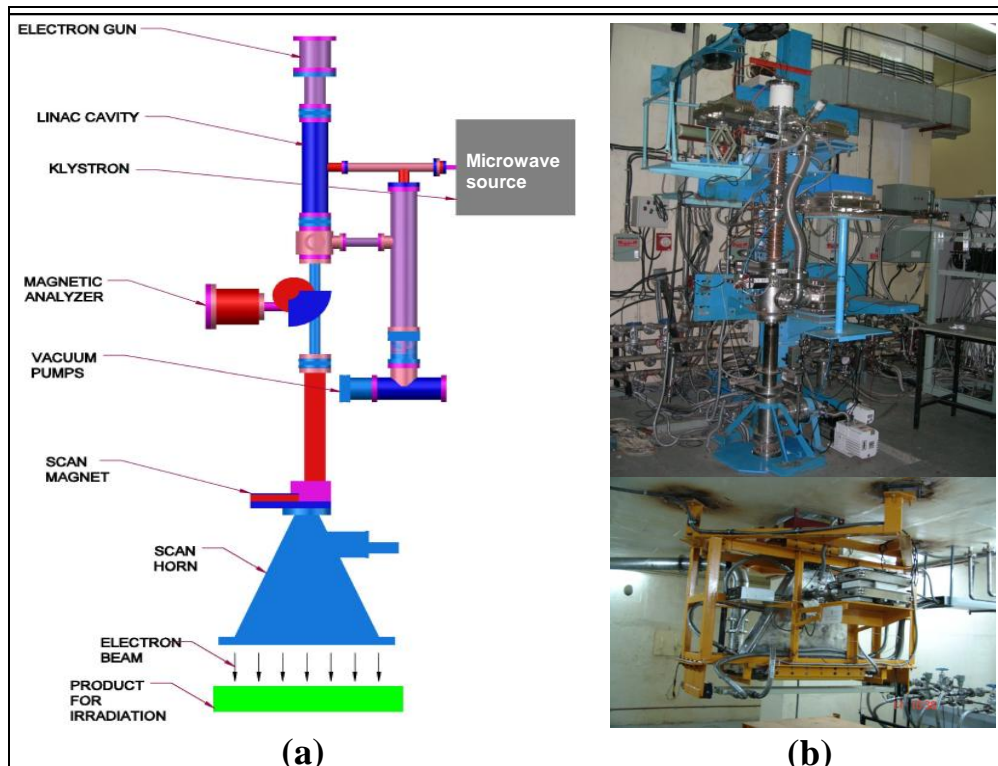


Figure 2.3: 10 MeV RF electron LINAC at EBC, BARC facility at Kharghar Navi Mumbai, India: (a) Schematic representation, (b) its photograph.

2.3.2 1-3 MeV DC accelerator

The basic principle of DC electron accelerator is to charge a large number of condensers connected in parallel and to discharge them in series when the voltage across them is equal to the sum of the voltages on the individual condensers. Thus it is a cascade generator which consists of identical stages containing capacitors and diodes and each stage is a voltage doubling circuit. There is a 1-3 MeV DC electron accelerator indigenously developed by BARC, situated in BARC facility at Electron Beam Centre (EBC) [29]. It

works on the philosophy of dynamitron acceleration and schematically represented in Fig. 2.4.

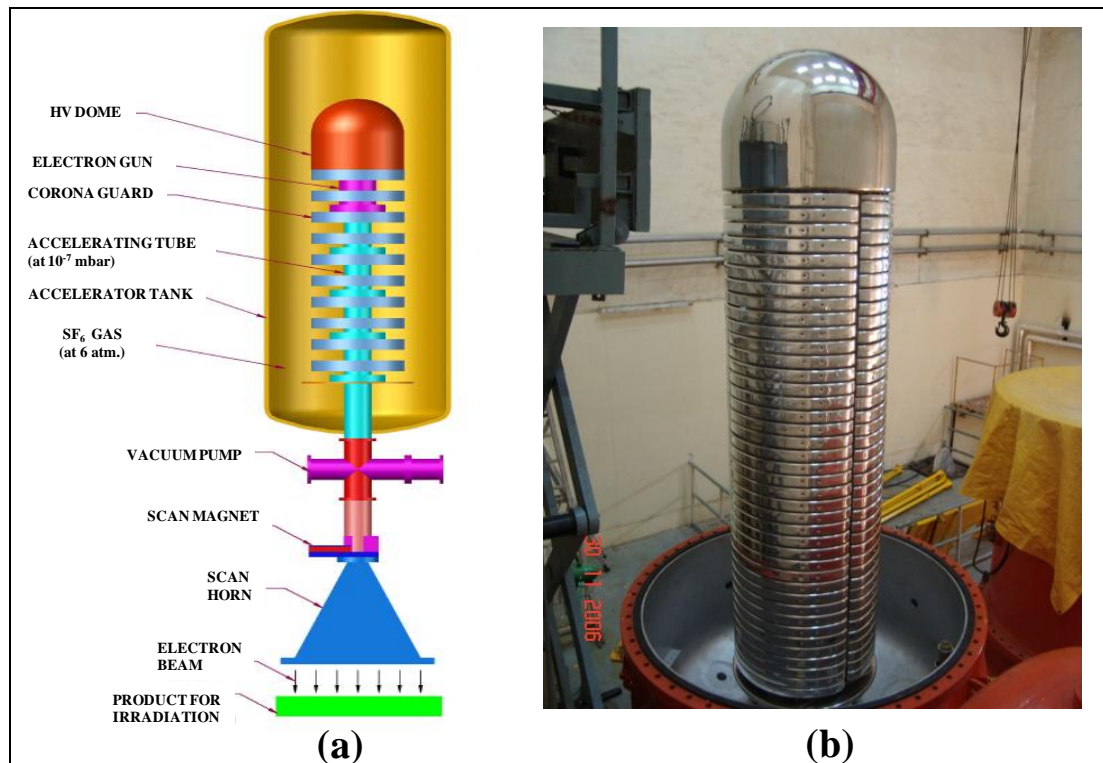


Figure 2.4: 1-3 MeV Dynamitron at EBC, BARC facility at Kharghar, Navi Mumbai, India: (a) Schematic representation, (b) its photograph.

It contains an accelerating column within a pressure vessel which is filled high pressure (~ 6 atm.) sulphur hexafluoride (SF_6) insulating gas. The column is composed of a number of rectifier tubes that are assembled in cascades. Semi-circular corona rings are attached to the anode and cathode of each rectifier in the cascade. Two RF electrodes are mounted near the inner surface of the tank and this circuit, with a resonance frequency around 100 kHz, is coupled inductively with an oscillator. Because of its high power, the oscillator is kept in a separate tank. Parallel coupling of the cascade to the liners is accomplished through the electrode to corona ring capacitance. The main advantage of this parallel coupling design is that it allows a much higher beam current to be transported than RF accelerator. Similar to 10 MeV, it also possess a scan magnet, exit window and product conveyor system.

2.3.3 Dosimetry characterization of accelerators

The dose rate and its uniformity over full scan length were verified by dosimetry experiments that are done with radio-chromic films. These radio-chromic films are basically a dye film which consists of 16.5 micron thick radiation sensitive pararosaniline cyanide dye precursor and is dissolved in polyvinyl butyral (PVB) [80]. As prepared film was colorless but because of electron beam radiation it turned to progressively darker shades of pink which occurred due to change of their optical density (absorbance). The net change in optical density is proportional to the radiation absorbed dose and it was measured using UV-Vis spectrophotometer (UVmini – 1240 type, Shimadzu, Japan). The photographs of spectrophotometer and radio-chromic films (detector) are shown in Fig. 2.5 along with the detector holder and movement system. The variation in absorbance with radiation dose and wavelength of reading light was deliberated during calibration of the film dosimeters in compliance with ISO/ASTM standards [81, 82]. The film shows maximum sensitivity at around 554 nm if scanned in UV to infrared wavelength regime (190 - 1100 nm). For calibration, set of radio-chromic film dosimeters (three in each) were exposed at different doses, along with three alanine pellets as a reference standard dosimeter which is based upon paramagnetic properties of alanine pellets; process is also called Electron Paramagnetic Resonance (EPR) dosimetry [83, 84]. The thickness normalized net absorbances were recorded and plotted against the absorbed dose as given by alanine pellet dosimeters (Fig. 2.6). From Fig. 2.6, the thickness independent response of film changes linearly, as dose changes, for the mentioned dose regime and also, the coefficient of determination (r squared) for the curve fitting is 0.995; which implies the best linear response.

In order to test the dose uniformity over the full scan length of 1 m the dose-rate profile has been generated at different conveyor speeds in case of 10 MeV. The output dose is 2 kGy at speed of 1m/min while when we switch on the speed 10 times lesser i.e. 0.1 m/min

dose becomes 10 times more and it rises upto 21 kGy with $\pm 5\%$ variation over full scan length, as given in Fig. 2.7a [27]. Similarly the dose uniformity experiments were done in 1 MeV DC accelerator at speed of 5.6 m/min (Fig. 2.7b).

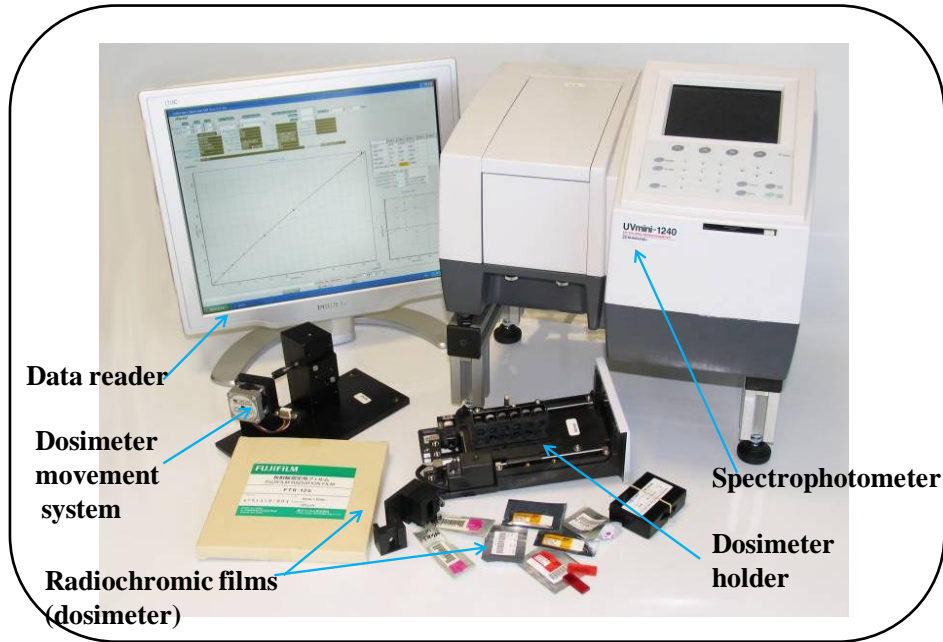


Figure 2.5: Photograph of spectrophotometer and radiochromic film dosimeters.

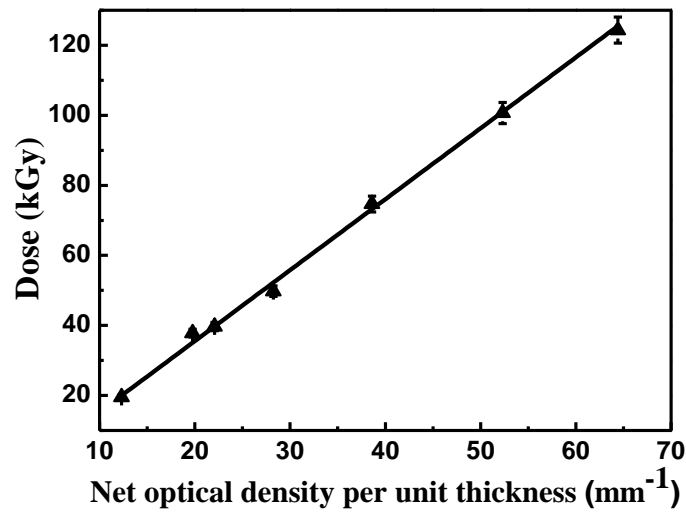


Figure 2.6: Calibration curve for dosimeter films that are used for the dose measurements in accelerators. The curve is perfectly linear fit with R^2 : 0.996.

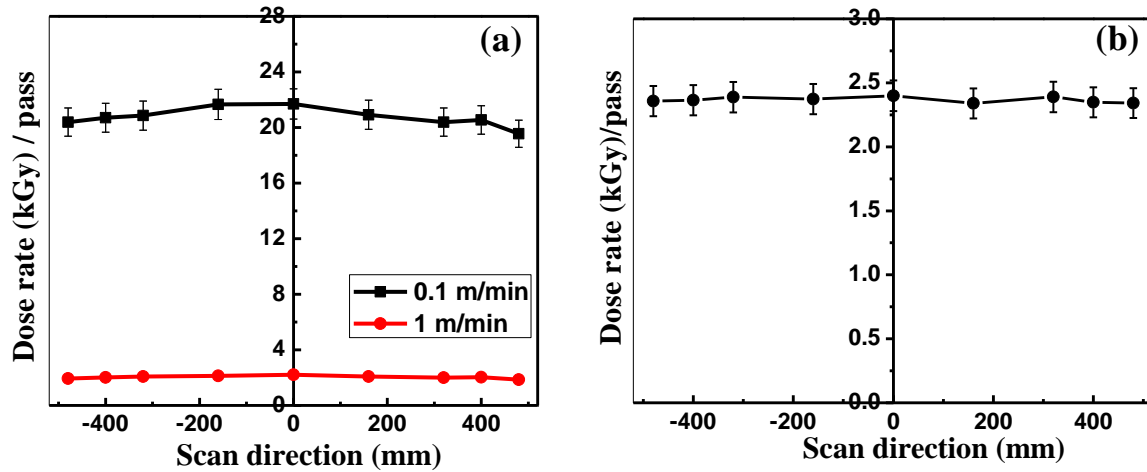


Figure 2.7: Dose profile over 1 m scan length in dynamic mode at different speeds for (a) 10 MeV RF accelerator, (b) 1 MeV DC accelerator.

2.4 Characterization techniques

The techniques that have been employed to characterize the samples during the research work are summarized as follow:

2.4.1 X-ray photoelectron spectroscopy (XPS)

XPS was developed as a surface analysis technique in the mid-1960s by Siegbahn and his coworkers [85]. Core level electrons have the binding energies matching to the energies of the photons that lie in x-ray region [85, 86]. XPS is based on the photoelectric effect in which an atom absorbs a photon with energy ($h\nu$) in excess of binding energy (E_b) of an electron, and as a result a photoelectron is emitted with kinetic energy according to the mathematical relation shown in Eq. 2.1 (schematic is shown in Fig. 2.8).

$$\text{K.E.} = h\nu - E_b \quad (2.1)$$

In XPS a soft x-ray source (Al-K α and Mg-K α) is used to ionize electrons (by knocking out the core-level electrons) from the surface of a solid sample (top few atomic layers). The estimation of the binding energies of these electrons being the characteristics of the elements provides the idea about surface composition. Binding energies of core electrons are not only element-specific but also contain chemical information, because the energy

levels of core electrons depend slightly on the chemical state of the atom. The shift in the energies of the core level electrons arising due to chemical state of electrons is known as chemical shift. The advantages of XPS technique are (a) detection of unknown element and chemical bond present in the sample (with the limitation of XPS analysis up to 10 nm depth only), (b) quantitative analysis of elements and chemical states of all elements except hydrogen and helium and (c) detection of conducting form of samples either conductors or semiconductors or insulators [87 - 89].

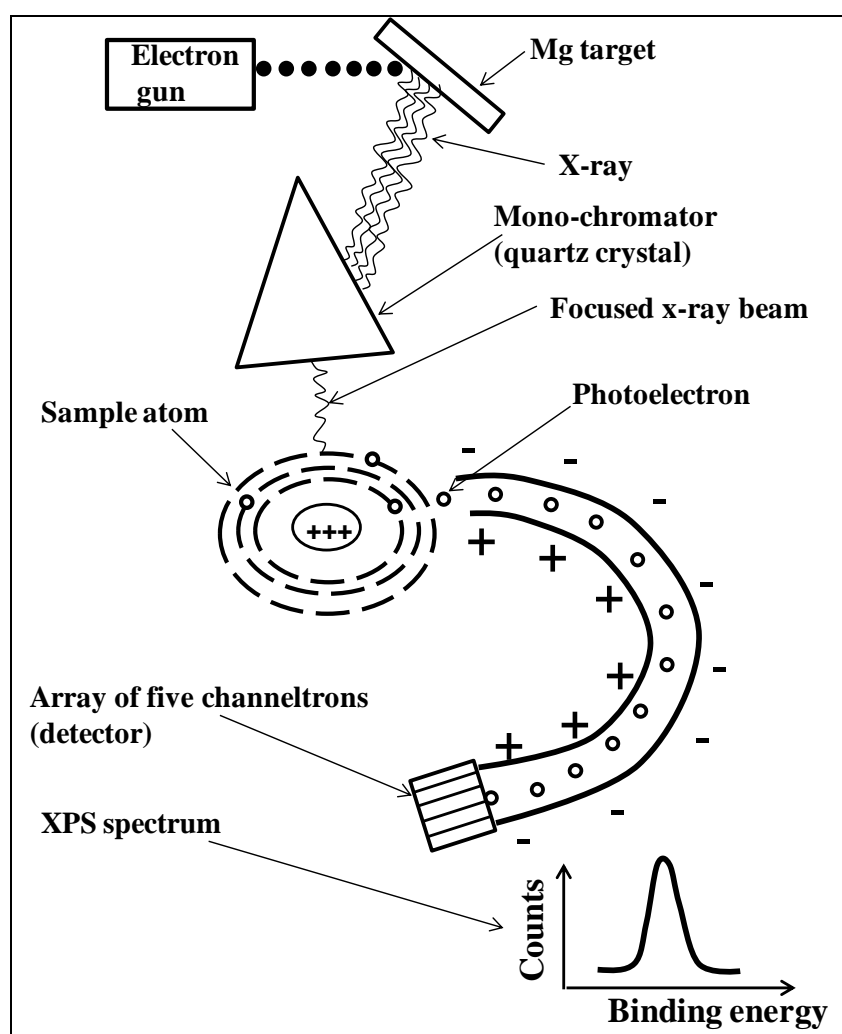


Figure 2.8: Schematic of XPS set up in which x-rays produced by electron bombardment on Mg anode. X-ray impinging on sample, producing photoelectrons that are detected after analysis in the electron energy analyzer.

In the present studies, we have used the XPS system (RIBER system model: FCX 700) consisting of Al-K α (1.7 keV) and Mg-K α (1.5 keV) x-ray sources and MAC-2 electron analyzer. The binding energy scale was calibrated with respect to Au-4f $_{7/2}$ line of 83.95eV. For charge referencing adventitious C1s peak set at 285eV was used. Each data set was first corrected for the non-linear emission background followed by fitting with Gaussian function to find the peak positions.

2.4.2 Fourier transform infrared spectroscopy (FTIR)

The frequencies and intensities of the vibrational modes observed in FTIR provide detailed information about the nature of the bonding in the molecule [90]. Bruker system (vertex 80V) has been used to record FTIR spectra. The important condition to be fulfilled for the infrared (IR) absorbance is the presence of permanent dipole moment or change in dipole moment of the chemical bond (between two atoms) when it interacts with IR. The absorption of IR leads to change in the vibration level and therefore IR absorption helps to identify the characteristic vibrational frequencies of organic functional groups. Normally the organic molecules have vibrational frequencies ranging from 4000 to 400 cm $^{-1}$. The working principle of FTIR is based upon that of interferometer which gives an interferogram i.e. a plot of light intensity versus optical path difference. The ray diagram of formation of interferogram is shown in the Fig. 2.9. Finally this interferogram is Fourier transformed to give a spectrum of infrared radiation intensity versus wave number.

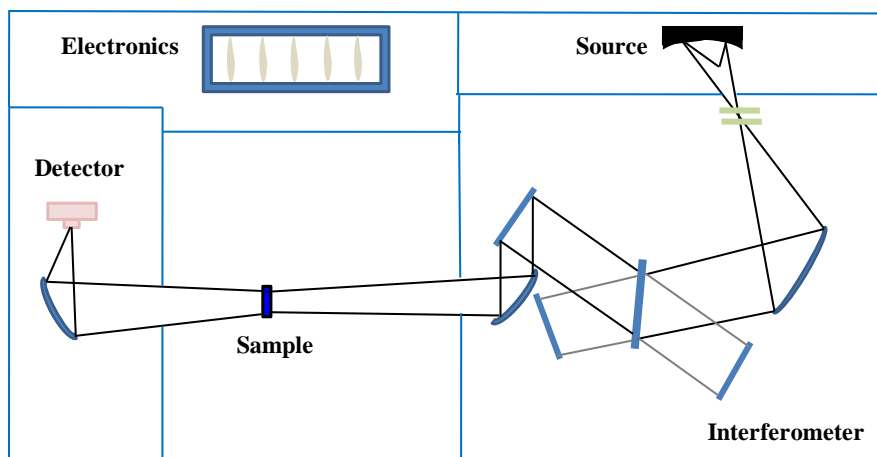


Figure 2.9: Ray diagram of recording FTIR spectra.

For our experimental purpose, FTIR spectra were recorded in two different spectroscopy modes: attenuated total reflection (ATR) and diffuse reflectance mode. In the ATR mode, an infrared beam is directed onto an optically dense crystal of high refractive index at a certain angle. This internal reflectance creates an evanescent wave (Fig. 2.10) that extends beyond the surface of the crystal into the sample which is held in contact with the crystal. This evanescent wave protrudes only upto few microns ($0.5 - 5 \mu\text{m}$) beyond the crystal surface to the sample. Consequently, there must be good contact between the sample and the crystal surface. In regions of the infrared spectrum where the sample absorbs energy, the evanescent wave will be attenuated or altered. The attenuated energy from each evanescent wave is passed back to the IR beam, which exits from the opposite end of the crystal and is passed to the detector in the IR spectrometer. The system then generates an infrared spectrum. This mode is a very good technique to measure FTIR spectra of the film.

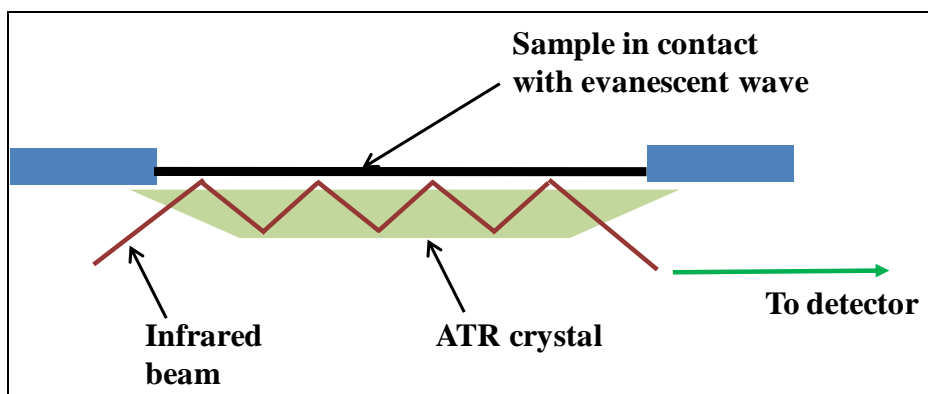


Figure 2.10: Ray diagram of recording FTIR spectra in ATR mode.

2.4.3 UV-Visible spectroscopy (UV-Vis)

UV Visible spectroscopic technique is used to characterize the bulk of thin films such as ZnPc and PANI-Ag. It measures the absorption of the ultraviolet (UV) or visible radiation as a function of wavelength. When UV or visible light is absorbed by molecules (containing π , σ or even non-bonding electrons) it causes electronic excitation among various energy levels within the molecule and thus the wavelength of absorption peaks can be correlated with the type of bonds that are present in the spices [91]. The absorption of radiations causes various kinds of electronic transitions that may occur in organic molecules as shown in Fig.

2.11. The transition between bonding and antibonding are of two types:

- (i) $\sigma - \sigma^*$ transition which requires large energies corresponding to absorption, most of the transitions occurs below 300 nm.
- (ii) $\pi - \pi^*$ transition which occurs within the molecules containing conventional double bond or triple bond.

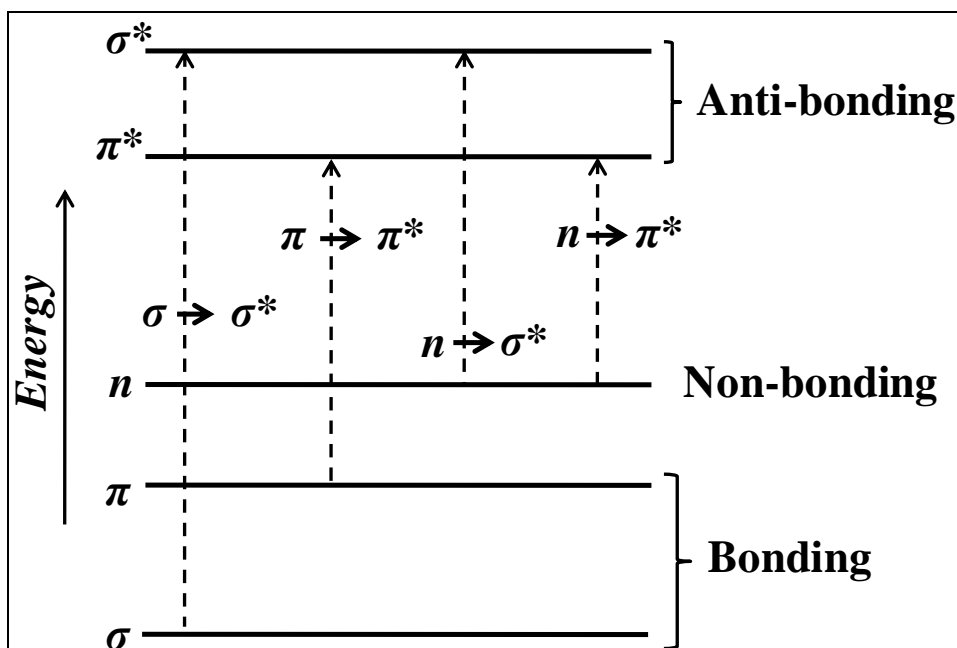


Figure 2.11: Electronic energy levels and possible electronic transitions of σ , π and n electrons.

Similar transitions between non-bonding and anti-bonding orbitals can take place as $n - \pi^*$ and $n - \sigma^*$. The absorption may sometime occur due to the d and f electron and also due to charge transfer electrons. So this absorption study is very important tool to indentify the molecule or functional group that can be present in the molecule. Most of the UV-Vis spectroscopic studies are carried out between 190 nm to 800 nm. Chemical functional groups that are responsible for absorption are referred as chromophore. Thus any species having colour, absorbs visible light and any species having an extended system with an alternating double and single bonds will absorb UV light. This enables the UV visible spectroscopy for application to a wide range of samples.

For our experiment we have used JASCO V530 spectrometer and the schematic of the double beam single monochromator spectrometer is represented in Fig. 2.12. In this spectrometer the transmitted intensity (I) of the beam passing through the sample is compared with the incident beam (I_0) and in output we get absorbance with respect to wavelength. The absorbance can be mathematically represented as $A = \log (I/I_0)$. Absorbance is directly

proportional to the numbers of absorbing molecules (concentration) in the light-path, path length and can be expressed as

$$A = \epsilon lc \quad (2.2)$$

where ϵ is the molar extinction coefficient, c is concentration of absorbing species and l is path length. This is called Beer-Lambert law.

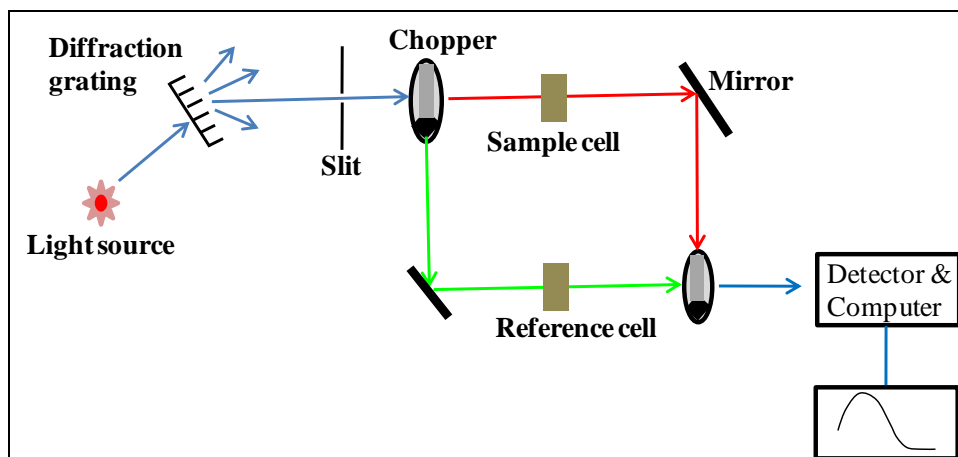


Figure 2.12: Block diagram of a typical double beam single monochromator UV-spectrometer.

2.4.4 Photoluminescence spectroscopy (PL)

Luminescence is a phenomenon which involves absorption of energy and subsequent emission of light. It is a contactless and non destructive method of probing the electronic structure of the materials. Emission of light from the materials (which get excited by light) can be categorized as fluorescence (means fast in ns time scale) and phosphorescence (means slow). The electronic transition causing photoluminescence can be visualized in Fig. 2.13.

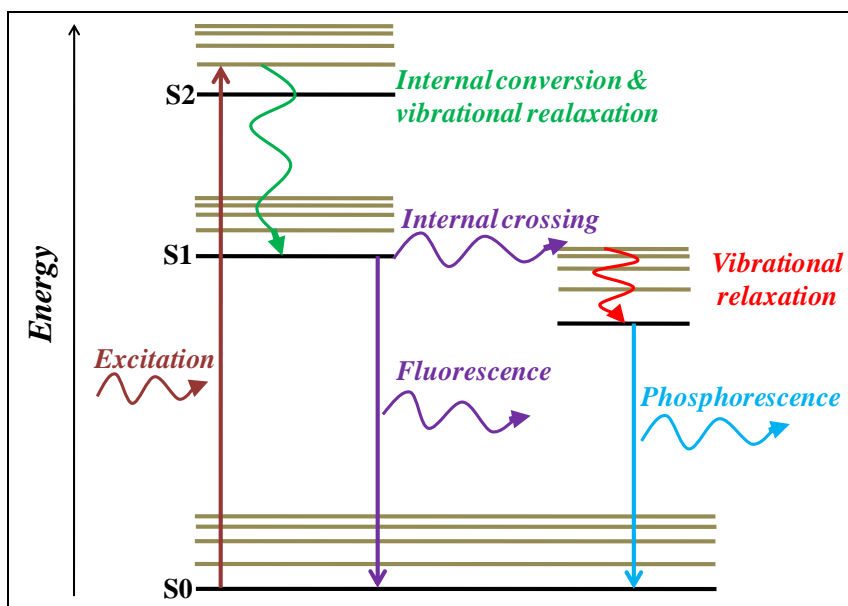


Figure 2.13: Energy diagram showing the photoluminescence.

The organic material can exhibit fluorescence or phosphorescence depending upon their structures. In PL studies there are two spectra used one is called excitation and other is called emission [92, 93]. These spectra are generated by an instrument called a spectrofluorimeter, which comprised two spectrometers: an illuminating spectrometer and an analyzing spectrometer. First, the sample is strongly illuminated by a color of light that is assumed to cause some fluorescence. A spectrum of the fluorescent emission is obtained by scanning the analyzing spectrometer using this fixed illumination color. The analyzer is then fixed at the brightest emission color, and a spectrum of the excitation is obtained by scanning with the illuminating spectrometer and measuring the variation in emission intensity at this fixed wavelength. For the purpose of designing filters, these spectra are normalized to a scale of relative intensity which is plotted with respect to wavelength.

Photoluminescence (PL) measurement was done at room temperature on ISS PC1 spectrophotometer using Xe lamp as source and ethanol as solvent. The excitation wavelength was kept at 300 nm for all the samples. A schematic representation of photoluminescence set up is shown in Fig. 2.14.

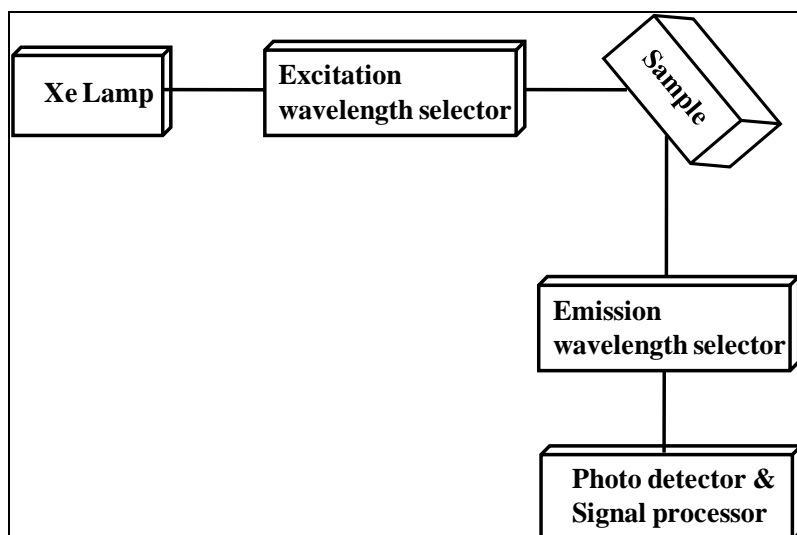


Figure 2.14: Schematic representation of photoluminescence set up.

2.4.5 X-Ray Diffraction (XRD)

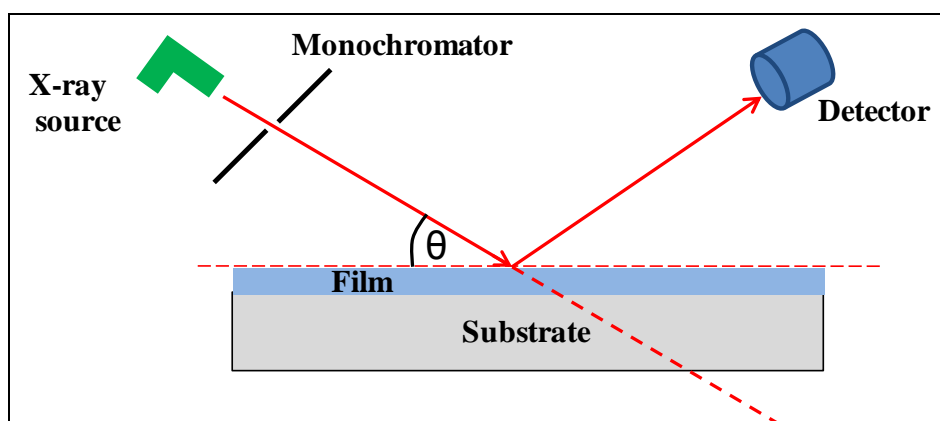


Figure 2.15: Schematic diagram of powder x-ray diffractometer.

X-ray diffraction (XRD) is used to find out the structure as well as orientation of the deposited films and it can be done in different configurations. We have used powder x-ray diffractometer (Seifert XRD 3003TT) in θ - 2θ scan mode to characterize the orientation and structure of the grown thin films. Fig. 2.15 shows the schematic diagram of the diffractometer, which consists of an x-ray source, a goniometer for mounting sample and x-ray detector. $\text{Cu K}\alpha$ having wavelength 1.54\AA was used and it has been selected using a Graphite mono-chromator. A specially designed Perspex holder (having a groove of

dimension 10 mm×10 mm×1mm) was employed to mount the thin films. The films were mounted on this groove using red wax so that x-rays will fall on the film plane. The wavelength (λ) of x-rays is comparable with the atomic spacing (d) in the solids, therefore, these x-rays get diffract in those orientations of 2θ for which the Bragg's diffraction condition is satisfied i.e. $2d \sin\theta = n\lambda$ (θ is the angle made by the incident beam with the sample plane) [94].

While recording the diffraction pattern with detector, the sample is synchronously rotated along with the detector, in such a way that the incident x-ray beam makes an angle θ with the plane of sample whereas detector is at angle 2θ with respect to incident beam. This is usually known as θ - 2θ scan of XRD. The recorded diffraction pattern is compared with standard pattern to get idea about the phase of the samples. The lattice parameters are obtained by fitting the recorded diffraction peaks using least-square fitting software.

In conventional θ - 2θ scan of x-ray diffraction measurements of thin films, normally a weak signal is produced from the film whereas an intense signal is generated from the substrate. To overcome this limitation the scan was performed with a fixed grazing angle of incidence. This mode of scanning is popularly known as grazing incidence x-ray diffraction (GIXRD). The fixed angle is chosen as higher than the critical angle of total internal reflection of the film material.

We have done the XRD in the powder diffraction mode with a PANalytical instrument (model EMPYREAN) using a Cu-K α source ($\lambda \sim 1.5418 \text{ \AA}$) with an emission current of 15 mA and voltage at 30 kV. Scans were collected over the 2θ in a step size of 0.01° and count time of 0.5 s/step.

2.4.6 Atomic force microscopy (AFM)

Atomic force microscopy (AFM) is a type of microscope in which a mechanical probe is used to study the surface feature of the material down to atomic resolution. It works upon the measurement of inter-atomic forces which come into play between the fine microscopic tip and the sample surface, as schematically depicted in Fig. 2.16a [95, 96]. The tip is attached to the free end of a cantilever (100 – 200 μm long) is brought very close to the sample surface.

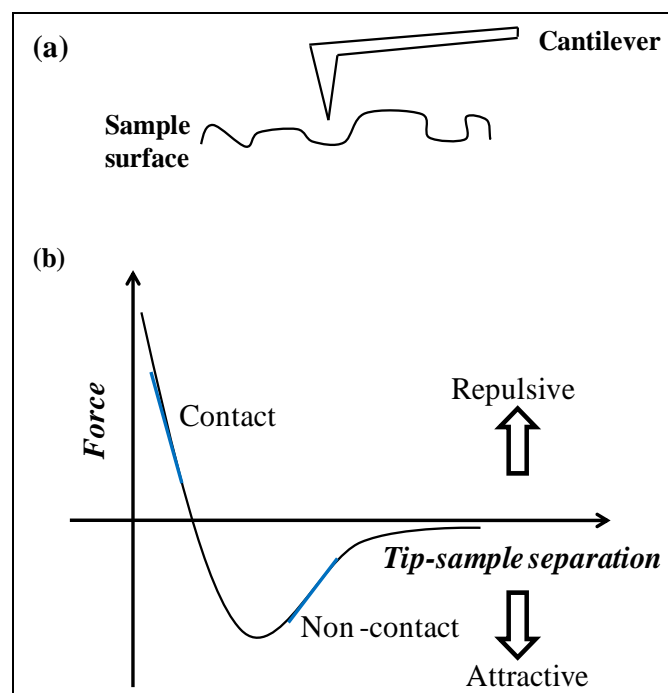


Figure 2.16: Schematic showing (a) interaction of the AFM tip with the sample surface, (b) variation in force with the separation between AFM tip and the sample surface.

The working principle of AFM is based upon the positive or negative deflection of a very sensitive cantilever due to repulsive or attractive forces between atoms on the sample surface and that at the cantilever tip. AFM operates in three different modes: contact mode, non-contact mode and tapping mode. At relatively large distance from the sample surface, the force of attraction between the tip and the sample surface dominates, whereas repulsive force is most significant at very small distance (up to few angstroms).

In non-contact mode or dynamic mode, the tip is held at the distance of the order of tens to hundreds of angstroms from the sample surface, and the inter-atomic force between the tip and sample is attractive (which is largely a result of the long-range vander Waals interactions). In contact mode, the force becomes repulsive as the tip is brought into close contact with sample surface less than a few angstroms. The resulting deflection by cantilever is monitored and measured by different detection techniques. For organic material, the foremost problem with this mode of operation is that the sample surfaces can be easily scratched or damaged because of the direct contact with the tip. These limitations are overcome by tapping mode. The resolution is usually the highest in the contact mode of operation because the force of attraction is much weaker than the repulsion.

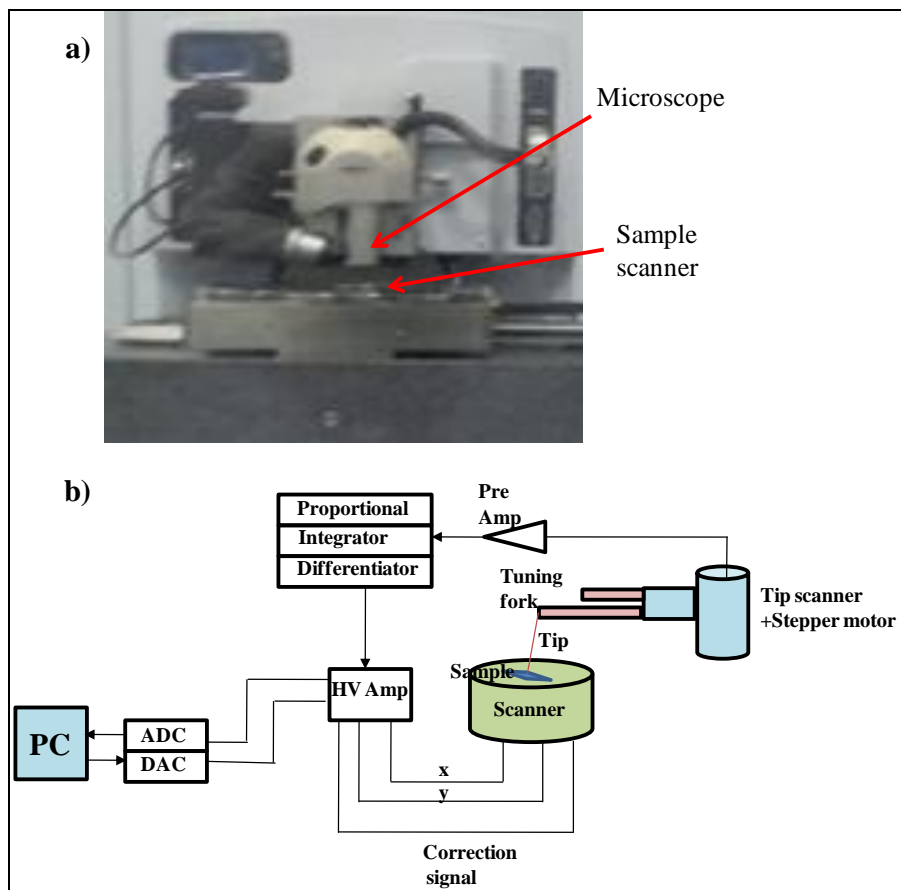


Figure 2.17: (a) Photograph showing Dimension Icon AFM system, (b) Block diagram of AFM.

The tapping mode brings together the advantages of contact and non-contact mode. In tapping mode, the cantilever oscillates close to its resonance frequency (100-500 kHz) with amplitude of approximately 20 nm so that the tip just comes into touch of (tapping) the surface. The amplitude of oscillation kept constant with the help of an electronic feedback loop, so that a constant tip-sample interaction is maintained during scanning. The resolution of image in tapping mode is nearly same as that in the contact mode. In addition, tapping mode is fast with the benefit of less damage to the sample. Fig. 2.17 shows the photograph of AFM set-up and its block diagram.

In the present study, Dimension Icon atomic force microscope, Bruker (CA, USA) make, was used to image the surface morphology of the samples. Scanasyst-air cantilever of 2 nm tip size and having 0.4 N/m force constant has been used and it worked in tapping mode.

2.4.7 Scanning electron microscopy (SEM)

Scanning electron microscopy (SEM) imparts information relating to topographical features, morphology and phase distribution [97, 98] SEM consists of an electron gun, a lens system, scanning coils, an electron collector and a display. The operational mechanism of SEM is described in Fig. 2.18. It is basically a type of electron microscope that produces images of a sample by scanning the surface with a focused beam of electron. The scanned electron beam is produced in an electron microscope column through heated cathode and arranged with the electric and magnetic fields in a proper direction to achieve the required incident beam at sample surface. A vacuum of the order of $10^{-5} - 10^{-6}$ mbar is required to be maintained at the sample locations. Electrons in the SEM are accelerated at voltages in the range 10-40 kV but for insulating samples the same should be in the order of hundred volts.

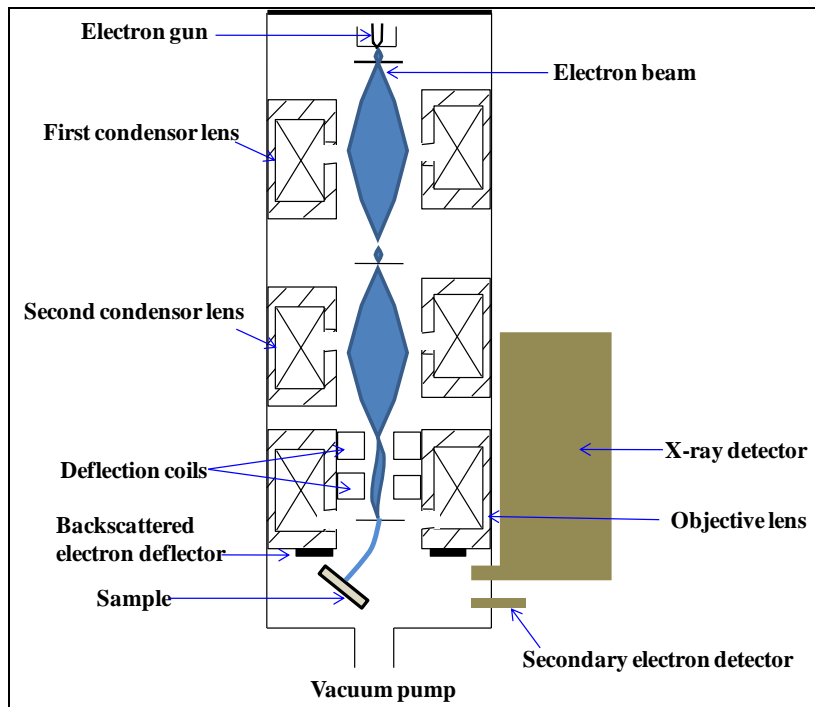


Figure 2.18: Typical sketch of scanning electron microscope.

Two types of interactions occur in between the electron beam and the atoms of the sample and those are elastic and inelastic. Elastic interaction occurs if the electron beam strikes the sample and there is a change in its direction without any change in its kinetic energy which results in backscattered electrons. Whereas, the inelastic interaction occurs when the beam of electron strikes an orbiting shell electron of the sample and results in the ejection of new electrons (secondary electrons). The vacancy created due to the ejection of a secondary electron is filled from a higher level orbital accompanied by the generation of a characteristic x-ray along with Auger electrons and sometimes with cathodoluminescence also (Fig. 2.19). These interactions reveal the important information about the sample to find out the surface characteristics and the chemical nature of the sample.

The most widely utilized signal is the secondary electron signal. Nearly all of secondary electrons come from a region very closer to the sample surface. The secondary electrons are characterized from other electrons by having energy less than 50 eV and emitted from K-shell of surface atoms of the specimen as an impact of the incident beam. It is the

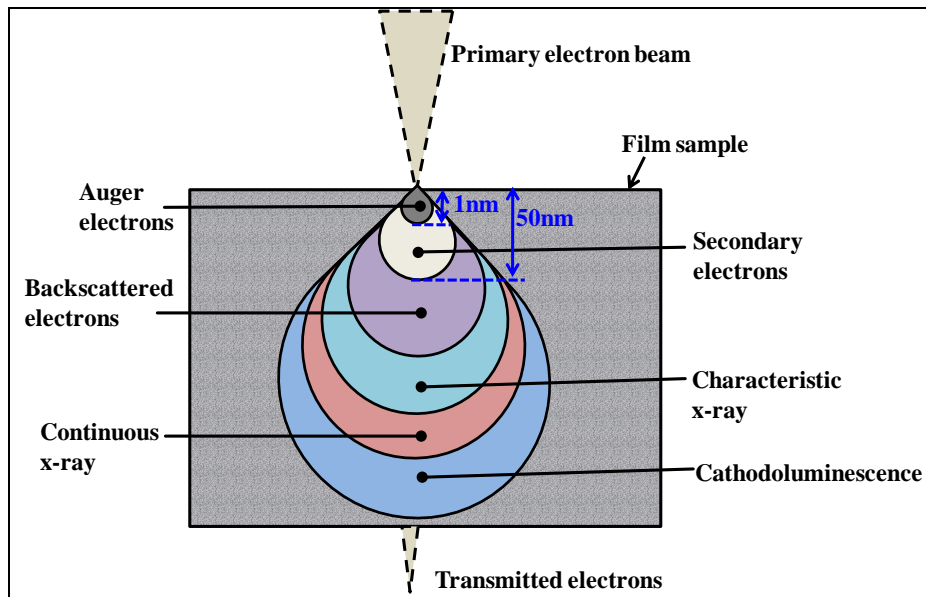


Figure 2.19: Schematic showing Tear drop model of electron interaction with sample and the depth/volume from which the different signals originates.

most useful signal for examining surface structure and gives the best resolution image better than 10 nm. Since the secondary electron intensity is a function of the surface orientation with respect to the beam and the detector and thus, produces an image of the specimen morphology. The secondary electron intensity is also influenced by the chemical bonding, charging effects and back scattered electron intensity, since the back scattered electron generated secondary electrons are significant part of the secondary electric signal. Backscattered electrons, consist of high-energy electrons (greater than 50 eV) that originates in the electron beam and are reflected or back-scattered out of the specimen interaction volume. The intensity of their signals increases with increase the atomic number. Backscattered electron signal is often used to show atomic number contrast, in which areas of higher average atomic number produce more back scattered electrons, and thus appear brighter than lower atomic number regions. The contrast in such images occurs not due to colour differences but due to different intensities of electrons that back-scatter from the layers with different average atomic number. The characteristics x-rays signal depends exclusively

on the atoms that produced it, hence can be used for chemical detection analysis. The EDS x-ray detector (also called EDX) measures the spectrum of x-ray which shows the number of emitted x-ray photons with respect to their energies. The energy of the x-ray is a characteristic of the element from which it is generated.

Cathodoluminescence (CL) is the emission of photons of characteristic wavelengths from a material that is under high-energy electron bombardment and used to study the internal structure of the material. The detector is Everhart-Thornley detector and it is composed of a scintillator followed by photo multiplier tube. At first electrons strike the positively biased scintillator and are converted to a burst of photons that travel through the light pipe to a photomultiplier tube which converts the photons of light into a voltage. The strength of this voltage depends on the intensity of secondary electrons that are striking the detector. Thus the secondary electrons that are produced from a small area of the specimen give rise to a voltage signal of a particular strength. This voltage is led out of the microscope column to an electric console, where it is processed and amplified to generate a point of brightness on the cathode ray tube screen. The contrast in SEM image appears due the difference in intensity which represents difference in signal that arise from corresponding picture elements on the sample. In the present study surface morphology of the films was imaged using scanning electron microscopy (SEM) (ZEISS SUPRA). SEM analysis is considered to be a non-destructive technique which means that the x-ray or electron generated through electron interactions do not result in volume loss of the sample and thus, it makes possible to analyze the same sample repeatedly.

2.4.8 Contact angle measurement

The hydrophobicity / hydrophilicity of the films have been determined by contact angle measurement. In this experiment a drop of liquid (de-ionized water) is allowed to expand on the film surface using a fine syringe. The contact angle is the tangent drawn on the

droplet from the solid surface of the film and solid surface (Fig. 2.20). The spread liquid drop on the film surface is imaged by CCD camera and software is used to measure the contact angle. We have used Data Physics (OCA20) system to measure the contact angle through liquid droplet method. A drop of de ionized water is proliferated on the surface of the film and a snap shot of the same has been taken using a CCD camera which is connected with computer software to measure the contact angle. The acute and obtuse contact angles are respective indication of hydrophilic and hydrophobic surfaces as seen from Fig. 2.20.

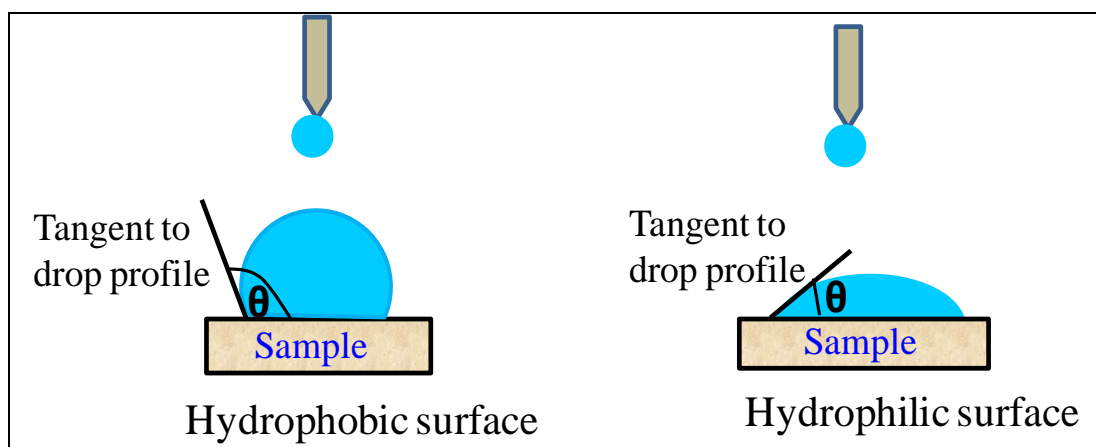


Figure 2.20: Schematic representation of contact angle measurement by water droplet method. Obtuse angle implies hydrophobic surface whereas acute angle represents hydrophilic.

2.4.9 Mechanical characterizations

The measurement of mechanical properties such as tensile strength, Young's modulus, elongation at break were carried out by using universal testing machine, Zwick Roell ZO10 (Zwick Roell, Germany), at a crosshead speed of 0.2 m/min (ASTM D2240) [99]. The typical schematic of mechanical properties measurement setup is given in Fig. 2.21. The set up consist of three main components load frame, a load cell and a cross head. For measurement of the mechanical properties, the samples were prepared in the form of dumbbell shape using a sharp edged steel die of standard dimensions (10 mm × 10 mm). The

dumbbell shaped specimen was fixed between the grips and a load is applied to the sample by moving the cross head apart. During the experiment the control system and associated software of the instrument recorded the load and extension of the samples from which mechanical properties such as tensile strength, elongation at break and Young's modulus of the samples can be estimated.

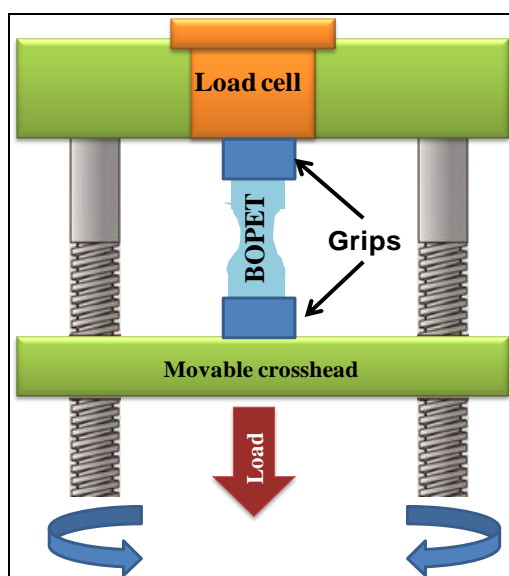


Figure 2.21: Schematic diagram of the mechanical property measurement setup.

2.4.10 Crosslinking analysis

Crosslinking is the most important effect of polymer irradiation because it can tailor the mechanical, thermal properties as well as chemical, environmental, radiation stabilities of preformed parts and also in case of bulk. Both polymer crosslinking and degradation by chain scission occur during radiation treatment, but one or the other of these effects may dominate at a specified time [100 - 102]. This distinction goes along with the chemical nature of polymers and the radiation dose. Materials with $G(S)/G(X)$ ratio below 1.0 (where $G(S)$ and $G(X)$ respectively defines the yield of scissioning and cross-linking) are favoured for crosslinking applications. $G(S)$ and $G(X)$ both change with increasing dose. So, it is possible that upon reaching a certain dose level, crosslinking dominated polymers, e.g. polyethylene or natural rubber latex can change to degradation dominated or vice versa. $G(X)$ and $G(S)$

also depend on irradiation conditions, such as temperature and atmosphere. To conclude the dominance of crosslinking or scissioning, some methods have been used in the present research work. One is called sol-gel analysis which is done by Soxhlet extraction method and is used only if the desired sample has the limited solubility in the said solvent. Another is solubility test method which can be applied when the desired sample has a significant solubility in the said solvent.

2.4.10.1 Sol-Gel test

For the sol-gel analysis, the samples were Soxhlet extracted at elevated temperature around 70°C, using proper solvent, for example o-chlorophenol (2-chlorophenol) or hexafluoroisopropanol (HFIP) for BOPET [103, 104]. Soxhlet extraction is a continuous solid-liquid extraction method and it consists of three important components: (i) the percolator which circulates the solvent and it contains heater and reflux, (ii) the thimble which is normally made of thick filter paper and it retains the solid to be laved and (iii) the siphon mechanism which periodically empties the thimble. The schematic of Soxhlet extractor set up is shown in Fig. 2.22.

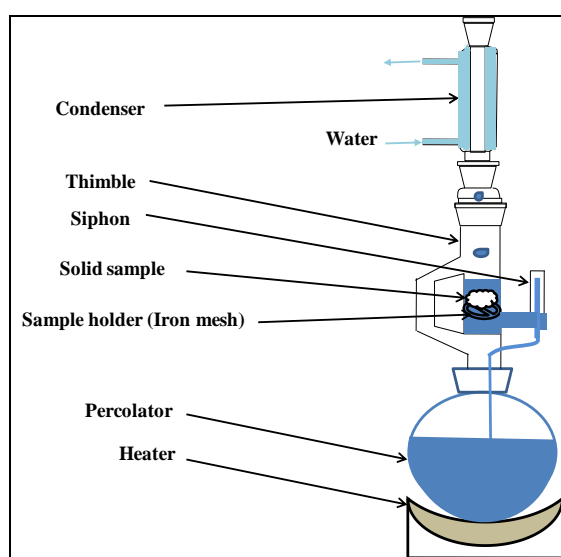


Figure 2.22: Schematic of Soxhlet-Extract setup.

The sample is kept inside the thimble and the solvent is heated to reflux. The vapors of solvent travel up through distillation arm where they get condensed and finally, flood into the chamber which houses the thimble of solid. The condenser ensures that any solvent vapor which has cooled down drips back into the chamber containing the solid sample. The chamber which contains solid sample is slowly filled with a warm solvent. Some of the sample gets dissolved in the warm solvent. When the Soxhlet chamber becomes almost full it is emptied by the siphon and the solvent is returned to the distillation flask. The thimble ensures that the rapid motion of the solvent does not allow transport of any solid material. The cycle may be allowed to repeat many times for hours. During each cycle, some fraction of the solid sample was dissolved in the solvent and after many cycles only the pure insoluble material remains in the distillation flask.

We took out the insoluble part at regular interval of around 15 minutes, dried under room conditions and weighed using microbalance (M/s AND Company Ltd., Japan make) having accuracy $\sim 100 \mu\text{g}$. After completion of some cycle it was found that the weight of insoluble part remains constant which is taken as insoluble fraction to calculate gel content using following relationship

$$\text{Gel content} = (W_g/W_i) \quad (2.3)$$

$$\text{Sol fraction} = 1 - \text{Gel content} \quad (2.4)$$

where W_g and W_i are the weight of insoluble fraction and initial weight respectively [105].

If the plot of gel content (also called gel fraction) of the sample with absorbed dose attains saturation then it implies that the crosslinking has become a dominant phenomenon. In order to quantitative evaluation of crosslinking and chain scission yields of irradiated samples, the Charlesby – Pinner equation (Equation 2.5) was used and a plot of $S + \sqrt{S}$ vs. $1/\text{absorbed dose}$ has been generated [106].

$$S + \sqrt{S} = \frac{p_0}{q_0} + \frac{1}{q_0 P_n D} \quad (2.5)$$

The symbols stand as S for sol fraction, p_0 and q_0 are for chain scission and crosslinking probabilities per unit dose (which is proportional to radiation chemical yields of chain scission and crosslinking) respectively, P_n is for the number average degree of polymerization and D is for radiation absorbed dose. The point of interception of Charlesby-Pinner plot gives the value of p_0/q_0 which concludes that whether the dominating phenomenon is crosslinking or scissioning. If the point of intercept, means p_0/q_0 , is less than 2, it implied that crosslinking was predominantly occurred [106].

2.4.10.2 Solubility test

The solubility test is another type of sol-gel test without using Soxhlet extract and it is applicable for samples having significant solubility in the said solvent. It has been conducted by leaving the samples in appropriate solvent (eg. dimethyl sulphoxide (DMSO) for polyaniline solid thin films) for fixed time (say 15 minutes), at room temperature or elevated temperature [107]. The insoluble part was taken out and dried at ambient conditions using hot air blower and weighed using microbalance as above. The cycle was repeated till the constant weight of sample was achieved and thus, the weight of insoluble part was estimated. In this way with reference to initial weight, the percentage solubility and also the percentage change in solubility with respect to pristine film was calculated. The high holding strength or low solubility of film has been attributed to longer chain length that results in good entanglement which clearly indicates crosslinking. Adversely, the loss of holding strength or more solubility concludes the dominance by chain scissioning.

2.5 Electrical characterizations

In the present study we have used standard two probe technique for electrical characterization and chemiresistive gas sensing measurements of the organic thin films.

Electrical characterizations have been carried out through current voltage (*I-V* or *J-V*) plot analysis using gold pads as electrodes. The gold pads were deposited on the films post electron beam irradiation. The irradiated film samples were sliced in two parts, one used for Au pad deposition and another for other characterizations. The gold pads having size 3 mm \times 3 mm were deposited on the film samples by thermal evaporation method. A metallic mask was used to deposit gold electrodes on the film with 12 μ m electrode spacing. The films were loaded in vacuum chamber which is connected to a TMP based vacuum pumping system and having base pressure 2×10^{-6} mbar. To deposit gold electrodes, 99.99% pure gold wire was loaded on a tungsten filament, which was resistively heated by external power supply. To prevent diffusion of gold atoms into the organic films, electrodes were deposited with very slow rate of 1 $\text{\AA}/\text{s}$. The deposition rate and thickness of the deposited electrodes were monitored through a quartz crystal monitor. The typical thickness of deposited gold pad was \sim 50 nm.

2.5.1 Electrical conductivity measurement

To measure the electrical conductivity *I-V* characterization have been done using Keithley 6487 picoammeter/voltage source and computer based data acquisition system which records the *I-V* plot. The electrical connections of gold pads with the picoammeter/voltage source, were made using silver wire (diameter \sim 100 μ m) and silver paint (Electrolube make). *I-V* measurement using two probe method is shown schematically in Fig. 2.23. All the measurements were carried out at room temperature and in dark to avoid photocurrent.

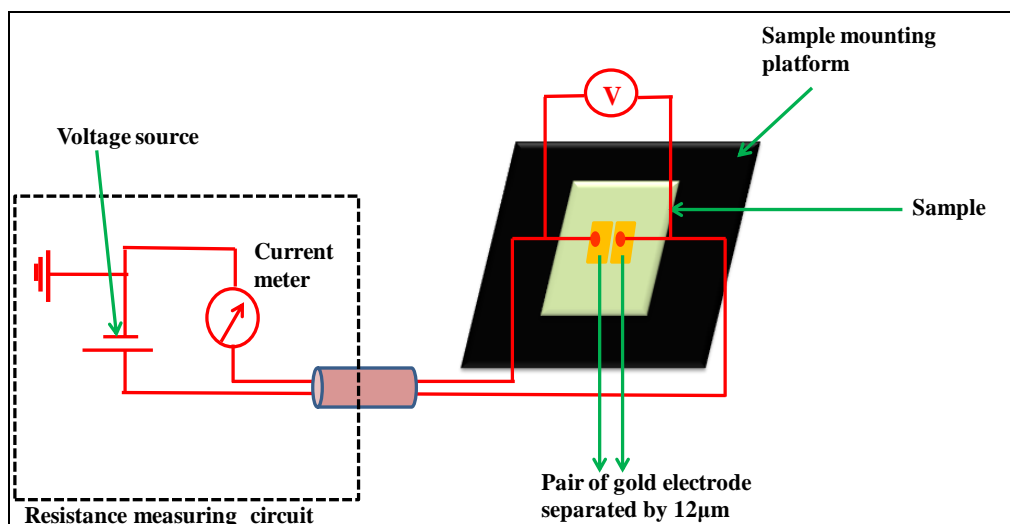


Figure 2.23: Schematic of two probe method for conductivity (I - V) measurements.

2.5.2 Chemiresistive gas sensing measurement

The chemiresistive gas sensing of thin films were performed in a static environment conditions with an in house-made gas sensing setup, as shown in Fig. 2.24. The sensor films are mounted on a metal surface and applying a fixed voltage to the sample. The sensor assembly was mounted in a leak tight stainless steel container having volume 1000 cm^3 and a known volume of gas (to be sensed) was injected into the closed chamber using a micro-syringe.

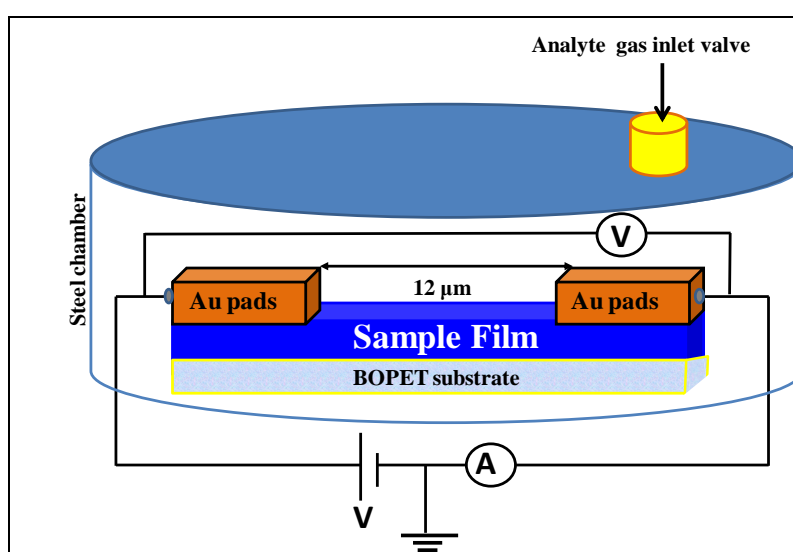


Figure 2.24: Schematic representation of gas sensing measurement setup.

To achieve the proper gas concentration, a desired volume of test gas was taken, in a micro syringe, from the commercially obtained gas cylinder. The gas cylinder contains nitrogen with test gas having concentration 1000 ppm. Since the original volume of test gas (as taken in syringe, V_1), original concentration of test gas (i.e. 1000 ppm, C_1) and new volume (volume of steel chamber, 1 L, V_2) are known. The actual concentration of test gas (C_2) in steel chamber has been estimated using standard titration equation $V_1C_1 = V_2C_2$. The current flowing through the circuit at fixed bias was monitored with time using picoammeter/voltage source and computer based data acquisition system. Once a steady state was achieved, recovery of films was recorded by exposing the sensor films to atmosphere by opening the lid of the steel chamber. The response (%) of the sensors was calculated from the response curves using the relation:

$$\text{Response (\%)} = \frac{|R_g - R_a|}{R_a} \times 100 \quad (2.6)$$

where R_g and R_a stand for the resistance values of the sensor films in test gas and fresh air respectively. Response and recovery times were defined as the times needed for 90% of total change in resistance upon exposure to test gas and fresh air, respectively.

CHAPTER-3

**ELECTRON BEAM INDUCED MODIFICATIONS
OF BIAXIALLY ORIENTED POLYETHYLENE
TEREPHTHALATE SHEETS**

In the present chapter, we have focused on the effects of electron beam irradiation (with dose ranging from 2 to 32 kGy) on mechanical and electrical properties of biaxially oriented polyethylene terephthalate (BOPET) sheets. BOPET is a flexible polymer of great interest due to its application as packaging material for food and medical commodities, insulation panel for electronic appliances as well as substrate for fabrication of flexible devices. The mechanical properties of BOPET, such as, tensile strength, elongation at break, Young's modulus, and electrical resistivity enhance with increase in dose and saturate for doses ≥ 8 kGy. The post irradiation characterizations which includes sol-gel analysis, Fourier transformation infra-red (FTIR), X-ray photoelectron spectroscopy (XPS) suggest partial crosslinking of PET chains through the diethylene glycol (DEG), and this crosslinking is responsible for modified mechanical and electrical characteristics. The improved mechanical properties and enhanced electrical resistivity of electron beam modified BOPET sheets can surely provide additional advantages in applications such as packaging materials for food, medical product sterilization and in electronic industries.

3.1 Introduction

Radiation is a popular and superior tool as compared to conventional processes like ethylene oxide sterilization, thermal sterilization, high pressure autoclave sterilization etc.; for sterilizing the food products and medical devices owing to its convenience and economical approach [108, 109]. The sterilization of food and medical products caused by ionizing radiation is usually carried out in fully packed conditions to avoid chances of recontamination [110]. High energy electron beam generated by linear radio frequency accelerator is generally utilized for sterilization and modification of the properties of materials. The beneficial aspect of electron beam generated by accelerators is their ability to provide a safe and flexible radiation source as the treatment stops as soon as power is switched off without leaving any radioactive waste or time delayed radioactivity [29]. Therefore the largest utilizations of electron accelerators for industrial applications include preservation of food and sterilization of medical products as well as the modification of the properties of polymers through cross-linking, degradation, curing and grafting. Since polymers have already shown their potential in the development of portable, flexible and foldable electronics, it has become very essential to investigate the effect of radiation on the electro-mechanical properties of polymeric materials [30]. The biaxially oriented polyethylene terephthalate (BOPET) is a flexible polymer which has drawn great interest due to its application as the packaging material for food and medical commodities, production of insulation panel for electronic appliances as well as substrate for fabrication of flexible devices. It has been reported that polyethylene terephthalate (PET) is a radiation resistant polymer in low dose range (i.e. up to 8 kGy) due to the presence of aromatic rings in its structure [111 - 113]. It is a well-known fact that PET is highly used in flexible organic thin film devices as substrate but BOPET facilitates the growth of thin film through “standing on” configurations, which assists easy intermolecular transport of the charge carriers. In addition

the molecular ordering, caused by the electrostatic interactions between oriented PET chains and organic film molecules as well as enhanced π - π interactions between organic molecules and oriented PET chains supports the mobility of charge carriers [114]. Thus the BOPET substrate based flexible thin films can have comparatively higher mobility of charge carriers. BOPET is prepared from molten sheet of PET, which is biaxially oriented by drawing and subsequently allowed to “heat set” under tension at temperature greater than 200°C [115]. The heat setting treatment process prevents the sheet from shrinking back to its original unstretched shape and locks the molecular orientation in the sheet plane. The molecular orientation also induces the formation of many crystal nuclei.

However, the modification of mechanical (*viz.* tensile strength, elongation at break, Young’s modulus) and electrical (such as sheet resistance) properties of BOPET sheets after electron beam irradiation has not been investigated extensively in the past; particularly in the dose regime that is required for the above mentioned applications. In the present chapter, we discuss about the findings when BOPET sheets were irradiated with 10 MeV electron beam at different radiation doses (up to 32 kGy) to tailor their mechanical and electrical properties. We demonstrate that electron-beam irradiation caused modification in both the mechanical and electrical properties of BOPET sheets. The sol-gel analysis, to verify existence of crosslinking, has been explained along with the FTIR results, both of which suggest structural modifications. Surface characterizations have been discussed with x-ray photoelectron spectroscopy and static contact angle measurements. The chapter is concluded by proposing the possible mechanisms for modification in chemical structure of BOPET that resulted in the change of mechanical and electrical properties. The tailored mechanical and electrical properties of electron beam modified BOPET sheets can have additional advantages in number of applications where PET is already being used.

3.2 Sample preparation & electron beam irradiation

The BOPET polymer sheet (M/s Dupont make), of thickness $\sim 100 \mu\text{m}$, were used for irradiation experiment and sliced in size of around $8 \text{ cm} \times 8 \text{ cm}$. They were ultrasonically cleaned using methanol followed by drying with nitrogen gas and finally packed in a plastic box for electron beam irradiation experiments. Three samples have been taken for each set of irradiation dose as well as pristine and each measurement (non destructive) has been repeated twice. The average was taken and deviation from average has been shown with error bars.

The BOPET samples were irradiated under 10 MeV electron beam generated by radio frequency linear accelerator (RF Linac) located at EBC, BARC facility, Navi Mumbai, India. The Linac delivered dose (that varied from 2 kGy to 32 kGy) to BOPET in steps so that any significant temperature changes or thermal damages to the BOPET could be avoided. For this, the BOPET samples were kept on a conveyor that was located just below the accelerator exit window and had the ability of doing to and fro motion with sufficient time gaps.

3.3 Mechanical characterizations

The measurement of mechanical properties such as tensile strength, Young's modulus, elongation at break were carried out by using universal testing machine, Zwick Roell ZO10 (Zwick Roell, Germany), at a crosshead speed of 0.2 m/min (ASTM D2240) [99]. The results of measurement experiments for pristine and irradiated BOPET sheets are shown in Fig. 3.1. From Fig. 3.1a, it can be seen that initially the tensile strength for irradiated BOPET samples increases up to 8 kGy and afterward, it gets saturated. The tensile strength of the BOPET has increased by around 1.5 times after irradiating with dose 8 kGy or more. Similar observations have been reported for tensile strength of PET by researchers [104, 116]. On the other hand the elongation at break (also known as fracture strain), as shown in Fig. 3.1b, decreases monotonically from 50 % for pristine to around 33 % in case of

8 kGy dose and with further increase in dose, it gets saturated. These results are in agreement with the observations made by Oliveira *et al*, for studies in PET [117].

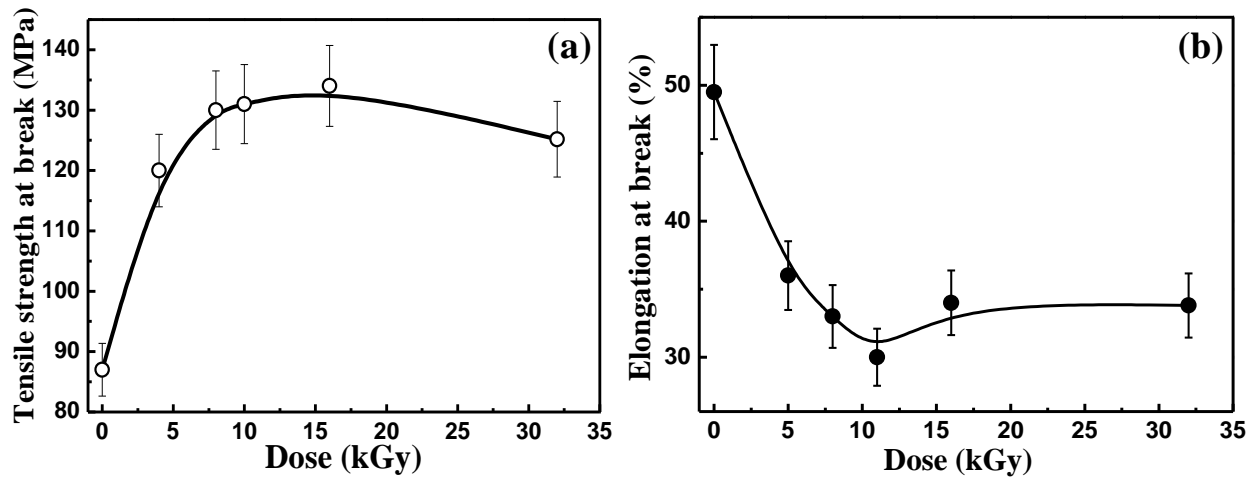


Figure 3.1: Variation in mechanical properties of BOPET with dose, (a) tensile strength, (b) elongation at break.

Another important mechanical property of polymer material is Young's modulus. The plot of calculated Young's modulus for BOPET samples as a function of dose is presented in Fig. 3.2 and it can be seen that Young's modulus initially increases with e-beam dose up to 12 kGy and after that it saturates.

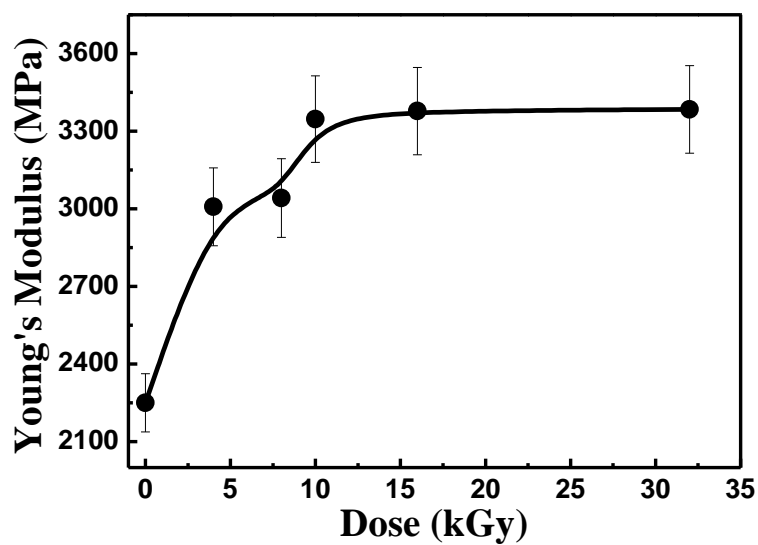


Figure 3.2: Variation in Young's modulus of BOPET with respect to dose.

The Young's modulus of BOPET also increases by 1.5 times than in case of pristine BOPET after being exposed to dose of 12 kGy. The results suggest that the increase of tensile strength is accompanied by the decrease of elongation at break with increasing radiation dose. It is well known fact that on irradiation polymers may predominantly undergo either crosslinking or degradation depending upon their chemical structure and irradiation conditions [29]. In literature it has also been reported that PET is a radiation resistant polymer because of aromatic rings present in the structure at low dose range (< 10 kGy) [80, 113]. However, our measurements along with some initial results (that have been published previously) suggest that mechanical properties of BOPET get modified even with low dose of electron beam irradiation perhaps due to modification of its chemical structure which is explained later.

3.4 Electrical characterizations

Sheet resistance of the films was checked using conventional two probe technique and the electrical contacts were prepared by thermally depositing two gold pads (50 nm thick, size $3\text{ mm} \times 3\text{ mm}$ at a spacing of $12\text{ }\mu\text{m}$) onto BOPET sheet. The electrical circuit (schematically shown in Fig. 2.23) consists of a voltage source with current meter and the response data was acquired by a personal computer equipped with softwares.

In order to measure sheet resistance of the BOPET, the current-voltage (I - V) characteristics were obtained in the bias range of $\pm 10\text{ V}$. Fig. 3.3a shows the typical I - V plots for pristine and irradiated BOPET with typical higher dose (16 kGy). The linear profile of I - V curve indicates the nature of conduction as ohmic for pristine BOPET which remains same for irradiated samples also. From I - V data, the sheet resistances of all samples were calculated and they have been plotted against the electron beam dose as given in Fig. 3.3b. The sheet resistance of pristine BOPET is $\sim 6\text{ T}\Omega$ which enhances by an order up to $\sim 65\text{ T}\Omega$ after receiving 8 kGy. The saturation has been observed for the samples irradiated with further

higher doses. Similar modifications in electrical properties, on electron beam irradiation, have been observed for PET sheet by Oproiu *et al* [118]. In polymer the charge carrier hops from one chain to another chain and such a hopping of charge carriers is majorly responsible for electrical conduction. After irradiation since PET chains become crosslinked which results in the increase of the molecular weight leading to swelling of molecules. It obstructs the charge carrier hopping, leads to increase in sheet resistance.

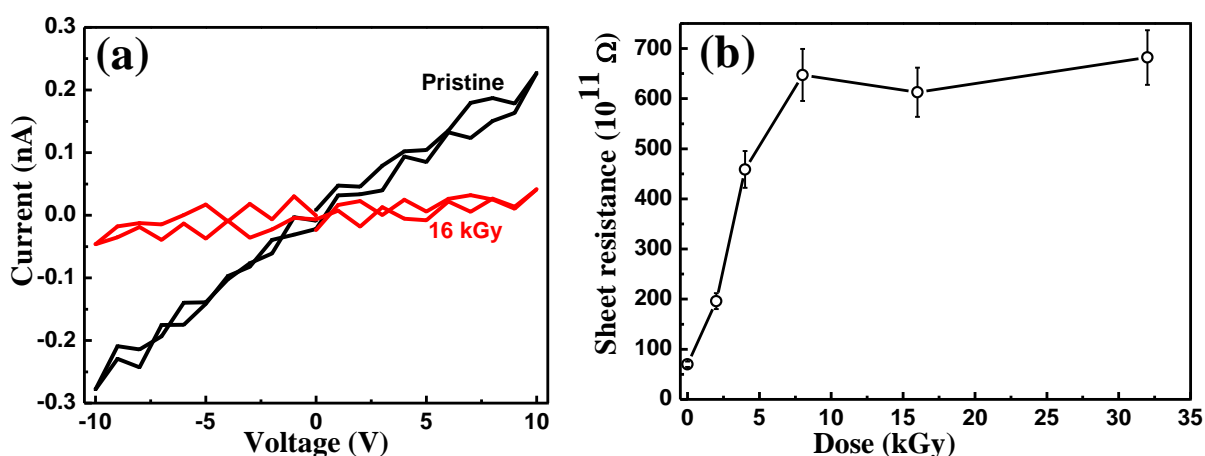


Figure 3.3: (a) Current-voltage characteristics of pristine and irradiated BOPET sheets, (b) variations of sheet resistance with dose.

3.5 Structural characterizations

Structure and morphology modifications in case of BOPET sheets have been investigated through the following characterization techniques.

3.5.1 FTIR spectroscopy

The structural modifications in BOPET as an impact of electron beam irradiation have been investigated using FTIR. FTIR spectrometry data of the pristine and EB irradiated BOPET samples were obtained using Bruker 80 V instrument in the transmission mode. The FTIR results for pristine and irradiated BOPET samples are shown in two wave number ranges and those are $1000\text{-}1350 \text{ cm}^{-1}$ (Fig. 3.4a) and $3350\text{-}3550 \text{ cm}^{-1}$ (Fig. 3.4b). From Fig. 3.4a, it is seen that in comparison to the pristine BOPET, the irradiated BOPET sheets exhibit

the presence of some additional strong absorption peaks at wave numbers of 1028 cm^{-1} , 1146 cm^{-1} and 1305 cm^{-1} . These peaks are attributed to the formation of additional C-O-C (ether) bonds in the irradiated samples [119, 120]. It has been observed that in the irradiated samples the peak at 1146 cm^{-1} shifts to the lower wave number 1142 cm^{-1} with increase of electron beam dose beyond 4 kGy. Similarly the peak at 1305 cm^{-1} which has been assigned to C-O-C stretching shifts to lower wave number 1302 cm^{-1} as the irradiation dose increases [121]. From Fig. 3.4b, it can be seen that all samples exhibit the absorption peak at 3430 cm^{-1} , which is a characteristic of -OH (hydroxyl) group. In pristine BOPET, the -OH group is the terminating group of the PET chains. In the irradiated samples, we observe a strong enhancement in the intensity of the -OH signal which suggest that new -OH groups were created on BOPET sheets as irradiation experiments were carried out in aerated conditions.

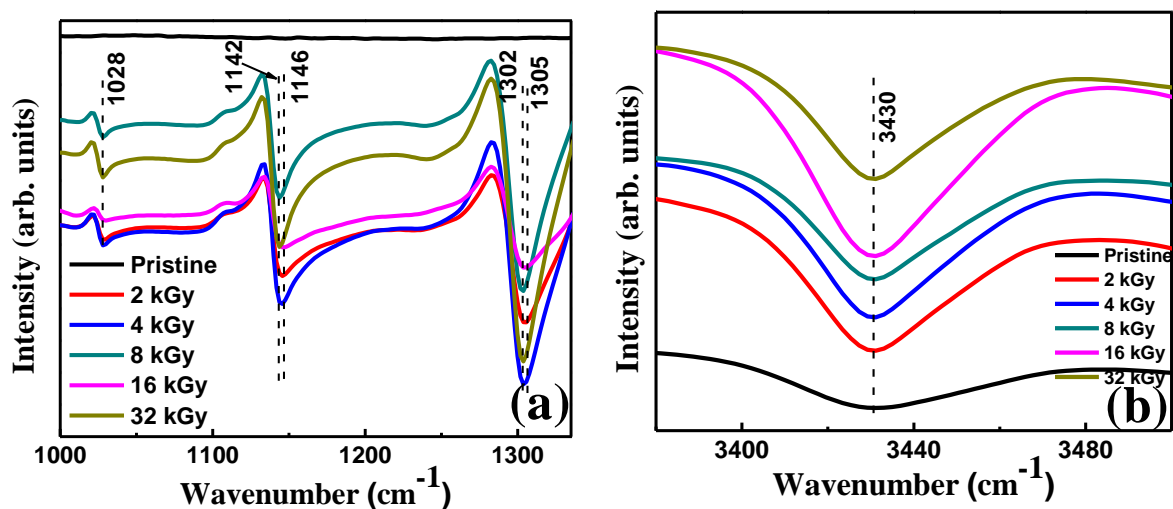


Figure 3.4: FTIR results for BOPET irradiated with different doses.

3.5.2 XRD

In order to see that whether there is a change in the semi-crystalline nature of the BOPET sheet as result of electron beam irradiation, x-ray diffraction (XRD) measurements were carried out. XRD was done in the powder diffraction mode with PANanalytical instrument (model EMPYREAN). Cu K_{α} x-ray was generated with emission current 15 mA,

voltage 30 kV and scans were collected ranging $2\theta = 20^\circ$ - 30° in step size of 0.01° . The results are shown in Fig. 3.5 and it can be seen that for pristine and irradiated BOPET samples the highest intensity diffraction peak appears at 26.06° without any change in the width of the diffraction peak. The full width of half maxima (FWHM) of diffraction peak corresponds to the measure of crystalline nature of the sample [114]. Therefore, from the present XRD results, it can be concluded that the semi-crystalline nature of BOPET sheet remains unaffected by the electron beam irradiation within the said dose regime.

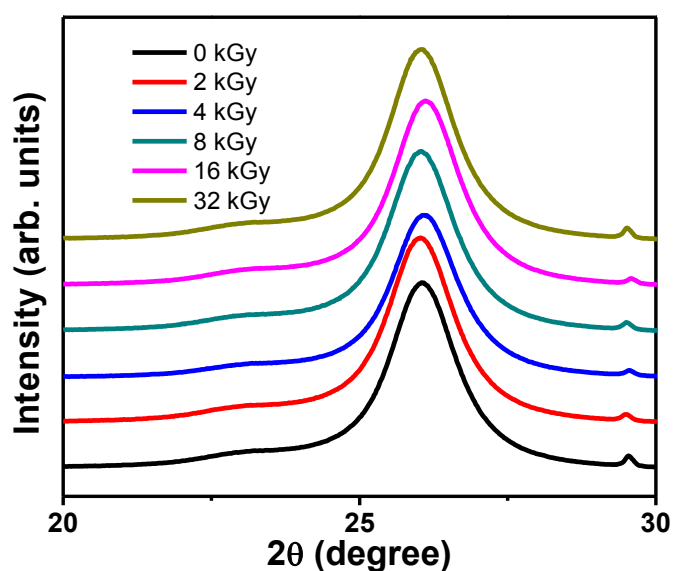


Figure 3.5: XRD data recorded for the pristine and irradiated BOPET samples.

3.6 Surface characterizations

3.6.1 XPS

The surface characterization has been done to check further insight of electron beam induced modifications in BOPET sheets as the irradiation was carried out in aerated condition. X-ray photoelectron spectroscopy (XPS) data were recorded with Mg K_α (1.5 keV) source using DESA-150 electron analyzer (M/s Staib Instruments, Germany). The binding energy scale was calibrated to Au- $4f_{7/2}$ line of 83.95eV. Elemental atomic concentrations were calculated from the XPS peak areas and the corresponding Scofield sensitivity factors

corrected for the analyzer transmission work function. XPS survey scans for pristine as well as EB irradiated BOPET samples are given in Fig. 3.6. It shows the presence of carbon and oxygen. To quantitatively understand the atomic concentrations and chemical bonds, the convoluted spectra of C1s and O1s have been plotted in Fig. 3.7. The C1s spectra for pure BOPET consists of three main peaks at 285 eV, 287 eV and 289 eV which correspond to three carbon environments namely C-C or C-H, C-O and O-C=O (ester group) respectively [122, 123]. Similarly the convoluted O-1s spectra of BOPET shows two separated peaks at 531.8 eV and 533.4 eV attributed to C=O (in ester group) and C-O respectively [124].

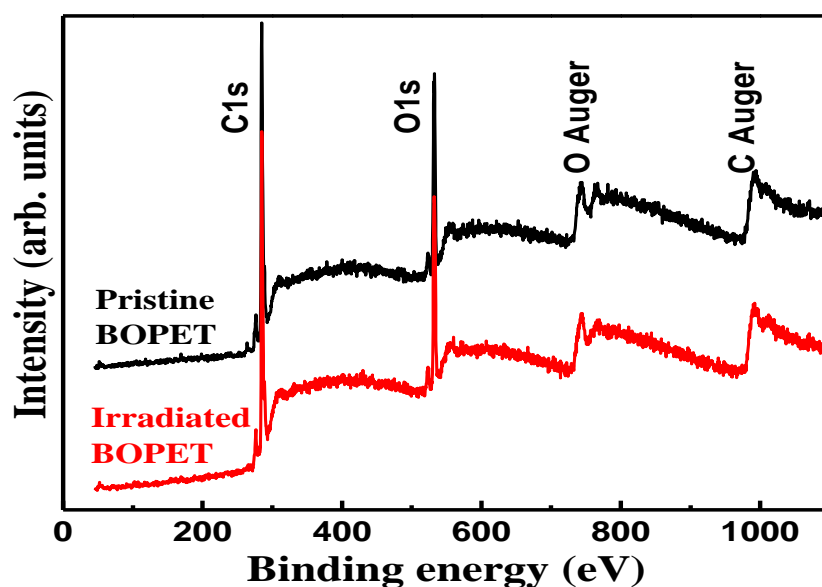


Figure 3.6: Survey XPS result for pristine and irradiated (16 kGy) BOPET sheets.

According to the XPS analysis for pristine BOPET the C/O ratio was found to be 3.0, which nearly matches with the chemical formula $(C_{10}H_8O_4)_n$ for BOPET. The convoluted spectra (shown in Fig. 3.7) were quantitatively analyzed and tabulated (Table-3.1).

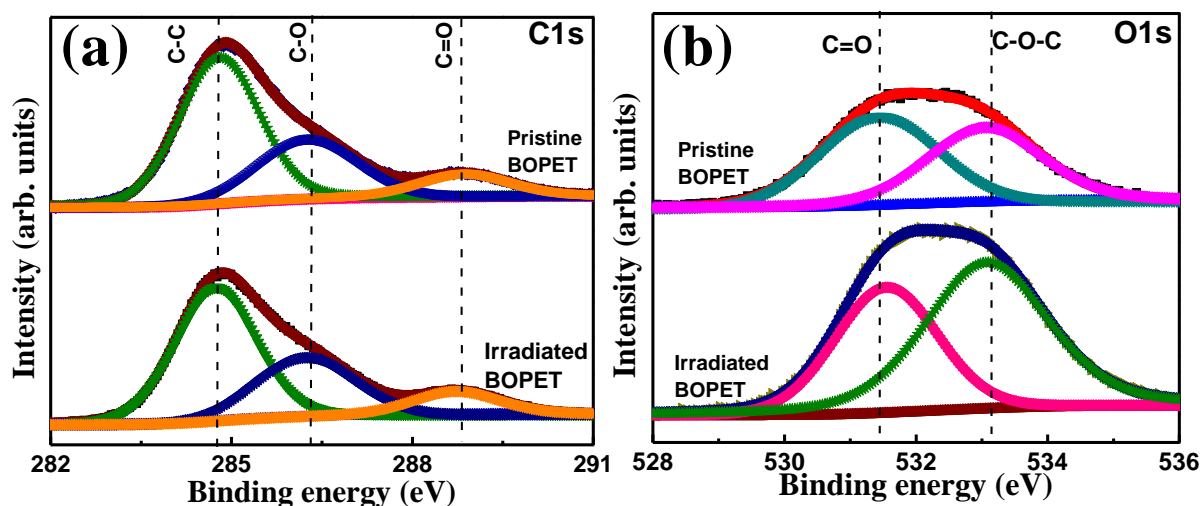


Figure 3.7: Convolved XPS result for pristine and irradiated (16 kGy) BOPET sheets (a) C1s spectra, (b) O1s spectra.

Table 3.1: Chemical composition of the pristine and irradiated BOPET surface determined from the analysis of XPS data.

Sample	C (%) for C-C or C-H	C (%) for C-O	C (%) for C=O	O (%) for C-O	O (%) for C=O
Pristine BOPET	59	29.6	11.4	40.1	59.9
Irradiated (16 kGy) BOPET	56	35.0	9	60.8	39.2

From Table-3.1 it can be seen that on electron-beam irradiation the C1s component corresponding to C-C or C-H decreases a little bit than in case of pristine whereas C-O increases a little simultaneously and C=O components remain nearly same. In addition for irradiated BOPET the major changes are seen in the O1s component corresponding to C-O group, which shows an increase from 40.1% to 60.8%; while C=O component shows a decrease from 59.9% to 39.2%. Interestingly for irradiated BOPET, the full width at half maximum (FWHM) of the O1s component for C=O bonds decreases from 2 to 1.8 eV, while the same for C-O component increases from 2 to 2.2 eV. These XPS results imply that on

irradiating BOPET with electron beam, some new C-O component containing polar groups increase. In addition it can also be concluded that some C-C/C-H bonds that were present in BOPET surface broke due to electron beam treatment, and they recombined with the oxygen to generate additional -OH group [125, 126]. This confirms the generation of new C-O-C bond and additional -OH and this shows well-agreement with FTIR results also.

3.6.2 Contact angle measurements

The static contact angle was determined by telescope- goniometry (M/s Dataphysics, Germany) using static water drop method. The measurements of water contact angles (error $\pm 8\%$) were performed using distilled water on five different positions and the diameter of water drop was around 10 μm . The contact angle variation with electron beam dose is plotted and given in Fig. 3.8.

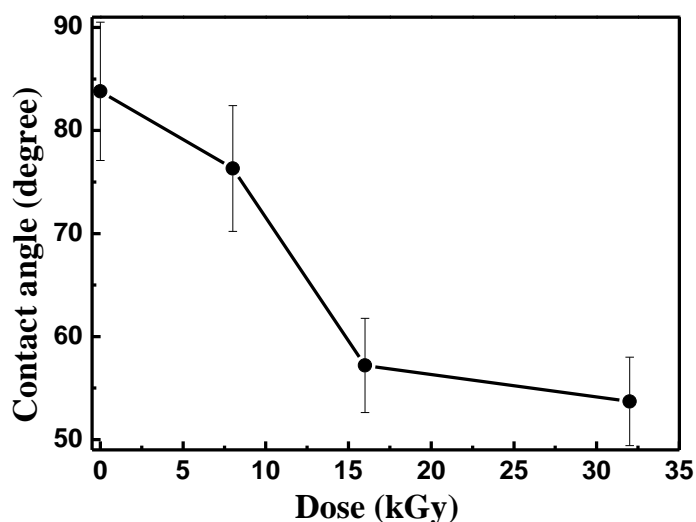


Figure 3.8: Static contact angle variations with electron beam dose for BOPET sheets.

It was observed that the contact angle decreases with electron beam dose which indicates the increase of hydrophilicity with dose. It suggests the production of some more oxygen which contain polar functional groups, especially (-OH) on BOPET surface as a result of electron beam irradiation [126, 127]. Thus the contact angle measurements are in

agreement with FTIR and XPS results also. In order to test the stability of the hydrophilic character of one of the irradiated BOPET sample (16 kGy) contact angle measurements were repeated after 45 days. The contact angle value was $\sim 57^\circ$ during the first day after irradiation and it remained nearly same ($\sim 58^\circ$) after 45 days. It can be concluded that a good stability of the hydrophilic groups created on BOPET surface after irradiation have good stability.

3.7 Sol-gel test for crosslinking analysis

Radiation effects on polymers can be interpreted by two main reactions crosslinking and degradation (or chain scissioning) process [128]. There are no absolute rules for determining the dominance of any one phenomenon for a given polymer. In other words, it cannot be stated that whether any given polymer will crosslink or degrade upon irradiation. In addition, it also depends upon the dose values, for instance, in case of a polymer, up to certain dose main chain scissioning can be a dominant phenomenon while for certain doses crosslinking can dominate or vice versa. Thus, when a polymer is treated by ionizing radiation there can be occurrence of different process like crosslinking or scissioning [129]. Such induced changes can lead to the formation of insoluble gel if crosslinking predominates over scission. By using a proper solvent for the polymer, one can estimate the gel content in the irradiated polymer. To confirm the crosslinking or degradation up on electron beam irradiation, sol-gel analysis has been carried out with Soxhlet extract at elevated temperature around 70°C , using o-chlorophenol as solvent that is regarded as favourable solvent for BOPET [103]. The insoluble gel part was dried under room conditions and weighed using microbalance (M/s AND Company Ltd., Japan make) having accuracy $\sim 100 \mu\text{g}$. Gel content was evaluated using following relationship

$$\text{Gel content} = (W_g/W_i) \quad (3.1)$$

Where W_g and W_i are the weight of insoluble fraction and initial weight respectively [88].

$$S + \sqrt{S} = \frac{p_0}{q_0} + \frac{1}{q_0 P_n D} \quad (3.2)$$

The estimated gel content for pristine and irradiated BOPET has been plotted as a function of dose and shown in Fig. 3.9a. For quantitative evaluation of crosslinking and chain scission yields of irradiated BOPET samples, the Charlesby – Pinner equation (equation 3.2) was used and a plot of $S + \sqrt{S}$ vs. $1/\text{absorbed dose}$ has been generated (shown in Fig. 3.9b) [130].

It is implied from Charlesby-Pinner plot (Fig. 3.9b) that p_0/q_0 is 1.65 and so crosslinking has predominantly been occurred as the ratio is less than 2 [106]. Thus the inferences from p_0/q_0 values, from sol-gel analysis, give an idea about the predominant process (crosslinking/degradation) which the polymer undergoes in the specified dose range. The enhancement in mechanical properties in irradiated samples also conveyed the same process.

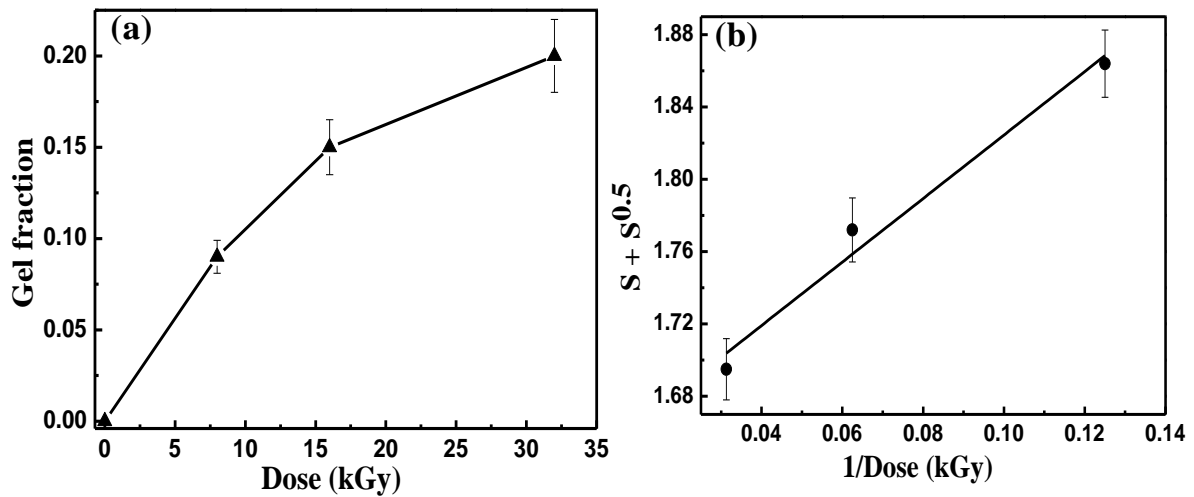


Figure 3.9: (a) Gel fraction of irradiated BOPET under different electron beam doses, (b) Charlesby-Pinner plot for electron beam irradiated BOPET samples. The plot is linearly fitted with $R^2 \sim 0.96$.

3.8 Plausible mechanism for modification of BOPET by EB irradiation

Based upon the characterization results, we describe about the changes that have been brought in the mechanical and electrical properties of BOPET sheet due to electron beam irradiation. Such changes occurred due to the modification of the chemical structure of the BOPET. In BOPET, the PET chains are usually terminated with the $-OH$ end group as shown in Fig. 3.10. In the presence of electron-beam, these $-OH$ end-groups from different PET chains interact and evolve as H^+ and OH^- ions. The end product of this reaction is basically the coupling of PET chains through the formation of diethylene glycol (DEG) and the suggested mechanism is shown in Fig. 3.10 [104, 130, 131]. The presence of C-O-C (ether) peak and high intensity $-OH$ peak in the FTIR data of the electron beam irradiated samples confirm the formation of DEG and creation of OH^- ion in these samples. Since OH^- ions are very reactive, therefore, they may either form H_2O or some peroxide. The enhanced intensity of the $-OH$ peak in FTIR suggests that the released $-OH$ groups are present on the surface of BOPET chain, which has been confirmed by both XPS analysis and contact angle measurements.

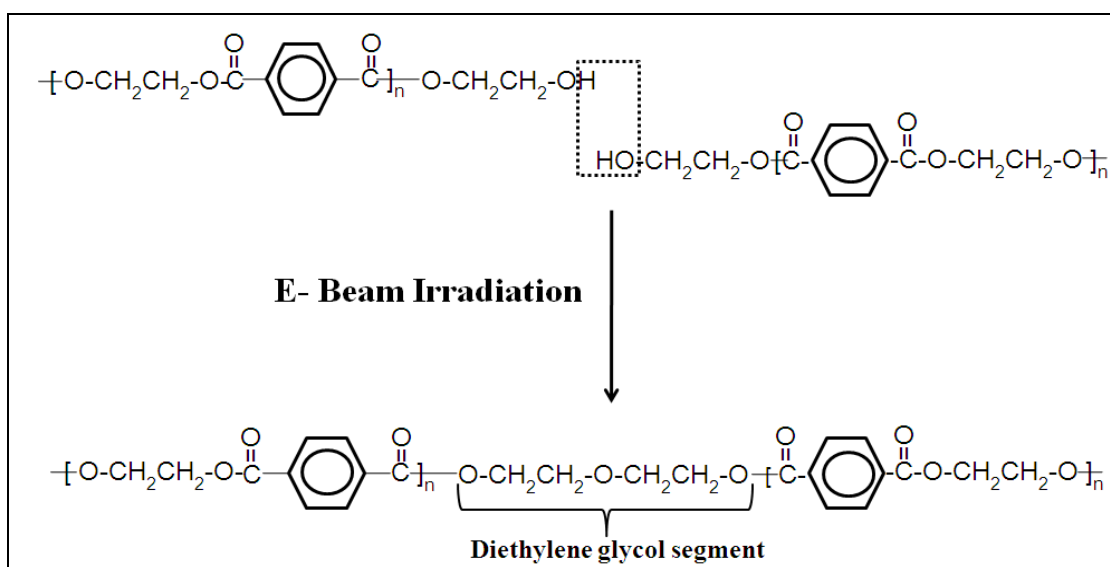


Figure 3.10: Schematic revealing the mechanism of the formation of DEG in BOPET polymer chains as a result of electron beam irradiation.

The sol–gel analysis suggests that crosslinking of PET chains through the DEG segment may result in the longer PET chain length. Such a modification of the internal chemical structure of BOPET may be responsible for the enhancement in mechanical and electrical properties. It is also important to mention that crosslinking and degradation of polymer may occur simultaneously on irradiation. All polymers exhibit an increase of tensile strength for the dose range where crosslinking predominates. However, when no further H-atoms are available to induce crosslinking, the polymer attains saturation or may start degrading [131]. As clear from the Fig. 3.1a, for the studied BOPET, an increase in tensile strength (more toughness/ductility) was observed up to a dose of ~12 kGy which suggests that crosslinking is predominant up to an absorbed dose of ~12 kGy and at further higher doses the saturation in tensile strength indicates that crosslinking has also saturated. It can also be concluded that BOPET sheet irradiated up to 32 kGy can be conveniently used if only strength is the criteria for their usage. Apart from high mechanical strength, the electron beam induced crosslinking has another advantage in usage of BOPET sheet with reference to the “migration phenomena i.e. transfer of substance through polymer sheet to food / medical products”. The migration would decrease as the extent of crosslinking enhances because denser network would hinder diffusion of trapped substances. Indeed, the migration phenomenon is a strong function of the size of trapped substance.

3.9 Conclusions

One of the major applications of BOPET is its use as a packaging material for sterilization of food products and medical devices which requires its irradiation within the practical dose regime (up to 30 kGy). The mechanical properties such as tensile strength, elongation at break, Young’s modulus of packaging material are equally important as sustainability of sterilized products (food and medical commodities) because these properties also determine the shelf life of these irradiated products to avoid recontamination. Our

detailed investigation proposes that the electron beam irradiation of BOPET sheets result in the formation of diethyleneglycol (DEG) chain due to initiation of crosslinking as an effect of irradiation. The study concludes that most of the mechanical properties of BOPET got enhanced on electron beam irradiation along with the electrical resistivity of the samples due to modification caused in its chemical structure. The improved mechanical properties and the electrical resistivity enable BOPET to be a suitable alternative of polyethylene in the packaging industries where stored items need to be radiation sterilized. The chance of degradation/breaking of polyethylene during high dose irradiation is more due to which whole needful aspects of sterilization can go in vain. In addition, this study suggests that BOPET can make possible utilization of flexible electronic components in the high radiation environment.

CHAPTER-4

**ELECTRON BEAM INDUCED MODIFICATIONS
IN ZINC PHTHALOCYANINE FILMS**

In this chapter we have analyzed the effect of electron beam irradiation on electrical and gas sensing characteristics of zinc phthalocyanine (ZnPc) thin film prepared on flexible BOPET sheets. The electron beam irradiation of ZnPc films was carried out using a 10 MeV RF Linear accelerator, under different radiation dose levels from 1 kGy to 30 kGy. The pristine and irradiated films were characterized by using X-ray photoelectron spectroscopy, Atomic force microscopy, UV-Visible spectroscopy and X-ray diffraction. Samples that were irradiated in the dose range of 1-18 kGy exhibited linear enhancement of electrical conductance due to increased adsorption of oxygen. Beyond 18 kGy, the samples exhibited saturation for the amount of adsorbed oxygen as well as in the electrical conductance. The pristine ZnPc films exhibit excellent chemiresistive response towards H₂S gas in 1-20 ppm range at room temperature. The response of the irradiated films decreases monotonically with increasing electron beam dose due to the strong binding of oxygen at the Zn sites. A plausible mechanism of electron beam induced modifications of ZnPc films and its implication on charge transport and chemiresistive gas sensing behavior have been discussed. The work highlights the utilization of ZnPc thin films as potential radiation dosimeter based upon linear rise in electrical conductance along with linear lowering of H₂S response with electron beam dose.

4.1 Introduction

The electron beam irradiation technology involves modification of the physico-chemical properties of organic materials [29]. The nature of interaction between electrons and organic materials depends on the energy as well as dose of the incident electron beam [27]. The metal phthalocyanines (MPcs) have been widely studied organic semiconductor because of their high thermal/environmental stability, low cost and wide range of application including gas sensors [132], organic solar cells [20, 133], organic field effect transistors [22] etc. The intrinsic MPcs are basically insulators and can be converted to p-type semiconductor even when they got exposed to the atmosphere because of the associated surface modifications. This implies that there exists a great possibility of tuning their electrical properties through other means which can introduce surface modifications. In the case of atmospheric exposure, the tailoring of electrical conductivity mainly arises due to the change in electron/hole concentrations because of adsorption of gas molecules at MPc surface [134 – 137]. Therefore, MPcs have been extensively considered as chemiresistive gas sensors. For an organic semiconductor bulk conductivity is a product of the density of charge carriers, their mobility and the charge of an electron/hole. Therefore the change in conductivity not only depends upon change in charge carrier density but crystallinity also, as better crystallinity implies better mobility [6].

Organic semiconductors can be utilized as various types of detectors/sensors, such as chemiresistive, field effect transistors, diode, surface acoustic wave (SAW) and optodes. The chemiresistive detectors are very simple and can be easily fabricated at low cost using organic semiconductors. Hence, we focus on the use of an organic semiconductor as chemiresistive detectors for gas sensing applications. A chemiresistive sensor is basically a resistor whose electrical resistance is very sensitive to the chemical environment. This device is simply an organic semiconductor having two electrical contacts (of metals like Au, Ag etc.)

made on it as shown in Fig. 4.1a and the change in the electrical resistance (i.e. change in electrical current under fixed voltage) is measured as the function of time for a known amount of exposed gas. An equivalent circuit diagram is shown in Fig. 4.1b, which consists of the contact resistances (R_c), bulk resistance of organic semiconductor film (R_B), resistance of interface layers at substrate-film (R_{sf}) and film air (R_{fa}). A change in any of these resistances will result in change of the overall resistance of the sensor.

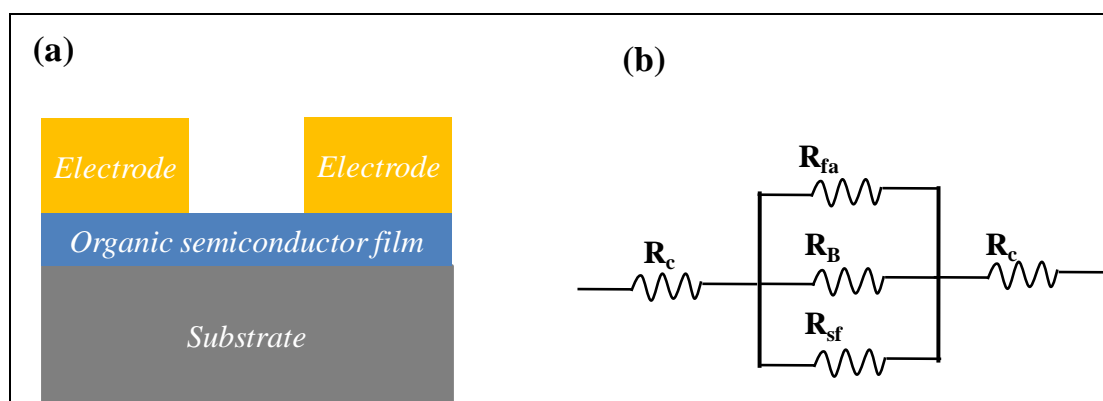


Figure 4.1: (a) Schematic configuration of chemiresistive sensor, (b) its equivalent circuit.

We have chosen zinc phthalocyanine (ZnPc) among other MPcs as it has been less investigated. In the present chapter, we have optimized the thickness of ZnPc films based upon their electrical conductivity and the optimized films have been analyzed further. The modifications that were caused in ZnPc thin films due to irradiation with electron beam (EB) at different doses up to 30 kGy has been investigated. In addition, the pristine as well as irradiated films were compared for the electrical and gas sensing studies. We demonstrate that the surface chemistry as well as bulk structure of pristine ZnPc films gets modified on interaction with electron beam that resulted in the linear enhancement of electrical conductivity up to 18 kGy dose and beyond that it achieved saturation. The linear enhancement in electrical conductivity with dose proposes the possibility of using these films as radiation dosimeters in the mentioned dose regime. The structural modifications, as result of electron beam irradiation, have been explained with the help of UV-Vis spectroscopy,

AFM and XRD. The XPS analysis has been elaborated in details to conclude the modification in surface chemistry of films because of EB irradiation. Film samples irradiated in the dose range of 1-18 kGy exhibited linear enhancements in conductivity because of increased content of adsorbed oxygen but beyond 18 kGy the samples exhibited saturation in the content of adsorbed oxygen on metallic site of ZnPc film. The selectivity of pristine ZnPc films for various gases has been checked and it was found that they exhibited very good sensitivity towards H₂S gas in ppm concentration range at the room temperature. Interestingly in spite of having high electrical conductivity of irradiated ZnPc films, there is a systematic lowering of the response towards H₂S gas with increasing EB dose. The chapter ends with the discussions on probable mechanisms of electron beam induced modification in ZnPc thin film and its implication on charge transport as well as chemiresistive gas sensing characteristics. The chapter also highlights the potential of electron beam irradiated ZnPc thin films for commercial applications. In the present study, three ZnPc film samples have been taken for each set of analysis and each measurement was repeated twice. The deviation from average value has been shown with error bars in the plots.

4.2 Deposition of flexible ZnPc films and thickness optimization

Thin films of ZnPc of desired thickness were deposited on flexible BOPET substrates by vacuum thermal evaporation technique. The ultrasonically cleaned BOPET sheet (size: 20 mm × 20 mm × 100 μm) were used as flexible substrate and the ZnPc film deposition was done at rate ~ 1 Å/s while keeping the substrate at room temperature followed by in-situ vacuum annealing at 100°C for 15 minutes. For electrical measurements, a few pairs of gold electrodes (thickness ~ 50 nm) of size 3 mm × 3 mm having separation of ~ 12 μm, were thermally evaporated on the ZnPc thin film using a metal mask. The electrical conductivity of the films was measured using conventional two probe technique. The linear current-voltage (*I-V*) plot of ZnPc film confirms its ohmic nature of conductivity. The typical current-voltage

characteristics of the films (thickness: 10 nm, 20 nm and 50 nm), that have been recorded during first and subsequent bias scans, in 0 - 100 V range, are shown in Fig. 4.2a – 4.2c.

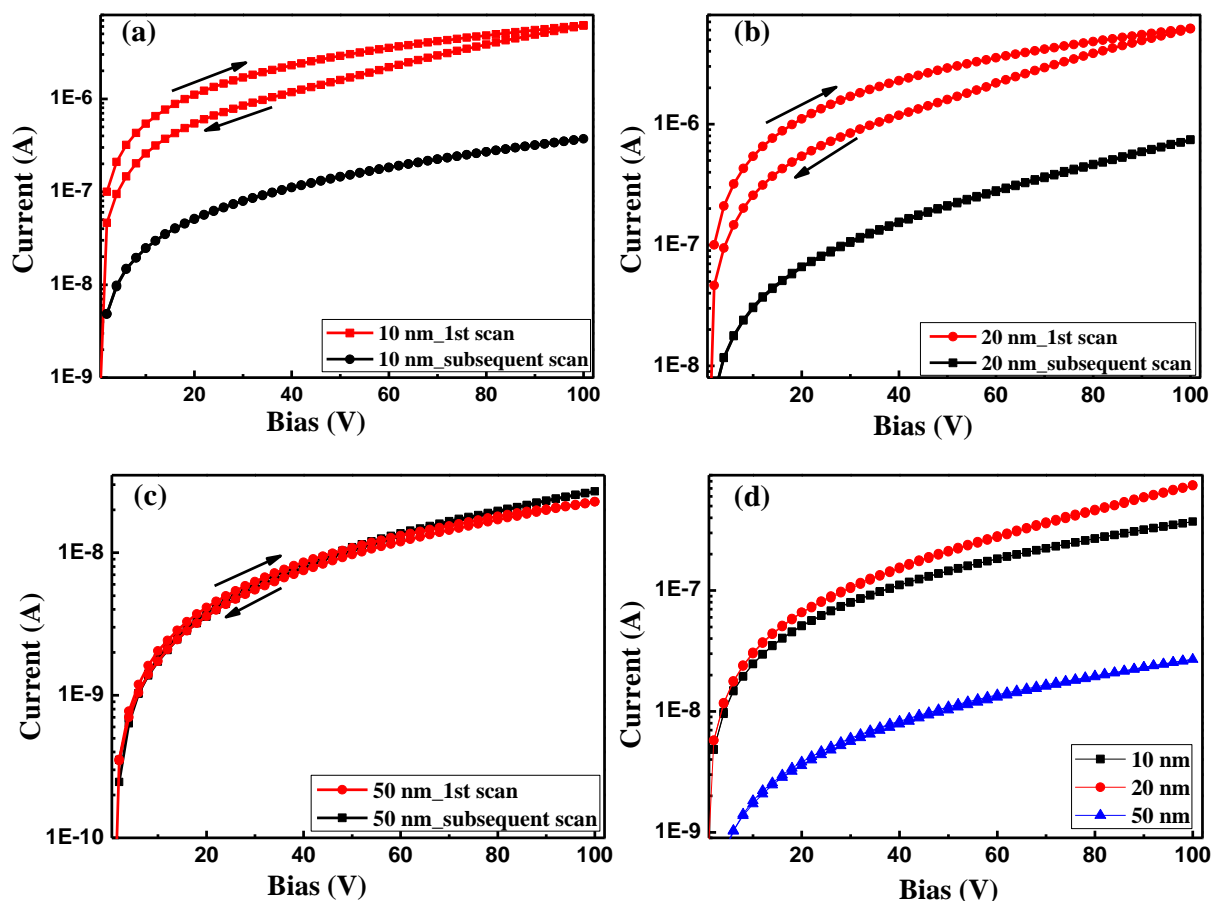


Figure 4.2: Current -voltage plots of ZnPc films during first and subsequent scans for thickness (a) 10 nm, (b) 20 nm and (c) 50 nm; (d) I - V plot for ZnPc films of different thicknesses under stable condition.

It is seen that films having 10 nm and 20 nm thickness show hysteresis in the first scan, which however disappears in the subsequent scans. The subsequent I - V scans are non-hysteretic and highly reproducible. The hysteresis during first scan in these films can be related with the presence of charge traps (probably arising due to the surface defects), which get filled during the first bias scan. During the scan when the field increases, space charge builds up in the ZnPc film due to localization of charge carriers in the traps, which opposes the charge injection during field decrease scan. Actually it is screening of applied bias

because of the existence of an internal electric field created by the trapped electrons [138, 139]. It justifies the lowering of current in decrease bias scan. Once these traps are filled the current becomes stable. On the other hand, 50 nm films show negligible hysteresis in the first bias scan, indicating that at higher thickness films do not have many defects. Under the stable conditions (shown in Fig. 4.2d), the values of current at 100 V for 10 nm, 20 nm and 50 nm films are 3.56×10^{-7} A, 7.67×10^{-7} A and 2.60×10^{-8} A respectively. No such hysteresis has been observed for irradiated 20 nm films which suggest that the traps were filled during e-beam treatments as the result of additional doping.

These results indicate that film having thickness 20 nm is more conductive than 10 nm and 50 nm films. At lower thickness (10 nm) the better structural ordering of ZnPc films on BOPET is attributed to two factors: (i) orientation of PET molecular chains in the substrate plane, resulted in very smooth surface and (ii) presence of polar groups like C=O and O-C=O in PET molecular chains which can electrostatically interact with ZnPc molecules and favors a relatively stronger π - π^* interaction among ZnPc molecules along the PET chains [114]. In such films although structural ordering is good but due to certain substrate roughness, the grain to grain connectivity may not be good hence current is low for films having thickness of 10 nm. With increasing thickness (up to 20 nm) though there exists the effect of molecule substrate interaction but at the same time grain to grain connectivity improves because of thick film surface and as a result, current enhances. With further increase of thickness molecules- substrate interaction becomes weak and thus random orientation of molecules leads to disorder which causes lowering of current [6]. Considering the thickness dependence of current under stable conditions, the optimized thickness of ZnPc films is found to be around 20 nm.

4.3 Electron beam irradiation of ZnPc films

The electron beam irradiation of ZnPc films has been carried out using a 10 MeV electron beam at EBC, BARC, Navi Mumbai, India [29]. The output dose rate is around 1 kGy per pass in the dynamic mode of irradiation under fixed operating parameters and the dose delivery was done by setting appropriate number of passes to get the dose in range of 1 kGy to 30 kGy in steps [131]. In order to protect from dust, the films were kept in a close plastic box of thickness around 2 mm which marginally attenuates 10 MeV electron beam. The irradiation experiments were carried out under atmospheric conditions.

4.4 Surface characterizations using XPS

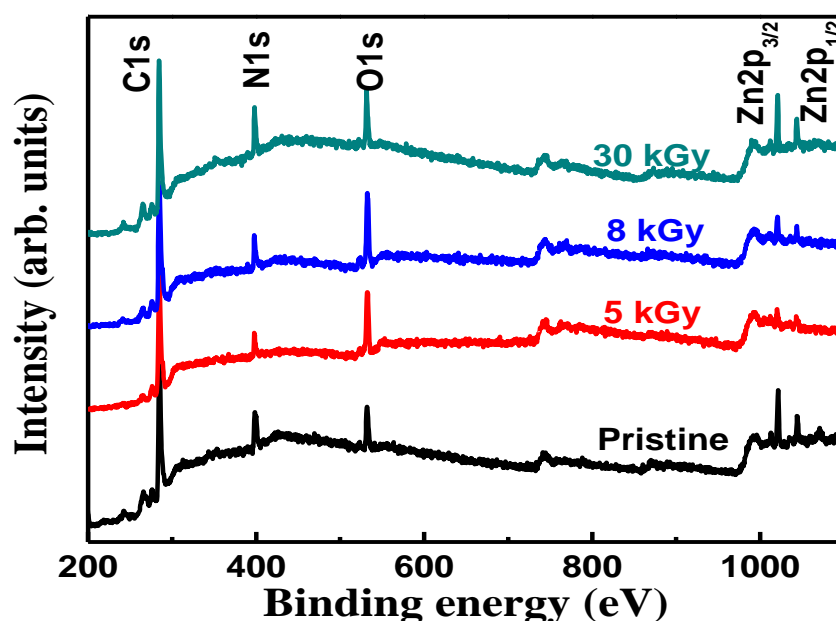


Figure 4.3: XPS survey spectrum of 20 nm ZnPc film grown on BOPET substrate.

The x-ray photoelectron spectroscopy (XPS) of samples was carried out using Mg K_{α} (1.5 keV) radiation under base pressure $\sim 2 \times 10^{-8}$ mbar and the recorded data were calibrated using C1s peak from the adventitious carbon-based contaminant with the binding energy of 284.6 eV. The elemental atomic concentrations were calculated from areas under the XPS peaks and the corresponding Scofield sensitivity factors were corrected for the analyzer

transmission work function. The survey scan XPS spectra of pristine and irradiated ZnPc films is shown in Fig. 4.3 which exhibits the presence of C1s, N1s, Zn2p (as doublet Zn2p_{3/2} and Zn2p_{1/2}) and O1s peaks in the spectrum. The spectrum is in conformity with other MPc [140].

The convoluted XPS spectra of each elements *viz.* C1s, N1s, Zn2p and O1s are shown in Fig. 4.4a - 4.4d. The atomic ratios have been found using area under curve for high resolution C1s, N1s, Zn2p and O1s peaks and respective elemental sensitivity factors. For pristine films the atomic ratios C/Zn and N/Zn were found to be 31.6 and 7.7 respectively which indicated that the pristine ZnPc films had the same chemical composition (C₃₂H₁₆N₈Zn) as that of the source ZnPc material.

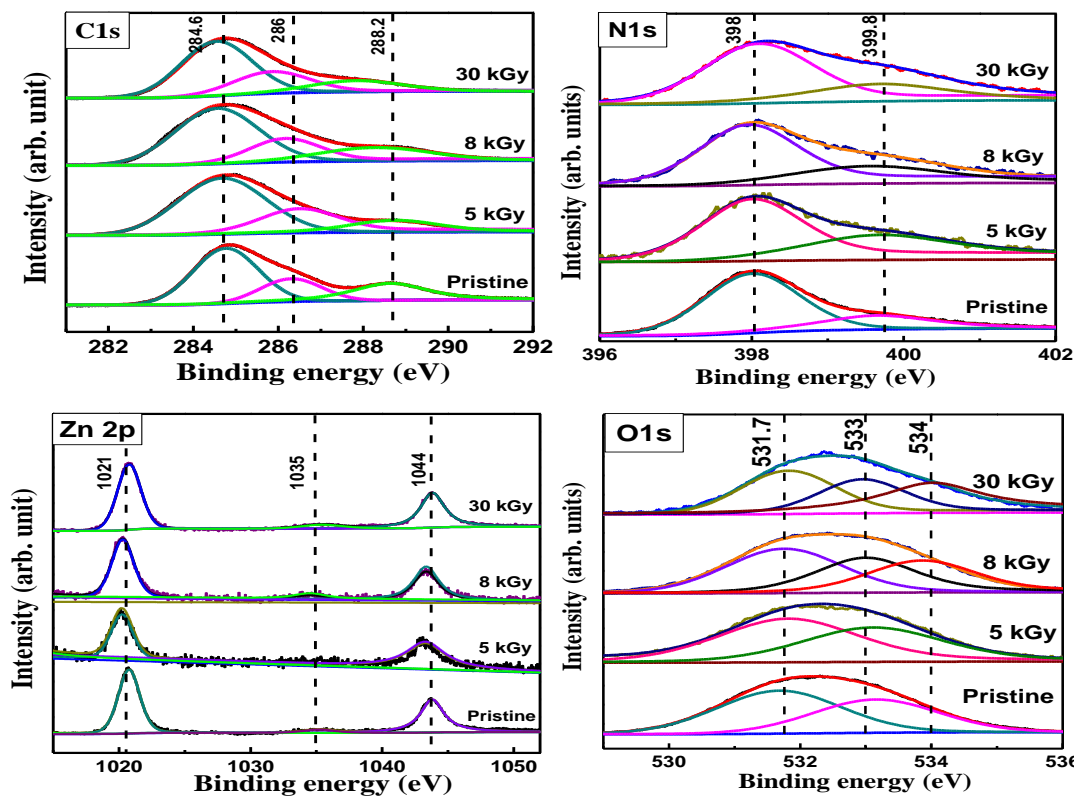


Figure 4.4: High resolution XPS spectra for pristine and irradiated ZnPc films (a) C1s, (b) N1s, (c) Zn2p, (d) O1s.

The high resolution C1s peak (Fig. 4.4a) consists of three main components at different binding energies and those at 284.6 eV attributed to aromatic carbon of the benzene rings, while at 286 eV corresponds to pyrrole carbon linked to nitrogen and the peak at 288.2 eV has been attributed to the shake-up satellite due to $\pi - \pi^*$ transitions [141].

The area ratio of first two peaks, which gives number of C atoms in benzene ring to the number of C atoms in pyrrole ring, is ~ 3 and it is in agreement with molecular structure of ZnPc. As for other PCs, the N1s spectra consist of two peaks; one centered at about 398 eV which corresponds to the pyrrole ring (C-N) without any coordination to the Zn atoms and other 399.8 eV corresponds to the N atom bonded with central Zn atoms (Fig. 4.4b). As seen from Fig. 4.4b, with increase in dose the overall N1s spectrum is extending more towards higher binding energy side. In case of irradiated films, the full width at half maximum (FWHM) for N1s (399.8 eV) peak enhances from 1.8 eV (for pristine ZnPc) and saturates at 2.3 eV. This enhancement of FWHM can be related to the adsorption of O at the Zn site (at the surface) that will pull electron cloud of Zn atoms which subsequently affect the charge distribution of N connected with Zn. XPS technique has a sampling depth of ~ 10 nm therefore overlap of surface N signal with the N buried within depth of 10 nm may give rise to broadening of N1s (399.8eV) peak. The XPS spectra given in Fig. 4.4c represents the Zn2p_{3/2} and Zn2p_{1/2} signal of ZnPc films at 1021 eV and 1044 eV respectively with area ratio of 2:1. In addition Zn-2p spectrum also shows the presence of a satellite peak at binding energy 1035 eV. For pristine films the O1s spectrum (Fig. 4.4d) consists of two peaks, one at 531.7 eV and the other at 533 eV which correspond to physisorbed and chemisorbed oxygen respectively. It is important to note that physisorbed oxygen does not alter the electrical properties of ZnPc. But interestingly it has been seen that with increase in electron beam dose > 5 kGy, the O1s spectrum shows the evolution of a third (new) peak at ~ 534 eV that

corresponds to a strongly bonded chemisorbed oxygen [142 – 144]. This is explained later with help of Fig. 4.5.

The possible explanations for the presence of an additional oxygen peak (at 534 eV) on the surface of irradiated ZnPc films may be due to the generation of ozone (O_3) resulting from the interactions between electron beam and atmospheric oxygen [145]. As a result of electron beam interaction the O_2 molecules dissociates into atomic oxygen, which is highly reactive and recombine with O_2 and makes O_3 . The O_3 easily decays into O_2 and atomic O. The highly reactive atomic O (created initially as well as from the decay of O_3) can easily get chemisorbed at the Zn site [146].

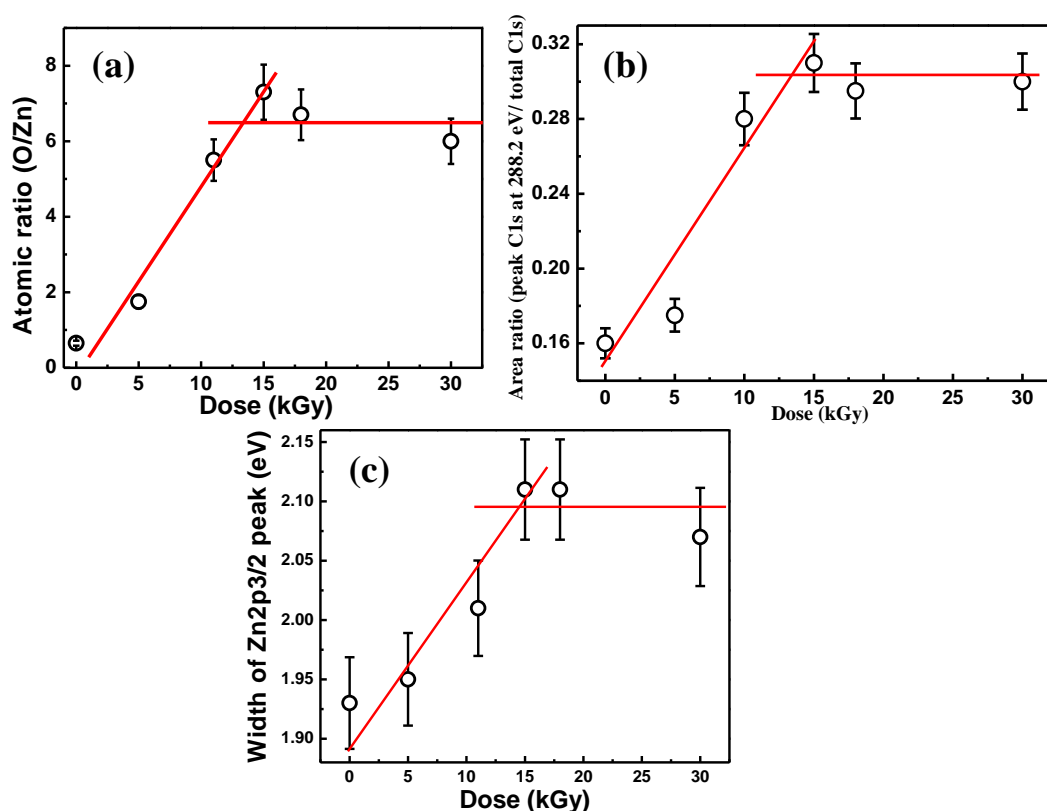


Figure 4.5: (a) Atomic ratios (O/Zn) with respect to dose, (b) variation in area ratio C1s peak at 288.2 eV to total C1s peak with dose, (c) FWHM of Zn 2p_{3/2} peak changes with dose.

This assumption is further supported by the atomic ratio of chemisorbed oxygen and zinc shown in Fig. 4.5a. It can be seen that the atomic ratio O/Zn for pristine films is less than

one which indicates that O is getting adsorbed at the selected Zn. The O/Zn atomic ratio increases (>1) with dose up to 18 kGy, which suggests that with increase in dose more and more oxygen is getting adsorbed at ZnPc surface. The adsorbed O at Zn will pull the electron cloud as a result FWHM of Zn2p peak will marginally enhance (Fig. 4.5c) due to good overlap of the broad peaks of Zn connected with N and Zn connected with O. The enhancement of FWHM of Zn2p_{3/2} as function of electron beam dose and its saturation above dose of 18kGy suggest full coverage of ZnPc films by adsorbed O above 18 kGy dose.

Moreover, it is seen that the relative area of C1s component (at ~ 288.2 eV) with respect to the total C1s peak area enhances with the electron-beam dose and saturates above 18 kGy which suggests delocalization of charge carriers after electron-beam exposure (Fig. 4.5b). Due to the low coordinated structure of ZnPc, the most preferable site for the chemisorption of oxygen is Zn atoms and the chemisorbed oxygen plays a very important role in the electrical conduction in case of ZnPc films. This is because oxygen from ambient gets chemisorbed at the film surface and induces hole as charge carrier in the films through the process: $ZnPc + O_2 \leftrightarrow (ZnPc + h^+) + O_2^-$. Particularly in case of copper phthalocyanine (CuPc) it has been demonstrated that the electrical conductivity increases by three orders of magnitude after exposure to oxygen [147].

In summary, results of XPS suggest that irradiation of ZnPc films with electron beam has chemically modified the surface of ZnPc films by increasing the content of adsorbed oxygen at the surface of films.

4.5 Structural and morphological characterizations

4.5.1 UV-Vis spectroscopy

The changes in bulk of ZnPc films after electron beam irradiation have been investigated using UV–Vis spectroscopy with a double beam spectrophotometer (Jasco, V 530). The typical UV–Vis spectrum of MPc originates from the molecular orbitals within the

aromatic 18- π electron systems and from overlapping orbitals on the central atom. In the near UV-region, the B-band or Sorret band represents the π - π^* transition and appears with a peak position in the range between 325 - 400 nm, depending upon the molecular stacking [148, 149]. However, in the present case, one absorption peak appeared at 340 nm irrespective of the irradiation dose (Fig. 4.6a).

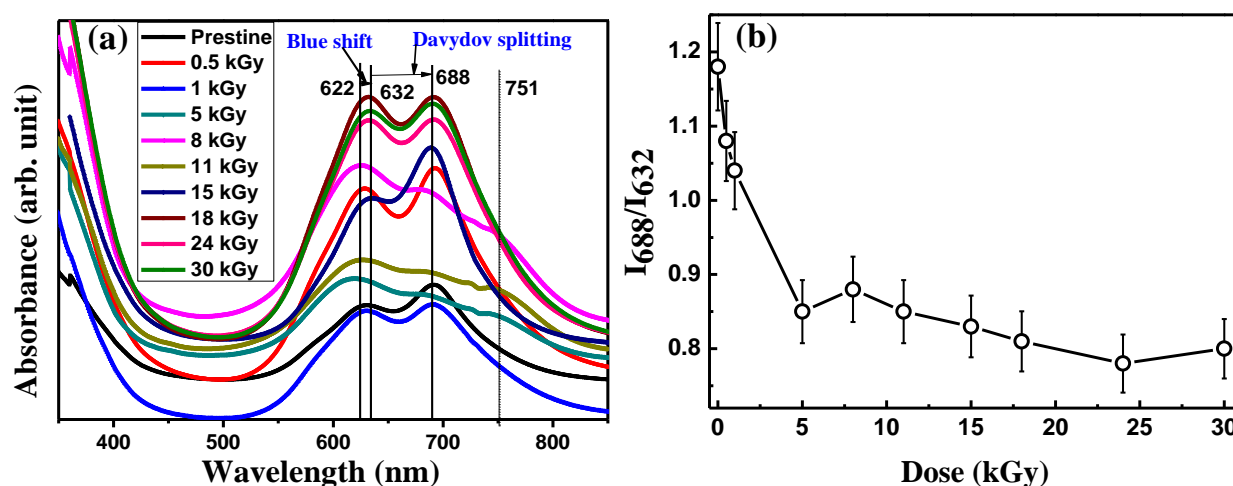


Figure 4.6: (a) UV-Visible spectra for pristine and EB irradiated ZnPc films, (b) variation of intensity ratio of Q band peaks at 688 to at 632 with dose.

The absorption band in the visible region (400-800 nm) which is usually referred to as the Q band, originates from the singlet π - π^* transition in the phthalocyanine ring (intramolecular excitation), and has a doublet due to the Davydov splitting [150]. The extent of Davydov splitting is related to the differences in the relative orientation of molecules, which are close enough to give electronic transitions, called interactions between transition dipole moments from adjacent molecules [151]. Based upon the results of UV-Vis spectra, three inferences can be drawn:

- (i) The relative intensity peaks of Q band at 632 nm and 688 nm change after irradiation.

For pristine films, the intensity of peak at 688 nm is higher comparative to peak at 632 nm (Fig. 4.6b) which suggests that in pristine films ZnPc molecules are arranged in β -

phase [152, 153]. For irradiated ZnPc samples, the relative intensity of peak reverses i.e. the ratio of intensities of peak at 688nm to peak at 632 nm diminishes and saturates after 5 kGy. It suggests that after irradiation the molecular orientation changes in comparison to the pristine films.

(ii) ZnPc films irradiated with electron beam dose ≥ 5 kGy, the Q band becomes broadened exhibiting a new peak around 751 nm (for up to 11 kGy and beyond that it merges with peak at 688 nm), which is an indication of oxidation of ZnPc surface to form a $(\text{ZnPc})^+$ species [154, 155].

(iii) The Q band peak at 632 nm for pristine sample exhibits a systematic blue shift on irradiation. It indicates the presence of electron acceptor gas, like oxygen (in excess) which causes oxidation of ZnPc to form $(\text{ZnPc})^+$ species, and results in the enhancement of electrical conductivity[156].

Thus the electron beam has modified the structural orientation of ZnPc films and also it oxidizes it to form conducting species $(\text{ZnPc})^+$. The oxidation or enhanced doping in ZnPc as a result of electron beam is also supported by XPS analysis.

4.5.2 X-ray diffraction

The structural changes were determined by x-ray diffraction (XRD) which was done in the powder diffraction mode with a PANalytical instrument (model EMPYREAN) using a Cu-K α source ($\lambda \sim 1.5418 \text{ \AA}$). Scans were collected over the 2θ range from 5.5° to 8° in a step size of 0.01° and count time of 0.5 scan/step. The XRD patterns of pristine and EB irradiated ZnPc thin films are shown in Fig. 4.7. It implies that the structural ordering of the pristine ZnPc film with presence of a broad Bragg peak at $2\theta \sim 6.8^\circ$ which corresponds to the (100) orientation of the β -ZnPc phase (as confirmed by UV-Vis also). This indicates that the film is crystalline with a-axis normal to the substrate plane [157, 158]. In addition the calculated value of lattice parameter 'a' (12.40 \AA) suggests that in pristine ZnPc films the molecules are

assembled in the “standing on” configuration [159]. In the “standing on” configuration, the π - π conjugation direction is parallel to the film plane, which is favorable for the in-plane charge transport.

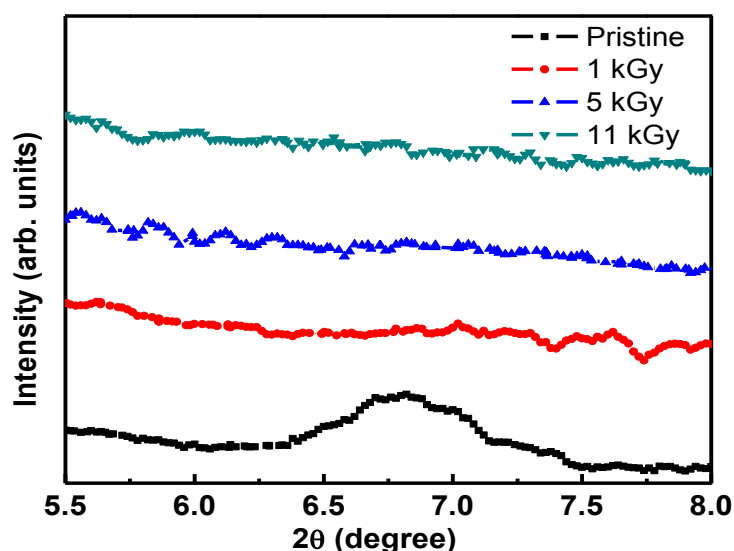


Figure 4.7: X-ray diffraction pattern for the pristine and EB irradiated ZnPc films.

It has been found that in case of the irradiated films the diffraction peak, which corresponds to ZnPc ordering, is missing which suggest that irradiation with electron beam creates structural disorder in the films [160, 161]. The critical analysis of XRD patterns for irradiated film samples indicates that there may be a possibility of presence of two peaks but they might have merged. It suggests that a mixture of both the phases (α and β) is present in the irradiated samples or intermediated phase development takes place as result of high energy electron beam irradiation.

4.5.3 Atomic force microscopy

The surface morphology of the film samples was imaged through Dimension Icon Atomic Force Microscope (AFM), M/s Bruker (CA, USA) make. For AFM Scanasyst-air cantilever of 2 nm tip size and having 0.4 N/m force constant has been used in tapping mode.

AFM images conclude that the surface morphology of ZnPc films got modified after electron beam exposure as shown in Fig. 4.8. It suggests that pristine ZnPc films are polycrystalline in nature and with increase in dose the grains become isolated. In addition it shows the rms value of roughness for the pristine films is around ~ 11 nm which decreases with irradiation and finally, reaches towards saturation.

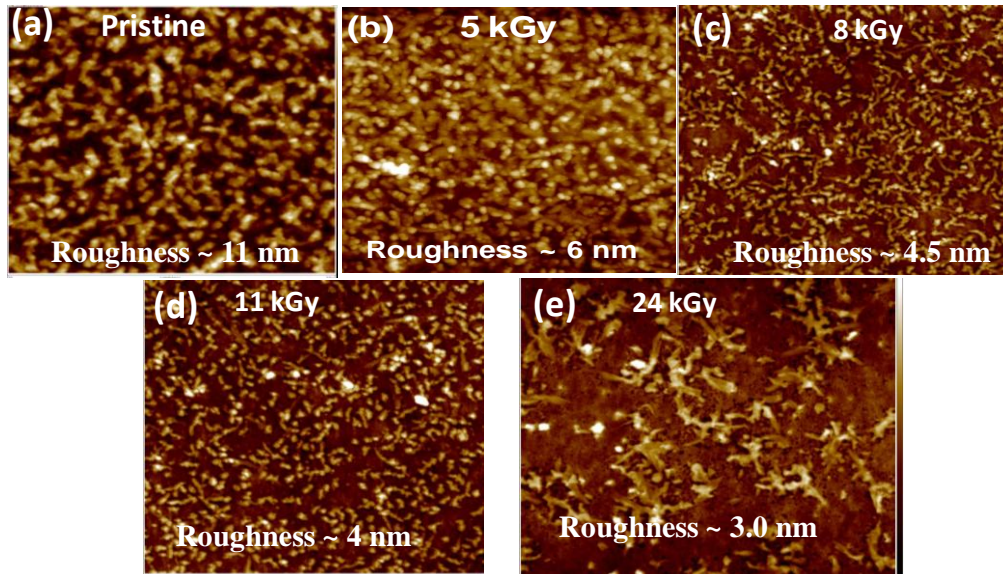


Figure 4.8: AFM images (size: $5\mu\text{m} \times 5\mu\text{m}$) of the pristine and irradiated ZnPc films. Respective dose of electron beam used for irradiation experiment is shown in each image.

4.6 Electrical characterizations

The electrical conductivity of the films was measured using conventional two probe technique. The electrical connections on the sample were made using silver wire of diameter $\sim 100 \mu\text{m}$ and silver paint (Electrolube make) was used to attach the wire with the gold electrodes that were deposited on the films. The current was measured using a voltage source/picoammeter (Model: Keithley 6487) and the data is stored in personal computer equipped with softwares. The Current-Voltage (I - V) curve was plotted by varying bias voltage in range of $\pm 50\text{V}$ (in steps of 1V) and measuring the current.

Typical room temperature I - V characteristics of pristine and irradiated ZnPc films under different doses are shown in Fig. 4.9a. A close observation indicates that I - V curve for pristine is not perfectly linear or ohmic, which is expected for planar device configuration, but it becomes linear in case of irradiated samples.

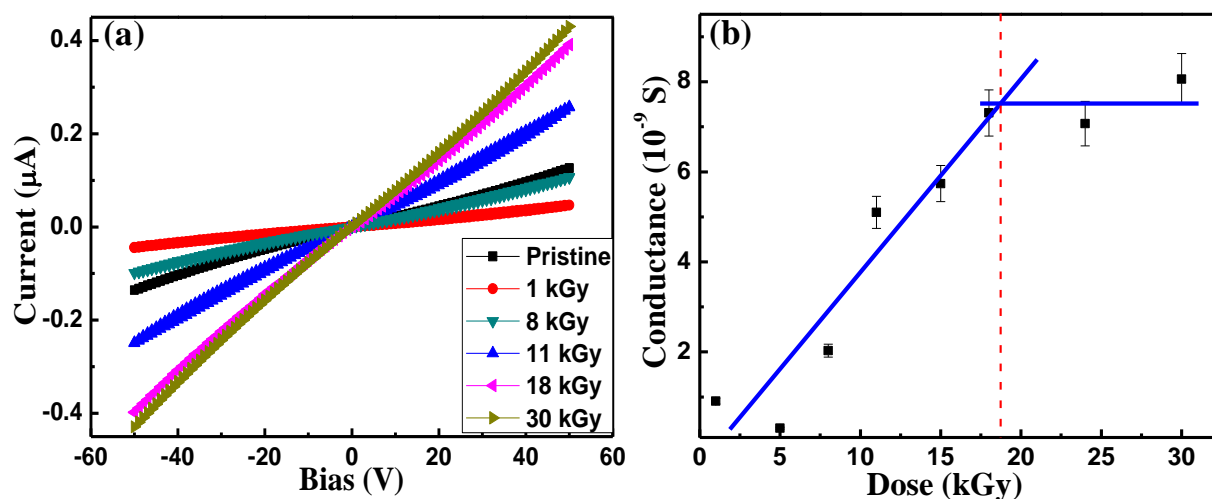


Figure 4.9: (a) Current-voltage characteristics of ZnPc films at room temperature, (b) electrical conductance variation with EB dose for ZnPc film.

The experimental results suggest that electron beam induces more p-type doping in ZnPc. At such improved doping of ZnPc the ohmic conduction (linear I - V) takes place in the films due to the fact that thermally generated charge carrier density is much higher than the injected charge carriers. In addition, there exists matching of Fermi levels of Au and ZnPc. The work function of Au is ~ 5.18 eV and the Fermi level of ZnPc has been reported ~ 4.31 eV [162]. The hole doping of ZnPc by adsorbed oxygen (because of e-beam irradiation) resulted in moving of its Fermi level away from the vacuum level. Hence with better matching of Fermi level of gold with doped ZnPc better charge injection is expected at Au/ZnPc electrode interface [163]. The variation in electrical conductance of ZnPc films with electron beam dose can be divided into two regions (Fig. 4.9b). From Fig. 4.9b, it is noticed that the conductance of ZnPc films increases up to 18 kGy and exhibits a tendency of

saturation beyond that. The explanation for variation in electrical conductance of ZnPc films with electron beam dose is given in section 4.8.

4.7 Chemiresistive gas sensing

For gas sensing the response curves (current versus time data) were recorded for ZnPc films using a static gas testing setup by applying a fixed voltage to the sample. A desired concentration of the test gas in the chamber was introduced by injecting a known quantity of gas using a micro-syringe. Once a steady state was achieved, recovery of films was recorded by exposing the sensor films to atmosphere by opening the lid of the chamber (as discussed in section 2.5.2).

The room temperature detection of H₂S in particular is very important from application point of view as it is a toxic, colorless, flammable, heavier than air, corrosive and inflammable gas produced in sewage, coal mines, oils and natural gas industries and also utilized in many chemical industries. The toxic threshold limit value (TLV) of H₂S gas is 10 ppm [67]. NO₂ is also very toxic gas which causes environmental pollution. It is generated from burning of fossil fuels like coal, diesel and petroleum gases. In addition, it is also responsible for acid rain and its TLV is 25 ppm [164].

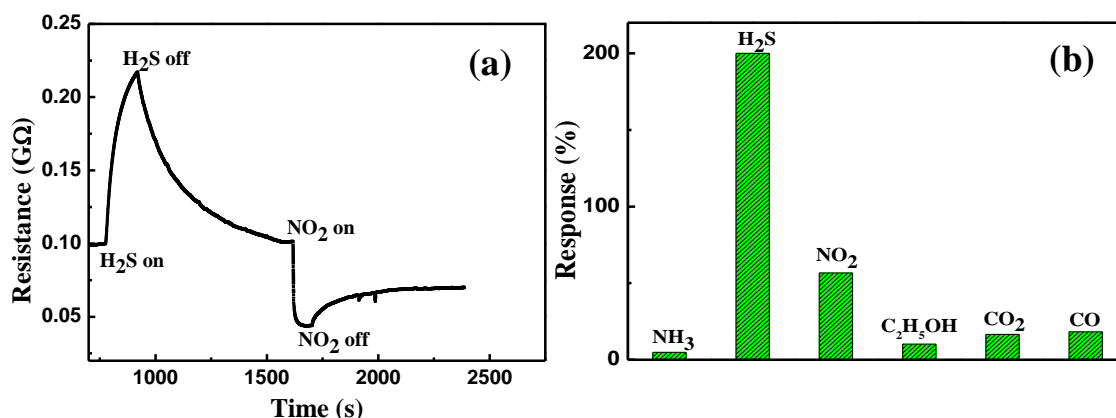


Figure 4.10: (a) Alteration in electrical resistance of the pristine ZnPc thin film on exposure to reducing gas H₂S and oxidizing gas NO₂, (b) selectivity histogram at 5 ppm of each gas of ZnPc thin film based chemiresistive gas sensor.

The chemiresistive gas sensing properties of pristine ZnPc films were studied by investigating the change in electrical resistance of the films on exposure to a fixed concentration of different gases such as NH_3 , H_2S , $\text{C}_2\text{H}_5\text{OH}$, NO_2 , CO etc. The results show that for ZnPc film, the resistance increases on exposure to H_2S while it decreases on exposure to NO_2 due to the opposite tendency (reducing/oxidizing) of these two gases (seen from Fig. 4.10a). Reducing gas donates electron to the ZnPc (a p-type semiconductor) and hence quenches holes as charge carriers, resulting in increase of electrical resistance. On the other hand oxidizing gas picks up the electron from ZnPc and hence lowers down the resistance. Fig. 4.10b shows the selectivity histogram for the ZnPc film based gas sensors and from this it can be seen that the highest response is observed for H_2S . Since ZnPc is p-type organic semiconductor having high hole concentrations in open atmosphere. The oxidizing gases doped more holes which increased its conductivity but not as much in comparison to open air conductivity because the semiconductor has already high hole concentration. The reducing gases neutralize the high hole concentration by donating more electrons and results in large reduction of electrical conductivity as compared to unexposed condition. Since the response (%) is measured as the ratio of change in conductivity with open air conductivity; p-type organic semiconductor is more responsive for reducing gases. H_2S has the highest reducing ability among the selected gases, hence ZnPc exhibited the highest response for this and therefore further emphasis is given for the sensing characteristics of the films for H_2S .

The typical response curve of pristine as well as irradiated ZnPc thin films towards different concentrations (up to 20 ppm) of H_2S gas is specified in Fig. 4.11a, 4.11b and 4.11c. In addition the repeatability of gas sensing characteristics for pristine ZnPc films was also checked at a fixed concentration (5 ppm) of H_2S and results are given in Fig. 4.11d. The obtained data suggest that the response characteristic is highly repeatable.

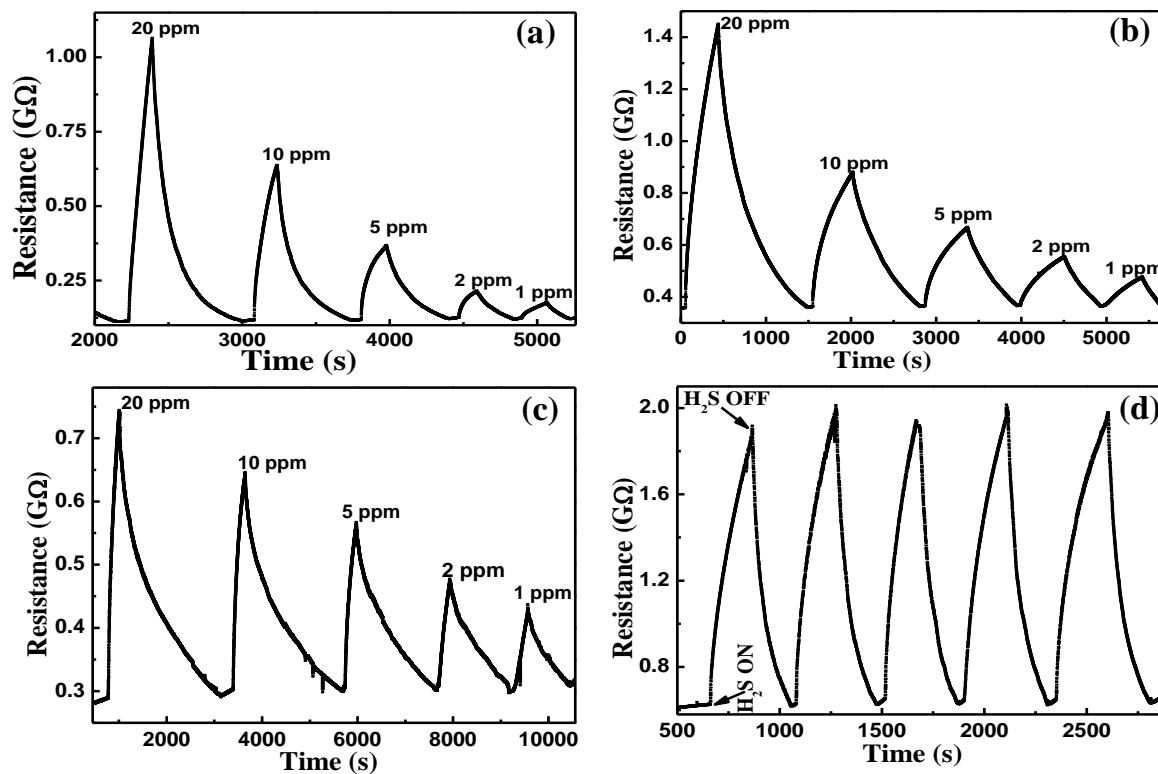


Figure 4.11: Response curves of ZnPc films, for different concentration of H₂S, irradiated with dose (a) pristine, (b) 11 kGy and (c) 18 kGy; (d) repeatability of the response curve at 5 ppm H₂S for pristine ZnPc films.

4.8 Charge transport and gas sensing behavior

Based on the characterization results of pristine and irradiated ZnPc films, we discuss about the charge transport and associated modifications in chemiresistive H₂S sensing behavior. Initially we comment on the variation of electrical conductance with the electron beam dose. As seen from XRD data and AFM images, exposure to electron beam disturbs the ordering of ZnPc molecules and hence one may expect a continuous lowering in electrical conductance with the dose of electron beam. On the other hand XPS and UV-visible data suggest that for higher doses, there is a strong adsorption of oxygen at the surface of the films which results in enhancement of electrical conductivity through hole doping effect. The characterization results also suggest that two phenomena occurred due to e-beam irradiation: one is additional doping and another is bulk disorder or changes. The e-beam exposure causes

additional doping in ZnPc film and it got saturated beyond 18 kGy which is consistent with data shown in Fig. 4.5a i.e. atomic ratio of O/Zn. XRD data (shown in Fig. 4.7) shows that even in case of films irradiated with 5 kGy there is no molecular ordering (absence of Bragg diffraction peak) which suggest that all the irradiated films are in disordered state. In addition UV-Vis results also suggest that the molecular orientation of ZnPc film changes with EB dose as compared to the pristine film but it also got saturated after 5 kGy (Fig. 4.6b). Thus it can be concluded that the structural disordering achieves saturation beyond 5 kGy and then the conductivity is only governed by doping. The conductivity thus attains saturation beyond 18 kGy with saturation of doping.

The enhancement in the electrical conductivity of ZnPc thin films with electron beam dose suggests two beneficial potential applications: (i) The linear enhancement in current with dose (Fig. 4.9b) offers the possibility of using these films as radiation dosimeters up to dose range 18 kGy; (ii) these films can be operated at lower voltage after irradiation, compared to pristine, to obtain sufficient current for different applications (like gas sensors) with the advantage of power-saving. For instance, it can be observed (from Fig. 4.9b) that the film irradiated with 18 kGy dose can deliver an amount of current at 5V bias only, whereas an as deposited ZnPc film requires 25 V bias to deliver almost same current.

The responses of ZnPc films irradiated with different doses of electron beam are plotted in Fig. 4.12. It may be noted that the response increases as H₂S concentration increases for both pristine as well as electron beam treated samples. A typical plot of the response as a function of electron beam dose at a particular concentration of H₂S (2 ppm and 5 ppm) is given in Fig. 4.13a & Fig. 4.13b respectively. Here it is observed that for irradiated films response decreases linearly with increasing electron beam dose and it can be nicely linear fitted with $R^2 = 0.965$ for 2 ppm and $R^2 = 0.895$ for 5 ppm.

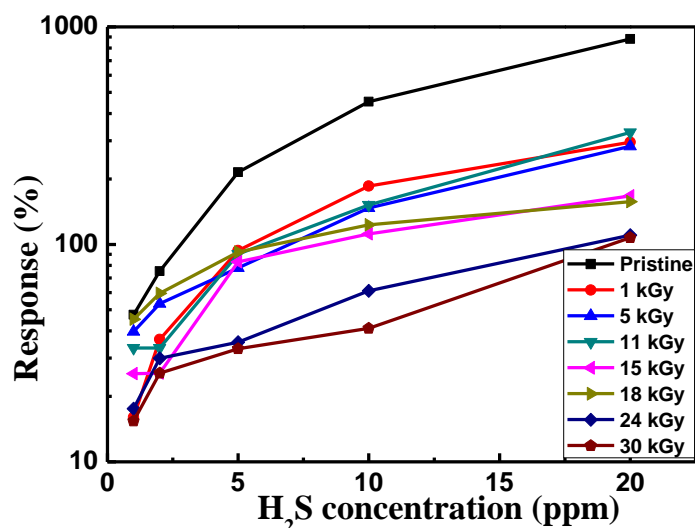


Figure 4.12: Response of pristine and EB irradiated ZnPc films towards H₂S gas sensing.

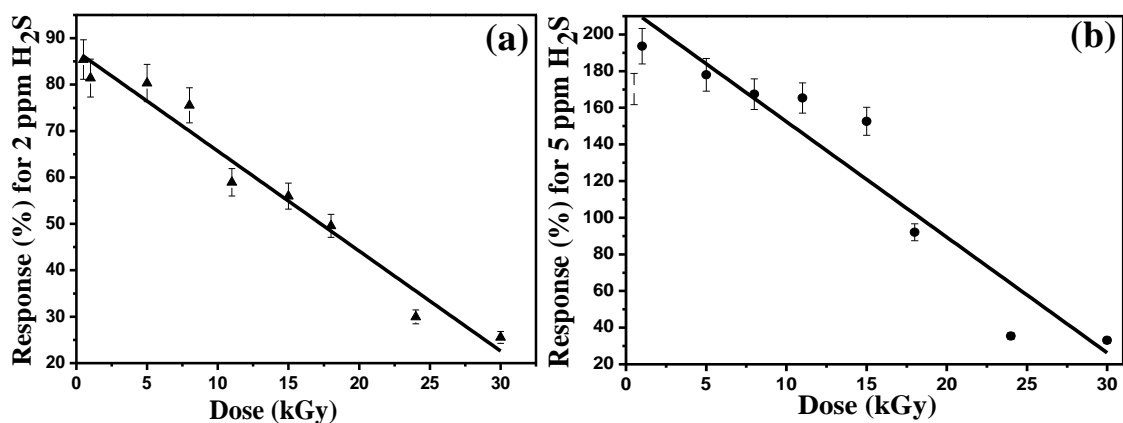


Figure 4.13: Variation in response of ZnPc films as function of irradiation dose for fixed concentration of H₂S gas (a) 2 ppm, (b) 5 ppm.

However, this linear variation in response of ZnPc thin film with electron beam dose (for a known concentration of H₂S gas) facilitates use of ZnPc thin films as potential electron beam dosimeter based upon their gas sensing ability under fixed H₂S concentration. In addition the variations in response and recovery time of pristine as well as irradiated ZnPc films are shown respectively in Fig. 4.14a and 4.14b. It can be observed that films irradiated with higher doses exhibit significant rise in response / recovery time.

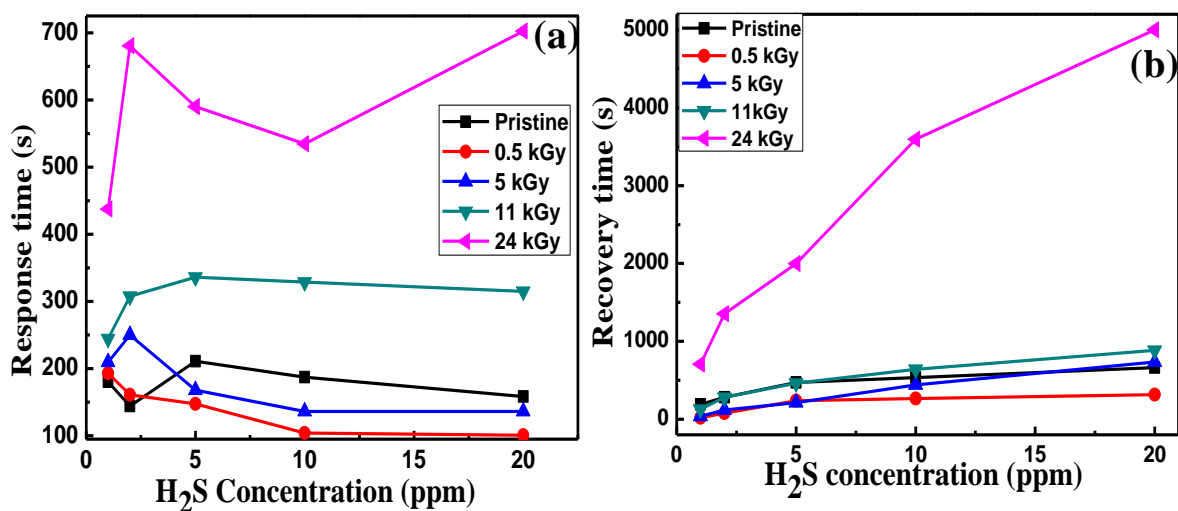


Figure 4.14: (a) Response time, (b) recovery time for pristine and EB irradiated ZnPc films for different concentrations of H₂S gas.

4.9 Plausible mechanism for electron beam induced change in gas sensing behavior

The mechanism of gas sensing in case of metal phthalocyanine thin films can be correlated with their electric conductance, which is regulated by the adsorption of oxygen from surrounding atmosphere. However in literature the interaction between gas molecules and organic semiconductors (OSC) films is attributed to various proposed mechanism such as (i) weak vander Waal interaction, (ii) hydrogen bonding, (iii) charge transfer, (iv) dipole-dipole interactions and (v) hydrophobic/hydrophilic interactions [165, 166]. In case of dipole-dipole interaction mechanism, the polar analytes creates image charges at the metal electrode/OSC interface (shown in Fig. 4.15) and the space charge polarization leads to the modification of work function of the metal contacts [167]. It thus results in facile carrier injection / ejection at films - electrode interface that gets reflected in amended current.

On the other hand Bohrer *et. al.*, reported that in case of metal phthalocyanine films the sensing property is mainly governed by formation of charge transfer complexes with oxidizing or reducing gases [48, 134]. Hence chemiresistive gas sensing mechanisms of organic semiconductor based devices are very complex and still a topic of ongoing exploration [166 168]. In the present study, the gas sensing mechanism in metal

phthalocyanine has been explained based upon the formation of charge transfer complex as shown in Fig. 1.18.

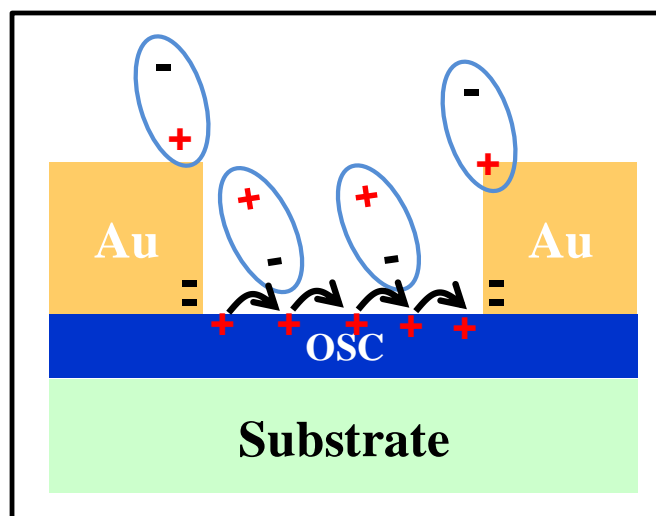
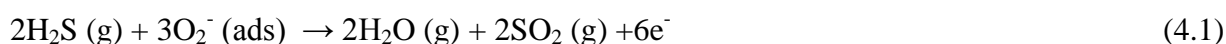


Figure 4.15: Gas analytes dipole interacting with image charges at metal-semiconductor interface and with the charge at grain boundary of p-type organic semiconductor.

As already discussed, ZnPc like other metal phthalocyanine, is an insulator with typical band gap of ~ 1.9 eV and it becomes a p-type semiconductor after adsorbing oxygen from the atmosphere [169]. For such a doped semiconductor, the surface dopant oxygen occupies only a fraction of the binding sites on the films, therefore there are two processes by which reducing/oxidizing gases interact with the ZnPc surface. These gases can bind either to open Zn surface coordination or they can compete with adsorbed oxygen for the occupied Zn surface sites. The competitive displacement of oxygen from the ZnPc surface by H_2S gas can be understood by equation:



When H_2S interacts with adsorbed oxygen groups of ZnPc film it releases large number of electrons in the film. The released electrons neutralize the holes of ZnPc films which results in an increase in the resistance of the samples on H_2S exposure and when the sample chamber is made open, the recovery takes place by picking up oxygen of atmosphere.

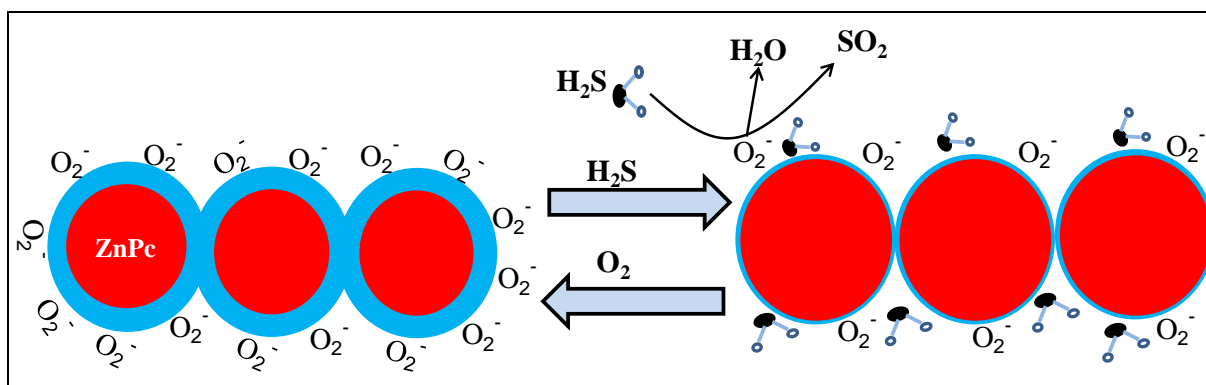


Figure 4.16: Schematic diagram showing the detection of H_2S gas by ZnPc thin film. The blue layer shows the density of hole as charge carriers in the ZnPc films.

The schematic of gas sensing mechanism can be explained with the help of Fig. 4.16, where the conducting layer (rich in holes) at the surface of ZnPc grains is shown by blue layers [136]. Here on exposure to H_2S gas the conducting layer shrinks and the resistance of films enhances. Now as confirmed by the XPS and UV-vis data that in an irradiated (with higher doses) ZnPc samples, there is extra strongly bonded oxygen (at binding energy of 534 eV) in addition to the weakly bonded oxygen (at binding energy of 532 eV) which undergoes a competitive displacement by H_2S . Such strongly bonded oxygen may primarily attach to the free Zn site (due to large electron density) as well as to the organic part of ZnPc [170]. The lowering of response and rise of response time in case of irradiated ZnPc films suggest that in such samples it may be difficult to replace such strongly bonded oxygen by H_2S gas. Therefore a reduction in interaction sites for H_2S gas resulted in the decrease of response with increasing dose of electron beam. In addition, we have also plotted the slope of response versus dose data for each concentration of H_2S gas (Fig. 4.17). It can be seen that slope increases with increase in H_2S concentration, suggests that gas sensing properties declines with increasing dose of electron beam. The increasing slope of the response versus dose curve with increasing H_2S concentration also implies the loss of interaction sites for H_2S gas [170].

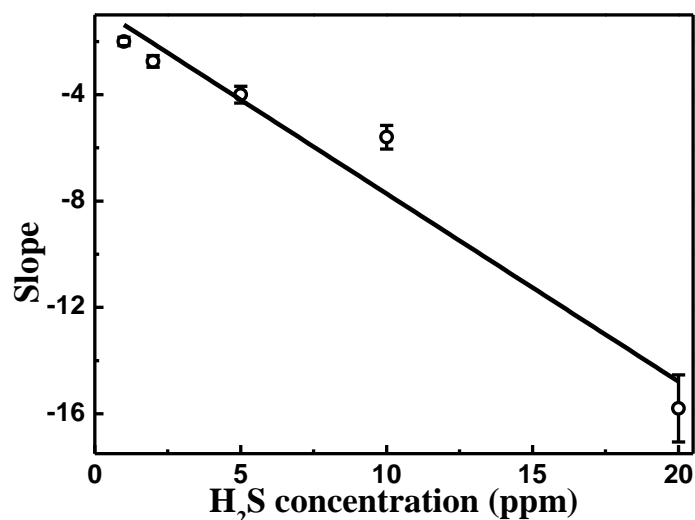


Figure 4.17: Slope of response versus dose as function of H₂S concentration.

However the important positive aspect of linear lowering of response (for a known concentration of H₂S gas, as evident from Fig. 4.13a & 4.13b) with electron beam dose is to facilitates the use of ZnPc thin films as potential electron beam dosimeter based upon their gas sensing ability.

4.10 Conclusions

The effect of electron beam irradiation on modification of flexible ZnPc thin films and consequences of such modification on electrical and chemiresistive gas sensing properties were investigated. Detailed characterizations of samples by UV-Visible spectroscopy, AFM and XRD suggest that the interaction of electron beam creates structural disorders in the films. XPS analysis indicates the presence of strongly bonded oxygen on the surface of irradiated ZnPc films with higher doses. Such strongly bonded oxygen enhanced hole doping in the film which resulted in linear rise in electrical conductance of the films with dose, up to 18 kGy. This linear variation of electrical current with dose facilitates the utilization of ZnPc thin films as potential radiation dosimeter. In addition, irradiated ZnPc films, having higher electrical conductance, can deliver more current at low voltages and

therefore, they can be operated at low bias for different device applications, like gas sensors, with the advantage of power saving.

The film dosimeters are most popular for routine dosimetry application in electron beam facilities because of their excellent material-material and material-air interface characteristics. They can be used inside bulk of the material to know the dose at point of interest. The thickness of film dosimeters is in the order of micron and therefore it didn't create any air void inside material which can hamper the dose uniformity. In addition it doesn't attenuate the beam energy significantly and in this way it doesn't interfere in irradiation of a product to get a requisite dose. One of the major drawbacks with conventional film dosimeters is its dependence on visible light. If these films are exposed pre or post irradiation with visible light, their optical density changes and thus the dose values cannot be accurately measured. To overcome the above problem ZnPc thin film based radiation dosimeter can act as a technical alternative because it is almost stable in visible light as well as normal environmental conditions.

In addition the pristine ZnPc films exhibited excellent chemiresistive response towards H₂S gas in 1-20 ppm range. The response of irradiated films decreased monotonically with increase in electron beam dose. Since strongly bonded oxygen atoms are attached to the Zn sites therefore such a loss of interaction sites for H₂S results in the decrease of response with the increasing electron dose. The essential part of linear drop of response (for a fixed concentration of H₂S gas) with electron beam dose is that it makes possible to use ZnPc thin films as potential electron beam dosimeter based upon their H₂S gas sensing abilities.

CHAPTER-5

**MODIFICATIONS IN CONDUCTING POLYMER
FILMS THROUGH ELECTRON BEAM**

This chapter deals with the electron beam irradiation effect on the conductivity and chemiresistive gas sensing characteristics of conducting polymer polyaniline-silver (PANI-Ag). PANI-Ag nanocomposite films doped with HCl were prepared on surface modified BOPET by in-situ photo-polymerization. The grown films were modified with 10 MeV electron beams at different doses (0-100 kGy). Post irradiation, the electrical conductivity of the PANI-Ag films was initially found to be enhanced by two orders of magnitude up to 30 kGy and later it falls with increasing dose. The rigorous characterizations of the films suggest that enhanced conductivity up to 30 kGy of electron beam dose is due to scissioning as well as additional doping of chlorine in PANI chains, through breaking of covalently bonded chlorine with PANI chains. At higher doses, crosslinking of polymer chains dominates and results in lowering of electrical conductivity. As compared to pristine film, electron beam modified PANI-Ag films exhibited higher sensitivity towards ppm level of H₂S gas.

The present chapter also includes the effect of high radiation on the electrical properties of PEDOT:PSS films to manifest the scope of this polymer in high radiation field and its suitability for radiation dosimeter applications. Thin films of PEDOT:PSS were deposited on flexible polyimide (Kapton) sheets and irradiated up to 75 kGy dose with 1 MeV electron beam. The conductivity of as deposited polymer film was ~ 3.2 S/cm which consistently falls to ~ 0.76 S/cm after getting 75 kGy. The detailed analysis of the samples using XPS, contact angle measurement and solubility test suggest that the lowering of electrical conductivity in irradiated sample can be attributed to the crosslinking of PEDOT chains and dissociation of PSS.

The study highlights the effect of electron beam irradiation on PANI-Ag and PEDOT:PSS films in terms of electrical conductivity, crosslinking and its inferences on H₂S sensing.

5.1 Introduction

In last two decades, conducting polymers have attracted broad interest because of its various applications in sensors [171], organic light emitting diodes (OLED) [172], batteries [173], solar cells, electromagnetic shielding [174], coating for metallic surfaces [175], thermoelectric etc. Conducting polymers are quite interesting for device applications because less expensive, flexible, solution processable and above all they are non-toxic in nature [176, 177]. Among many conducting polymers, polyaniline (PANI) is one of the most extensively studied conducting polymer due to its unique acid base chemistry, ease of synthesis, biocompatibility, stable electrical conduction and high environmental stability [52, 178]. Nanostructures of PANI have received much attention as sensor materials because of high surface area and fast diffusion of gas molecules into the structures [179 - 181]. PANI nanostructures in the form of nanofibers, nanorods and nanowires can be prepared by different methods such as templates, surfactants, interfacial polymerization and electro-spinning. However there exists a new class of materials called conducting polymer-metal nanocomposites which can provide device design possibility with new functionality, by combining the properties of both the organic/inorganic realms [182 - 187]. Embedding metallic nanoparticles in PANI is one of the attractive strategies to harness its sensing [188], electrochemical [189] and catalytic properties [190]. In the context of chemiresistive gas sensor based on PANI, the incorporation of suitable metal in PANI matrix not only improves the sensitivity but also the selectivity towards a particular gas [191, 192]. In literature, nanocomposites of PANI with different metals including PANI-Ag [193], PANI-Au [194], PANI-Pt [195] and PANI-Cu [196, 197] have also been reported.

In the midst of various nanocomposites, PANI-Ag is gaining extensive consideration because it can be simply prepared by in-situ approach i.e. using direct oxidation of aniline by Ag^+ in the presence of UV irradiation [198], γ irradiation [199] or chemical polymerization in

ionic liquid media [200]. For device applications such as displays, electronics, gas sensors, super capacitors etc, PANI-Ag nanocomposite films deposited on flexible substrates are required. In order to improve the adhesion and uniformity of the deposited PANI-Ag films over flexible plastic substrate, the surface modification of substrate using suitable coupling agents is necessary [201].

In addition to polyaniline-silver (PANI-Ag) nanocomposite, poly(3,4-ethylenedioxythiophene):poly(styrenesulphonate) i.e. PEDOT:PSS, owing to its high conductivity and commercial availability, is also presently considered as one of the most successful polymer for various device applications including thermoelectric, organic light emitting diodes etc. Scope of conducting polymers in various device applications is determined by their electrical conductivity. However charge transport mechanism in polymers is governed by inter and intra-chain hopping. Exposure to high energy radiation often leads to crosslinking or scissioning of polymer chains. Hence on irradiation structure as well as morphology of polymers gets modified resulting in modification of conductivity. Therefore we have investigated the effect of high radiation on the electrical conductivity of conducting polymer films of PANI-Ag and PEDOT:PSS to manifest the scope of these polymers in high radiation field and also to use it as potential radiation dosimeter.

In this chapter, we report electron beam induced modification in PANI-Ag nano composites films grown on flexible APTMS modified BOPET substrates by in-situ photopolymerization as well as the same for PEDOT:PSS films deposited on flexible polyimide by drop cast method. The PANI-Ag films were modified with high energy (10 MeV) electron beams at different doses (0-100 kGy) using Linear accelerator. After electron beam exposure the electrical conductivity of the PANI-Ag films was initially found to be enhanced by two orders of magnitude up to 30 kGy of dose and later it lowered down with increase in dose. The detailed characterization including FTIR, PL, XPS, UV-Vis, SEM and solubility analysis

have been carried out and results have been discussed. The chapter highlights the effect of electron beam irradiation on PANI-Ag films in terms of electrical conductivity and its inferences on H₂S gas sensing.

Thin films of PEDOT:PSS were irradiated up to 75 kGy dose with 1 MeV electron beam. The conductivity of as deposited polymer film was ~ 3.2 S/cm which consistently reduced to ~ 0.76 S/cm after getting 75 kGy. The modification in surface morphology and plausible mechanism which is responsible for tailoring the electrical conductivity of PEDOT:PSS films because of electron beam irradiation have been discussed in the present chapter.

5.2 Photo-polymerization of PANI-Ag nanocomposite films

In-situ deposition of polyaniline-silver on BOPET surface through photo-polymerization has been described as follows.

5.2.1 Modification of BOPET substrate using APTMS

As obtained aniline (Sigma-Aldrich, purity 98 %) solution was purified through vacuum distillation process, before utilization. The deionized (DI) water was used for washing and solution preparation. BOPET sheets of thickness ~ 100 µm, procured from M/s DuPont, were cut into desired size for the experiments. The pieces of BOPET were ultrasonically washed. It is desirable to provide very good adhesion and directional growth of PANI-Ag films on flexible BOPET substrate. Therefore surface modification of BOPET was carried out by a surface anchoring group (3-aminopropyl)trimethoxysilane (APTMS) layer which was used as received from M/s Sigma-Aldrich having purity ~ 97%. For this purpose, first the surface of BOPET was hydroxylated by dipping it in the potassium hydroxide (KOH) containing dimethyl sulphoxide (DMSO) solution. The solution is prepared by dissolving 160 mg KOH in 30 ml of DMSO and 5 ml DI H₂O. The sheets were left to react with KOH

solution for 30 minutes, then thoroughly washed in distilled water and dried. The hydroxylated BOPET sheets were now dipped in an APTMS solution which contains 112 μl APTMS in 25 ml of ethanol and 1 ml of acetic acid. The hydroxylated BOPET sheets were left in solution for 72 hours to allow reaction to take place. Later these modified BOPET sheets were thoroughly cleaned using ethanol and dried for 1 hr at 60°C in an oven. The scheme for grafting of APTMS layer at hydroxylated BOPET surface is elaborated in Fig. 5.1. This process is also called ‘silanization’ which can be briefly explained in two steps.

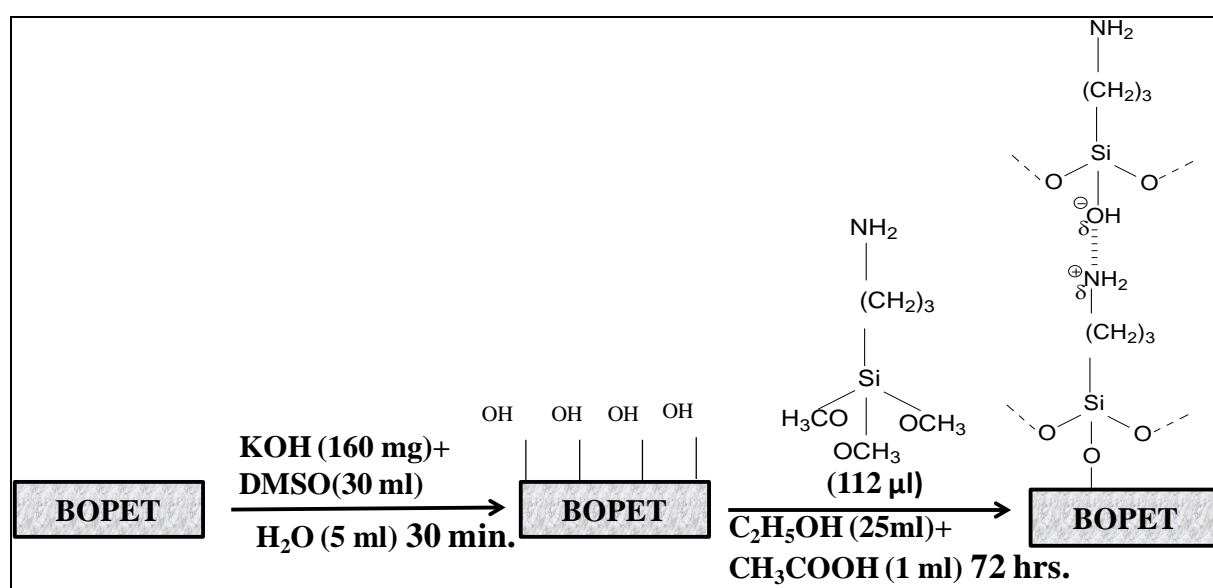


Figure 5.1: Representative schemes for surface modification of BOPET substrate with APTMS.

First step includes the hydrolyses of silane head groups which reach close to the substrate due to adsorbed water layer (inherently present) on the surface. While the second step includes formation of covalent bonds between $\text{Si}(\text{OH})_3$ and hydroxyl groups on BOPET. Thus APTMS layer has been grafted upon BOPET surface and the modified BOPET has been characterized through XPS. The XPS survey scan, shown in Fig. 5.2, suggests that untreated BOPET possess two peaks corresponding to C1s and O1s whereas the APTMS modified BOPET shows two additional peaks at 400 eV and 102 eV which confirms the presence of N1s and Si2p respectively at the surface of BOPET [164, 202]. The ratio of N/Si was around

2.0 which closely agreed to the reported value for silanes grafted on ITO surface [202, 203].

The convoluted spectra of N1s and Si2p have been shown in Fig. 5.3.

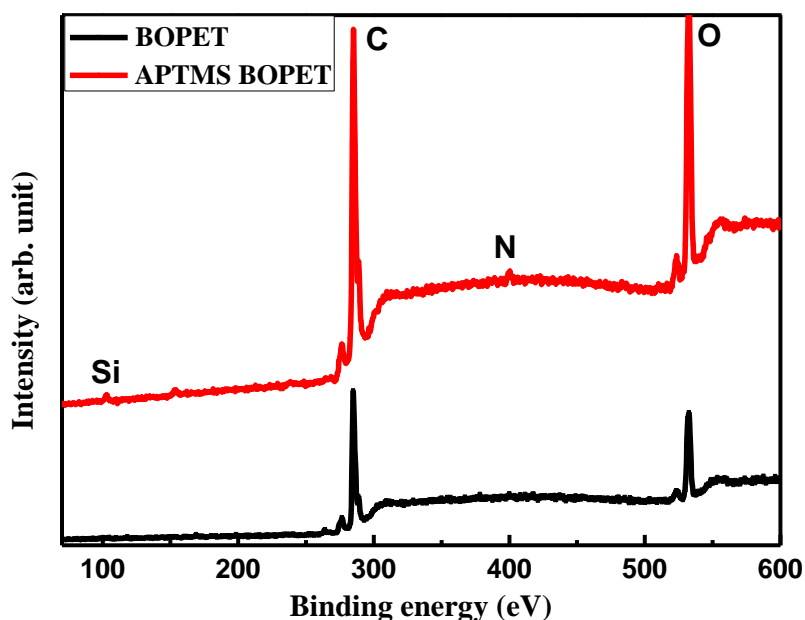


Figure 5.2: XPS survey spectra of BOPET and APTMS treated BOPET substrate.

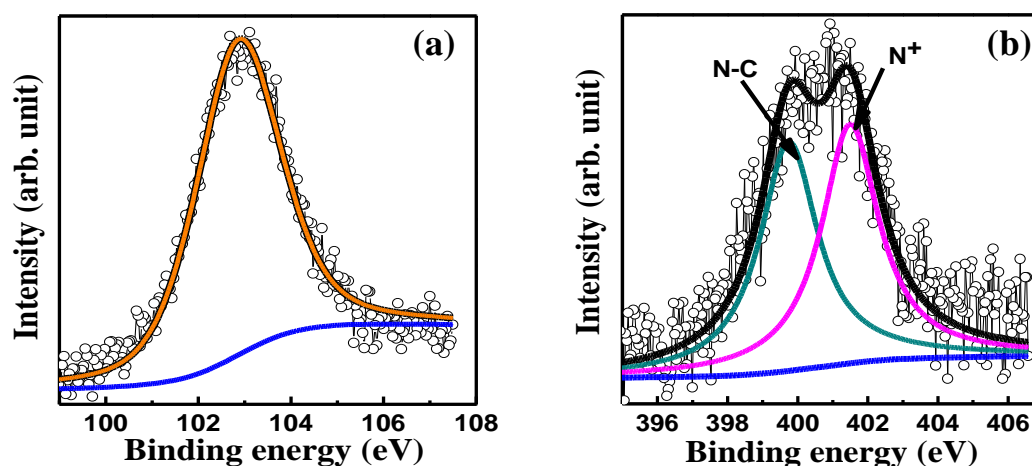


Figure 5.3: XPS convoluted spectra of (a) Si2p, (b) N1s for APTMS treated BOPET.

The presence of Si2p peak at 103 eV indicates the existence of SiO kind of layer. N1s spectra of APTMS modified BOPET shows two peaks at binding energy values 399.8 (attributed to nitrogen in N-C) and at 402.1 eV (attributed to positively charged nitrogen in -NH₂ group). The presence of positively charged nitrogen insinuates the prospect of

multilayered APTMS formation [202]. The process of multilayer formation can be explained by the interaction of head group of the hydrolyzed APTMS molecules i.e. $\text{Si}(\text{OH})_3$ (which is a weak acid) with the surface $-\text{NH}_2$ groups (which are basic in nature) of the monolayer through the dipole-dipole interaction in presence of adsorbed water layer as shown in Fig. 5.5 (for schematic representation).

When the substrate (APTMS modified BOPET) is kept in mixed solution of protonated aniline and AgNO_3 , the NH_2 group in APTMS layers got converted into radical on exposure to UV. These amino radicals initiate the growth of PANI by photo polymerization and facilitate the PANI-Ag films to attach firmly on the substrate.

5.2.2 Preparation of PANI-Ag nanocomposite films on APTMS modified BOPET

Silver nitrate (Sigma-Aldrich, purity ~ 99.9%) was used as received to prepare the PANI-Ag nanocomposite films. At first protonation of aniline monomer has been done using distilled aniline 0.913 ml (1M) along with 0.84 ml (2 M) HNO_3 and 10 ml of DI water. HNO_3 is added to aniline for the protonation of monomer. Followed by protonation, 3.4 g (2 M) AgNO_3 is added in protonated aniline solution and a uniform mixing has been done using magnetic stirrer. Now the solution is kept in leak tight glass bottle with APTMS modified BOPET sheets for photo-polymerization. The glass bottle containing the solution and substrate was placed under a UV lamp (Spectrolinker, XL-1500UV cross linker) set at wavelength ~ 365 nm and intensity ~5 mW/cm². The distance of UV source to sample is ~13 cm and it was left for 6 hours. After UV exposure the samples were thoroughly cleaned with DI H_2O and ethanol to remove the unreacted monomer species. This washing treatment may partially de-dope the PANI-Ag films and therefore the films were subsequently exposed to the HCl vapors for about 3 minutes.

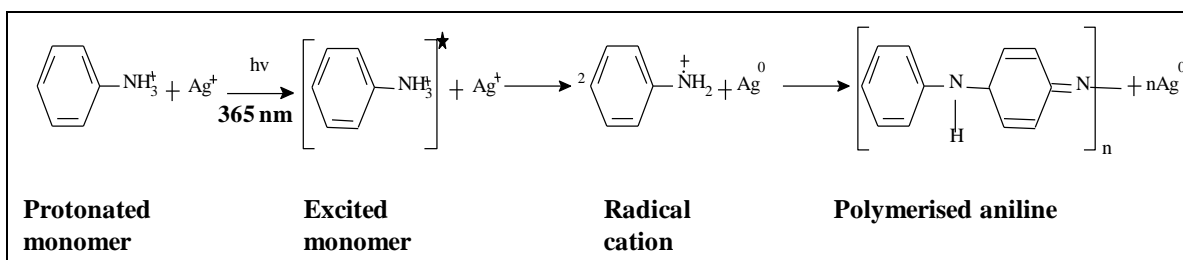


Figure 5.4: Mechanism of photo-polymerization of PANI in presence of AgNO_3 .

The mechanism of photo-polymerization of aniline is briefly represented in Fig. 5.4. The UV light acts as catalyst which excites the aniline monomer and the electrons transferred from excited monomer to Ag^+ ions leaving aniline radical cation. This radical cation further reacts with another radical cation and consequences to polymerization of aniline. In this process, Ag^+ ions got reduced to metallic state and embedded in the polymer matrix to form nanocomposite [193].

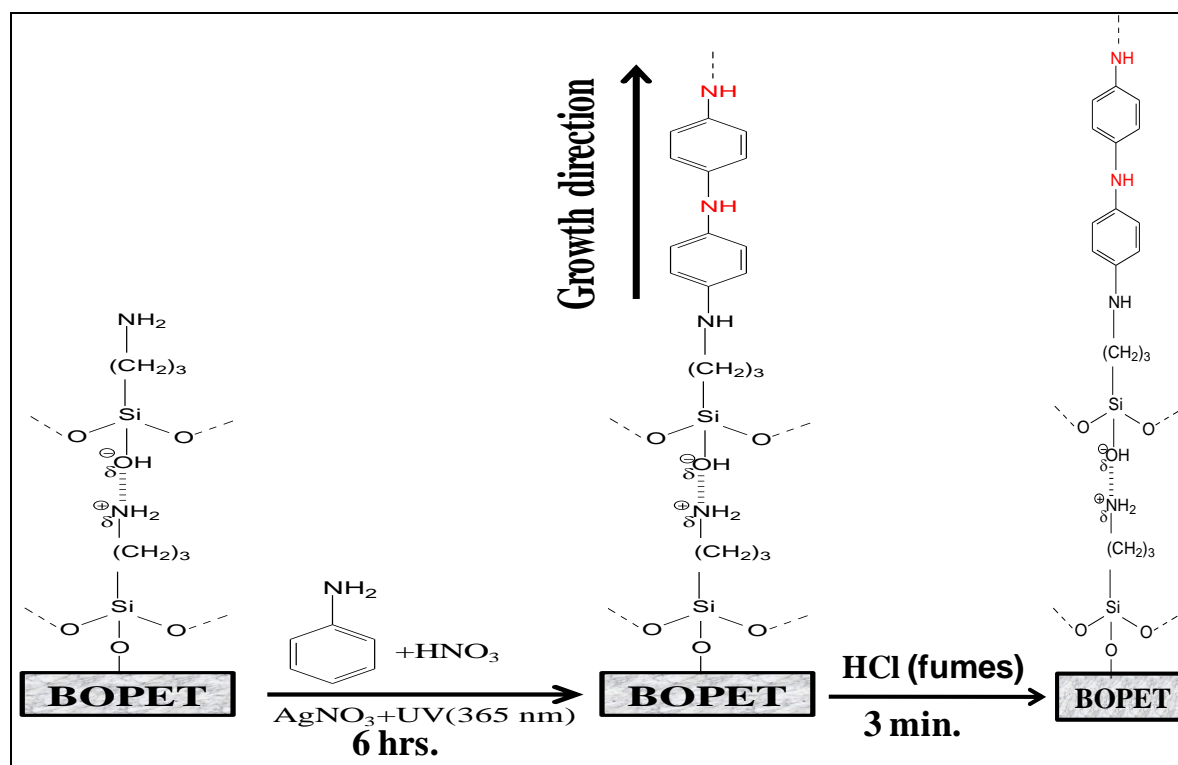


Figure 5.5: Representative scheme for growth of PANI-Ag nanocomposite films on APTMS modified BOPET substrate. Red colored N shows nitrogen of aniline whereas black colored N stands for nitrogen of APTMS layer.

UV light also acts as catalyst to convert the surface NH_2 groups of APTMS layer into amino radicals (NH_2^+) [204]. These amino radicals initiate the growth of PANI on APTMS modified BOPET substrate as represented in Fig. 5.5. The detailed synthesis procedure of PANI-Ag films on APTMS modified BOPET sheet is given in references and our previous study [164, 202]. Three PANI-Ag nano-composite film samples were taken for each set of analysis and also each measurement (non destructive) has been replicated twice. The mean results are shown along with error bars.

5.3 Preparation of PEDOT:PSS flexible polymer films

Thin film of conducting polymer PEDOT:PSS has been prepared on flexible polyimide (Kapton) substrate by drop cast method. PEDOT:PSS solution was procured from M/s Ossila (make-M122 PH1000) and subjected to ultrasonication before deposition. The films were dried in air and annealed at $160\text{ }^\circ\text{C}$ for 45 minutes. Each set of film comprises three PEDOT:PSS samples for the analysis and each measurement (non devastating) has been repeated two times. The variations from average have been shown with error bars. The structure of PEDOT:PSS composite has been shown in Fig. 5.6.

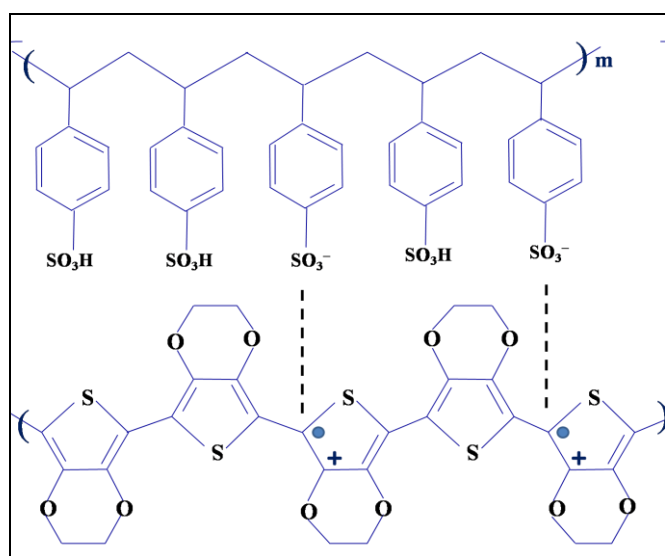


Figure 5.6: Structure of PEDOT:PSS composite film.

5.4 Electron beam irradiation of conducting polymer films

The electron beam irradiation of PANI-Ag films has been done at the EBC, BARC facility, Navi Mumbai, India [29]. The dose was delivered to the PANI-Ag film samples in steps up to 100 kGy in dynamic mode using 10 MeV RF Linac. Similarly the irradiation of PEDOT:PSS films were done up to 75 kGy in steps with 1 MeV DC electron accelerator, at EBC, BARC, in dynamic mode. In order to protect from dust the films were kept in a close plastic box of thickness around 1 mm which did not attenuate the electron beam appreciably. The irradiation experiments were carried out in atmospheric conditions.

5.5 Surface and morphological characterizations of PANI-Ag nanocomposite films

5.5.1 Scanning electron microscopy

The morphology of the electron beam irradiated PANI-Ag films was characterized by scanning electron microscopy (SEM) (ZEISS SUPRA) and the images are shown in Fig. 5.7.

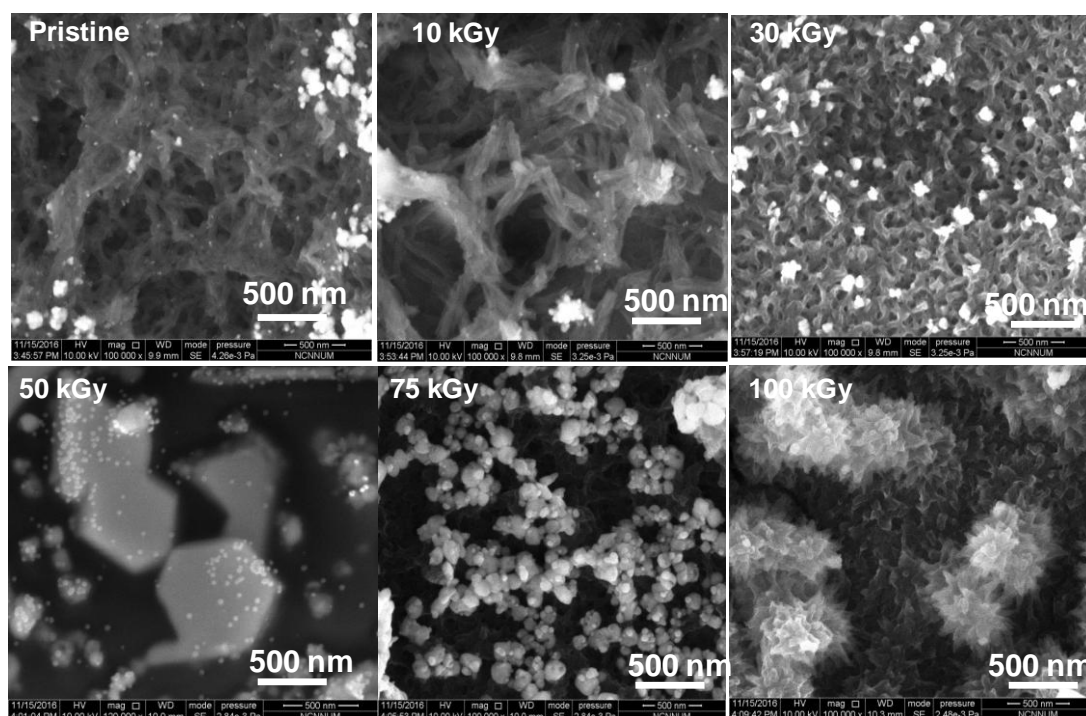


Figure 5.7: FE-SEM images of pristine and EB irradiated PANI-Ag films.

The SEM image of as synthesized PANI-Ag film reveals the growth of nano-fibers. It shows smooth morphology which suggests that the presence of APTMS layers at the BOPET surface controls the photopolymerization of aniline in the direction normal to the substrate as represented in Fig. 5.5. It has been observed that with increasing dose up to ~10 kGy the diameter of nano-fibers increases and it is interesting to note that sample irradiated with 30 kGy dose exhibit nicely interconnected microstructure. The same becomes further dense with increasing dose up to 100 kGy [205].

5.5.2 X-ray photoelectron spectroscopy

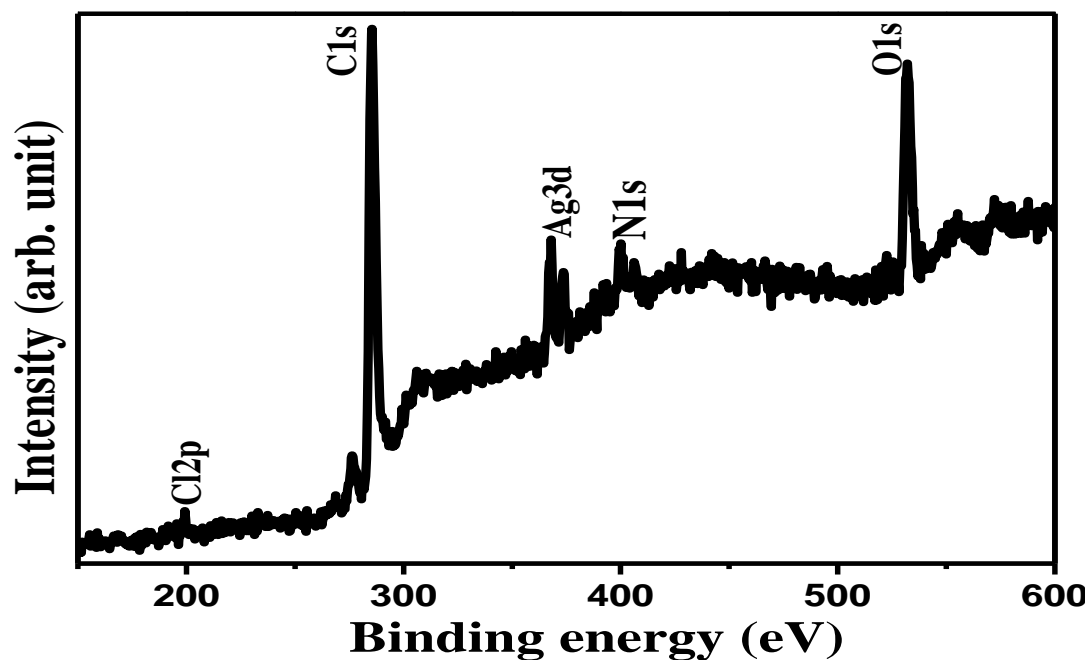


Figure 5.8: XPS survey scan of pristine PANI-Ag films.

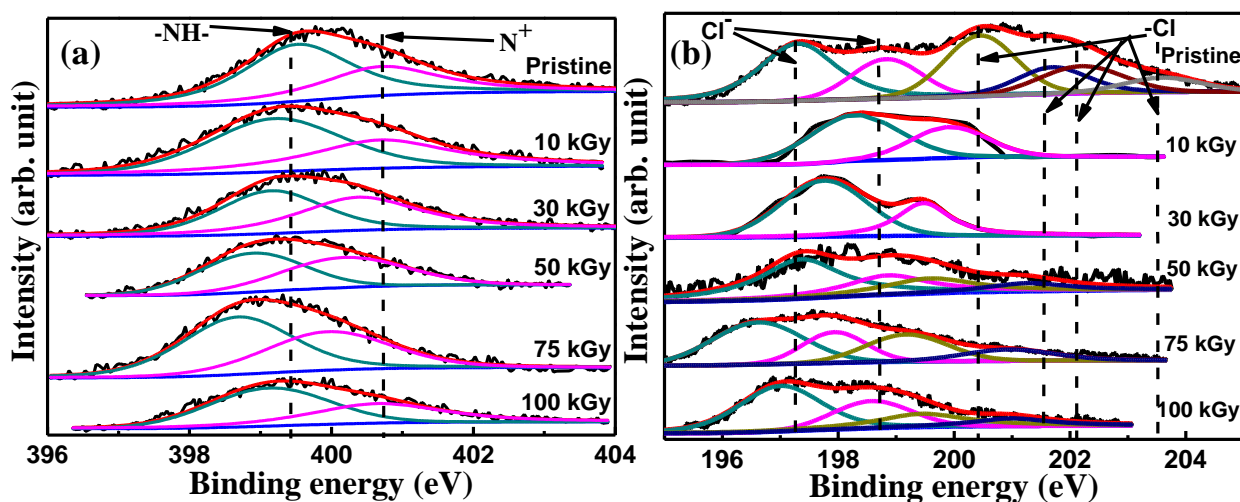


Figure 5.9: Convolved XPS for (a) N1s, (b) Cl2p of PANI-Ag films pre and post EB irradiation.

The X-ray photoelectron spectroscopy (XPS) of samples was carried out using Mg K α (1253.6 eV) radiation and the recorded data have been calibrated using C1s peak from the adventitious carbon-based contaminant with the binding energy of 284.6 eV. The XPS survey scan of pristine PANI-Ag films is given in Fig. 5.8, which shows the presence of chlorine (Cl2p ~ 199 eV), carbon (C1s ~ 285 eV), Ag doublet (Ag5d ~ 368eV and Ag3d ~ 374 eV), nitrogen (N1s ~ 400eV) and oxygen (O1s ~ 532 eV) [170, 206 - 208]. In order to obtain the quantitative information about doping level, high resolution XPS spectra of N1s and Cl2p were recorded and analyzed as shown in Fig. 5.9. In N1s spectra (Fig. 5.9a) there are two major peaks, at 399.4 eV and at 401.2 eV which are attributed to amine (-NH-) nitrogen and positively charged nitrogen respectively [209]. The convolved Cl2p core level XPS spectra of PANI-Ag films are shown in Fig. 5.9b. In case of pristine PANI-Ag film there are peaks corresponding to chloride ion at binding energy less than 199 eV ($2p_{3/2}$ & $2p_{1/2}$) and two different type of covalently attached chlorine at higher binding energy (> 199 eV) [210 - 212]. It is interesting to observe that in the samples irradiated with dose up to 30 kGy, only one peak is present which corresponds to chloride ions (dopants). It suggests that the covalently attached chlorine gets detached from PANI chains when it is exposed to low dose

(10 kGy & 30 kGy) of electron beam. The variation in N^+/N ratio is given in table 5.1 which shows an enhancement in N^+/N ratio for 10 kGy & 30 kGy samples as compared to pristine films. It also suggests that there is a possibility that some part of the released chlorine gets trapped as ions in the PANI matrix and it contributes to the doping of PANI.

For samples irradiated at dose > 30 kGy, one can see the presence of ionic chlorine as well as covalently bonded chlorine (at binding energy >200 eV). It implies that in the samples irradiated with higher dose of electron beam, covalently bonded chlorine is not fully removed from the PANI chains. From table 5.1 it can also be seen that for samples with high dose (> 30 kGy) the N^+/N ratio slightly decreases, which also support the fact that less chlorine is released due to cleaving at higher doses

Table 5.1: N^+/N ratio of pristine and electron beam irradiated PANI-Ag film based up on XPS.

Sample	N^+/N
Pristine	0.38
10 kGy	0.42
30 kGy	0.50
50 kGy	0.48
75 kGy	0.42
100 kGy	0.42

5.6 Structural characterization of PANI-Ag nanocomposite films

5.6.1 Fourier transform infrared spectroscopy

The pristine and post irradiated PANI-Ag films were characterized by Fourier-transform infrared spectroscopy (Bruker 80V). The bands observed at 1597 cm^{-1} and 1501 cm^{-1} (shown in Fig. 5.10) are assigned to the ring stretching vibration of quinoid (Q) and benzenoid (B) respectively. The quantitative analysis of FTIR area ratio provides the detailed

link up in structural changes due to electron beam irradiation. The ratio of peak area (I_Q/I_B) gives the degree of oxidation of PANI [213, 214]. In the present case I_Q/I_B is almost one and it remains same for all pristine as well as EB irradiated PANI-Ag films as seen from table 5.2. This indicates that electron beam irradiation caused only marginal effect on the oxidation level (i.e. ratio of benzenoid to quinoid units in the chains) of PANI-Ag films. It is understood that doping of PANI is a non redox type of process which involves addition/removal of electron from polymer back bone [53].

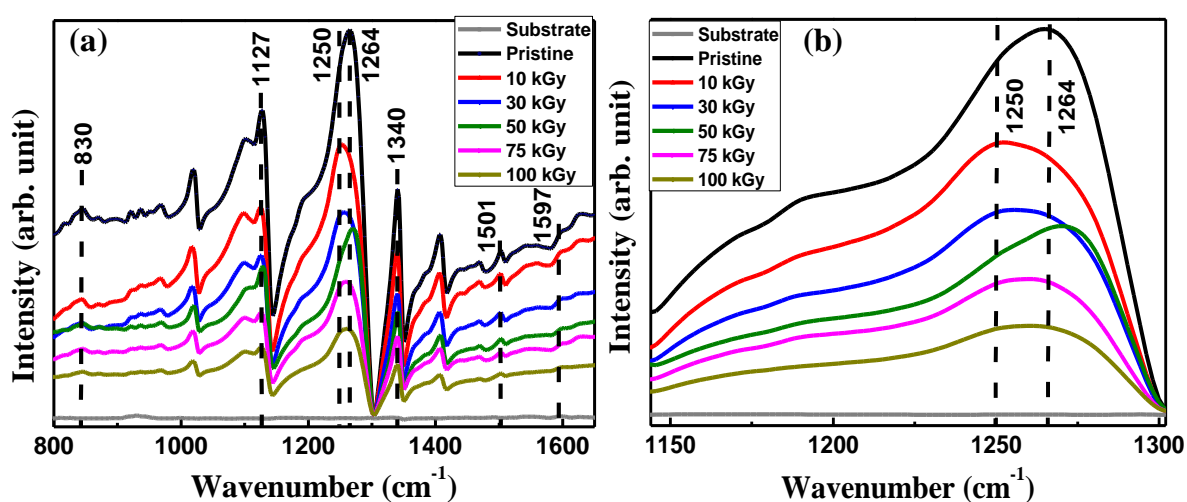


Figure 5.10: FTIR spectra of (a) APTMS treated BOPET substrate and pristine as well as EB irradiated PANI-Ag films, (b) characteristic conductive band showing shift from 1264 cm^{-1} to 1250 cm^{-1} after irradiation up to 30 kGy.

The band at 1127 cm^{-1} is due to protonation chain vibration of structure $-\text{NH}^+=$ which is formed in the acid doping process of the film and characterizes the electrical conductivity [215, 216]. The area ratio of peak at 1127 cm^{-1} and peak at 830 cm^{-1} (signifying the amount of chlorine added to PANI) gives the estimation of doping levels [217]. The ratio, given in table 5.2, increases from 1.59 (for pristine) to 1.92 (for 30 kGy) and then (for doses > 30 kGy) it decreases up to 1.70 (in case of 100 kGy), which shows agreement with XPS results of doping level (N^+/N). The band present at 1264 cm^{-1} is attributed to the stretching of $\text{C}-\text{N}^+$ polaron structure of PANI-Ag film [213]. This is the characteristic band of the electrically

conductive form of doped polyaniline. There is a shift observed in this band towards lower wave number to 1250 cm^{-1} after EB irradiation up to 30 kGy dose and beyond that the band again shifted towards the original position (Fig. 5.10b).

Table 5.2 FTIR band intensity ratio of pristine and EB irradiated PANI-Ag films.

Sample	I_{1597}/I_{1501} (I_Q/I_B)	I_{1127}/I_{830}
Pristine	1.19	1.59
10 kGy	1.15	1.88
30 kGy	1.14	1.92
50 kGy	1.14	1.75
75 kGy	1.14	1.70
100 kGy	1.15	1.70

These results support that non-redox doping of irradiated (with dose up to 30 kGy) PANI-Ag samples is greater as compared to pristine film [218]. This doping of PANI-Ag film favors the movement of π electrons and justifies the shift of corresponding band to lower wavenumber. The band present at 1340 cm^{-1} is assigned to stretching of C-N bonds next to quinoid ring (C-N=Q=N-C).

5.6.2 Photoluminescence spectroscopy

Photoluminescence (PL) measurement was done at room temperature on ISS PC1 spectrophotometer using Xe lamp as source and ethanol as solvent. Conducting polymers in general does not exhibit PL but there are some exceptions such as PANI. The benzenoid units in PANI demonstrate fluorescence while the quinoid units reveal no observable fluorescence because the intra-chain energy migration enables the quinoid groups to act as excitation traps and quench the PL [219, 220]. PL emission spectra of pristine and electron beam irradiated PANI-Ag films with excitation wavelength as 300 nm are presented in Fig. 5.11.

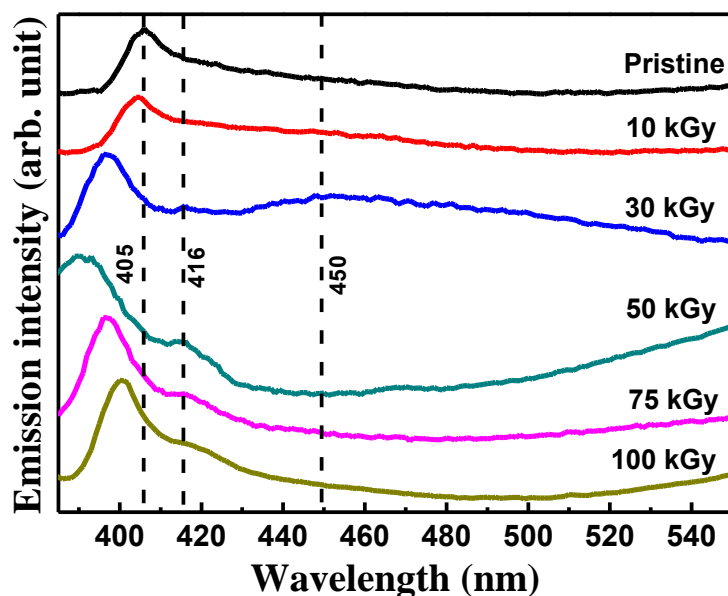


Figure 5.11: Photoluminescence spectra of pristine and EB irradiated PANI-Ag films.

The exciton wavelength was taken as 300 nm so that it exists well within the range of π - π^* absorption band of the benzenoid units which are centered at 376 in case of HCl doped PANI as emeraldine salt. It is also confirmed from UV-Vis results (discussed in next section) that the absorption began from wavelength around 305 nm and thus 300 nm is chosen as exciton wavelength for the PL. In the emission spectrum of pristine films, peak at 405 nm along with a broad tail (probably superposition of few more peaks of low intensity) at higher wavelength is observed. The peak at 405 nm for pristine films is attributed to the presence of leucoemeraldine base sequence in PANI chains. The peak at 416 nm is attributed to the emeraldine base form of PANI and peak observed at 450 nm (seen more clearly in 10kGy and 30 kGy samples) is attributed to the reduction of HOMO-LUMO gap (due to improved conjugation) along with the presence of high amount of conducting portions in PANI chains [221, 222]. In case of films irradiated at 30 kGy, main peak is blue shifted to 400 nm and new peaks become visible at \sim 416 nm and 450 nm. For films irradiated with 50 kGy, the main peak shows more blue shift to \sim 390 nm while the other peak remains at 416 nm. With further increase of dose in the range of 75-100 kGy, the main peak exhibits red shift while other peak

remains at 416 nm. It is interesting to observe that the peak at ~ 450 nm is absent for the films irradiated at dose ≥ 50 kGy. The analysis of PL results can be correlated with the HOMO/LUMO gap change because of EB irradiation. The peak at 416 nm in case of 10 kGy and 30 kGy is very weak and it can be considered as red shifting to 450 nm. But in case of samples irradiated with dose above 30 kGy the peak at 450 nm is blue shifted to 416 nm. Since the PL spectrum is related to HOMO/LUMO absorption transition and so a change in HOMO/LUMO energy gap would lead to a change in photoluminescence spectrum. When a polyaniline film is doped and converted from emeraldine base form to emeraldine salt state, the HOMO/LUMO energy gap of the benzenoid π - π^* transition decreases as seen through the red shift of band from 416 nm to 450 nm or vice versa. This change in π - π^* absorption may be related to either the doping of the emeraldine base sequences and/or to the protonation of the leucoemeraldine units. Thus the decrease in energy gap leads to a decrease in energy of the PL spectrum or red shifting of characteristic emeraldine base peak [222, 223]. The absence of 450 nm peak in the PL spectra of the films irradiated with dose > 30 kGy is consistent with the low electrical conductivity of these films [224].

5.6.3 UV-Vis spectroscopy

The UV-Visible spectroscopy has been done to examine the effect of EB irradiation on electronic property of PANI-Ag films and results are shown in Fig. 5.12. The UV-Visible spectroscopy has been performed in diffused reflectivity mode using Cary-60 UV VIS-NIR spectrophotometer with measuring wavelength range of 190 nm to 800 nm and the beam spot size was around 1.5 mm in diameter. It is observed that the films exhibit two bands: one at 376 nm and another is a broad band at 690 nm. The band at 376 nm is attributed to π - π^* transition in the benzenoid unit of PANI chains [225 - 227].

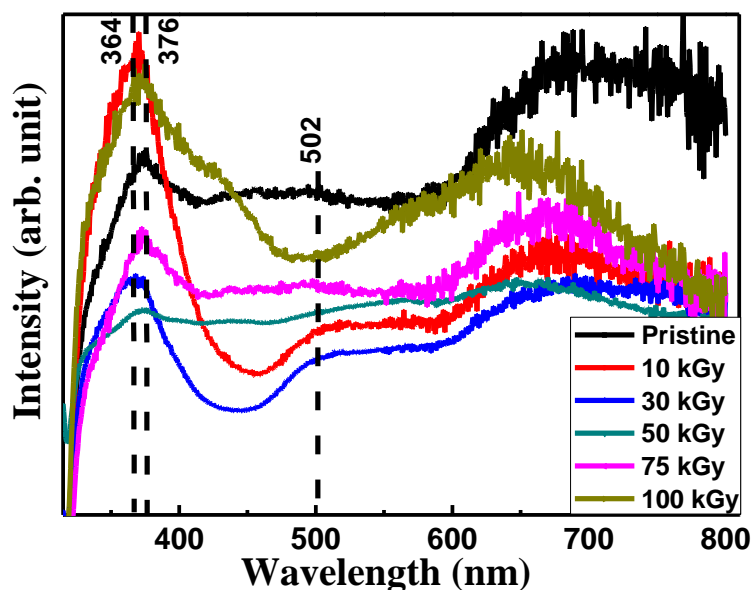


Figure 5.12: UV-Visible spectra of pristine and EB irradiated PANI-Ag films.

From UV-Vis spectra, it is clearly seen that there is a shift in band at 376 nm to 364 nm in case of films irradiated with dose up to 30 kGy [227]. The films irradiated up to a dose of 30 kGy exhibit a new band at 502 nm which is attributed to the surface plasmon resonance of Ag nanoparticles in the PANI matrix [228, 229]. The band at 690 nm corresponds transition from polaron band to π^* band and it is closely related to the charge carriers that are responsible for the electrical conductivity. The lower energy shift of band (or red shift) implies an increase in mobility and ease of electronic transition of the charge carriers i.e. doping of the polymer to the conductive regime [230]. It has been observed from UV-Vis spectra that the band at 690 nm gets blue shifted at dose > 30 kGy which is clearly reflected in the reduced electrical conductivity of the samples. In summary, the changes appeared in the UV-Visible spectra of PANI-Ag films on exposure to electron-beam suggest that the internal structure of PANI units got modified due to irradiation.

5.7 Crosslinking characterizations

In order to understand the electron beam induced chain scissioning or crosslinking dominance in polymer chains of PANI-Ag films in the analyzed dose regime, the solubility

test has been carried out. The solubility test has been conducted by leaving the samples in solvent dimethyl sulphoxide (DMSO) for 10 minutes, at room temperature. The insoluble part was dried under room conditions and weighed using microbalance (M/s AND Company Ltd., Japan) having accuracy ~ 0.1 mg. Pure PANI is less soluble in available solvents because of very strong intermolecular force of attraction present in PANI which originated from its structure, polarity and crystallinity. The protonated PANI is very soluble in common organic solvents like dimethyl sulphoxide (DMSO) and dimethyl formamide (DMF) at room temperature whereas it is less soluble in benzene and chloroform [107, 200]. This suggests that the solubility of PANI is due to reduced inter-chain interactions because of large size of counter anion. The solubility test of pristine and EB irradiated samples were carried out using DMSO as solvent at room temperature. The actual photographs of PANI-Ag films after DMSO solubility test have been shown in Fig. 5.13 which indicates in case of 10 kGy and 30 kGy only substrates are left with little film.

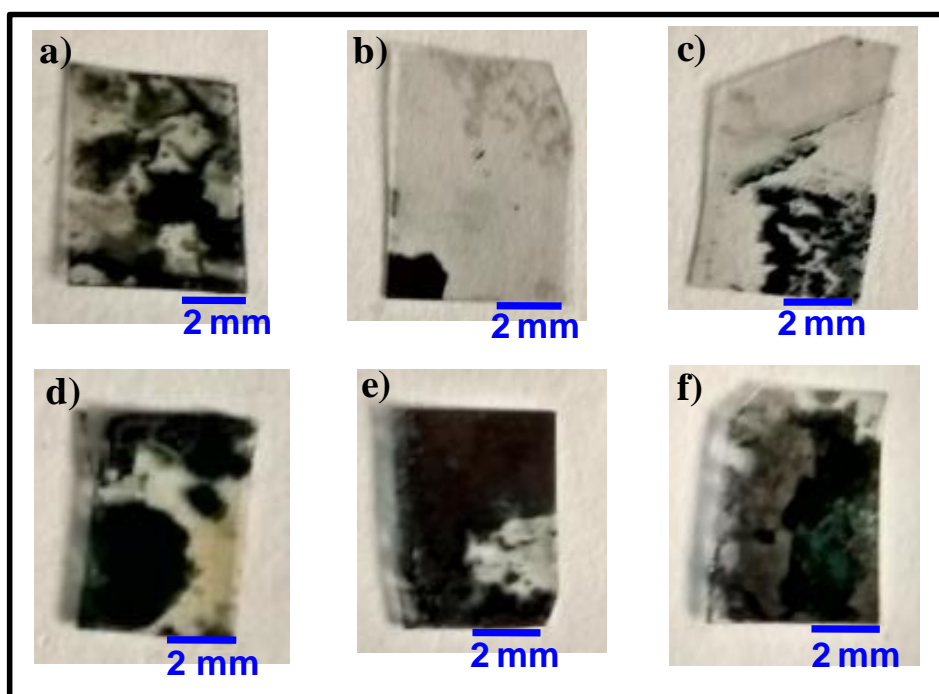


Figure 5.13: Actual photographs of PANI-Ag film on APTMS treated BOPET after solubility test: (a) pristine, (b) 10 kGy, (c) 30 kGy, (d) 50 kGy, (e) 75 kGy, (f) 100 kGy.

The relative change in solubility of EB irradiated films as compared to pristine samples is plotted in Fig. 5.14 and it can be seen that in case of pristine films PANI chains exhibit low solubility. However with increase in electron beam dose the solubility enhances and reaches maximum at 30 kGy. With further increase of dose beyond 30 kGy solubility is found to decrease. The high holding strength or low solubility of pristine PANI-Ag films is attributed to longer chain length that results in good entanglement. With increasing dose upto 30 kGy, the chain scissioning dominates that result in loss of holding strength. With further increase of dose beyond 30 kGy, the crosslinking of PANI chains dominates which superseded the chain scission process and results in decline of solubility [231].

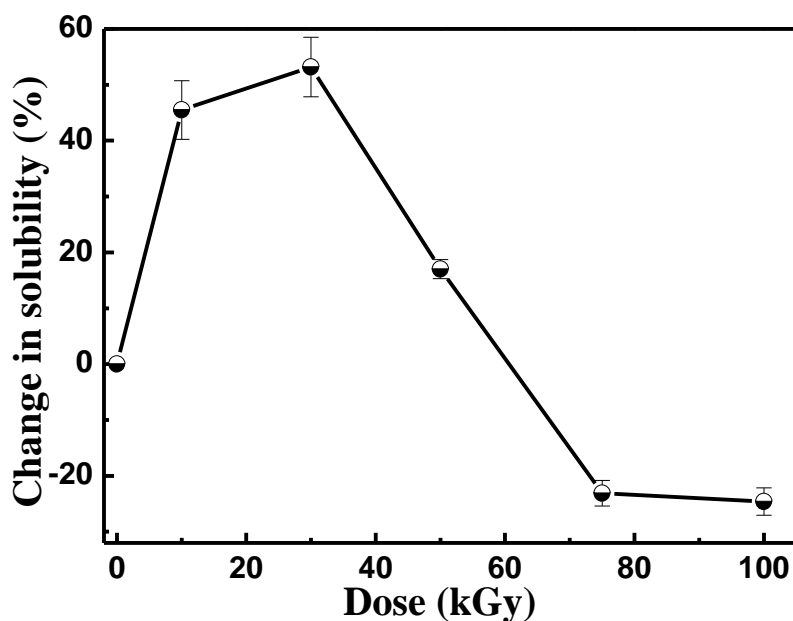


Figure 5.14: Change in solubility of PANI-Ag film in DMSO with electron beam dose as compared to pristine film.

5.8 Electrical characterizations and charge transport analysis

Since the PANI-Ag film is well known intrinsic conducting polymer and therefore the effect of electron beam on its electrical conductivity was investigated. The electrical conductivity of the PANI-Ag films was measured using conventional two probe technique. Electrical connections on the sample were made using silver wire of diameter $\sim 100 \mu\text{m}$ and

silver paint (Electrolube make) was used to attach the wire on the gold electrodes that were deposited (using thermal evaporation) on the films. The separation between two gold electrodes was $\sim 12 \mu\text{m}$. The Current-Voltage (I - V) curve was plotted by varying bias voltage in range of $\pm 1\text{V}$ (in steps of 0.1V) and measuring the current. Typical room temperature I - V characteristic of pristine and EB irradiated PANI-Ag films are shown in Fig. 5.15a. I - V plots are linear which reveal that ohmic conducting nature of PANI-Ag films did not alter as a result of electron-beam irradiation. The electrical conductivity enhances with dose up to 30 kGy by two orders as compared to pristine films (Fig. 5.15b). As seen from Fig. 5.15b, the conductivity rises sharply with dose and attains a maximum at 30 kGy followed by an abrupt lowering with dose up to 75 kGy, thereafter the change is relatively very small.

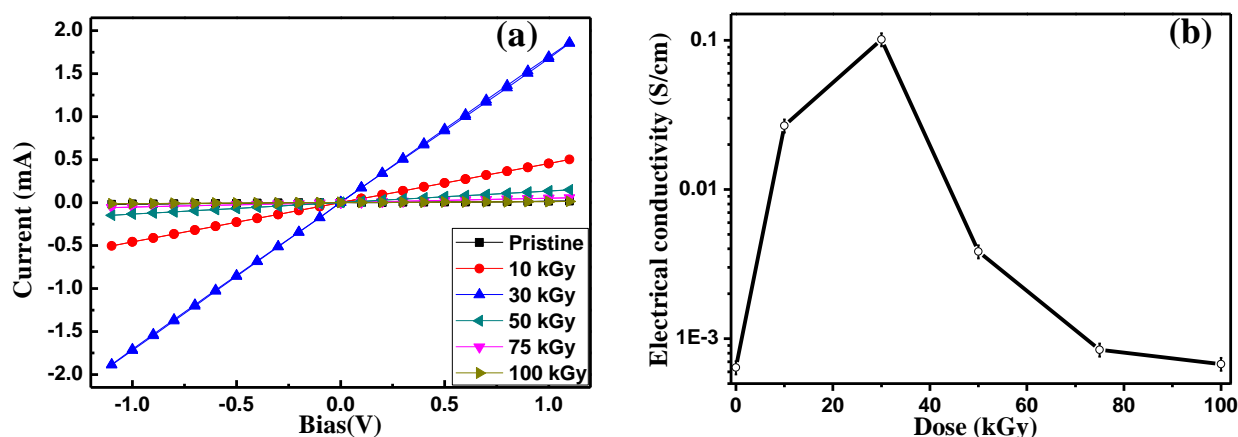


Figure 5.15: (a) I - V characteristics of pristine and EB irradiated PANI-Ag film, (b) electrical conductivity as function of dose.

It is well known that the electrical conductivity of PANI predominantly depends upon its oxidation state as well as on the level of doping [232, 233]. As per XPS analysis the pre irradiated PANI-Ag films were doped with HCl. Due to electron-beam irradiation the covalently bonded chlorine ($-\text{Cl}$) with PANI-Ag chains gets dissociated and as a result, chlorine is released. These newly formed chlorine further dissociated into Cl^- and/or Cl^* which acts as counter ion to form more N^+ (enhanced degree of doping) and promote

enhancement of conductivity in PANI-Ag films. In addition, the degree of doping which enhanced up to 30 kGy has also been confirmed by FTIR analysis but at the same time it can be concluded that the doping which took place due to electron-beam irradiation in case of PANI-Ag films was of non-redox nature.

As seen, from solubility test, samples that were irradiated with dose > 30 kGy, exhibited crosslinking of polymer chains along with slightly reduced doping (i.e. reduction in N^+/N , as revealed by the XPS data) as compared to the films irradiated with 30 kGy dose. The conductivity of doped PANI also depends upon degree of crystallinity, charge carrier concentration and their mobility [234]. As result of increased crystallinity, the conductivity increases because the structure becomes more organized following on to escalate the intra-molecular mobility of charged species along the chain. Also, it encourages the intermolecular hopping of charge carriers because of better packing to some extent. This can be well concluded from SEM images as well as from the lower wave-number shift in characteristic FTIR band up to 30 kGy.

Now we discuss why cross-linking of polymer chains results in lowering of electrical conductivity. Molecular weight or molecular chain length is another important parameter that influences the conductivity of a polymer. The conductivity of the system does not increase significantly until a molecule attains a certain definite size. It is mainly due to formation of long range delocalization of electron cloud because of the creation of conjugated double bond and this cannot occur until the molecule attains a definite size. However at a very high molecular weight, some kind of imperfections developed which in turn adversely affects the continuous charge delocalization process intra-chain or inter-chain. Since cross-linking results in chains having very high molecular length (or molecular weight), in such long chains the imperfections like distortion in chain symmetry or cluster formation may localize the charges. The distortion in chain symmetry as well as cluster formation can be observed

from SEM images of the samples that were irradiated with dose above 30 kGy. In addition, the high molecular weight chains cause swelling of samples which result in increase in the inter-chain distance and hence, negatively affect the charge carriers' hopping between two chains [231, 235 - 237].

Thus, the increase in the electrical conductivity of PANI-Ag films up to 30 kGy of electron beam dose can be attributed to the increase in the number of radicals through chain scission. The occurrence of chain scission has been identified from the solubility test. In addition, the more doping took place in PANI as the result of cleavage of covalently bond chlorine by electron beam. At further higher doses, the decrease in conductivity might have occurred due to crosslinking dominance which could cause imperfection like distortions in chain symmetry and badly affected the charge delocalization. Also, de-doping in the PANI chains has been observed under higher electron-beam dose [217, 238].

5.9 Chemiresistive gas sensing

For gas sensing experiments the response curves (current versus time) were recorded by applying a fixed voltage to the sample. A desired concentration of the test gas in the chamber was introduced by injecting a known quantity of gas using a micro-syringe (as discussed in section 2.5.2). Once a steady state was achieved, the new concentration of the gas has been introduced to achieve new steady state and finally the recovery of films was recorded by exposing the sensor films to atmosphere by opening the lid of the chamber. The chemiresistive gas sensing properties of PANI-Ag films have already been previously studied by our group and it was found that its response towards H₂S was the best out of gases that included NH₃, Cl₂, NO, NO₂, CO, CH₄ and C₂H₅OH [164]. Therefore the effect of electron beam irradiation on H₂S gas sensing of PANI-Ag film has been analyzed. The response curve of PANI-Ag film for different concentrations of H₂S gas is shown in Fig. 5.16a which shows a decrease in electrical resistance of PANI-Ag film on exposure to H₂S. In view of electron

donating nature of reducing gas (H_2S), the decrease in resistance instead of expected increase for PANI-Ag films is quite appealing. PANI gives a vigorous response to strong acids as they have the ability to fully dope PANI and results in a very large change of electrical conductivity. H_2S is weak acid and hence the response of PANI towards it is expected to be minimal. Therefore, in order to improve the response of PANI for H_2S , PANI-metal composites were used [194, 239 - 242].

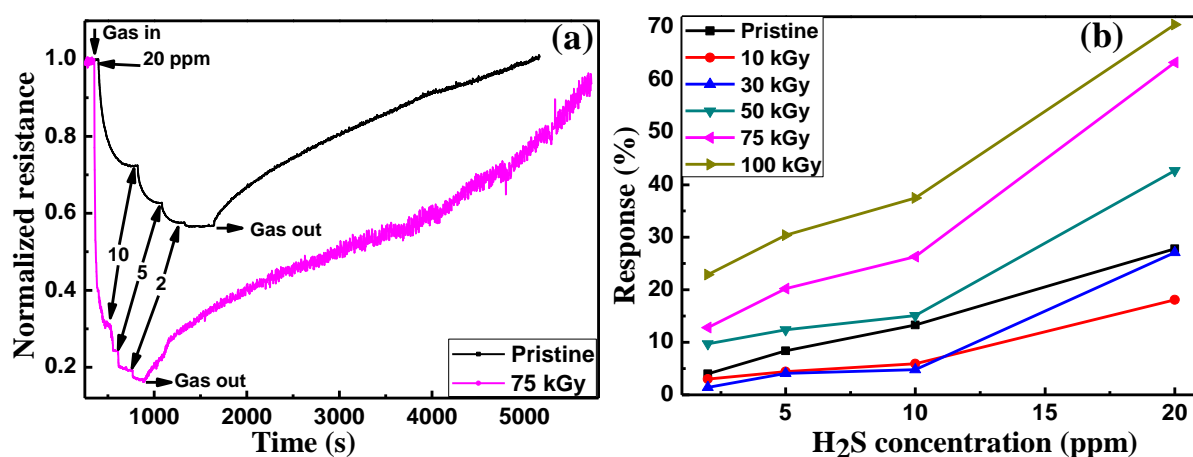


Figure 5.16: (a) Response curve of pristine and irradiated with 75 kGy EB dose PANI-Ag film at various H_2S concentrations, (b) response of pristine and irradiated PANI-Ag film towards various H_2S concentrations.

In literatures various mechanism have been proposed to explain the interaction of H_2S with PANI based composites but the most suitable one is related to the dissociation of H_2S on metal surface under ambient conditions as it is a weak acid having dissociation constant $pK_a = 7.05$ [243]. H_2S got dissociated into H^+ and HS^- ions due to presence of Ag. The HS^- ions neutralizes the positive N^+ charge in the PANI chain but simultaneously a proton (H^+) is also liberated which has higher mobility than heavy HS^- ions [239, 244]. This process results in decrease in electrical resistance of films on exposure to H_2S as seen from Fig. 5.16a.

The response of EB irradiated PANI-Ag films with respect to H_2S concentration is shown in Fig. 5.16b. It is interesting to note that response initially decreases marginally with

electron beam dose up to 30 kGy and after that it starts increasing. This dependence of response on electron beam dose can be explained by the fact which is related to the availability of more interaction sites. The films irradiated at higher doses (> 30 kGy) exhibit crosslinking as dominant phenomena and therefore additional interaction sites become available for H_2S in crosslinked PANI chains. It results in increased response for H_2S . The EB irradiation thus induces modifications in PANI-Ag films which helped to enhance its sensitivity towards H_2S gas.

5.10 Characterization of PEDOT:PSS films

We have also investigated the effect of high radiation on the electrical conductivity of commercial polymer PEDOT:PSS films to manifest the scope of this polymer in high radiation field. Thin films of PEDOT:PSS were grown on flexible Kapton sheets and irradiated up to 75 kGy dose with 1 MeV electron beam. It was found that the electrical conductivity of as deposited polymer films was ~ 3.2 S/cm which consistently falls to ~ 0.76 S/cm after getting 75 kGy. The detailed characterizations have been carried out to understand the conductivity amendment in PEDOT:PSS films due to 1 MeV electron beam irradiation.

5.10.1 XPS

The surface characterizations of pristine and EB irradiated PEDOT:PSS samples were done by XPS using Mg $K\alpha$ (1253.6 eV). The recorded data were calibrated using C1s peak similar as done in previous sections. The XPS survey scan of pristine PEDOT:PSS film has been shown in Fig. 5.17, which shows the presence of sulphur (S2p ~ 167 eV), carbon (C1s ~ 285 eV) and oxygen (O1s ~ 532 eV) [245 - 249].

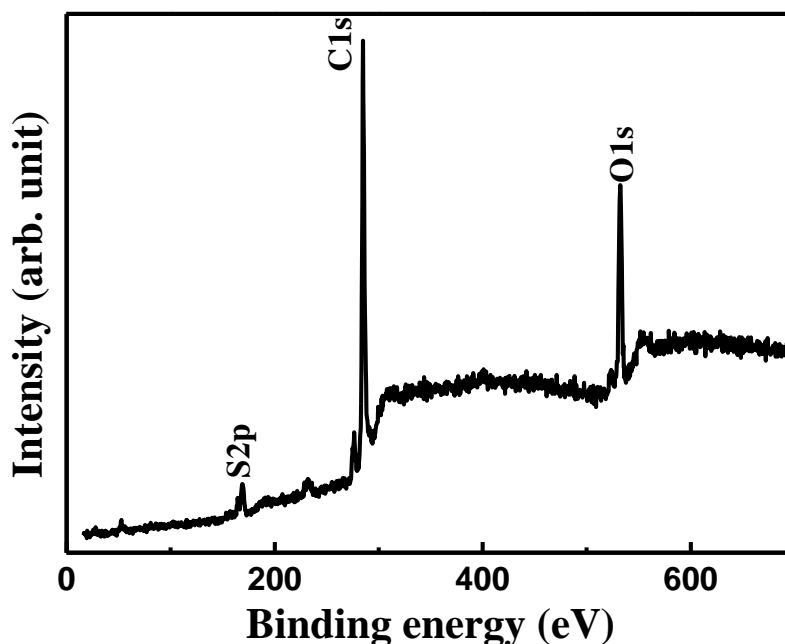


Figure 5.17: XPS survey spectra of pristine PEDOT:PSS film.

The convoluted spectra of S2p has been recorded and analyzed to obtain the relative composition of PEDOT and PSS quantitatively after EB irradiation (Fig. 5.18). S2p spectrum has two components, one at ~ 165 eV and another at ~ 169 eV, attributed to S2p of thiophene group in PEDOT and S2p of sulphonate group in PSS respectively [250]. In high resolution spectra each components of S2p has been resolved in two parts lower energy represents S2p_{3/2} and higher one represents S2p_{1/2} as shown in Fig. 5.18. The variation in area ratio of S2p components of PEDOT and PSS is given in table 5.3, which indicates a fall in PSS and enrichment in PEDOT components in the film composite, as result of EB irradiation. This demonstrates that the intensity of S2p from sulphonate group of PSS deteriorates after EB irradiation whereas the same for thiophene group in PEDOT increases [251].

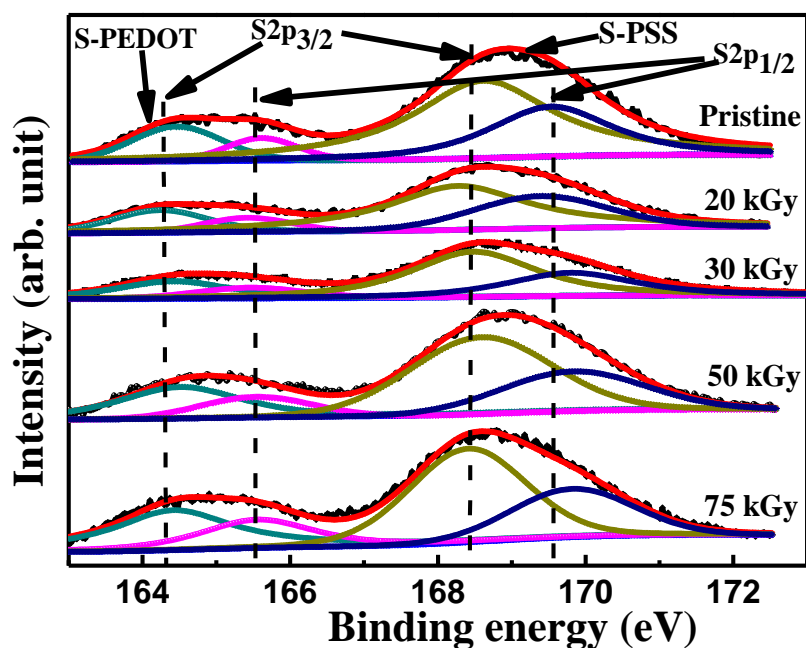


Figure 5.18: Convolved XPS for S2p of PEDOT:PSS films pre and post EB irradiation.

Table 5.3: Area ratio of sulphonate group (S2p) of PSS and thiophene group (S2p) of PEDOT in pristine and EB irradiated PEDOT:PSS film samples.

Sample	PEDOT	PSS	PSS/PEDOT
Pristine	0.175	0.825	4.7
20 kGy	0.209	0.791	3.8
30 kGy	0.255	0.745	2.9
50 kGy	0.297	0.703	2.4
75 kGy	0.392	0.608	1.6

5.10.2 Contact angle measurement

It is well known fact that PEDOT is hydrophobic molecule whereas PSS is hydrophilic in nature. In order to understand the relative existence of PEDOT and PSS post electron beam treatment, the static contact angle was determined with telescope- goniometry (M/s Dataphysics, Germany) using static water drop method. The measurements of water contact angles (error $\pm 8\%$) were performed using distilled water on five different positions

and the water drop diameter was around 10 μm . The contact angle variation with electron beam dose is plotted in Fig. 5.19.

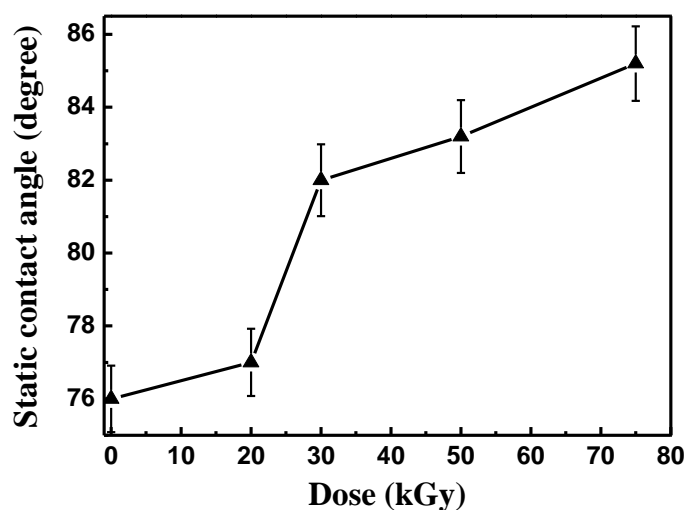


Figure 5.19: Static contact angle variations with electron beam dose for PEDOT:PSS films.

It has been observed that the contact angle increases with electron beam dose which indicates the increase of hydrophobicity with dose. It implies that the transition of film properties from hydrophilicity to hydrophobicity after irradiation. It also suggests that the hydrophilic molecules PSS are removed by settling down and thus, the film top surface becomes enriched by hydrophobic PEDOT molecules after electron beam irradiation for the said dose regime up to 75 kGy [250, 252, 253].

5.10.3 Solubility test

The solubility test has been carried out to check the electron beam induced chain scissioning or crosslinking dominance in polymer chains of PEDOT:PSS films. The solubility test has been conducted by leaving the samples in solvent dimethyl sulphoxide (DMSO) for 15 minutes, at elevated temperature $\sim 60^{\circ}\text{C}$ [254, 255]. The insoluble part has been dried under room conditions through hot air dryer and weighed using microbalance (M/s AND Company Ltd., Japan) having accuracy ~ 0.1 mg. Pristine PEDOT:PSS film is highly

soluble in the said solvents because of weak intermolecular force of attraction present in PEDOT originating from its structure, polarity and crystallinity. The actual photographs of polymer films PEDOT:PSS, after DMSO solubility test, is shown in Fig. 5.20 and it can be concluded that in case of pristine whole film got dissolved whereas with the increase in dose solubility of the film decreased.

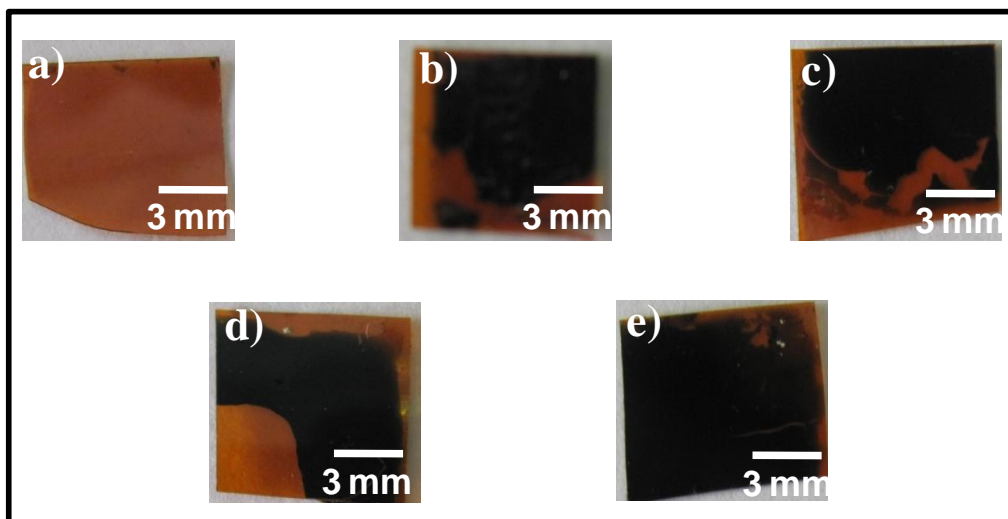


Figure 5.20: Actual photographs of PEDOT:PSS film grown on Kapton after solubility test using DMSO as solvent: (a) pristine, (b) 20 kGy, (c) 30 kGy, (d) 50 kGy, (e) 75 kGy.

In order to quantitatively understanding the relative change in solubility of EB irradiated films, as compared to pristine samples, is plotted with dose (Fig. 5.21). It can be concluded that the solubility of PEDOT:PSS films reduced with electron beam dose because the high solubility or weak holding strength of pristine films is attributed to shorter chain length resulting in poor entanglement. As EB dose increases the crosslinking of chain dominates to cause better grip between chains and as a result decline in solubility was observed [256].

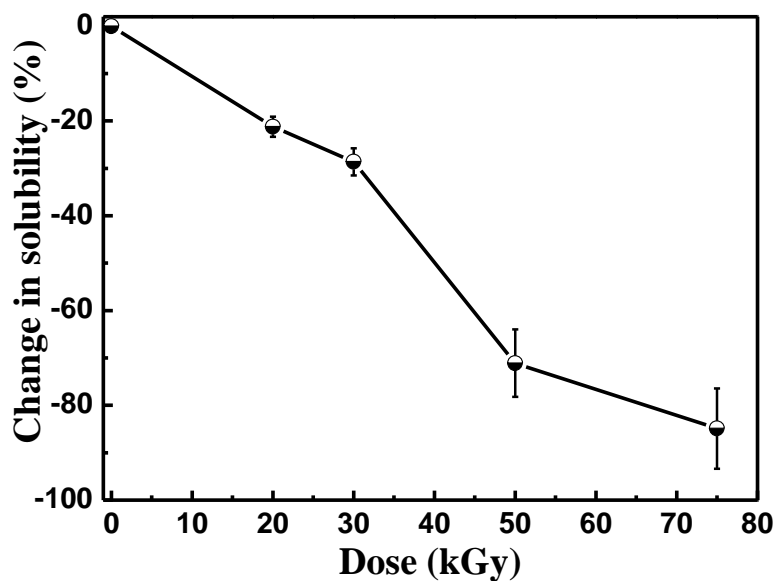


Figure 5.21: Relative change in solubility of PEDOT:PSS film in DMSO with electron beam dose as compared to pristine.

5.10.4 Electrical conductivity

PEDOT is eminent intrinsic conducting polymer used commercially for device applications and therefore the effect of electron beam on its electrical conductivity was investigated. The electrical conductivity of the PEDOT:PSS films were measured using conventional two probe technique. The gold pads have been deposited on the film, using thermal evaporation techniques, with the separation of ~ 1 mm between two pads. Electrical connections on the sample were made using silver wire of diameter ~ 100 μm and silver paint (Electrolube make) was used to attach the wire on the gold pads deposited on the films. The Current-Voltage (I - V) curve was plotted by varying bias voltage in range of ± 0.1 V (in steps of 0.01 V) and measuring the current. Typical room temperature I - V plot of as prepared and EB irradiated PEDOT:PSS films are linear which concludes that conduction is ohmic and EB irradiation doesn't alter the nature of conduction in these polymer films (Fig. 5.22a). The electrical conductivity of pristine film is 3.2 S/cm which falls monotonically as EB dose increases up to 50 kGy and afterward it shows very weak dependence on dose (shown in Fig.

5.22b). The conductivity reduced by approximately four times to 0.76 S/cm after irradiating with dose of 75 kGy.

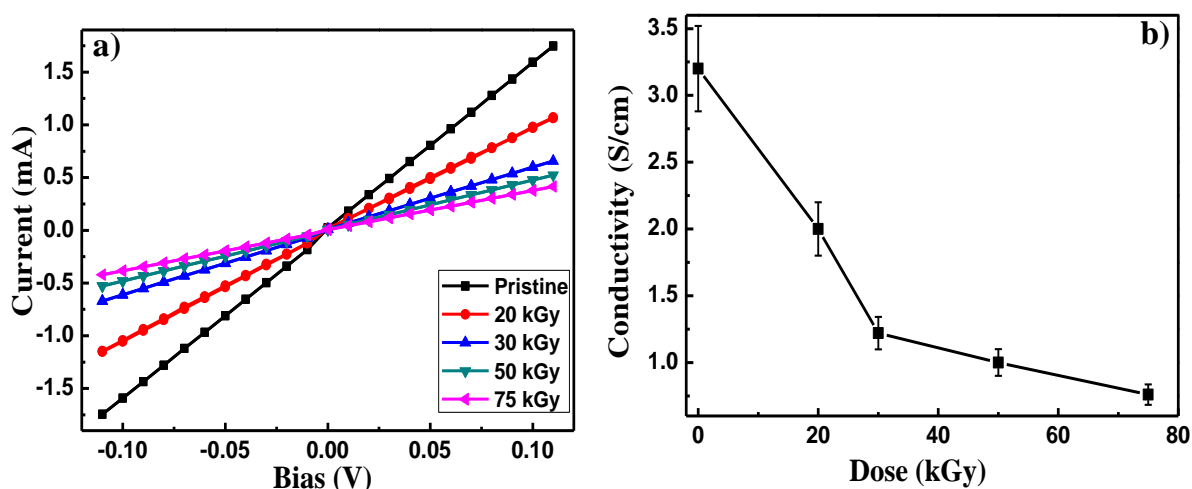


Figure 5.22: (a) *I-V* plot of pristine and EB treated PEDOT:PSS films, (b) electrical conductivity of PEDOT:PSS films as function of dose.

Based on the detailed characterization of the samples, we have discussed the effect of irradiation on the electrical conductivity of PEDOT:PSS films. PEDOT is conducting but hydrophobic and to make it soluble, hydrophilic but insulating poly(styrenesulphonate) (PSS) is added to it in the appropriate ratio. Therefore, any loss of the insulating PSS component from the films can positively influence the electrical conductivity [251, 257]. The XPS analysis indicates that the irradiated samples show lowering of PSS content in the films. In case of PEDOT:PSS, the PSS has very poor polymerization kinetics because of incompatibility between highly ionized sulphonic acid groups surrounded by a large hydration spheres and hydrophobic polymer backbones [258]. This results in scissioning or unbinding of the coiled PSS which cause reduction of PSS component under electron-beam irradiation. The lowering of PSS content in the irradiated sample is also supported by enhanced hydrophobicity of these samples. Hence in such irradiated samples, one may expect the enhancement of electrical conductivity due to better connectivity of PEDOT chains due to

removal of insulating PSS. However obtained results are in contrast to it. The solubility test suggests that there is continuous fall in solubility of PEDOT:PSS film after irradiation which implies that the crosslinking has taken place dominantly due to EB irradiation [256, 259, 260]. Crosslinking results in chains with very high molecular length (or molecular weight) and in such long chains some kinds of imperfections like distortion in chain symmetry or cluster formation may localize the charge carriers. In addition the high molecular weight chains results in swelling of samples causing increase in inter-chain distance and hence affects the charge carrier hopping between two chains. Both the charge localization and reduced hopping result in lowering of the electrical conductivity [261 - 263]. Therefore it can be concluded that in spite of the removal of insulating PSS, electrical conductivity of PEDOT:PSS films that reduced on electron-beam irradiation can be explained on the basis of crosslinking phenomenon.

5.11 Conclusions

The effect of high energy electron beam irradiation on electrical and gas sensing properties of PANI-Ag nanocomposite films on flexible APTMS modified BOPET substrate have been investigated. It has been observed that the electrical conductivity of the films enhances with electron beam dose up to 30 kGy. Films irradiated with dose of 30 kGy exhibited electrical conductivity higher by two orders of magnitude in comparison to the pristine films because of enhanced doping and scissioning in polymer chains. Whereas the films irradiated at doses above 30 kGy exhibited reduced electrical conductivity due to dominance of crosslinking (of PANI chains) and induced structural defects. The effect of electron beam induced modifications of PANI-Ag films can also be witnessed in their chemiresistive gas sensing properties. At higher doses (above 30 kGy) crosslinking of polymer chains dominates which creates more sites for interaction of gas with the polymer. Such increase in interaction sites resulted to higher response for gas sensing. In addition the

linear enhancement of electrical conductivity with electron beam dose up to 30 kGy, suggests that these films can be used as a flexible potential radiation dosimeter within the dose range up to 30 kGy. The electron beam induced modifications in electrical conductivity and H₂S gas sensing characteristics of flexible PANI-Ag films has been summarized in Fig. 5.23.

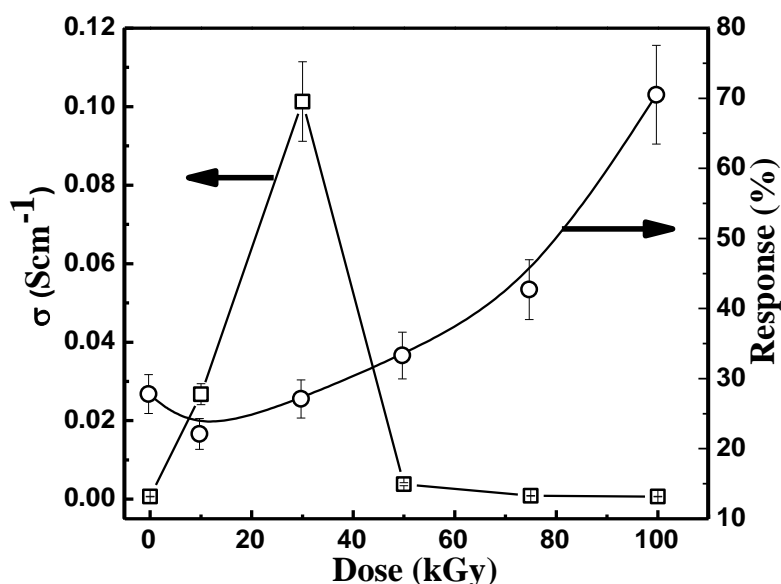


Figure 5.23: Electrical conductivity and H₂S response of flexible PANI-Ag films as function of EB dose.

Also we have investigated the effect of high radiation on the electrical conductivity of commercial polymer PEDOT:PSS films to manifest the scope of this polymer in high radiation field. Thin films of PEDOT:PSS were grown on flexible Kapton sheets and irradiated up to 75 kGy dose with 1 MeV electron beam. The conductivity of as deposited polymer film was ~ 3.2 S/cm and it consistently reduced to ~ 0.76 S/cm after getting 75 kGy. Such a high dose of electron beam though caused loss of insulating PSS but despite that electrical conductivity was reduced due to crosslinking of PEDOT chains under the effect of electron beam irradiation. The crosslinking of PEDOT results in swelling of molecules (and longer chain length) which discourages the inter chain hopping of charge carriers that ultimately resulted in reduction of electrical conductivity of the PEDOT:PSS films. The

observed systematic dependence of electrical conductivity of PEDOT:PSS on EB dose (in the said dose regime) may facilitate its application in radiation dosimetry. The study also suggests the importance of electron-beam as an alternative to tedious chemical crosslinking approaches that are used for various polymers.

SUMMARY

The high energy electron beam, as a source of radiation, is more acceptable and outweighs the conventional gamma-ray sources. In addition it is much suitable for the treatment of moderately thick materials like organic thin films, polymer sheets etc. In the present thesis the electron beam induced modifications in electrical and mechanical characteristics of all the three important categories of organic films, *viz.* insulating (BOPET), semiconducting (ZnPc) and conducting (doped PANI and doped PEDOT), have been investigated. The pristine and electron beam irradiated organic film samples were characterized through XPS, FTIR, XRD, UV-Vis, PL, AFM, SEM and crosslinking analysis using solubility test as well as sol gel analysis. The electrical conductance and chemiresistive gas sensing properties of the samples were analyzed with conventional two probe methods at room temperature. The electron beam irradiation effect in tailoring the mechanical and electrical parameters of BOPET has been observed and analyzed. The electron beam induced crosslinking in BOPET has been found responsible for chemical structure modifications which ultimately tuned its electrical and mechanical characteristics.

The organic semiconducting ZnPc thin films were deposited on flexible BOPET substrate using thermal evaporation techniques. The film growth parameters (*viz.* thickness ~ 20 nm, deposition rate 1Å/s and in situ post deposition vacuum annealing of film sample at 100°C for 15 minutes) were optimized to get high mobility ZnPc films with reproducibility. The increased electrical conductivity as a result of EB irradiation has been explained on the basis of induced additional oxygen doping. Associated charge transport mechanism has been studied along with the chemiresistive gas sensing behavior *viz.* selectivity, sensitivity, repeatability etc.

Conducting polymer- metal nanocomposite is an interesting class of materials which enable the device-design opportunity with new functionality by exploiting the features of both organic and inorganic components. Polyaniline-silver (PANI-Ag) nanocomposite films

have been grown on flexible BOPET substrate through in situ photo polymerization. Prior to film deposition, the surface of BOPET substrate was modified with APTMS to induce a better adhesion between film and substrate along with asserting the directional growth of film. The electrical conductivity enhances up to two orders after irradiating with 30 kGy EB dose and further it falls as dose increased. The rigorous analysis conclude that in initial dose regime (up to 30 kGy) additional non redox doping takes place in polymer backbone along with scissioning of polymer chain as dominant phenomenon over crosslinking. While at the higher doses, the doping sites got saturated and also crosslinking dominated. The chemiresistive gas sensing response of PANI-Ag film also increases with electron beam dose for ppm level of H₂S.

The influence of high dose of electron beam on conductivity of commercial polymer (PEDOT) doped with organic molecule (PSS) has also been studied. The conductivity consistently declined with dose because of crosslinking in polymer chains.

The conclusions of the important outcomes obtained during the thesis work have been mentioned in the end of respective chapters. Here we summarize the important results as follows:

- (i) The irradiation of BOPET sheets by electron beam, in dose range 2-32 kGy, results in modification of chemical structure through creation of diethylene glycol that crosslinks the PET chains. It ultimately causes improved mechanical properties and enhanced electrical resistivity.
- (ii) ZnPc films having thickness 20 nm have been deposited on flexible BOPET substrate and irradiated with 10 MeV electron beam in the dose range 0 - 30 kGy. The electron beam exposure of ZnPc films up to 18 kGy results in a linear enhancement in the electrical conductance which got saturated with higher doses. The selectivity experiment, for chemiresistive gas sensing, concludes that 20 nm ZnPc film has the

best response for H₂S. The response graph of ZnPC towards H₂S sensing shows a linear fall with dose. Mechanism behind increased conductivity of ZnPC films has been explained on the basis of additional oxygen doping which got induced due to irradiation being carried out in aerated conditions at room temperature. Beyond a certain dose (18 kGy) all the doping sites in the film (particularly central metal atom) become blocked with oxygen and no additional oxygen can further attach with the film surface resulting in saturation of electrical conductance. The linear enhancement in electrical current with dose at fixed bias and concomitant fall in response of fixed concentration of H₂S gas with dose implies their possible application as radiation dosimeter in the mentioned dose regime. In addition, the enhancement in electrical conductivity after electron-beam irradiation with 18 kGy dose provides that ZnPC thin films can be operated at lower voltage to achieve sufficient current for different device applications including gas sensors, with the benefit of power-saving.

(iii) Conducting polymer PANI-Ag nanocomposite films have been grown on flexible APTMS treated BOPET substrate and the electron beam irradiation resulted in tailoring of electrical conductivity as well as sensitivity towards ppm level of H₂S. The reasons of such modifications are the enhanced doping, scissioning and crosslinking of PANI chains. The interesting part of linear enhancement of electrical conductivity with electron beam dose up to 30 kGy suggests that the grown films can be used as a flexible potential radiation dosimeter within the said dose range. Also the augmentation in electrical conductivity by around two orders after irradiation with 30 kGy dose can facilitate the use of irradiated PANI-Ag film based devices to operate at lower bias for different applications like gas sensors. The increased response of PANI-Ag films irradiated with 100 kGy, for fixed concentration of H₂S, concludes that EB irradiation can be utilized as tool to enhance the sensitivity of PANI-Ag films based

chemiresistive gas sensor. It can be adopted as technical alternative of tedious and uncontrolled chemical tuning process to augment the gas sensitivity.

(iv) Commercial conducting polymer PEDOT:PSS film grown on flexible Kapton sheets and irradiated with 1 MeV electron beam to manifest the scope of this polymer in high radiation field. The electrical conductivity of the film falls by around four times after getting dose of 75 kGy as compared to as deposited pristine films and for higher doses, it didn't much. The analysis concludes that the crosslinking in PEDOT polymer chain takes place as result of electron beam irradiation which covers the conducting polymer PSS and discourages the hopping of charge carriers. This ultimately results in reduced electrical conductivity of PEDOT:PSS. This study also suggests the importance of electron beam as an alternative of tedious chemical crosslinking approaches that are used for modifying the properties of polymers.

The outcomes of thesis can be narrated with the help of Fig. 6.1.

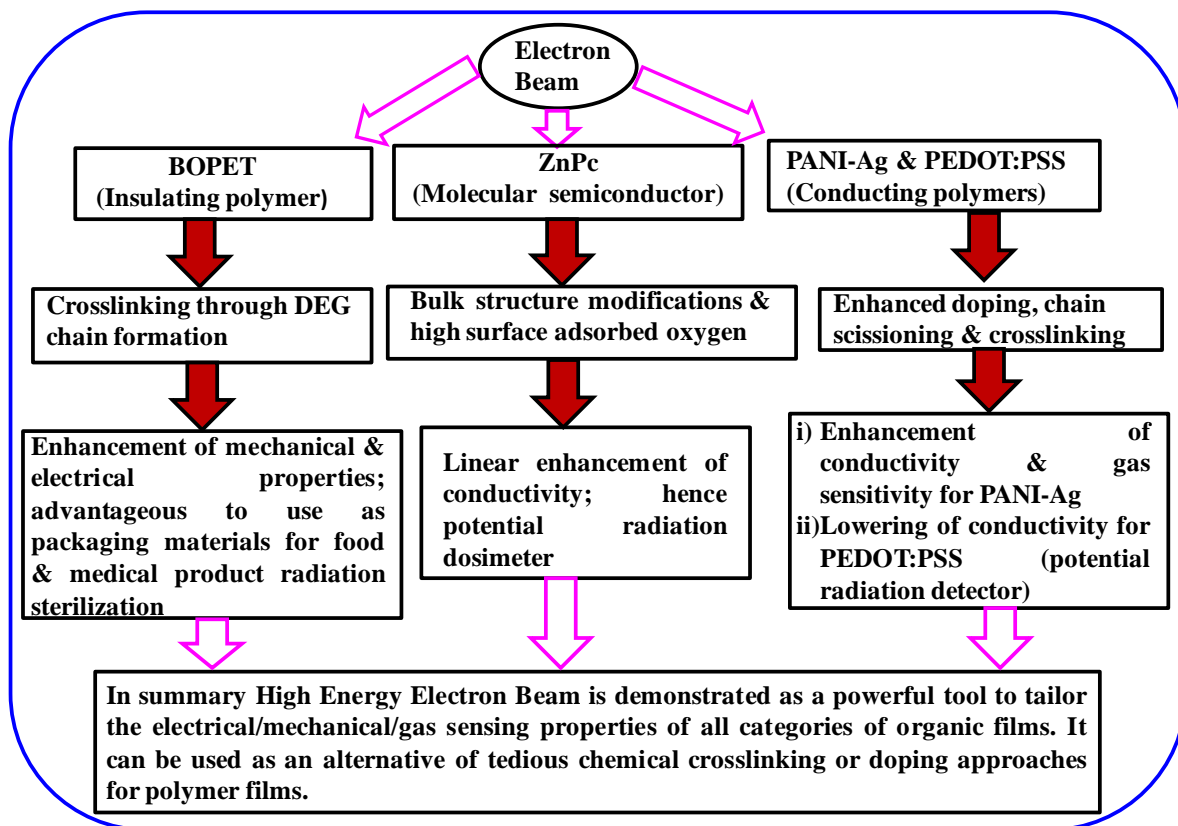


Figure 6.1: Schematic summarizing the outcomes of the present research work.

The results obtained out of present research work clearly manifest the significance of electron beam irradiation to tailor the properties of organic films as well as organic film based devices. The thesis unlocks important points that can be taken in near future:

- (i) The food and medical products needs to be irradiated for sterilization and storage. As per the international standards the dose required for preservation of dry food products (like spices, coriander powder etc) is ranging from 10 kGy- 14 kGy [264, 265] while for the sterilization of medical products the required threshold dose is 25 kGy [266]. It is also essential that the packaging material should not break during irradiation and be able to sustain the high radiation. The study provides that the mechanical properties of BOPET enhance due to irradiation and thus, it is feasible to utilize it as a packaging material for said applications as an alternative to other conventional approaches which have more probability of damage during irradiation.
- (ii) The actual applicability of ZnPc film and PEDOT:PSS film for radiation dosimeters can be explored.
- (iii) The feasibility to utilize the irradiated ZnPc and PANI-Ag film based devices to get enhanced current under low bias can be looked at.
- (iv) Irradiated PANI-Ag films with higher dose can be used for gas sensing applications to have enhanced response towards gases.
- (v) Electron beam irradiation can be utilized to crosslink the conducting polymers, for various applications, as an alternative of tedious chemical approaches.

References

- [1] H. Y Choi, S. H. Kim and J. Jang, *Adv. Mater.* 2004, **16**, 732-736.
- [2] C. D. Dimitrakopoulos and P. R. L Malenfant, *Adv. Mater.* 2002, **14**, 99-117.
- [3] J. Park, S. Lee and H. H. Lee, *Org. Electron.* 2006, **7**, 256-260.
- [4] H. Sirringhaus, *Adv. Mater.* 2005, **17**, 2411-2425.
- [5] D. K. Aswal, S. Lenfant, D. Guerin, J. V. Yakhmi and D. Vuillaume, *Analyt. Chim. Acta.* 2006, **568**, 84-108.
- [6] D. K. Aswal and J. V. Yakhmi, “*Molecular and Organic Electronics Devices*” Nova Science Pub Inc. 2010, New York, USA.
- [7] C. Joachim, J. K. Gimzewski and A. Aviram, *Nat.* 2000, **408**, 541-548.
- [8] S. P. Koiry, D. K. Aswal, A. K. Chauhan, V. Saxena, S. K. Nayak, S. K. Gupta and J. V. Yakhmi, *Chem. Phys. Lett.* 2008, **453**, 68-72.
- [9] S. P. Koiry, P. Jha, D. K. Aswal, S. K. Nayak, C. Majumdar, S. Chattopadhyay, S. K. Gupta and J. V. Yakhmi, *Chem. Phys. Lett.* 2010, **485**, 137-141.
- [10] D. J. Wold and C. D. Frisbie, *J. Am. Chem. Soc.* 2000, **122**, 2970-2971.
- [11] C. K. Chiang, C. R. Fincher, Jr., Y. W. Park, A. J. Heeger, H. Shirakawa, E. J. Louis, S. C. Gau and A. G. MacDiarmid, *Phys. Rev. Lett.* 1977, **39**, 1098-1101.
- [12] L-L. Chua, J. Zaumseil, J-F. Chang, E. C. W. Ou, P. K. H. Ho, H. Sirringhaus and R. H. Friend, *Nat.* 2005, **434**, 194-199.
- [13] V. Podzorov, S. E. Sysoev, E. Loginova, V. M. Pudalov and M. E. Gershenson, *Appl. Phys. Lett.* 2003, **83**, 3504-3506.
- [14] Y. Zhang, J. R. Petta, S. Ambily, Y. Shen, D. C. Ralph and G. G. Malliaras, *Adv. Mater.* 2003, **15**, 1632-1635.
- [15] M. Mas-Torrent and C. Rovira, *Chem. Rev.* 2011, **111**, 4833-4856.
- [16] S. R. Forrest, *Nat.* 2004, **428**, 911-918.

- [17] N. Karl and J. Marktanner, *Mol. Cryst. Liq. Cryst.* 1998, **315**, 163-168.
- [18] W. Warta, R. Stehle and N. Karl, *Appl. Phys. A: Mater. Sci. Proc.* 1985, **36**, 163-170.
- [19] M. Bouvet, V. Parra, C. Locatelli and H. Xiong, *J. Porphyr. Pthalocyanines* 2009, **13**, 84-91.
- [20] S. Gunes, H. Neugebauer and N. S. Sariciftci, *Chem. Rev.* 2007, **107**, 1324-1338.
- [21] H. Hoppe and N. S. Sariciftci, *J. Mater. Res.* 2004, **19**, 1924-1945.
- [22] Z. Bao, A. J. Lovinger and A. Dodabalapur, *Appl. Phys. Lett.* 1996, **69**, 3066.
- [23] S. M. Abdou and R. I. Mohamed, *J. Phys. Chem. Solids* 2002, **63**, 393 – 398.
- [24] U. Henniges, M. Hasani, A. Potthast, G. Westman and T. Rosenau, *Materials* 2013, **6**, 1584 - 1598.
- [25] N. K. Pramanik, R. S. Haldar, Y. K. Bhardwaj, S. Sabharwal, U. K. Niyogi and R. K. Khandal, *Radiat. Phys. Chem.* 2009, **78**, 199 – 205.
- [26] A. Chapiro “*Radiation Effects in Polymers*”, Elsevier Ltd. Encyclopedia of Materials: Science and Technology ISBN: 0-08-043152-6, Elsevier Ltd. 2004, 1–8.
- [27] R. H. Chilkulwar, S. D. Sharma, N. Chaudhary, S. Acharya, Y. S. Mayya, K. C. Mittal and L. M. Gantayet, *Radiat. Measur.* 2012, **47**, 628-633.
- [28] R. J. Woods and A. K. Pikaev, Applied Radiation Chemistry: Radiation Processing, John Wiley & Sons, Inc. 1994, NewYork, U.S.A.
- [29] N. Chaudhary, A. Singh, A. K. Debnath, S. Acharya and D. K. Aswal, *Solid State Phenomena* 2015, **239**, 72-97.
- [30] S. K. Gupta, P. Jha, A. Singh, M. M. Chehimi and D. K. Aswal, *J. Mater. Chem. C* 2015, **3**, 8468-8479.
- [31] W. A. MacDonald, M. K. Looney, D. MacKerron, R. Eveson, R. Adam, K. Hashimoto and K. Rakos, *J. Soc. Inform. Disp.* 2007, **15(12)**, 1075-1083.

- [32] M. Schwoerer and H. C. Wolf, *“Introduction in Organic Molecular Solids”*, Wiley-VCH 2008, Verlag GmbH.
- [33] Y. Gok and S. Z. Yildiz, *J. Coord. Chem.* 1995, **36**, 175-181.
- [34] C. E. Dent, R. P. Linstead and A. R. Lowe, *J. Chem. Soc. (Resumed) 1934*, **217**, 1033-1039.
- [35] C. C. Leznoff and A. B. P. Lever, *“Phthalocyanines: properties and applications”*, Wiley-VCH 1996, Verlag GmbH.
- [36] M-S. Liao and S. Scheiner, *J. Chem. Phys.* 2001, **114**, 9780-9791.
- [37] Z. Bao, A. J. Lovinger and J. Brown, *J. Am. Chem. Soc.* 1998, **120**, 207-208.
- [38] B. Crone, A. Dodabalapur, Y. Y. Lin, R. W. Filas, Z. Bao, A. LaDuca, R. Sarpeshkar, H. E. Katz and W. Li, *Nat.* 2000, **403**, 521-523.
- [39] Y-Y. Lin, A. Dodabalapur, R. Sarpeshkar, Z. Bao, W. Li, K. Baldwin, V. R. Raju and H. E. Katz, *Appl. Phys. Lett.* 1999, **74**, 2714-2716.
- [40] A. K. Debnath, S. Samanta, A. Singh, D. K. Aswal, S. K. Gupta and J. V. Yakhmi, *Chem. Phys. Lett.* 2009, **480**, 185-188.
- [41] T. Higuchi, T. Murayama, E. Itoh and K. Miyairi, *Thin Solid Films* 2006, **499**, 374-379.
- [42] F. Yakuphanoglu, M. Caglar, Y. Caglar and S. Ilican, *Synth. Met.* 2010, **160**, 1520-1523.
- [43] H. Yanagi, H. Kataura and Y. Ueda, *J. Appl. Phys.* 1994, **75**, 568-576.
- [44] C. J. Brown, *J. Chem. Soc. A: Inorg. Phys. Theor.* 1968, **0**, 2488-2493.
- [45] R. D. Gould, *Coord. Chem. Rev.* 1996, **156**, 237-274.
- [46] N. Uyeda, M. Ashida and E Suito, *J. Appl. Phys.* 1965, **36**, 1453-1460.
- [47] S. M. Bayliss, S. Heutz, G. Rumbles and T. S. Jones, *Phys. Chem. Chem. Phys.* 1999, **1**, 3673-3676.

- [48] F. I. Bohrer, A. Sharoni, C. Colesniuc, J. Park, I. K. Schuller, A. C. Kummel and W. C. Trogler, *J. Am. Chem. Soc.* 2007, **129**, 5640- 5646.
- [49] J. Zwart and J. H. M. C. van Wolput, *J. Mol. Catalysis.* 1979, **5**, 51-64.
- [50] D. W. Hatchett and M. Josowicz, *Chem. Rev.* 2008, **108**, 746-769.
- [51] J. Stejskal and R. G. Gilbert, *Pure Appl. Chem.* 2002, **74**, 857-867.
- [52] A. G. MacDiarmid and A. J. Epstein, *Faraday Discuss. Chem. Soc.* 1989, **88**, 317.
- [53] J. Y. Shimano and A. G. MacDiarmid, *Synth. Met.* 2001, **123**, 251-262.
- [54] W.E. Spicer, I. Lindau, P.E. Gregory, C.M. Garner, P. Pianetta and P.W. Chye, *J. Vac. Sci. Technol.* 1976, **13**, 780-785.
- [55] W.E. Spicer, Z. Liliental-Weber, E. Weber, N. Newman, T. Kendelewicz, R. Cao, C. McCants, P. Mahowald, K. Miyano and I. Lindau, *J. Vac. Sci. Technol. B* 1988, **6** 1245.
- [56] H. Vazquez, R. Oszwaldowski, P. Pou, J. Ortega, R. Perez, F. Flores and A. Kahn, *Euro. Phys. Lett.* 2004, **65**, 802 - 808.
- [57] H. Vazquez, F. Flores, R. Oszwaldowski, J. Ortega, R. Perez and A. Kahn, *Appl. Surf. Sci.* 2004, **234**, 107 – 112.
- [58] S. M. Sze, *Physics of Semiconductor Devices, 2nd edition*, Wiley 1981, New York.
- [59] C. R. Crowell, *Solid State Electron.* 1965, **8**, 395 – 399.
- [60] J.G. Simmons, *Phys. Rev.* 1968, **166**, 912.
- [61] F. Gutmann, L. E. Lyons, H. Keyzer, Organic semiconductors, *R. E. Krieger Pub. Co.* 1983.
- [62] B. H. Hamadani, Electronic charge injection and transport in organic field effect transistors, *Rice University* 2007.
- [63] U. Gohs, H. Dorschner, G. Heinrich, M. Stephan, U. Wagenknecht, R. Bartel and O. Roder, “Requirements on Electron Accelerators for Innovative Applications in

- Polymer Industry, Russian Accelerator Conference (RuPAC) 2006*”, Novosibirsk, Russia.
- [64] S. Cheng and D. R. Kerluke, “*Radiation Processing for Modification of Polymers, Annual Technical Conference of the Society of Plastic Engineering (ANTEC) 2003*”, Nashville, U.S.A.
- [65] A. Bhattacharya, *Prog. Polym. Sci.* 2000, **25**, 371–401.
- [66] ASTM ISO/ASTM51538-09, “*Standard Practice for Use of the Ethanol-Chlorobenzene Dosimetry System*”, ASTM International, West Conshohocken, PA, 2002, www.astm.org.
- [67] D. K. Aswal and S. K. Gupta, “*Science and technology of chemiresistive gas sensors*”, Nova Publishers 2007, New York, U.S.A.
- [68] B. Schollhorn, J. P. Germain, A. Pauly, C. Maleysson and J. P. Blanc, *Thin Solid Films* 1998, **326**, 245-250.
- [69] A. Glidle, P. E. Pearson, E. L. Smith, J. M. Cooper, R. Cubitt, R. M. Dalglish, A. R. Hillman and K. S. Ryder, *J. Phys. Chem. B* 2007, **111**, 4043-4053.
- [70] G. Li, M. Josowicz, and J. Janata, *Synth. Met.* 2001, **125**, 273-278.
- [71] D. Blackwood and M. Josowicz, *J. Phys. Chem.* 1991, **95**, 493-502.
- [72] M. Ono, T. Sueyoshi, Y. Zhang, S. Kera and N. Ueno, *Mol. Cryst. Liq. Cryst.* 2016, **455**, 251-256.
- [73] S. H. Yoo, J. M. Kum and S. O Cho, *Nanoscale Res. Lett.* 2011, **6**, 545-552.
- [74] J. J. Kim, J. M. Ha, H. M. Lee, H. S. Raza, J. W. Park and S. O. Cho, *Appl. Mater. Inter.* 2016, **8**, 19192-19196.
- [75] J. J. Kim, H. M. Lee, J. W. Park and S. O. Cho, *J. Mater. Chem. C* 2015, **3**, 2650-2655.
- [76] H. N. Raval, D. S. Sutar and V. R. Rao, *Org. Electron.* 2013, **14**, 1281-1290.

- [77] H. N. Raval, D. S. Sutar, P. R. Nair and V. R. Rao *Org. Electron.* 2013, **14**, 1467-1476.
- [78] Aneesh Kumar K.V, H. B. Ravikumar, S. Ganesh, and C. Ranganathaiah, *IEEE Trans. Nuclear. Sci.* 2015, **62**, 306-313.
- [79] S. Raghu, K. Archana, C. Sharanappa, S. Ganesh and H. Devendrappa, *J. Radiat. Res. Appl. Sci.* 2016, **9**, 117-124.
- [80] A. Miller, W. Batsberg and W. Karman, *Radiat. Phys. Chem.* 1988, **31**, 491-496.
- [81] *ISO/ASTM 2002, "Guide for Selection and Calibration of Dosimetry Systems for Radiation Processing"* ISO/ASTM 51261.
- [82] *ISO/ASTM 2004, "Practice for use of a Radiochromic Film Dosimetry System"* ISO/ASTM 51275.
- [83] *ISO/ASTM 2004, "Standard Practice for Use of Alanine-EPR Dosimetry System"* ISO/ASTM 51607.
- [84] *ISO/ASTM 2005, "Practice for Dosimetry in an Electron Beam Facility for Radiation Processing at Energies between 300 keV and 25 MeV"* ISO/ASTM 51649.
- [85] S. Zhang, L. Li and A. Kumar, "*Materials characterization techniques*", CRC Press, 2009.
- [86] D. P. Woodruff and T. A. Delchar, "*Modern Techniques of Surface Science*", Cambridge University Press 1994, Cambridge, U. K.
- [87] D. Briggs and M. P. Seah, "*Practical surface analysis by auger and x-ray photoelectron spectroscopy*", John Wiley & Sons Ltd. 1983, Chichester, U. K.
- [88] J. F. Watts and J. Wolstenholme, "*An introduction to surface analysis by XPS and AES*", John Wiley & Sons Ltd. 2003, Chichester, U. K.

- [89] J. F. Moulder, "*Handbook of x-ray phototelectron spectroscopy: A reference book of standard spectra for identification and interpretation of XPS data*", *Physical Electronics* 1995.
- [90] W. Kemp, "*Organic spectroscopy*", *Macmillan* 1987.
- [91] D. A. Skoog, F. J. Holler and S. R. Crouch, "*Principles of instrumental analysis*", *Thomson Brooks/Cole* 2007.
- [92] C. Ronda, "*Luminescence from theory to applications*", *Wiley-VCH* 2008, New York, U.S.A.
- [93] K. N. Shinde, S. J. Dhoble, H. C. Swart and K. Park, "*Phosphate phosphors for solid state lighting*", *Springer series in material science* 2013, **174**, Springer, Berlin, Germany.
- [94] B. D. Cullity, "*Elements of x-ray diffraction*", *BiblioBazaar* 2011.
- [95] G. Binning, C. F. Quate and Ch. Gerber, *Phys. Rev. Lett.* 1986, **56**, 930-933.
- [96] N. Yao and Z. L. Wang, "*Handbook of microscopy for nanotechnology*", *Springer* 2005.
- [97] P. J. Goodhew, J. Humphreys and R. Beanland, "*Electron microscopy and analysis*", *Taylor & Francis* 2001, New York, U.S.A.
- [98] I. M. Watt, "*The principles and practice of electron microscopy*", *Cambridge University Press* 1997, Cambridge, U. K.
- [99] K. A. Dubey, Y. K. Bhardwaj, K. Rajkumar, L. Panicker, C. V. Chaudhari, S. K. Chakraborty and S. Sabharwal, *J. Polym. Res.* 2012, **19**, 9876-9885.
- [100] A. Charlesby, "*Atomic radiation and polymers*", *Pergamon Press* 1960, New York.
- [101] A. Charlesby, *Radiat. Phys. Chem.* 1977, **9**, 17-29.
- [102] J. Silverman, *Radiat. Phys. Chem.* 1977, **9**, 1-15.
- [103] L. Martin, M. Lavine and S. T. Balke, *Intl. GPC Symp.* 1991, **99-0900**, 585-596.

- [104] D. H. Jeon, K. H. Lee and H. J. Park, *Radiat. Phys. Chem.* 2004, **71**, 1059-1064.
- [105] K. A. Dubey, Y. K. Bhardwaj, C. V. Chaudhari, V. Kumar, N. K. Goel and S. Sabharwal, *eXPRESS Polym. Lett.* 2009, **3**, 492-500.
- [106] K. Makuuchi and S. Cheng, “*Radiation processing of polymer materials and its industrial applications*”, John Wiley & Sons 2012, New Jersey, U. S. A.
- [107] S. Li, Y. Cao and Z. Xue, *Synth. Met.* 1987, **20**, 141-149.
- [108] L. Fengmei, W. Ying, L. Xiaoguang and Y. Baoyu, *Radiat. Phys. Chem.* 2000, **57**, 435-439.
- [109] L. Woo, M. K. Ling, S. Y. Ding and S. P. Westphal, *Thermochim. Acta* 1988, **324**, 179-189.
- [110] Codex Alimentarius Commission, 2003. *General standard for irradiated foods, CODEX STAN 106-1983 REV.1-2003. FAO / WHO standards, www.codexalimentarius.net.*
- [111] M. Mizani, N. Sheikh, S. N. Ebrahimi, A. Gerami and F. A. Tavakoli, *Radiat. Phys. Chem.* 2009, **78**, 806-809.
- [112] E. A. B. Moura, A. V. Ortiz, H. Wiebeck, A. B. A. Paula, A. L. A. Silva and L. G. A. Silva, *Radiat. Phys. Chem.* 2004, **71**, 201-204.
- [113] U. Ravasio, G. Consolati, A. Faucitano, M. Mariani and F. Quasso, *Euro. Polym. J.* 2007, **43**, 2550-2556.
- [114] A. Singh, A. Kumar, A. Kumar, S. Samanta, A. K. Debnath, P. Jha, R. Prasad, Z. Salmi, S. Nowak, M. M. Chehimi, D. K. Aswal and S. K. Gupta, *Appl. Phys. Lett.* 2012, **101**, 222102.
- [115] W. A. MacDonald, M. K. Looney, D. MacKerron, R. Eveson, R. Adam, K. Hashimoto and K. Rakos, *J. Soc. Inf. Disp.* 2007, **15**, 1075-1084.
- [116] M. Zenkiewicz, *Radiat. Phys. Chem.* 2004, **69**, 373-378.

- [117] V. M. Oliveira, A. V. Ortiz, N. L. Del Mastro and E. A. B. Moura, *Radiat. Phys. Chem.* 2009, **78**, 553-560.
- [118] C. Opriou, D. Martin, M. Toma, S. Marghitu and A. Jianu, *Nucl. Instr. and Meth. B* 2000, **166-167**, 669-675.
- [119] R. L. Hudson, M. H. Moore and A. M. Cook, *Adv. Space Res.* 2005, **36**, 184-189.
- [120] R. M. Silverstein, G. C. Bassler and T. C. Morrill, “*Spectrometric Identification of Organic Compounds*”, 4th edition, *John Wiley and Sons* 1981, New York, U.S.A.
- [121] K. Shameli, M. Bin Ahmad, S. Davoud Jazayeri, S. Sedaghat, P. Shabanzadeh, H. Jahangirian, M. Mahdavi and Y. Abdollahi, *Int. J. Mol. Sci.* 2012, **13**, 6639-6650.
- [122] A. Singh, Z. Salmi, N. Joshi, P. Jha, A. Kumar, H. Lecoq, S. Lau, M. M. Chehimi, D. K. Aswal and S. K. Gupta, *RSC Adv.* 2013, **3**, 5506-5523.
- [123] M. K. Lei, Y. Liu and Y. P. Li, *Appl. Surf. Sci.* 2011, **257**, 7350-7358.
- [124] G. Beamson and D. Briggs, “*High Resolution XPS of Organic Polymers: The ScientaESCA300 Database*”, *JohnWiley & Sons* 1992, U. K.
- [125] M. Aflori and M. Drobot, *Dig. J. Nano. Mat. Biostr.* 2015, **10**, 587-593.
- [126] P. Slepicka, N. Slepickova Kasalkova, E. Stranska, L. Bacakova and V. Svorcik, *eXPRESS Polym. Lett.* 2013, **7**, 535-545.
- [127] K. Gotoh, A. Yasukawa and Y. Kobayashi, *Polym. J.* 2011, **43**, 545-551.
- [128] M. H. van de Woorde, “*Effects of radiation on materials and components, CERN 70-75*”, 1970.
- [129] J. M. Rosiak, *Radiat. Phys. Chem.* 1998, **51**, 13-17.
- [130] J-W Chen and L-W Chen, *J. Polym. Sci.: Polym. Chem.* 1998, **36**, 3073-3080.
- [131] N. Chaudhary, S. P. Koiry, A. Singh, A. R. Tillu, P. Jha, S. Samanta, A. K. Debnath, D. K. Aswal, R. K. Mondal, S. Acharya and K. C. Mittal, *Mat. Chem. Phys.* 2017, **189**, 237-244.

- [132] M. Bouvet, V. Parra, C. Locatelli and H. Xiong, *J. Porphyr. Pthalocyanines* 2009, **13**, 84-91.
- [133] H. Hoppe and N. S. Sariciftci, *J. Mater. Res.* 2004, **19**, 1924-1945.
- [134] F. I. Bohrer, C. N. Colesniuc, J. Park, M. E. Ruidiaz, I. K. Schuller, A. C. Kummel and W. C. Trogler, *J. Am. Chem. Soc.* 2009, **131**, 478–485.
- [135] S. Singh, G. S. S. Saini and S. K. Tripathi, *Sens. Actuators B* 2014, **203**, 118–121.
- [136] A. Kumar, N. Joshi, S. Samanta, A. Singh, A. K. Debnath, A. K. Chauhan, M. Roy, R. Prasad, K. Roy, M. M. Chehimi, D. K. Aswal and S. K. Gupta, *Sens. Actuators. B* 2015, **206**, 653–662.
- [137] K-C Ho, C-M Chen and J-Y Liao, *Sens. Actuators B* 2005, **108**, 418-426.
- [138] D. I. Son, D. H. Park, W. K. Choi, S. H. Cho, W. T. Kim and T. W. Kim, *Nanotechnol.* 2009, **20**, 195203.
- [139] A. Singh, A. Joshi, S. Samanta, A. K. Debnath, D. K. Aswal, S. K. Gupta and J. V. Yakhmi, *Appl. Phys. Lett.* 2009, **95**, 202106.
- [140] M. Krzywiecki, L. Grzadziel, L. Ottaviano, P. Parisse, S. Santucci and J. Szuber, *Mater. Sci. Pol.* 2008, **26**, 287-294.
- [141] K. Nakua, H. T. Ng and E. G. Hanson, *MRS Proc.* 2010, **1270**, 14-33.
- [142] O. Berger, W. J. Fischer, B. Adolphi, S. Tierbach, V. Melev and J. Schreiber, *J. Mater. Sci.: Mater. Electron.* 2000, **11**, 331-346.
- [143] H. Mockert, D. Schmeisser and W. Gopel, *Sens. Actuators* 1989, **19**, 159-176.
- [144] A. Rager, B. Gompf, L. Durselen, H. Mockert, D. Schmeisser and W. Gopel, *J. Mol. Electron.* 1989, **5**, 227-238.
- [145] I. V. Vasiljeva, S. V. Mjakin, A. V. Makarov, A. N. Krasovsky and A. V. Varlamov, *Appl. Surf. Sci.* 2006, **252**, 8768-8775.

- [146] J. H. Park, J. E. Royer, E. Chagarow, T. Kaufman-Osborn, M. Edmonds, T. Kent, S. Lee, W. C. Trogler and A. C. Kummel, *J. Am. Chem. Soc.* 2013, **135**, 14600-14609.
- [147] M. E. Azim-Araghi, S. H. M. Mohamadi and Z. Bisadi, *Acta. Phys. Pol. A* 2014, **125**, 87-92.
- [148] A. A. Zanfolim, D. Volpati, C. A. Olivati, A. E. Job and C. J. L. Constantino, *J. Phys. Chem. C* 2010, **114**, 12290-12299.
- [149] G. Gumrukcu, M. U. Ozgur, A. Altnadal, A. R. Ozkaya, B. Salih and O. Bekaroglu, *Synth. Met.* 2011, **161**, 112-123.
- [150] T. N. Misra, *Rev. Pure Appl. Chem.* 1965, **15**, 39.
- [151] S. Karan and B. Mallik, *J. Phys. Chem. C* 2007, **111**, 7352-7365.
- [152] N. Padma, A. Joshi, A. Singh, S. K. Deshpande, D. K. Aswal, S. K. Gupta and J. V. Yakhmi, *Sens. Actuators. B* 2009, **143**, 246–252.
- [153] M. Kozlik, S. Paulke, M. Grunewald, R. Forker and T. Fritz, *Org. Electron.* 2012, **13**, 3291-3295.
- [154] T. Richardson, V. C. Smith, A. Topacli, J. Jiang and C. H. Huang, *Supramol. Sci.* 1997, **4**, 465-470.
- [155] J. M. Green and L. R. Faulkner, *J. Am. Chem. Soc.* 1983, **105**, 2951-2955.
- [156] J. A. de Saja and M. L. Rodriguez-Mendez, *Adv. Colloid Interface Sci.* 2005, **116**, 1-11.
- [157] JCPDS Card no. 11-0893.
- [158] L. Gaffo, M. R. Cordeiro, A. R. Freitas, W. C. Moreira, E. M. Giroto and V. Zucolotto, *J. Mater. Sci.* 2010, **45**, 1366-1370.
- [159] S. Senthilarasu, Y. B. Hahn and S. H. Lee, *J. Appl. Phys.* 2007, **102**, 043512.
- [160] J. C. Hsieh, C. J. Liu and Y. H. Ju, *Thin Solid Films* 1998, **322**, 98-103.
- [161] M. M. El-Nahass, A. A. M. Farag and A. A. Atta, *Synth. Met.* 2009, **159**, 589–594.

- [162] W. Gao and A. Kahn, *Org. Electron.* 2002, **3**, 53-63.
- [163] W Gao and A. Kahn, *Appl. Phys. Lett.* 2001, **79**, 4040-4042.
- [164] A. Mekki, N. Joshi, A. Singh, Z. Salmi, P. Jha, P. Decorse, S. Lau-Truong, R. Mahmoud, M. M. Chehimi, D. K. Aswal and S. K. Gupta, *Org. Electron.* 2014, **15**, 71–81.
- [165] D. Duarte and A. Dodabalapur, *J. Appl. Phys.* 2012, **111**, 044509.
- [166] C. Zhang, P. Chen and W. Hu, *Chem. Soc. Rev.* 2015, **44**, 2087-2107.
- [167] A. Klug, M. Denk, T. Bauer, M. Sandholzer, U. Scherf, C. Slugovc and E. J. W. List, *Org. Electron.* 2014, **13**, 500-504.
- [168] T. Cramer, A. Campana, F. Leonardi, S. Casalini, A. Kyndiah, M. Murgia and F. Biscarini, *J. Mater. Chem. B* 2013, **1**, 3728-3741.
- [169] S. H. Park, J. G. Jeong, H. Kim, S. Park, M. Cho, S. W. Cho, Y. Yi, M. Y. Heo and H. Sohn, *Appl. Phys. Lett.* 2010, **96**, 013302.
- [170] N. Chaudhary, A. Singh, D. K. Aswal, A. K. Debnath, S. Samanta, S. P. Koiry, S. Sharma, K. Shah, S. Acharya, K. P. Muthe and S. C. Gadkari, *Synth. Met.* 2017, **231**, 143-152.
- [171] D. E. Tallman, G. Spinks, A. Dominis and G. G. Wallace, *J. Solid State Electrochem.* 2002, **6**, 73-84.
- [172] J. W. Schultze and H. Karabulut, *Electrochim. Acta.* 2005, **50**, 1739-1745.
- [173] D. E. Tallman, Y. Pae and G.P. Bierwagen, *Corrosion* 2000, **56**, 401-410.
- [174] S. K. Dhawan, N. Singh and D. Rodrigues, *J. Sci. Technol. Adv. Mater.* 2003, **4**, 105-113.
- [175] H. Tsutumi, S. Yamashita and T. Oishi, *J. Appl. Electrochem.* 1997, **27**, 477-481.
- [176] M. He, F. Qiu and Z. Lin, *Energy Environ Sci.* 2013, **6**, 1352–1361.
- [177] C. Han, Z. Li and S.X. Dou, *Chin Sci. Bull.* 2014, **59**, 2073-2091.

- [178] J. Stejskal and R. G. Gilbert, *Pure Appl. Chem.* 2002, **74**, 857-867.
- [179] S. Virji, J. Huang, R. B. Kaner and B. H. Weiller, *Nano Lett.* 2004, **4**, 491-496.
- [180] J. Huang, S. Virji, B. H. Weiller and R. B. Kaner, *Chem. Eur. J.* 2004, **10**, 1314-1319.
- [181] H. Liu, J. Kameoka, D. A. Czaplewski and H. G. Craighead, *Nano Lett.* 2004, **4**, 671-675.
- [182] M. Mumtaz, E. Clotet, C. Labrugere, G. Hadziioannou and H. Cramail, *Polym. Chem.* 2013, **4**, 615-622.
- [183] S. Wang, Y. Kang, L. Wang, H. Zhang, Y. Wang and Y. Wang, *Sens. Actuator. B* 2013, **182**, 467-481.
- [184] X. Lu, W. Zhang, C. Wang, T-C Wen, and Y. Wei, *Prog. Polym. Sci.* 2011, **36**, 671-712.
- [185] O. M. Folarin, E. R. Sadiku and A. Maity, *Int. J. Phys. Sci.* 2011, **6**, 4869-4882.
- [186] S. Kango, S. Kalia, A. Celli, J. Njuguna, Y. Habibi and R. Kumar, *Prog. Polym. Sci.* 2013, **38**, 1232-1261.
- [187] M. Trchova, Z. Moravkova, I. Sedenkova and J. Stejskal, *Chem. Pap.* 2012, **66**, 415-445.
- [188] C. M. Hangarter, N. Chartuprayoon, S. C. Hernandez, Y. Choa and N. V. Myung, *Nano Today* 2013, **8**, 39-55.
- [189] A. B. Afzal, M. J. Akhtar, M. Nadeem, M Ahmad, M. M. Hassan, T Yasin and M. Mehmood, *J. Phys. D: Appl. Phys.* 2009, **42**, 015411.
- [190] C. Yuan, Y. Xu, L. Zhong, L. Zhang, C. Yang, B. Jiang, Y. Deng, B. Zeng, N. He, W. Luo and L. Dai, *Nanotechnol.* 2013, **24**, 185602.
- [191] C. Liu, K. Hayashi and K. Toko, *Sens. Actuator. B* 2012, **161**, 504-509.
- [192] S. Sharma, C. Nirkhe, S. Pethkar and A. A. Athawale, *Sens. Actuator. B* 2002, **85**, 131-136.

- [193] Y. Xia, J. M. Wiesinger and A. G. MacDiarmid, *Chem. Mater.* 1995, **7**, 443-445.
- [194] T. Berzina, K. Gorshkov, A. Pucci, G. Ruggeri and V. Erokhin, *RSC Adv.* 2011, **1**, 1537-1541.
- [195] S. Peng, J. Liang, S. G. Mhaisalkar and S. Ramakrishna, *J. Mater. Chem.* 2012, **22**, 5308-5311.
- [196] Y. Zhang, J. Yin, K. Wang, P. Chen and L. Ji, *J. Appl. Polym. Sci.* 2013, **128**, 2971-2976.
- [197] S. L. Lim, K. L. Tan and E. T. Kang, *Langmuir* 1998, **14**, 5305-5313.
- [198] D. S. Patil, J. S. Shaikh, S. A. Pawar, R. S. Devan, Y. R. Ma, A. V. Moholkar, J. H. Kim, R. S. Kalubarme, C. J. Park and P. S. Patil, *Phys. Chem. Chem. Phys.* 2012, **14**, 11886-11895.
- [199] S. K. Pillalamarri, F. D. Blum, A. T. Tokuhiko and M. F. Bertino, *Chem. Mater.* 2005, **17**, 5941-5944.
- [200] C. M. Correa, R. Faez, M. A. Bizeto and F. F. Camilo, *RSC Adv.* 2012, **2**, 3088-3093.
- [201] D. S. Sutar, N. Padma, D. K. Aswal, S. K. Deshpande, S. K. Gupta and J. V. Yakhmi, *Sens. Actuator. B* 2007, **128**, 286-292.
- [202] A. K. Chauhan, D. K. Aswal, S. P. Koiry, S. K. Gupta, J. V. Yakhmi, C. Surgers, D. Guerin, S. Lenfant and D. Vuillaume, *Appl. Phys. A* 2008, **90**, 581-589.
- [203] D. Cossement, F. Plumier, J. Delhalle, L. Hevesi and Z. Mekhalif, *Synth. Met.* 2003, **138**, 529-536.
- [204] S. S. Patil, S. P. Koiry, P. Veerender, D. K. Aswal, S. K. Gupta, D. S. Joag and M. A. More, *RSC Adv.* 2012, **2**, 5822-5827.
- [205] S. Saravanan, C. J. Mathai, M. R. Anantharaman, S. Venkatachalam and P. V. Prabhakaran, *J. Phys. Chem. Solids* 2006, **67**, 1496-1501.

- [206] Y. Gao, D. Shan, F. Cao, J. Gong, X. Li, H. Ma, Z. Su and L. Qu, *J. Phys. Chem. C* 2009, **113**, 15175–15181.
- [207] J. Yue and A. J. Epstein, *Macromolecules* 1991, **24**, 4441-4445.
- [208] S. Golczak, A. Kanciurowska, M. Fahlamn, K. Langer and J. J. Langer, *Sol. St. Ion.* 2009, **179**, 2234-2239.
- [209] E. T. Kang, K. G. Neoh, T. C. Tan, S. H. Khor and K. L. Tan, *Macromolecules* 1990, **23**, 2918-2926.
- [210] B. Zhao, K. G. Neoh, F. T. Liu, E. T. Kang and K. L. Tan, *Langmuir* 2000, **16**, 10540-10546.
- [211] L. Zhao, K. G. Neoh and E. T. Kang, *Chem. Mater.* 2002, **14**, 1098-1106.
- [212] B. Zhao, K. G. Neoh, E. T. Kang and K. L. Tan, *Chem. Mater.* 2000, **12**, 1800-1806.
- [213] S. M. Reda and S. M. Al-Ghannam, *Adv. Mater. Phys. Chem.* 2012, **2**, 75-81.
- [214] S. Bhadra, N. K. Singha and D. Khastgir, *J. Appl. Polym. Sci.* 2007, **104**, 1900-1904.
- [215] A. Drury, S. Chaure, M. Kroll, V. Nicolosi, N. Chaure and W. J. Blau, *Chem. Mater.* 2007, **19**, 4252-4258.
- [216] S. Bhadra, N. K. Singha and D. Khastgir, *Polym. Int.* 2007, **56**, 919–927.
- [217] O. Guven, *Radiat. Phys. Chem.* 2007, **76**, 1302-1307.
- [218] E. C. Gomes and M. A. S. Oliveira, *Am. J. Polym. Sci.* 2012, **2**, 5-13.
- [219] R. G. Thorne, J. G. Master, S. A. Williams, A. G. MacDiarmid and R. M. Hochstrasser, *Synth. Met.* 1992, **49/50**, 423-428.
- [220] M. Wan and J. J. Yang, *Appl. Polym. Sci.* 1995, **55**, 399-405.
- [221] B. V. Raigaonkar, L. P. Vijayan, S. Chawla, R. N. Dubey and M. S. Qureshi, *Synth. Met.* 2011, **161**, 348–353.
- [222] D. Phillips, “*Polymer Photophysics: Luminescence, Energy Migration and Molecular Motion in Synthetic Polymers*”, Chapman & Hall 1985, Cambridge, U. S. A.

- [223] M. Cochet, J.-P. Buisson, J. Wery, G. Jonusauska, E. Faulques and S. Lefrant, *Synth. Met.* 2001, **119**, 389-390.
- [224] D. M. Bubb, S. M. O'Malley, C. Antonacci, R. Belmont, R. A. McGill and C. Crimi, *Appl. Phys. A* 2005, **81**, 119–125.
- [225] J.A. Malmonge and L.H.C. Mattoso, *Synth. Met.* 1997, **84**, 779-780.
- [226] S. Dhibar and C. K. Das, *Ind. Eng. Chem. Res.* 2014, **53**, 3495–3508.
- [227] V. K. Shukla, P. Yadav, R. S. Yadav, P. Mishra and A. C. Pandey, *Nanoscale* 2012, **4**, 3886-3893.
- [228] M. R. Karim, J. H. Yeum, Min-Y. Lee, M. S. Lee and K. T. Lim, *Polym. Adv. Technol.* 2009, **20**, 639–644.
- [229] M. M. Ayad, N. Prastomo, A. Matsuda and J. Stejskal, *Synth. Met.* 2010, **160**, 42–46.
- [230] M Angelopoulos, J. M. Shaw, R. D. Kaplan and S. Perreault, *J. Vac. Sci. Technol.* 1989, **B7(6)**, 1519.
- [231] S. Bhadra and D. Khastgir, *Polym. Degrad. Stab.* 2007, **92**, 1824-1832.
- [232] S. Stafstrom, J. L. Bredas, A. J. Epstein, H. S. Woo, D. B. Tanner, W. S. Huang and A. G. MacDiarmid, *Phys. Rev. Lett.* 1987, **59**, 1464-1467.
- [233] V. Luthra, R. Singh, S. K. Gupta and A. Mansingh, *Curr. Appl. Phys.* 2003, **3**, 219-222.
- [234] A. Choudhury, *Sens. Actuator. B* 2009, **138**, 318–325.
- [235] Z. Li, F. D. Blum, M. F. Bertino and C. Kim, *Sens. Actuator. B* 2012, **161**, 390–395.
- [236] A. Fattoum, M. Arous, F. Gmati, W. Dhaoui and A. B. Mohamed, *J. Phys. D: Appl. Phys.* 2007, **40**, 4347–4354.
- [237] A. G. MacDiarmid, *Synth. Met.* 1997, **84**, 27-34.
- [238] H. Bodugoz and O. Guven, *Nucl. Instrum. Methods Phys. Res. B* 2005, **236**, 153-159.

- [239] M. D. Shirsat, M. A. Bangar, M. A. Deshusses, N. V. Myung and A. Mulchandani, *Appl. Phys. Lett.* 2009, **94**, 083502.
- [240] K. Crowley, A. Morrin, R. L. Shepherd, M. in het Panhuis, G. G. Wallace, M. R. Smyth and A. J. Killard, *IEEE Sens. J.* 2010, **10**, 1419-1426.
- [241] B. T. Raut, P. R. Godse, S. G. Pawar, M. A. Chougule, D. K. Bandgar and V. B. Patil, *Measurements* 2012, **45**, 94-100.
- [242] B. T. Raut, M. A. Chougule, S. R. Nalage, D. S. Dalavi, S. Mali, P. S Patil and V. B. Patil, *Ceram. Int.* 2012, **38**, 5501-5506.
- [243] C. Qin and J. L. Whitten, *Surf. Sci.* 2005, **588**, 83-91.
- [244] N. E. Agbor, M. C. Petty and A. P. Monkman, *Sens. Actuator. B* 1995, **28**, 173-179.
- [245] P. Gobbo, S. Novoa, M. C. Biesinger and M. S. Workentin, *Chem. Commun.* 2013, **49**, 3982-3984.
- [246] J. Zhou, E. Q. Li, R. Li, X. Xu, I. A. Ventura, A. Moussawi, D. A. Anjum, M. N. Hedhili, D. M. Smilgies, G. Lubineau and S. T. Thoroddsen, *J. Mater. Chem. C* 2015, **3**, 2528-2538.
- [247] H. Yan and H. Okuzaki, *Synth. Met.* 2009, **159**, 2225-2228.
- [248] H. Ling, J. Lu, S. Phua, H. Liu, L. Liu, Y. Huang, D. Mandler, P. S. Lee and X. Lu, *J. Mater. Chem. A* 2014, **2**, 2708-2717.
- [249] S. Ma, K. Anderson, L. Guo, A. Yousuf, E. C. Ellingsworth, C. Vajner, H-T. Wang and G. Szulczewski, *Appl. Phys. Lett.* 2014, **105**, 073905.
- [250] G. H. Kim, L. Shao, K. Zhang and K. P. Pipe, *Nat. Mater.* 2013, **12**, 719-723.
- [251] E. J. Bae, Y. H. Kang, K-S. Jang and S. Y. Cho, *Nature Scientific Reports* 2016, **6:18805**, doi: 10.1038/srep18805.
- [252] C. Duc, A. Vlandas, G. G. Malliaras and V. Senez, *Soft Matter.* 2016, **12**, 5146-5153.

- [253] M. Marzocchi, I. Gualandi, M. Calienni, I. Zironi, E. Scavetta, G. Castellani and B. Fraboni, *Appl. Mater. Inter.* 2015, **7**, 17993-18003.
- [254] A. Elschner, S. Kirchmeyer, W. Lovenich, U. Merker and K. Reuter, “*PEDOT: Principles and applications of intrinsically conductive polymer*”, Taylor Francis 2011, CRC Press.
- [255] O. P. Dimitriev, D. A. Grinko, Y. V. Noskov, N. A. Ogurtsov and A. A. Pud, *Synth. Met.* 2009, **159**, 2237-2239.
- [256] H. Yin, C. Lee and W. Chiu, *Polym.* 2011, **52**, 5065-5074.
- [257] H. Shi, C. Liu, Q. Jiang and J. Xu, *Adv. Electron. Mater.* 2015, **1**, 1500017.
- [258] M. M. Nasef, H. Saidi and K. Z. M. Dahlan, *Radiat. Phys. Chem.* 2011, **80**, 66-75.
- [259] T. M. Huang, S. Batra, J. Hu, T. Miyoshi and M. Cakmak, *Polym.* 2013, **54**, 6455-6462.
- [260] N. Chaudhary, M. Bharti, A. Singh, D. K. Aswal, S. P. Koiry, A. K. Debnath and S. Acharya, *Vacuum* 2018, **152**, 243-247.
- [261] J. Edberg, D. Landolo, R. Brooke, X. Liu, C. Musumeci, J. W. Andreasen, D. T. Simon, D. Evans, I. Engquist and M. Berggren, *Adv. Funct. Mater.* 2016, **26**, 6950-6960.
- [262] W. Cho, S. Im, S. Kim, S. Kim and J. H. Kim, *Polym.* 2016, **8**, 189.
- [263] D. Mantione, I. del Agua, W. Schaafsma, M. ElMahmoudy, I. Uguz, A. S. Sanchez, H. Sardon, B. Castro, G. G. Malliaras and D. Mecerreyes, *Appl. Mater. Inter.* 2017, **9**, 18254-18262.
- [264] IAEA-TECHDOC-639, 1992.
- [265] D. G. Olson, *Food Technol.* 1998, **52**, 56-62.
- [266] IAEA-TECHDOC- 539, 1990.